

Adaptive Techniques for Multiuser OFDM

Thesis submitted by
Eric Phillip LAWREY BE (Hons)
in December 2001

for the degree of Doctor of Philosophy
in Electrical and Computer Engineering
School of Engineering
James Cook University

Access to Thesis

I, the undersigned, the author of this thesis, understand that James Cook University will make it available for use within the University Library and, by microfilm or other photographic means, allow access to users in other approved libraries. All users consulting this thesis will have to sign the following statement:

"In consulting this thesis I agree not to copy or closely paraphrase it in whole or in part without the written consent of the author; and to make proper written acknowledgement for any assistance which I have obtained from it."

Beyond this, I do not wish to place any restriction on access to this thesis.

.....

(signature)

.....

(date)

Declaration

I declare that this thesis is my own work and has not been submitted in any form for another degree or diploma at any university or other institution of tertiary education. Information derived from the published work of others has been acknowledged in the text and a list of references is given.

.....

(signature)

.....

(date)

Acknowledgements

I wish to convey warmest thanks to my parents; Cheryl and Michael, who have given me endless support, and provided me with the opportunity to reach this far with my studies.

I wish to thank my supervisor A/Prof Cornelis Jan Kikkert for his support and encouragement.

I also thank A/Prof Greg Allen, and Dr. Graham Woods of the Department of Electronic and Computer Engineering at James Cook University for their expert help and recommendations.

I would like to thank Craig Blackburn for the many hours of white board discussion, and support.

I would also like to thank both Noel Lovisa and Noel Lovisa (senior) for their support as friends and for sharing my excitement of discoveries made during this thesis.

I would particularly like to thank Dr. Nicole Kessissoglou for her motivational discussions about research and publications, without which, I would probably still be not finished.

I also would like to thank all staff of the School of Engineering at James Cook University for their kind help.

ABSTRACT

The demand for high-speed mobile wireless communications is rapidly growing. OFDM technology promises to be a key technique for achieving the high data capacity and spectral efficiency requirements for wireless communication systems of the near future.

This thesis presents an investigation into methods for maximising the spectral efficiency of Orthogonal Frequency Division Multiplexing (OFDM) systems. As part of this, an investigation of detrimental effects on OFDM is presented, showing the effect of: band pass filtering, the use of a raised cosine guard period, clipping distortion, Additive White Gaussian Noise (AWGN) on modulation BER rate, time synchronisation error, and frequency offset errors.

An investigation of two adaptive techniques is also presented. These techniques utilise knowledge obtained by dynamically tracking the radio channel response, to optimise the user frequency, and subcarrier modulation. Adaptive modulation independently optimises the modulation scheme applied to each subcarrier so that the spectral efficiency is maximised, while maintaining a target Bit Error Rate (BER). For a fading channel, adaptive modulation results in an improvement of 12 - 16 dB in the Signal to Noise Ratio (SNR) required to maintain a given BER, as compared with fixed modulation. Adaptive user allocation exploits the difference in frequency selective fading between users, to optimise user subcarrier allocation. In a multipath environment the fading experienced on each subcarrier varies from user to user, thus by utilising user/subcarrier combinations that suffer the least fading, the overall performance is maximised. Adaptive user allocation results in an additional average signal power improvement of 3 - 5 dB.

The simulated performance of the adaptive techniques is presented using a set of measured wide bandwidth (70 MHz) frequency response measurements taken at 1

GHz. These measurements show the changes in the frequency selective fading with small increments in space, allowing the effects of different tracking rates for the adaptive allocations schemes to be investigated.

This thesis also presents a method for maximising the signal strength within buildings, by using transmission repeaters. This is similar to the Single Frequency Networks used in DAB and DVB systems, except applied to small-scale bi-directional communications. Using multiple repeaters causes multipath problems in most conventional systems, however OFDM has a sufficiently high multipath tolerance to combine the multipath energy. It was found to decrease the path loss by 7 dB for an indoor system with two repeaters, and up to 20 dB for eight repeaters.

In addition, two techniques are presented for reducing the Crest Factor (peak to average power ratio of the RF signal envelope) of OFDM signals. The first technique is a phasing scheme for OFDM pilot symbols, which uses genetic algorithms to optimise the phase angle of each subcarrier. This technique achieves a lower CF than any previously published techniques, obtaining a CF as low as 0.65 dB, which is 2 dB lower than commonly used techniques. The second technique reduces the CF of data carrying symbols, by including additional subcarriers that are optimised in amplitude and phase to cancel out the peaks in the overall OFDM symbol. This was found to produce a net improvement of 4 dB to the worst-case symbol CF.

TABLE OF CONTENTS

Abstract.....	v
Table of Contents	vii
List of Tables.....	xiii
List of Figures.....	xv
Glossary	xxiv
Simulation Files	xxviii
Chapter 1 Introduction.....	1
1.1 Third Generation Wireless Systems	2
1.2 4 th Generation Systems and beyond	3
1.3 Orthogonal Frequency Division Multiplexing.....	4
1.3.1 Digital Audio Broadcasting.....	5
1.3.2 Digital Video Broadcasting.....	7
1.3.3 Multiuser OFDM.....	9
1.3.4 HiperLAN2 and IEEE802.11a	10
1.4 Thesis outline and contributions to the field.....	11
1.4.1 Chapter 2 Basic Principles of OFDM	11
1.4.2 Chapter 3 Radio Propagation	12
1.4.3 Chapter 4 Multiuser OFDM	13
1.4.4 Chapter 5 Access Point Repeaters.....	14
1.4.5 Chapter 6 Generation of low Crest Factor Multi-Tone Signals .	14
1.4.6 Chapter 7 Crest Factor Minimisation of OFDM Data Symbols .	15
1.4.7 Chapter 8 Summary.....	15

Chapter 2 Basic Principles of OFDM.....	16
2.1.1 Orthogonality	18
2.1.2 Frequency Domain Orthogonality.....	20
2.2 OFDM Generation and Reception.....	21
2.2.1 Serial to Parallel Conversion.....	22
2.2.2 Subcarrier Modulation.....	23
2.2.3 Frequency to Time Domain Conversion.....	25
2.2.4 RF Modulation	26
2.2.5 Real verses Complex OFDM generation	27
2.3 Guard Period	30
2.3.1 Protection against Time Offset.....	32
2.3.2 Protection against ISI.....	32
2.3.3 Guard Period Overhead and Subcarrier Spacing.....	36
2.4 Bandlimiting of OFDM and windowing.....	37
2.4.1 Band Pass Filtering.....	39
2.4.2 Computational Complexity of FIR band pass filtering	42
2.4.3 Effect of band pass filtering on OFDM performance	43
2.5 Raised Cosine Guard Period	48
2.6 Effect of Additive White Gaussian Noise on OFDM.....	51
2.6.1 Modulation schemes.....	52
2.6.2 OFDM verses Single Carrier Transmission.....	53
2.6.3 Modulation Limitations of systems.....	55
2.6.4 Simulation Set up	56
2.6.5 Gray Coding	57
2.6.6 Coherent Modulation.....	62
2.6.7 Differential Phase Modulation.....	62
2.6.8 Differential QAM	64
2.6.9 Simulation Results.....	67
2.7 Effect of pilot symbol channel equalisation in coherent modulation.....	69
2.8 Effect of Distortion on OFDM	72
2.8.1 Distortion Modelling	74
2.8.2 Spectral SpreadinG from Distortion Clipping.....	77
2.8.3 Effective SNR from Clipping Distortion	79

2.8.4	Effect of pilot symbol type on the BER with distortion.....	80
2.9	Reduction of spectral spreading by Pre-filter Clipping	82
2.10	Effect of Time Synchronisation Error	86
2.11	Effect of Frequency Synchronisation Error.....	88
Chapter 3 Radio Propagation	91	
3.1	Path loss and Attenuation.....	91
3.2	Shadowing and slow fading.....	93
3.3	Multipath Effects	95
3.4	Delay Spread.....	97
3.5	Short term fading	99
3.6	Frequency selective fading	100
3.7	Frequency-Space Fading	102
3.7.1	Equalisation.....	103
3.8	Frequency Space Fading measurements	104
3.8.1	Measurement Locations	104
3.8.2	Measurement Results	107
3.9	Rate of change of radio channels	109
3.9.1	Experimental Set up	110
3.9.2	Scope and Scaling of the Results	112
3.9.3	Measurement Location.....	113
3.9.4	Effect of walking toward the transmitter channel response	114
3.9.5	Effect of typing on a keyboard near the transmitter on the channel response	117
3.9.6	Effect of a moving person on the channel response	119
Chapter 4 Multiuser OFDM.....	122	
4.1	Network Structure.....	123
4.1.1	Peer-to-peer Networking	123
4.1.2	Single Cell Base Station.....	123
4.1.3	Forward Channel.....	124
4.1.4	Reverse Channel.....	125
4.2	Adaptive modulation	127

4.2.1	Limitations of Adaptive Modulation.....	130
4.2.2	Effective SNR measurement	131
4.2.3	Single User Adaptive Modulation.....	133
4.3	Multiuser Subcarrier Allocation	138
4.3.1	Fixed frequency grouped subcarriers	140
4.3.2	Random frequency hopping	143
4.3.3	Time Division Multiple Access Allocation.....	146
4.3.4	Comb Spread Subcarriers	149
4.3.5	Adaptive User Allocation and Adaptive Bandwidth.....	151
4.3.6	Summary of user allocation scheme performance	158
4.4	Tracking Rate Required for Adaptive Modulation and Adaptive User Allocation.....	159
4.4.1	Effect of delay on the performance of adaptive modulation....	163
Chapter 5 Access Point Repeaters	165	
5.1	Spatial Diversity by multiple repeat transmissions	167
5.1.1	APR spacing for HiperLAN2 system.....	170
5.2	Implementation of an Access Point Repeater.....	173
5.3	Experimental Set up	174
5.4	Discussion of measured results.....	177
5.5	Reduction in cellular interference.....	179
5.6	Shadow Modelling	179
5.6.1	Intercept calculations	181
5.6.2	Spacial Anti-Aliasing	183
5.6.3	Model Verification.....	183
5.6.4	Simulated Results	184
5.7	Access Point Repeater Performance with a moving interferer.....	188
5.7.1	SNR calculation.....	188
5.7.2	Results	189
5.8	Conclusion.....	193
Chapter 6 Generation of low Crest Factor Multi-Tone Signals.....	194	
6.1	Crest Factor Measurement.....	196

6.1.1	Random Phase DMT symbols.....	197
6.1.2	Measurement of Crest Factor	199
6.1.3	Estimation of error in CF measurements.....	200
6.1.4	Simulated Results	203
6.1.5	CF Errors in Practice.....	204
6.2	Crest Factor Minimisation using Genetic Algorithms	204
6.2.1	Shapiro-Rudin Phases	205
6.2.2	Newmann Phases.....	206
6.2.3	S. Narahashi and T. Nojima phasing scheme	208
6.2.4	Genetic Algorithm Phase Optimisation.....	210
6.3	Phasing Schemes for Null Symbol Synchronisation.....	219
6.3.1	Spectral Flatness.....	221
6.3.2	Experimental Verification.....	224
Chapter 7 Crest Factor Minimisation of OFDM Data Symbols	228	
7.1	Background	228
7.2	Peak Reduction Carriers	229
7.3	Results.....	230
7.4	Effect of PRC Position.....	232
7.5	Grouped PRCs	234
7.6	Spread PRCs	234
7.7	Conclusion.....	237
Chapter 8 Summary.....	238	
8.1	Future Work	238
8.2	Conclusion.....	241
References.....	244	
Publications resulting from this PhD	256	
Appendix A Window functions	257	
A.1	Window function transition width and side-lobe power.....	259
A.2	Window function performance when used for FIR filters	260
A.3	Window Loss	263

A.4	Lawrey Window Function.....	264
Appendix B	BER verses SNR for OFDM in AWGN.....	266
B.1	Coherent Quadrature Amplitude Modulation.....	266
B.2	Coherent Phase Shift Keying.....	270
B.3	Differential QAM	272
B.4	Differential Phase Shift Keying.....	274
Appendix C	RF Measurements	277
C.1	Diversity	283
Appendix D	Phase tables for evolved low Crest Factor Discrete Multi-Tone signals	285
D.1	Phase difference between evolved low CF DMT symbols and Newmann's phasing scheme	292

LIST OF TABLES

Table 1-1, DAB Transmission parameters for each transmission mode [20]	6
Table 1-2, DVB transmission parameters [18].....	8
Table 1-3, SNR required and net bit rate for a selection of the coding and modulation combinations for DVB	9
Table 1-4, Summary of characteristics of IEEE802.11b, IEEE802.11a and HiperLAN2. Derived from [97]	11
Table 1-5, Physical Layer for HiperLAN2 and IEEE802.11a. Derived from [99]	11
Table 2-1, 4 bit Gray coding in binary.....	58
Table 2-2, IQ diagrams for modulations used in the OFDM simulations. (script s0045)	59
Table 2-3, Phase mapping for differential QPSK.....	63
Table 2-4, SNR degradation in dB due to imperfect channel estimation.	71
Table 3-1, Table of typical path loss exponent for different environments.....	95
Table 3-2, Measured delay spread for a variety of environments.	99
Table 4-1, Required SNR to maintain a BER below a given threshold.	132
Table 4-2, Summary of system performance when using different user allocation schemes. Note: all schemes used adaptive modulation.	158
Table 5-1, Material properties of the internal walls.....	184
Table 6-1, Shapiro-Rudin phase sequences for generating low CF DMT signals	205
Table 7-1, Optimised positions found for 10 BPSK data subcarriers.....	237

Table A - 1, Transition width and side-lobe power of different window functions. (script s0039)	260
Table A - 2, Side-lobe power of different window functions when used with the window method of FIR filter design. (script s0071)	261
Table A - 3, Transition of FIR filters using different window functions. (script s0071)	262
Table A - 4, Window loss for different window functions (script s0075)	264
Table A - 5, Coefficients for Lawrey5 and Lawrey6 window functions, and other common window functions.....	265

LIST OF FIGURES

Figure 1-1, Current and future mobile systems. The general trend will be to provide higher data rates and greater mobility. Derived from [12] and [13].....	4
Figure 2-1, Time domain construction of an OFDM signal.	19
Figure 2-2, Frequency response of the subcarriers in a 5 tone OFDM signal. (script 0006)	21
Figure 2-3, Block diagram showing a basic OFDM transceiver.....	22
Figure 2-4, Example IQ modulation constellation. 16-QAM, with gray coding of the data to each location. (script s0045).....	24
Figure 2-5, IQ plot for 16-QAM data with added noise. (script s0083).....	25
Figure 2-6, OFDM generation, IFFT stage.....	26
Figure 2-7, RF modulation of complex base band OFDM signal, using analog techniques.....	26
Figure 2-8, RF modulation of complex base band OFDM signal, using digital techniques. (DDS = Direct Digital Synthesis)	27
Figure 2-9, DC offset OFDM signal, W - bandwidth, f_{off} - frequency offset from DC, f_c centre frequency.....	28
Figure 2-10, Construction of the subcarriers for generating a real output time domain waveform.....	29
Figure 2-11, Construction of the subcarriers for complex signal representation of OFDM signals	30
Figure 2-12, Addition of a guard period to an OFDM signal	31
Figure 2-13, Function of the guard period for protecting against ISI.	33
Figure 2-14, Effectiveness of adding a guard period for removal of ISI. (script s0082)	36
Figure 2-15, Time waveform of a single carrier OFDM signal, showing 3 symbols.	37

Figure 2-16, Spectrum of a 52 subcarrier OFDM signal with no band-limiting. (script s0050)	38
Figure 2-17, Spectrum of a 1536 subcarrier OFDM signal with no band-limiting. (script s0050)	38
Figure 2-18, Spectrum of a 20 subcarrier OFDM, with and without band pass filtering. Centre subcarrier was not used. (script s0050)	41
Figure 2-19, Effective SNR as a function of the time offset for a band pass filtered 52 subcarrier OFDM signal. (script s0057)	44
Figure 2-20, Section of the waveform that the receiver FFT is taken from depending on the time offset.....	44
Figure 2-21, Effective SNR for each subcarrier as a result of band pass filtering. (script s0057)	45
Figure 2-22, Subcarrier effective SNR, due to band pass filtering. (script s0085)	47
Figure 2-23, Construction of a RC guard period.	48
Figure 2-24, Envelope of OFDM symbols with a flat guard period and an overlapping raised cosine guard period.	48
Figure 2-25, Side-lobe power for an OFDM signal with 20 subcarriers as the length of the RC guard period is varied. (script s0050)	50
Figure 2-26, Side-lobe power for an OFDM signal with 100 subcarriers as the length of the RC guard period is varied. (script s0050)	50
Figure 2-27, Side-lobe power for an OFDM signal with 4000 subcarriers as the length of the RC guard period is varied. (script s0050)	51
Figure 2-28, IQ plot of 16-PSK using gray coding. Note that each successive IQ location changes by only a single bit.	58
Figure 2-29, IQ data mapping for differential 16-QAM.	64
Figure 2-30, Bit Error Rate verses the Energy per Bit to Noise Ratio for a selection of OFDM modulation schemes. (script s0041)	67
Figure 2-31, SNR required to maintain a BER of $< 1 \times 10^{-5}$, for all the simulated modulation schemes. (script s0046)	69
Figure 2-32, Effect of distortion on a 2 tone signal, showing harmonics and IMD. (script s0049)	72

Figure 2-33, Measured Input verses Output for an MAR6 amplifier, showing distortion.....	75
Figure 2-34, Input verses Output for a power limited linear amplifier.....	76
Figure 2-35, Spectrum of OFDM signal with clipping distortion. (script s0048)	78
Figure 2-36, Strength of the spectral spreading as a function of the Output Power Backoff. (script s0048)	78
Figure 2-37, Crest Factor distribution verses number of subcarriers for an OFDM signal. (script s0032)	79
Figure 2-38, Effective SNR of an OFDM transmission verses the Output Power Backoff for 8, 64 and 512 transmission subcarriers. (script s0052)	79
Figure 2-39, Effective SNR verses output power backoff using different pilot symbols. (script s0054).....	81
Figure 2-40, Pre-filter clipping is to reduce spectral spreading due to clipping in the power amplifier.	82
Figure 2-41, Spectrum of a 64 subcarrier OFDM signal with pre-filter clipping. (script s0063)	85
Figure 2-42, Side-lobe power caused by IMD as a result of clipping in the power amplifier, for different levels of pre-filter clipping. (script s0063)	85
Figure 2-43, Effective SNR of the OFDM transmission as a function of the OBO in the Power Amplifier, and the Pre-filter clipping used. (script s0062)	86
Figure 2-44, Effective SNR of an OFDM signal with a time offset error, using a flat guard period of 40 samples. (script s0053)	87
Figure 2-45, Effective SNR of an OFDM signal with a time offset error, using a raised cosine guard period. (script s0069)	88
Figure 2-46, Effective SNR for Coherent QAM with frequency offset error. (script s0068)	90
Figure 3-1, Expanding RF pulse from a central transmitter. (script s0029)	92
Figure 3-2, Effect of receiver position on the relative strength of the received direct, reflected and diffracted signals.....	94
Figure 3-3, Impulse response and phasor plot for multipath channel.	96
Figure 3-4, Example channel impulse response for a 2.4 km transmission at 910 MHz on Manhattan Island, New York City [71].	97

Figure 3-5, Plot of fast fading with distance. This is measured data for a short indoor link. (script s0030)	100
Figure 3-6, Two path transmission to demonstrate frequency selective fading. (see text)	101
Figure 3-7, Frequency selective fading for a short indoor link. (script s0028)	102
Figure 3-8, Short term fading, showing fading dependence on distance and frequency. (script s0030)	103
Figure 3-9, Plan of measurement locations for frequency space fading measurements.....	105
Figure 3-10, Set up of equipment for frequency space fading measurements.....	105
Figure 3-11, Experimental set up for measuring the radio channel response as a function of distance.....	106
Figure 3-12, Measured frequency space measurement for a 14.9 m non-LOS indoor link. (script s0030)	107
Figure 3-13, Path loss of the measurements taken. (script s0030)	108
Figure 3-14, Fading probability distribution for each of the measurement locations. (script s0030)	109
Figure 3-15, Experimental set up. The Network Analyser was used to measure the amplitude and phase of the channel. The Digital Oscilloscope was used to capture the results for further processing.	112
Figure 3-16, Photo of the room where the propagation measurements were taken.....	113
Figure 3-17, Plan view of the test room, showing the layout of the benches, and the position of the transmitter and receiver. Note: All lengths are in metres.....	113
Figure 3-18, Movement of the person in the test room during the measurement period	114
Figure 3-19, Radio channel response variation due to a person walking toward the transmitter. (At 940 MHz) (script s0028)	116
Figure 3-20, Fading causes by a person pretending to type on a keyboard 15 cm from the transmitter antenna. (script s0028)	118
Figure 3-21, Movement of the person relative to the transmitter and receiver.....	120
Figure 3-22, Fading caused by a person walking in the same room as the transmitter and receiver. (script s0028).....	121
Figure 4-1, Peer-to-peer network. Users communicate directly to each other, with no centralised control.....	123

Figure 4-2, Base Station connected system. All data passes through the base station.....	124
Figure 4-3, Forward Link in a single cell system.....	125
Figure 4-4, Reverse link of an OFDM system using a single cell network and FDM for user allocation.....	126
Figure 4-5, Adaptive Modulation. The modulation scheme is set based on the SNR of the channel.....	129
Figure 4-6, Algorithm for estimating the signal plus noise, to noise ratio ((S+N)/N) for a subcarrier. This approximates the SNR when the noise is significantly smaller than the signal power.....	131
Figure 4-7, Signal to Noise Ratio of wide band radio channel used for single user adaptive modulation simulation. (script s0059)	134
Figure 4-8, Modulation scheme allocated to each subcarrier. (script s0059)	135
Figure 4-9, Location of the bit errors for the adaptive modulation simulation. (script s0059)	136
Figure 4-10, Location of bit errors for fixed modulation of QPSK, for the same channel as used for the adaptive modulation simulation (script s0059).....	137
Figure 4-11, Frequency allocations for the fixed frequency group of subcarriers simulation. (script s0059)	141
Figure 4-12, Simulated performance from allocating a fixed frequency group of subcarriers to each user. (script s0059)	142
Figure 4-13, Frequency allocations for each user with random frequency hopping. (script s0059)	144
Figure 4-14, Simulated performance for randomly hopped groups of subcarriers. (script s0059)	145
Figure 4-15, Frequency allocations for each user with TDMA. (script s0059)	147
Figure 4-16, Simulated performance for TDMA allocation. (script s0059)	148
Figure 4-17, Frequency allocations for each user with a comb frequency pattern. (script s0059)	149
Figure 4-18, System performance when using adaptive modulation and comb frequency allocation. (script s0059)	150
Figure 4-19, Simulated adaptive user allocation, utilising adaptive bandwidth, adaptive frequency, and adaptive modulation. (script s0059)	156

Figure 4-20, Continuation of results from Figure 4-19	157
Figure 4-21, BER as a function of the distance between tracking points for a multiuser system using adaptive modulation and adaptive user allocation. (script s0061)	160
Figure 4-22, Calculated BER for adaptive modulation. (script s0065)	163
Figure 4-23, BER as a function of the delay between channel measurement and adaptive modulation allocation (script s0085)	164
Figure 4-24, Location of the bit errors in a single user adaptive modulation scheme at a SNR of 42 dB. Channel measurement Figure A - 12 was used for this simulation. (script s0059)	164
Figure 5-1, Methods for obtaining spatial diversity.....	166
Figure 5-2, Pictorial demonstration showing the difference in shadowing when using a single transmitter (a), and 4 transmitters (b).....	167
Figure 5-3, Increase in the multipath delay spread as a result of using Access Point Repeaters.....	170
Figure 5-4, Possible implementation of an Access Point Repeater.....	173
Figure 5-5, Path loss measurement locations in the ECE building for APR testing.....	175
Figure 5-6, Photo of the mobile receiver trolley, showing the rotating antenna on top, spectrum analyser in the middle, and the battery for powering the pre-amp.....	176
Figure 5-7, Transmitter set up simulating Access Point Repeaters. The total transmitter power from Tx2a and Tx2b were matched to the Tx1 power.....	176
Figure 5-8, The receiver antenna was swept over a circle to average out effect of fading.....	177
Figure 5-9, Measured path loss with one transmitter over the area of the ECE building at 990 MHz. (script s0011)	177
Figure 5-10, Measured path loss for two transmitters over the area of the ECE building at 990 MHz. (script s0011)	178
Figure 5-11, Probability of path loss over the measured area of the building. (script s0011)	179
Figure 5-12, Attenuation calculations for a ray passing through two objects.....	180

Figure 5-13, Diagram showing the method for find the intercepts between a ray and an object.....	182
Figure 5-14, Polar to rectangular conversion used for plotting of simulated path loss.....	182
Figure 5-15, Example of spatial aliasing due to finite number of rays used.....	183
Figure 5-16, Cumulative Distribution Function of the path loss within the measured and simulated building. (script s0011)	184
Figure 5-17, Simulated path loss for one transmitter at 990 MHz. (script s0011)	185
Figure 5-18, Simulated path loss for two transmitters at 990 MHz. (script s0011)	186
Figure 5-19, Simulated path loss for four transmitters for 990 MHz. (script s0011)	186
Figure 5-20, Simulated path loss for 8 transmitters for 990 MHz. (script s0011)	187
Figure 5-21, Cumulative Probability Distribution for simulated results, showing the result for 1, 2, 4 and 8 transmitters. (script s0011)	187
Figure 5-22, Received signal power for interferer and wanted signal. (script s0010)	191
Figure 5-23, Average spectral efficiency over the area of the top building, as a function of the movement of the interferer. (script s0009)	192
Figure 5-24, Quality of service provided in the top building in the simulation. (script s0009)	192
Figure 6-1, The magnitude of the complex base band DMT signal (shown in red) represents the envelope. (script s0001)	195
Figure 6-2, Envelope for 26 tone DMT symbol for different phasing schemes. (script s0005)	197
Figure 6-3, Crest Factor probability distribution function (split into 40 bins) for simulated random phase DMT signals, with 8, 32 and 128 tones (script s0032)	198
Figure 6-4, CF distribution of phase modulated OFDM signals verses the number of tones. (script s0032)	199
Figure 6-5, Accurate measurement of CF requires accurate measurement of the peaks in the waveform, which can be found using interpolation. (script s0004)	200
Figure 6-6, Worst case peak estimation sampling.	200
Figure 6-7, Maximum error in CF measurements as a function of over sampling of the DMT signals. (script s0002).....	203

Figure 68, Crest Factor of a multitone signal when using Shapiro-Rudin's phasing scheme. (script s0067)	205
Figure 69, Time envelope and spectrogram for DMT based Shapiro-Rudin's phasing scheme. (script s0055)	206
Figure 6-10, Crest Factor for Newmann's Phasing scheme. (script s0067)	207
Figure 6-11, Time envelope and spectrogram for DMT based on Newmann's quadratic phasing scheme. (script s0055)	207
Figure 6-12, Crest Factor as a function of the number of tones for S. Narahashi and T. Nojima phasing scheme [106] (script s0067)	208
Figure 6-13, Time envelope and spectrogram for DMT based on S. Narahashi and T. Nojima's quadratic phasing scheme. (script s0055)	209
Figure 6-14, Crest Factor for the steepest descent optimised phasing scheme proposed in [107]. (script s0034)	209
Figure 6-15, Genetic Algorithm used to minimise the CF of the DMT waveforms.....	213
Figure 6-16, Best crest factor found using GA verses the number of tones in the signal. (script s0020)	214
Figure 6-17, Power distribution of the time waveform for DMT signals generated using a range of phasing schemes. (script s0055)	214
Figure 6-18, Crest factor distribution as a function of the simulated generations. (script s0021)	215
Figure 6-19, Effect of population size for genetic algorithm optimisation of CF, for 26 tone signal. (script s0021).....	216
Figure 6-20, Effect of percentage population used to breed the next generation for genetic algorithm optimisation of CF. (population = 100). (script s0021)	217
Figure 6-21, Effect of changing the amplitude of the mutation noise for genetic algorithm optimisation of CF. (script s0021)	217
Figure 6-22, Effect of initial phase sequence used for genetic algorithm optimisation of the CF. (script s0021)	218
Figure 6-23, (a) Crest factor and (b) time spectral flatness as a function of the phase equation coefficient A . (script s0056)	222
Figure 6-24, Fitness of the phase scheme for null symbol time synchronisation as a function of the phase gain coefficient A . (script s0056)	223

Figure 625, Crest Factor and Time spectral flatness as a function of the number of tones. (script s0056)	224
Figure 626, Time waveform and spectrogram of a 224 tone OFDM signal using the time spectral flatness optimised phasing scheme. (script s0055)	224
Figure 6-27, Experimental set up for investigating the performance of the time synchronisation method.....	225
Figure 6-28, Measured time synchronisation accuracy for different reference symbols.	227
Figure 7-1, CF verses number of edge grouped PRCs (8 BPSK data subcarriers).....	230
Figure 7-2, Maximum CF verses number of data subcarriers and edge grouped PRCs, where M is the number of PRCs.....	231
Figure 7-3, Net CF improvement verses number of edge grouped PRCs. (10 BPSK data subcarriers).....	232
Figure 7-4, PRC position combinations	232
Figure 7-5, CF verses position of 2 grouped PRCs (10 BPSK data subcarriers)	233
Figure 7-6, CF verses position of 4 grouped PRCs (10 BPSK data subcarriers)	233
Figure 7-7, CF verses the number of spread PRCs (10 BPSK data subcarriers).....	235
Figure 7-8, Net improvement in CF, position optimised PRCs (10 BPSK data subcarriers).....	236

GLOSSARY

2G	Second Generation mobile phone system (GSM, IS-95)
3G	Third Generation mobile phone system (systems using WCDMA)
4G	Fourth Generation mobile phone system
AC	Alternating Current (Frequency above 0 Hz)
ADSL	Asymmetric Digital Subscriber Line
alpha	Path loss exponent (rate of path loss change with distance)
AM	Amplitude Modulation
APR	Access Point Repeater
ASK	Amplitude Shift Keying
AWGN	Additive White Gaussian Noise
b/s/Hz	Bits per second per hertz (unit of spectral efficiency)
BER	Bit Error Rate
bps	Bits per second
BPSK	Binary Phase Shift Keying
BS	Base Station
CD	Compact Disc
CDMA	Code Division Multiple Access
CF	Crest Factor (peak to average power ratio of the RF envelope)
DAB	Digital Audio Broadcasting
dB	Decibel (ratio in log scale)
dBc	Decibel relative to main signal power
dBm	Decibel relative to 1 milliwatt
DC	Direct Current (0 Hz)
DDS	Direct Digital Synthesiser
DFT	Discrete Fourier Transform

DMT	Discrete Multi-Tone
DPSK	Differential Phase Shift Keying
DSBSC	Double Side Band Suppressed Carrier
DS-CDMA	Direct Sequence Code Division Multiple Access
DSP	Digital Signal Processing
DSSS	Direct Sequence Spread Spectrum
DVB	Digital Video Broadcasting
DVB-C	Digital Video Broadcasting – Cable
DVB-S	Digital Video Broadcasting – Satellite
DVB-T	Digital Video Broadcasting - Terrestrial
EBNR	Energy per Bit to Noise Ratio
FDM	Frequency Division Multiplexing
FEC	Forward Error Correction
FFT	Fast Fourier Transform
FIR	Finite Impulse Response (digital filter)
FM	Frequency Modulation
Fs	Sample Frequency
FSK	Frequency Shift Keying
GA	Genetic Algorithm
GHz	Gigahertz - 10^9 Hz
GMSK	Gaussian Minimum Shift Keying
GSM	Global System for Mobile communications
HDTV	High Definition Television
HiperLAN2	HIgh PErfomance Radio Local Area Network, WLAN standard (Europe) based on OFDM, with a maximum data rate of 54 Mbps. Similar to IEEE802.11a
Hz	Hertz (cycles per second)
ICI	Inter-Carrier Interference
IEEE802.11a	WLAN standard (U.S.) based on OFDM, with a maximum data rate of 54 Mbps. Similar to HiperLAN2

IEEE802.11b WLAN standard (U.S.) based on DSSS, with a maximum data rate of 11 Mbps

IF	Intermediate Frequency
IFFT	Inverse Fast Fourier Transform
IMD	Inter-Modulation Distortion
IQ	Inphase Quadrature
ISI	Inter-Symbol Interference
ISM	Industrial Scientific Medical
IS-95	Mobile phone standard using CDMA transmission method.
JCU	James Cook University
K	Kelvin
kbps	Kilo bits per second (10^3 bps)
kHz	Kilohertz - 10^3 Hz
km	Kilometer (10^3 m)
l	Lambda - RF wavelength
LO	Local Oscillator
LOS	Line Of Sight
m	Metre
Mbps	Mega bits per second (10^6 bps)
MHz	Megahertz - 10^6 Hz
MPEG	Moving Picture Experts Group (Video compression standard)
NF	Receiver Noise Figure
OBO	Output power BackOff
OFDM	Orthogonal Frequency Division Multiplexing
PAPR	Peak to Average Power Ratio
PC	Personal Computer
PDA	Personal Digital Assistant
π	Pi (3.14159265)
PLL	Phase Locked Loop
PM	Phase Modulation
PRC	Peak Reduction Carriers

PRS	Pseudo Random Sequence
PSK	Phase Shift Keying
QAM	Quadrature Amplitude Modulation
QOS	Quality Of Service
QPSK	Quadrature Phase Shift Keying
RAKE	Multiple tap multipath equalisation for CDMA
RC	Raised Cosine (Guard Period)
RF	Radio Frequency
RMS	Root Mean Squared
SFN	Single Frequency Network
SHARC	Super Harvard ARChitecture, Digital Signal Processor by Analog Devices)
SIR	Signal to Interference Ratio
SNR	Signal to Noise Ratio
SSB	Single Side Band
SSPA	Solid State Power Amplifier
TDM	Time Division Multiplexing
TDMA	Time Division Multiple Access
TWTA	Travelling Wave Tube Amplifier
mm	Micrometre (10^{-6} m)
UMTS	Universal Mobile Telecommunications System
ms	Microsecond (10^{-6} s)
VSB	Vestigal Side Band
W	Watt (energy per unit time, one joule per second)
W-CDMA	Wide-band Code Division Multiple Access
WLAN	Wireless Local Area Network
WLL	Wireless Local Loop

SIMULATION FILES

Each of the simulation plots shown in this thesis were produced using a Matlab simulation script. Each of these simulation files was assigned a unique script number. The start of the script file name is shown on each of the plots, for example: *script s0059* corresponds to a complete filename of s0059_aofdm.m. The simulation files for this thesis are included in electronic format on CD. This CD is available from the Department of Electrical and Computer Engineering at James Cook University, Australia. The script corresponding to each plot can be found by using a file search tool.

Most of the simulation files generate several plots from a single simulation; see the comments in each simulation file for more details. Where possible the simulation scripts were written to produce the plots shown in this thesis. There are however several scripts that were modified to produce a series of figures. The settings in these scripts must be set to the required application to produce the required plot.

CHAPTER 1 INTRODUCTION

Wireless communications is an emerging field, which has seen enormous growth in the last several years. The huge uptake rate of mobile phone technology, Wireless Local Area Networks (WLAN) and the exponential growth of the Internet have resulted in an increased demand for new methods of obtaining high capacity wireless networks.

Most WLAN systems currently use the IEEE802.11b standard, which provides a maximum data rate of 11 Mbps [96]. Newer WLAN standards such as IEEE802.11a [100] and HiperLAN2 [98], [99] are based on OFDM technology and provide a much higher data rate of 54 Mbps. However systems of the near future will require WLANs with data rates of greater than 100 Mbps, and so there is a need to further improve the spectral efficiency and data capacity of OFDM systems in WLAN applications.

For cellular mobile applications, we will see in the near future a complete convergence of mobile phone technology, computing, Internet access, and potentially many multimedia applications such as video and high quality audio. In fact, some may argue that this convergence has already largely occurred, with the advent of being able to send and receive data using a notebook computer and a mobile phone. Although this is possible with current 2G (2nd Generation) Mobile phones, the data rates provided are very low (9.6 kbps – 14.4 kbps) and the cost is high (typically \$0.20 - \$1.30 AUD per minute) [24], [25], limiting the usefulness of such a service.

The goal of third and fourth generation mobile networks is to provide users with a high data rate, and to provide a wider range of services, such as voice communications, videophones, and high speed Internet access. The higher data rate of future mobile networks will be achieved by increasing the amount of spectrum

allocated to the service and by improvements in the spectral efficiency. OFDM is a potential candidate for the physical layer of fourth generation mobile systems. This thesis presents techniques for improving the spectral efficiency of OFDM systems applied in WLAN and mobile networks.

1.1 THIRD GENERATION WIRELESS SYSTEMS

Third generation mobile systems such as the Universal Mobile Telecommunications System (UMTS) [1], [2], [3], [4] and CDMA2000 [6] will be introduced over the next 1-5 years (2002 onwards) [5]. These systems are striving to provide higher data rates than current 2G systems such as the Global System for Mobile communications (GSM) [22], [23] and IS-95. Second generation systems are mainly targeted at providing voice services, while 3rd generation systems will shift to more data oriented services such as Internet access.

Third generation systems use Wide-band Code Division Multiple Access (W-CDMA) as the carrier modulation scheme [10]. This modulation scheme has a high multipath tolerance, flexible data rate, and allows a greater cellular spectral efficiency than 2G systems. Third generation systems will provide a significantly higher data rate (64 kbps – 2 Mbps) [1] than second-generation systems (9.6 – 14.4 kbps). The higher data rate of 3G systems will be able to support a wide range of applications including Internet access, voice communications and mobile videophones. In addition to this, a large number of new applications will emerge to utilise the permanent network connectivity, such as wireless appliances, notebooks with built in mobile phones, remote logging, wireless web cameras, car navigation systems, and so forth. In fact most of these applications will not be limited by the data rate provided by 3G systems, but by the cost of the service.

The demand for use of the radio spectrum is very high, with terrestrial mobile phone systems being just one of many applications vying for suitable bandwidth. These applications require the system to operate reliably in non-line-of-sight environments with a propagation distance of 0.5 - 30 km, and at velocities up to 100 km/hr or higher. This operating environment limits the maximum RF frequency to 5 GHz, as operating above this frequency results in excessive channel path loss, and excessive

Doppler spread at high velocity. This limits the spectrum available for mobile applications, making the value of the radio spectrum extremely high.

In Europe auctions of 3G licenses of the radio spectrum began in 1999. In the United Kingdom, 90 MHz of bandwidth [8] was auctioned off for £22.5 billion [9]. In Germany the result was similar, with 100 MHz of bandwidth raising \$46 billion (US) [7]. This represents a value of around \$450 Million (US) per MHz. The length of these license agreements is 20 years [8] and so to obtain a reasonable rate of return of 8% on investment, \$105 Million (US) per MHz must be raised per year. It is therefore vitally important that the spectral efficiency of the communication system is maximised, as this is one of the main limitations to providing a low cost high data rate service.

1.2 4TH GENERATION SYSTEMS AND BEYOND

Research has just recently begun on the development of 4th generation (4G) mobile communication systems. The commercial rollout of these systems is likely to begin around 2008 - 2012, and will replace 3^d generation technology. Few of the aims of 4G networks have yet been published, however it is likely that they will be to extend the capabilities of 3G networks, allowing a greater range of applications, and improved universal access. Ultimately 4G networks should encompass broadband wireless services, such as High Definition Television (HDTV) (4 - 20 Mbps) and computer network applications (1 - 100 Mbps). This will allow 4G networks to replace many of the functions of WLAN systems. However, to cover this application, cost of service must be reduced significantly from 3G networks. The spectral efficiency of 3G networks is too low to support high data rate services at low cost. As a consequence one of the main focuses of 4G systems will be to significantly improve the spectral efficiency.

In addition to high data rates, future systems must support a higher Quality Of Service (QOS) than current cellular systems, which are designed to achieve 90 - 95% coverage [11], i.e. network connection can be obtained over 90 - 95% of the area of the cell. This will become inadequate as more systems become dependent on wireless networking. As a result 4G systems are likely to require a QOS closer to 98 - 99.5%.

In order to achieve this level of QOS it will require the communication system to be more flexible and adaptive. In many applications it is more important to maintain network connectivity than the actual data rate achieved. If the transmission path is very poor, e.g. in a building basement, then the data rate has to drop to maintain the link. Thus the data rate might vary from as low as 1 kbps in extreme conditions, to as high as 20 Mbps for a good transmission path. Alternatively, for applications requiring a fixed data rate, the QOS can be improved by allocating additional resources to users with a poor transmission path.

A significant improvement in spectral efficiency will be required in order for 4G systems to provide true broadband access. This will only be achieved by significant advances in multiple aspects of cellular network systems, such as network structure, network management, smart antennas, RF modulation, user allocation, and general resource allocation. This thesis will focus on several aspects, primarily RF modulation, user allocation and network structure.

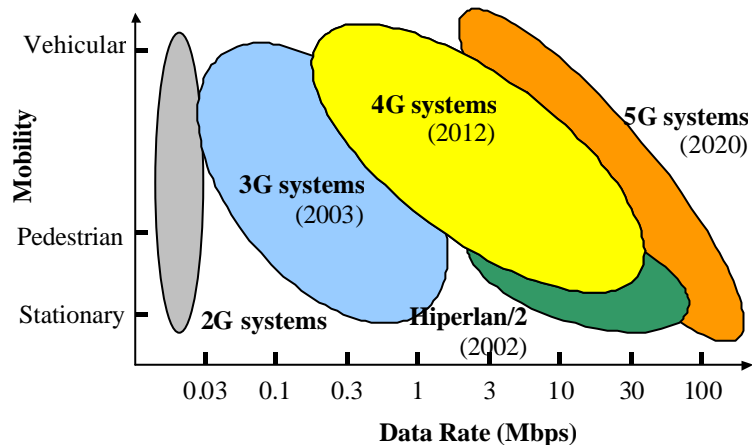


Figure 1-1, Current and future mobile systems. The general trend will be to provide higher data rates and greater mobility. Derived from [12] and [13].

1.3 ORTHOGONAL FREQUENCY DIVISION MULTIPLEXING

Orthogonal Frequency Division Multiplexing (OFDM) is an alternative wireless modulation technology to CDMA. OFDM has the potential to surpass the capacity of CDMA systems and provide the wireless access method for 4G systems.

OFDM is a modulation scheme that allows digital data to be efficiently and reliably transmitted over a radio channel, even in multipath environments. OFDM transmits data by using a large number of narrow bandwidth carriers. These carriers are regularly spaced in frequency, forming a block of spectrum. The frequency spacing and time synchronisation of the carriers is chosen in such a way that the carriers are orthogonal, meaning that they do not cause interference to each other. This is despite the carriers overlapping each other in the frequency domain. The name ‘OFDM’ is derived from the fact that the digital data is sent using many carriers, each of a different frequency (Frequency Division Multiplexing) and these carriers are orthogonal to each other, hence Orthogonal Frequency Division Multiplexing.

The origins of OFDM development started in the late 1950’s [30] with the introduction of Frequency Division Multiplexing (FDM) for data communications. In 1966 Chang patented the structure of OFDM [32] and published [31] the concept of using orthogonal overlapping multi-tone signals for data communications. In 1971 Weinstein [33] introduced the idea of using a Discrete Fourier Transform (DFT) for implementation of the generation and reception of OFDM signals, eliminating the requirement for banks of analog subcarrier oscillators. This presented an opportunity for an easy implementation of OFDM, especially with the use of Fast Fourier Transforms (FFT), which are an efficient implementation of the DFT. This suggested that the easiest implementation of OFDM is with the use of Digital Signal Processing (DSP), which can implement FFT algorithms. It is only recently that the advances in integrated circuit technology have made the implementation of OFDM cost effective. The reliance on DSP prevented the wide spread use of OFDM during the early development of OFDM. It wasn’t until the late 1980’s that work began on the development of OFDM for commercial use, with the introduction of the Digital Audio Broadcasting (DAB) system.

1.3.1 DIGITAL AUDIO BROADCASTING

DAB was the first commercial use of OFDM technology [19], [20]. Development of DAB started in 1987 and services began in U.K and Sweden in 1995. DAB is a replacement for FM audio broadcasting, by providing high quality digital audio and information services. OFDM was used for DAB due to its multipath tolerance.

Broadcast systems operate with potentially very long transmission distances (20 - 100 km). As a result, multipath is a major problem as it causes extensive ghosting of the transmission. This ghosting causes Inter-Symbol Interference (ISI), blurring the time domain signal.

For single carrier transmissions the effects of ISI are normally mitigated using adaptive equalisation. This process uses adaptive filtering to approximate the impulse response of the radio channel. An inverse channel response filter is then used to recombine the blurred copies of the symbol bits. This process is however complex and slow due to the locking time of the adaptive equaliser. Additionally it becomes increasing difficult to equalise signals that suffer ISI of more than a couple of symbol periods.

OFDM overcomes the effects of multipath by breaking the signal into many narrow bandwidth carriers. This results in a low symbol rate reducing the amount of ISI. In addition to this, a guard period is added to the start of each symbol, removing the effects of ISI for multipath signals delayed less than the guard period (see section 2.3 for more detail). The high tolerance to multipath makes OFDM more suited to high data transmissions in terrestrial environments than single carrier transmissions.

Parameter	Transmission Mode			
	I	II	III	IV
Bandwidth	1.536 MHz	1.536 MHz	1.536 MHz	1.536 MHz
Modulation	DQPSK	DQPSK	DQPSK	DQPSK
Frequency Range (Mobile reception)	≤ 375 MHz	≤ 1.5 GHz	≤ 3 GHz	≤ 1.5 GHz
Number of subcarriers	1536	384	192	768
Symbol Duration	1000 μ s	250 μ s	125 μ s	500 μ s
Guard Duration	246 μ s	62 μ s	31 μ s	123 μ s
Total Symbol Duration	1246 μ s	312 μ s	156 μ s	623 μ s
Maximum Transmitter Separation for SFN	96 km	24 km	12 km	48 km

Table 1-1, DAB Transmission parameters for each transmission mode [20]

Table 1-1 shows the system parameters for DAB. DAB has four transmission modes. The transmission frequency, receiver velocity and required multipath tolerance all determine the most suitable transmission mode to use.

Doppler spread is caused by rapid changes in the channel response due to movement of the receiver through a multipath environment. It results in random frequency

modulation of the OFDM subcarriers, leading to signal degradation. The amount of Doppler spread is proportional to the transmission frequency and the velocity of movement. The closer the subcarriers are spaced together, the more susceptible the OFDM signal is to Doppler spread, and so the different transmission modes in DAB allow trade off between the amount of multipath protection (length of the guard period) and the Doppler spread tolerance.

The high multipath tolerance of OFDM allows the use of a Single Frequency Network (SFN), which uses transmission repeaters to provide improved coverage, and spectral efficiency. For traditional FM broadcasting, neighbouring cities must use different RF frequencies even for the same radio station, to prevent multipath causes by rebroadcasting at the same frequency. However, with DAB it is possible for the same signal to be broadcast from every area requiring coverage, eliminating the need for different frequencies to be used in neighbouring areas.

The data throughput of DAB varies from 0.6 - 1.8 Mbps depending on the amount of Forward Error Correction (FEC) applied. This data payload allows multiple channels to be broadcast as part of the one transmission ensemble. The number of audio channels is variable depending on the quality of the audio and the amount of FEC used to protect the signal. For telephone quality audio (24 kbps) up to 64 audio channels can be provided, while for CD quality audio (256 kb/s), with maximum protection, three channels are available.

More information on DAB can be found in [20] and [21].

1.3.2 DIGITAL VIDEO BROADCASTING

The development of the Digital Video Broadcasting (DVB) standards was started in 1993 [14]. DVB is a transmission scheme based on the MPEG-2 standard, as a method for point to multipoint delivery of high quality compressed digital audio and video. It is an enhanced replacement of the analogue television broadcast standard, as DVB provides a flexible transmission medium for delivery of video, audio and data services [17]. The DVB standards specify the delivery mechanism for a wide range of applications, including satellite TV (DVB-S), cable systems (DVB-C) and terrestrial transmissions (DVB-T) [15]. The physical layer of each of these standards

is optimised for the transmission channel being used. Satellite broadcasts use a single carrier transmission, with QPSK modulation, which is optimised for this application as a single carrier allows for large Doppler shifts, and QPSK allows for maximum energy efficiency [16]. This transmission method is however unsuitable for terrestrial transmissions as multipath severely degrades the performance of high-speed single carrier transmissions. For this reason, OFDM was used for the terrestrial transmission standard for DVB. The physical layer of the DVB-T transmission is similar to DAB, in that the OFDM transmission uses a large number of subcarriers to mitigate the effects of multipath. DVB-T allows for two transmission modes depending on the number of subcarriers used [18]. Table 1-2 shows the basic transmission parameters for these two modes. The major difference between DAB and DVB-T is the larger bandwidth used and the use of higher modulation schemes to achieve a higher data throughput. The DVB-T allows for three subcarrier modulation schemes: QPSK, 16-QAM (Quadrature Amplitude Modulation) and 64-QAM; and a range of guard period lengths and coding rates. This allows the robustness of the transmission link to be traded at the expense of link capacity. Table 1-3 shows the data throughput and required SNR for some of the transmission combinations.

DVB-T is a uni-directional link due to its broadcast nature. Thus any choice in data rate versus robustness affects all receivers. If the system goal is to achieve high reliability, the data rate must be lowered to meet the conditions of the worst receiver. This effect limits the usefulness of the flexible nature of the standard. However if these same principles of a flexible transmission rate are used in bi-directional communications, the data rate can be maximised based on the current radio conditions. Additionally for multiuser applications, it can be optimised for individual remote transceivers.

Parameter	2k Mode	8k Mode
Number subcarriers	1705	6817
Useful Symbol Duration (T_u)	896 μ s	224 μ s
Carrier Spacing (1/ T_u)	1116 Hz	4464 Hz
Bandwidth	7.61 MHz	7.61 MHz

Table 1-2, DVB transmission parameters [18].

Subcarrier Modulation	Code Rate	SNR for BER = $2^{-10^{-4}}$ after Viterbi (dB)		Bit rate (Mbps)	
		Gaussian Channel	Rayleigh Channel	Guard Period (Fraction of Useful symbol duration)	1/4
					1/32
QPSK	$\frac{1}{2}$	3.1	5.4	4.98	6.03
QPSK	$\frac{7}{8}$	7.7	16.3	8.71	10.56
16-QAM	$\frac{1}{2}$	8.8	11.2	9.95	12.06
16-QAM	$\frac{7}{8}$	13.9	22.8	17.42	21.11
64-QAM	$\frac{1}{2}$	14.4	16.0	14.93	18.10
64-QAM	$\frac{7}{8}$	20.1	27.9	26.13	31.67

Table 1-3, SNR required and net bit rate for a selection of the coding and modulation combinations for DVB

Note: Code rate can be any of the following values: 1/2, 2/3, 3/4, 5/6, 7/8. The Guard Period duration can be any following values: 1/4, 1/8, 1/16, 1/32. Derived from [18].

1.3.3 MULTIUSER OFDM

DAB and DVB systems are only uni-directional from the base station to the users. Not much work has been done on using OFDM for two-way communications or for multiuser applications. These applications include wireless modems, Wireless Local Area Networks (WLAN's), Wireless Local Loop (WLL), mobile phones, and mobile high speed internet. This thesis aims to look at applying OFDM to such applications, and to look at the resulting advantages and problems. This thesis also presents some new techniques that can be used to improve broadcast and multiuser OFDM systems. This thesis presents the performance of adaptive modulation and adaptive user allocation schemes in a multiuser OFDM system. These techniques improve the spectral efficiency and QOS.

Fattouche [81] patented a method for implementing a wireless multiuser OFDM system in 1992, predating any published research in this field. This system used half duplex Time Division Multiplexing (TDM) to allow multiuser access, with the base stations and portable units taking turns to transmit. Carrier modulation was fixed and used D8-PSK (Differential 8 Phase Shift Keying). The system was bandwidth limited by using a raised cosine guard period. Fattouche is the founder WiLan Inc., which is one of the few companies currently producing multiuser OFDM modems.

Williams and Prodan [82], patented the use of multiuser OFDM in cable applications in 1995. This introduced the use of a hybrid user allocation, using Frequency

Division Multiplexing (FDM) and TDM. In this system the users were allocated time and frequency slots depending on the data demand. This patent however, fails to address problem of obtaining and maintaining accurate time and frequency synchronisation between users, which is critical for maintaining orthogonality between users.

Cimini, Chuang, Sollenberger [83] outlined an Advanced Cellular Internet Service using multiuser OFDM. The aim of this system was to provide Internet access at a data rate of 1 – 2 Mbps. This system uses time synchronised base stations, which are allocated time slots in a self-organising fashion. These base station time slots are then broken down in to time slots for users. In addition to TDM, users are allocated subcarriers dynamically based on the channel Signal to Interference Ratio (SIR), to allow minimisation of inter-cellular interference.

Wahlqvist [84] described one possible implementation of multiuser OFDM in a wireless environment, outlining a user allocation scheme where users were allocated small blocks of time and frequency. In this scheme, each transmission block consists of a small group of subcarriers, (5 - 10) and a small number of symbols, about 11 in length. The aim of this structure is to allocate time and frequency slots to utilise the high correlation between neighbouring subcarriers, and the small channel variation between a small group of symbols. This allows the block to be characterised with a simple pilot tone structure.

1.3.4 HIPERLAN2 AND IEEE802.11A

Development of the European Hiperlan standard was started in 1995, with the final standard of HiperLAN2 being defined in June 1999. HiperLAN2 pushes the performance of WLAN systems, allowing a data rate of up to 54 Mbps [97]. HiperLAN2 uses 48 data and 4 pilot subcarriers in a 16 MHz channel, with 2 MHz on either side of the signal to allow out of band roll off. User allocation is achieved by using TDM, and subcarriers are allocated using a range of modulation schemes, from BPSK up to 64-QAM, depending on the link quality. Forward Error Correction is used to compensate for frequency selective fading.

IEEE802.11a has the same physical layer as HiperLAN2 with the main difference

between the standard corresponding to the higher-level network protocols used.

HiperLAN2 is used extensively as an example OFDM system in this thesis. Since the physical layer of HiperLAN2 is very similar to the IEEE802.11a standard these examples are applicable to both standards.

Standard	802.11b	802.11a	HiperLAN2
Spectrum	2.4 GHz	5.2 GHz	5.2 GHz
Modulation Technique	DSSS	OFDM	OFDM
~ Max physical rate	11 Mbps	54 Mbps	54 Mbps
~ Max data rate, layer 3	5 Mbps	32 Mbps	32 Mbps
Medium access control	CSMA/CA		TDMA/TDD
Connectivity	Conn. less	Conn. less	Conn. orientated

Table 1-4, Summary of characteristics of IEEE802.11b, IEEE802.11a and HiperLAN2. Derived from [97]

Parameter	Value
Channel Spacing	20 MHz
IFFT used for 20 MSPS	64
Data Subcarriers	48
Pilot Subcarriers	4
Carrier Spacing (F_c)	312.5 kHz (=20 MHz/64)
Nominal Bandwidth	16.25 MHz (=312.5 kHz × 52)
Useful Symbol Period	3.2 μ sec (=1/ F_c)
Guard Period	0.8 μ sec
Modulation Schemes	BPSK, QPSK, 16-QAM, 64-QAM
Coding Rate	1/2, 2/3, 3/4

Table 1-5, Physical Layer for HiperLAN2 and IEEE802.11a. Derived from [99]

1.4 THESIS OUTLINE AND CONTRIBUTIONS TO THE FIELD

1.4.1 CHAPTER 2 BASIC PRINCIPLES OF OFDM

Chapter 2 provides an introduction to OFDM in general and outlines some of the problems associated with it. This chapter describes what OFDM is, and how it can be generated and received. It also looks at why OFDM is a robust modulation scheme and some of its advantages over single carrier modulation schemes. Detrimental effects such as noise, band pass filtering, distortion, time synchronisation error and frequency synchronisation error are described. In addition to this, an investigation into the effectiveness of using raised cosine guard periods for side-lobe suppression

is presented. This chapter establishes the performance of OFDM over a wide range of modulation schemes from BPSK through to 4096-QAM and over a range of detrimental effects. This work forms the foundation for the development of adaptive modulation schemes that are presented in Chapter 4.

1.4.2 CHAPTER 3 RADIO PROPAGATION

This chapter presents an introduction to radio propagation effects such as path loss, frequency selective fading, Doppler spread and multipath delay spread. The performance of any wireless communication systems is highly dependent on the propagation channel, and so a detailed knowledge of radio propagation is important for optimisation of wireless communications. Chapter 4 presents a method for exploiting the effects of multipath propagation in multiuser OFDM applications in order to improve the spectral efficiency of the system and so an understanding of radio propagation characteristics is needed before different forms of multiuser OFDM can be discussed. This chapter provides a review of well-known propagation effects and extends these to look at the effects on wide bandwidth transmissions.

Most radio fading models in literature are based on statistical results, making them of little use for investigating the performance of the adaptive modulation scheme presented in Chapter 4. The performance of this technique is dependent on the correlation of the frequency selective fading and how fast the fading changes with position of the transceiver. To overcome this problem this chapter includes an experimental investigation of small-scale frequency selective fading of multipath environments, which is a measure of the variation in the multipath fading with small changes in position. This work is used in Chapter 4 to simulate the performance of adaptive modulation.

Also presented is an experiment measuring the rate of change of the radio channel with movement of nearby people. This also looks at the error in tracking the channel under these conditions, giving a guide to how fast adaptive schemes must actively track the radio channel characteristics.

1.4.3 CHAPTER 4 MULTIUSER OFDM

This chapter looks at methods for applying OFDM in multiuser applications. It provides a study into user allocation schemes, and the application of adaptive modulation mobile RF environments.

Adaptive modulation is a method for obtaining a high spectral efficiency in a fading environment. The HiperLAN2 and IEEE802.11a standard use system wide modulation tracking, allowing the modulation of all subcarriers to be changed to match the channel SNR. The modulation used in such systems is based on the average subcarrier SNR, and so the effects of fading still cause large increases in the error rate.

This thesis proposes that the adaptive modulation is applied on a subcarrier by subcarrier basis, as a method for combating the effects of frequency selective fading. Each subcarrier in the OFDM system transmits a different amount of data based on the Signal to Noise Ratio (SNR) for that subcarrier. The channel performance is tracked on a regular basis using the bi-directional nature of the link to ensure that both the transmitter and receiver know what modulation scheme is currently being used on each subcarrier.

This technique has been applied to wire line (telephone cable) OFDM systems such as xDSL (x – Asymmetric or Symmetric, Digital Subscriber Loop) [87]. Such a technique is relatively easy to apply to copper cables, due to the static nature of the channel response. In a mobile environment the frequency response of the radio channel changes as a result of the relative movement of the transmitter, receiver and the surrounding objects. This response changes significantly for movements as small as a fraction of a wavelength, which is typically 10-30 cm. This dynamic nature of the channel makes it difficult to track its response, especially when mobile users are travelling faster than walking speed.

Work has been done studying the use of adaptive modulation in single carrier systems [90] - [93], however not much work has been published on use of adaptive modulation in OFDM systems.

This chapter outlines applying adaptive modulation to OFDM systems in a multiuser mobile environment. Additionally an adaptive frequency allocation scheme is

presented for optimisation of user subcarrier frequency. This chapter investigates the feasibility of such techniques and the possible advantages such as increased capacity, improved quality of service, and a significant reduction in required forward error correction.

1.4.4 CHAPTER 5 ACCESS POINT REPEATERS

OFDM can withstand high levels of multipath delay spread. This property can be exploited to reduce the path loss in WLAN systems. For example the signal from single base station signal can be simultaneously transmitted from multiple locations within a cell. This simple technique reduces shadowing caused by walls and obstructions, improving the coverage of WLAN systems. The signals from the multiple transmitters appear as multipath at the receiver, but can be compensated for by the high multipath tolerance of OFDM. These multiple transmitters are referred to as Access Point Repeaters (APR) because the process is reversible in that the base station transmits and receives from these APRs. This technique is similar to Single Frequency Networks used in DAB [14], and DVB systems [20]. The main difference is this technique is proposed for bi-directional communications and for small-scale systems. Using APRs coupled with adaptive modulation allows WLAN OFDM systems to operate at very high spectral efficiencies while maintaining a high Quality Of Service (QOS), and so this technique provides a significant advance.

1.4.5 CHAPTER 6 GENERATION OF LOW CREST FACTOR MULTI-TONE SIGNALS

OFDM signals require highly linear amplification to prevent Inter-Carrier Interference (ICI) and spectral spreading due to Inter-Modulation Distortion (IMD) [54]. Linear amplifiers have a low energy efficiency making them difficult to use in battery-operated equipment. Additionally OFDM signals have a high Crest Factor (CF) (peak to average power ratio of the envelope of the RF signal) due to the multi-carrier modulation. As a result of the high CF, the output power of the amplifier must be kept low to prevent clipping and distortion.

This chapter describes how the CF of a sampled signal can be measured accurately, and outlines a new phasing technique for generating OFDM pilot reference symbols

with a very low CF.

The new phasing scheme uses genetic algorithms to optimise the phase of the subcarriers to minimise the CF of the waveform. This form of optimisation has never been applied to this application. The result of this process is that symbols with a CF as low as 0.65 dB are possible. This is 0.7 dB lower than any previously known algorithm. The very low CF of the OFDM signals makes them useful for pilot symbols in coherent modulation or for adaptive modulation to allow tracking of the radio channel. Because of their ultra low CF the average power of these symbols can be boosted significantly (~6 dB) while still maintaining a lower peak power than data symbols. This improves the SNR of the channel estimation, reducing the number of pilot symbols needed, and potentially the channel estimation speed.

1.4.6 CHAPTER 7 CREST FACTOR MINIMISATION OF OFDM DATA SYMBOLS

This chapter describes a technique for a better than 5 dB reduction in the CF for data carrying OFDM signals. This improvement is achieved by inserting additional subcarriers into the signal referred to as peak reduction carriers (PRC). These PRC are set in phase and amplitude, using a codebook, to minimise the overall symbol CF. The codebook is obtained using a search of all possible signal combinations. This technique is optimised for signals using a low number of subcarriers, and low modulation schemes such as BPSK and QPSK, due to the brute force searching technique employed.

1.4.7 CHAPTER 8 SUMMARY

A conclusion is provided, which summarises the major results obtained this thesis, and outlines possible future work in this field.

CHAPTER 2 BASIC PRINCLIPES OF OFDM

Orthogonal Frequency Division Multiplexing (OFDM) is very similar to the well-known and used technique of Frequency Division Multiplexing (FDM). OFDM uses the principles of FDM to allow multiple messages to be sent over a single radio channel. It is however in a much more controlled manner, allowing an improved spectral efficiency.

A simple example of FDM is the use of different frequencies for each FM (Frequency Modulation) radio stations. All stations transmit at the same time but do not interfere with each other because they transmit using different carrier frequencies. Additionally they are bandwidth limited and are spaced sufficiently far apart in frequency so that their transmitted signals do not overlap in the frequency domain. At the receiver, each signal is individually received by using a frequency tuneable band pass filter to selectively remove all the signals except for the station of interest. This filtered signal can then be demodulated to recover the original transmitted information.

OFDM is different from FDM in several ways. In conventional broadcasting each radio station transmits on a different frequency, effectively using FDM to maintain a separation between the stations. There is however no coordination or synchronisation between each of these stations. With an OFDM transmission such as DAB, the information signals from multiple stations is combined into a single multiplexed stream of data. This data is then transmitted using an OFDM ensemble that is made up from a dense packing of many subcarriers. All the subcarriers within the OFDM signal are time and frequency synchronised to each other, allowing the interference between subcarriers to be carefully controlled. These multiple subcarriers overlap in the frequency domain, but do not cause Inter-Carrier Interference (ICI) due to the

orthogonal nature of the modulation. Typically with FDM the transmission signals need to have a large frequency guard-band between channels to prevent interference. This lowers the overall spectral efficiency. However with OFDM the orthogonal packing of the subcarriers greatly reduces this guard band, improving the spectral efficiency.

All wireless communication systems use a modulation scheme to map the information signal to a form that can be effectively transmitted over the communications channel. A wide range of modulation schemes has been developed, with the most suitable one, depending on whether the information signal is an analogue waveform or a digital signal. Some of the common analogue modulation schemes include Frequency Modulation (FM), Amplitude Modulation (AM), Phase Modulation (PM), Single Side Band (SSB), Vestigial Side Band (VSB), Double Side Band Suppressed Carrier (DSBSC) [121], [122]. Common single carrier modulation schemes for digital communications include, Amplitude Shift Keying (ASK), Frequency Shift Keying (FSK), Phase Shift Keying (PSK) and Quadrature Amplitude Modulation (QAM) [121] - [123].

Each of the carriers in a FDM transmission can use an analogue or digital modulation scheme. There is no synchronisation between the transmission and so one station could transmit using FM and another in digital using FSK. In a single OFDM transmission all the subcarriers are synchronised to each other, restricting the transmission to digital modulation schemes. OFDM is symbol based, and can be thought of as a large number of low bit rate carriers transmitting in parallel. All these carriers transmit in unison using synchronised time and frequency, forming a single block of spectrum. This is to ensure that the orthogonal nature of the structure is maintained. Since these multiple carriers form a single OFDM transmission, they are commonly referred to as ‘subcarriers’, with the term of ‘carrier’ reserved for describing the RF carrier mixing the signal from base band. There are several ways of looking at what make the subcarriers in an OFDM signal orthogonal and why this prevents interference between them.

2.1.1 ORTHOGONALITY

Signals are orthogonal if they are mutually independent of each other. Orthogonality is a property that allows multiple information signals to be transmitted perfectly over a common channel and detected, without interference. Loss of orthogonality results in blurring between these information signals and degradation in communications. Many common multiplexing schemes are inherently orthogonal. Time Division Multiplexing (TDM) allows transmission of multiple information signals over a single channel by assigning unique time slots to each separate information signal. During each time slot only the signal from a single source is transmitted preventing any interference between the multiple information sources. Because of this TDM is orthogonal in nature. In the frequency domain most FDM systems are orthogonal as each of the separate transmission signals are well spaced out in frequency preventing interference. Although these methods are orthogonal the term OFDM has been reserved for a special form of FDM. The subcarriers in an OFDM signal are spaced as close as is theoretically possible while maintaining orthogonality between them.

OFDM achieves orthogonality in the frequency domain by allocating each of the separate information signals onto different subcarriers. OFDM signals are made up from a sum of sinusoids, with each corresponding to a subcarrier. The baseband frequency of each subcarrier is chosen to be an integer multiple of the inverse of the symbol time, resulting in all subcarriers having an integer number of cycles per symbol. As a consequence the subcarriers are orthogonal to each other. Figure 2-1 shows the construction of an OFDM signal with four subcarriers.

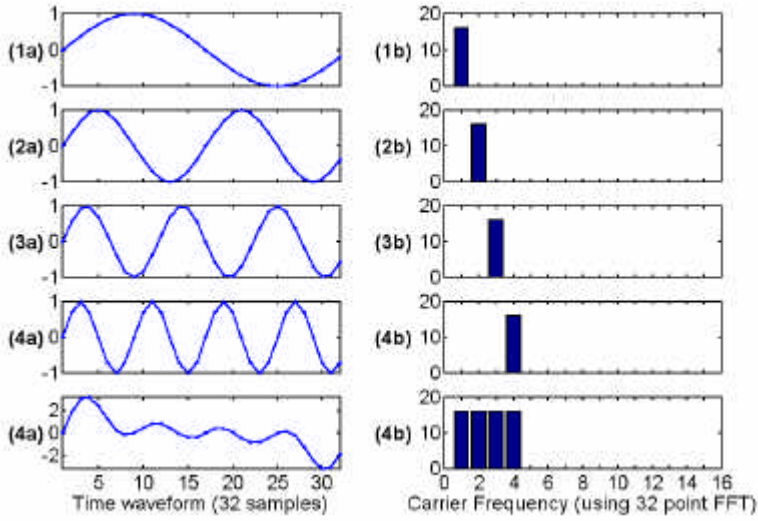


Figure 2-1, Time domain construction of an OFDM signal.

(1a), (2a), (3a) and **(4a)** show individual subcarriers, with 1, 2, 3, and 4 cycles per symbol respectively. The phase on all these subcarriers is zero. Note, that each subcarrier has an integer number of cycles per symbol, making them cyclic. Adding a copy of the symbol to the end would result in a smooth join between symbols. **(1b), (2b), (3b)** and **(4b)** show the FFT of the time waveforms in **(1a)**, **(2a)**, **(3a)** and **(4a)** respectively. **(4a)** and **(4b)** shows the result for the summation of the 4 subcarriers.

Sets of functions are orthogonal to each other if they match the conditions in equation (2-1). If any two different functions within the set are multiplied, and integrated over a symbol period, the result is zero, for orthogonal functions. Another way of thinking of this is that if we look at a matched receiver for one of the orthogonal functions, a subcarrier in the case of OFDM, then the receiver will only see the result for that function. The results from all other functions in the set integrate to zero, and thus have no effect.

$$\int_0^T s_i(t)s_j(t)dt = \begin{cases} C & i = j \\ 0 & i \neq j \end{cases} \quad (2-1)$$

Equation (2-2) shows a set of orthogonal sinusoids, which represent the subcarriers for an unmodulated real OFDM signal.

$$s_k(t) = \begin{cases} \sin(2\pi k f_o t) & 0 < t < T \quad k = 1, 2, \dots M \\ 0 & otherwise \end{cases} \quad (2-2)$$

where f_o is the carrier spacing, M is the number of carriers, T is the symbol period. Since the highest frequency component is Mf_o the transmission bandwidth is also Mf_o .

These subcarriers are orthogonal to each other because when we multiply the waveforms of any two subcarriers and integrate over the symbol period the result is zero. Multiplying the two sine waves together is the same as mixing these subcarriers. This results in sum and difference frequency components, which will always be integer subcarrier frequencies, as the frequency of the two mixing subcarriers has integer number of cycles. Since the system is linear we can integrate the result by taking the integral of each frequency component separately then combining the results by adding the two sub-integrals. The two frequency components after the mixing have an integer number of cycles over the period and so the sub-integral of each component will be zero, as the integral of a sinusoid over an entire period is zero. Both the sub-integrals are zeros and so the resulting addition of the two will also be zero, thus we have established that the frequency components are orthogonal to each other.

2.1.2 FREQUENCY DOMAIN ORTHOGONALITY

Another way to view the orthogonality property of OFDM signals is to look at its spectrum. In the frequency domain each OFDM subcarrier has a sinc, $\sin(x)/x$, frequency response, as shown in Figure 2-2. This is a result of the symbol time corresponding to the inverse of the carrier spacing. As far as the receiver is concerned each OFDM symbol transmitted for a fixed time (T_{FFT}) with no tapering at the ends of the symbol. This symbol time corresponds to the inverse of the subcarrier spacing of $1/T_{FFT}$ Hz¹. This rectangular, boxcar, waveform in the time domain results in a sinc frequency response in the frequency domain. The sinc shape has a narrow main lobe, with many side-lobes that decay slowly with the magnitude of the frequency difference away from the centre. Each carrier has a peak at the centre frequency and nulls evenly spaced with a frequency gap equal to the carrier spacing.

¹ OFDM signals typically use a time domain guard period. This guard period extends the length of the transmitted OFDM symbol, but is removed at the receiver (see section 2.3). As a result we can ignore its effect on the spectrum seen by the receiver.

The orthogonal nature of the transmission is a result of the peak of each subcarrier corresponding to the nulls of all other subcarriers. When this signal is detected using a Discrete Fourier Transform (DFT) the spectrum is not continuous as shown in Figure 2-2 (a), but has discrete samples. The sampled spectrum are shown as ‘o’s in the figure. If the DFT is time synchronised, the frequency samples of the DFT correspond to just the peaks of the subcarriers, thus the overlapping frequency region between subcarriers does not affect the receiver. The measured peaks correspond to the nulls for all other subcarriers, resulting in orthogonality between the subcarriers.

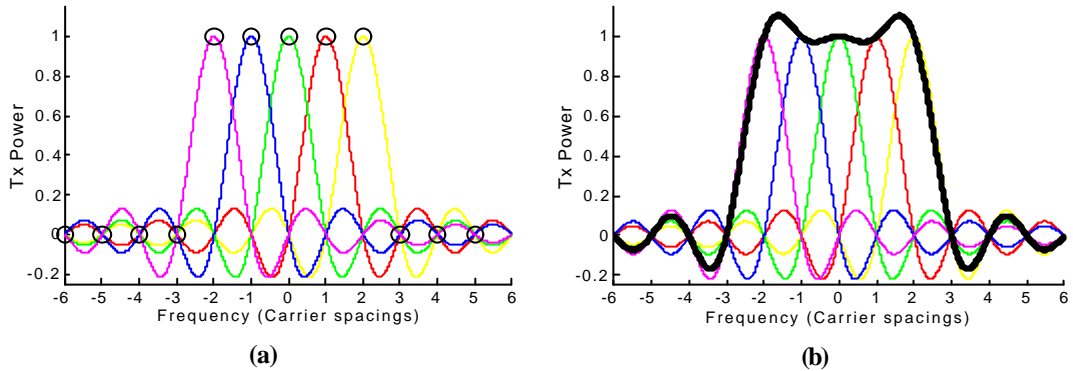


Figure 2-2, Frequency response of the subcarriers in a 5 tone OFDM signal.
(script 0006)

(a) shows the spectrum of each carrier, and the discrete frequency samples seen by an OFDM receiver. Note, each carrier is sinc, $\sin(x)/x$, in shape. **(b)** Shows the overall combined response of the 5 subcarriers (thick black line).

2.2 OFDM GENERATION AND RECEPTION

OFDM signals are typically generated digitally due to the difficulty in creating large banks of phase lock oscillators and receivers in the analog domain. Figure 2-3 shows the block diagram of a typical OFDM transceiver. The transmitter section converts digital data to be transmitted, into a mapping of subcarrier amplitude and phase. It then transforms this spectral representation of the data into the time domain using an Inverse Discrete Fourier Transform (IDFT). The Inverse Fast Fourier Transform (IFFT) performs the same operations as an IDFT, except that it is much more computationally efficient, and so is used in all practical systems. In order to transmit the OFDM signal the calculated time domain signal is then mixed up to the required frequency.

The receiver performs the reverse operation of the transmitter, mixing the RF signal to base band for processing, then using a Fast Fourier Transform (FFT) to analyse the signal in the frequency domain. The amplitude and phase of the subcarriers is then picked out and converted back to digital data.

The IFFT and the FFT are complementary function and the most appropriate term depends on whether the signal is being received or generated. In cases where the signal is independent of this distinction then the term FFT and IFFT is used interchangeably.

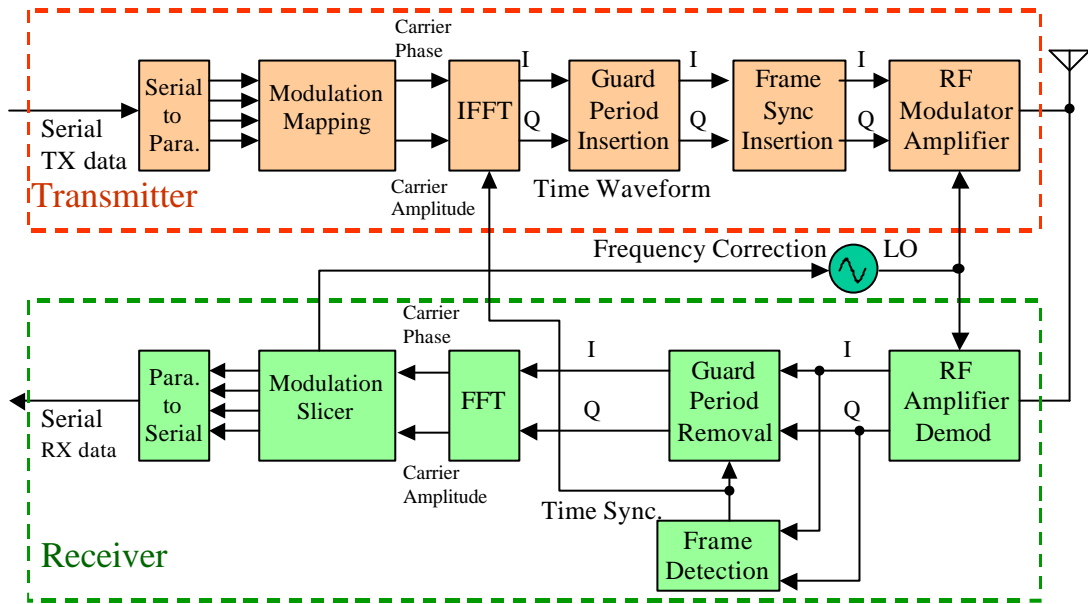


Figure 2-3, Block diagram showing a basic OFDM transceiver.

2.2.1 SERIAL TO PARALLEL CONVERSION

Data to be transmitted is typically in the form of a serial data stream. In OFDM, each symbol typically transmits 40 - 4000 bits, and so a serial to parallel conversion stage is needed to convert the input serial bit stream to the data to be transmitted in each OFDM symbol. The data allocated to each symbol depends on the modulation scheme used and the number of subcarriers. For example, for a subcarrier modulation of 16-QAM each subcarrier carries 4 bits of data, and so for a transmission using 100 subcarriers the number of bits per symbol would be 400.

For adaptive modulation schemes such as described in section 4.2, the modulation scheme used on each subcarrier can vary and so the number of bits per subcarrier

also varies. As a result the serial to parallel conversion stage involves filling the data payload for each subcarrier. At the receiver the reverse process takes place, with the data from the subcarriers being converted back to the original serial data stream.

When an OFDM transmission occurs in a multipath radio environment, frequency selective fading can result in groups of subcarriers being heavily attenuated, which in turn can result in bit errors. These nulls in the frequency response of the channel can cause the information sent in neighbouring carriers to be destroyed, resulting in a clustering of the bit errors in each symbol. Most Forward Error Correction (FEC) schemes tend to work more effectively if the errors are spread evenly, rather than in large clusters, and so to improve the performance most systems employ data scrambling as part of the serial to parallel conversion stage. This is implemented by randomising the subcarrier allocation of each sequential data bit. At the receiver the reverse scrambling is used to decode the signal. This restores the original sequencing of the data bits, but spreads clusters of bit errors so that they are approximately uniformly distributed in time. This randomisation of the location of the bit errors improves the performance of the FEC and the system as a whole.

2.2.2 SUBCARRIER MODULATION

Once each subcarrier has been allocated bits for transmission, they are mapped using a modulation scheme to a subcarrier amplitude and phase, which is represented by a complex In-phase and Quadrature-phase (IQ) vector. Figure 2-4 shows an example of subcarrier modulation mapping. This example shows 16-QAM, which maps 4 bits for each symbol. Each combination of the 4 bits of data corresponds to a unique IQ vector, shown as a dot on the figure. A large number of modulation schemes are available allowing the number of bits transmitted per carrier per symbol to be varied. An analysis of the performance of a range of commonly used modulation schemes is presented in section 2.6.

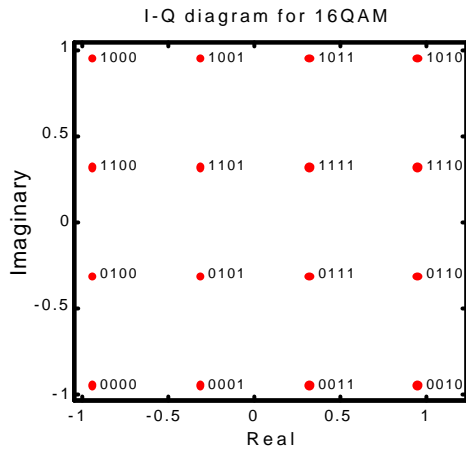


Figure 2-4, Example IQ modulation constellation. 16-QAM, with gray coding of the data to each location. (script s0045)

Subcarrier modulation can be implemented using a lookup table, making it very efficient to implement.

In the receiver, mapping the received IQ vector back to the data word performs subcarrier demodulation. During transmission, noise and distortion becomes added to the signal due to thermal noise, signal power reduction and imperfect channel equalisation. Figure 2-5 shows an example of a received 16-QAM signal with a SNR of 18 dB. Each of the IQ points is blurred in location due to the channel noise. For each received IQ vector the receiver has to estimate the most likely original transmission vector. This is achieved by finding the transmission vector that is closest to the received vector. Errors occur when the noise exceeds half the spacing between the transmission IQ points, making it cross over a decision boundary.

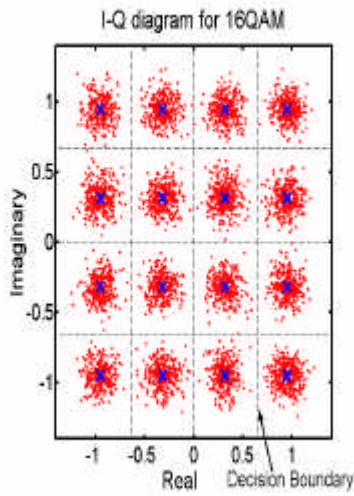


Figure 2-5, IQ plot for 16-QAM data with added noise. (script s0083)

2.2.3 FREQUENCY TO TIME DOMAIN CONVERSION

After the subcarrier modulation stage each of the data subcarriers is set to an amplitude and phase based on the data being sent and the modulation scheme; all unused subcarriers are set to zero. This sets up the OFDM signal in the frequency domain. An IFFT is then used to convert this signal to the time domain, allowing it to be transmitted. Figure 2-6 shows the IFFT section of the OFDM transmitter. In the frequency domain, before applying the IFFT, each of the discrete samples of the IFFT corresponds to an individual subcarrier. Most of the subcarriers are modulated with data. The outer subcarriers are unmodulated and set to zero amplitude. These zero subcarriers provide a frequency guard band before the nyquist frequency and effectively act as an interpolation of the signal and allows for a realistic roll off in the analog anti-aliasing reconstruction filters.

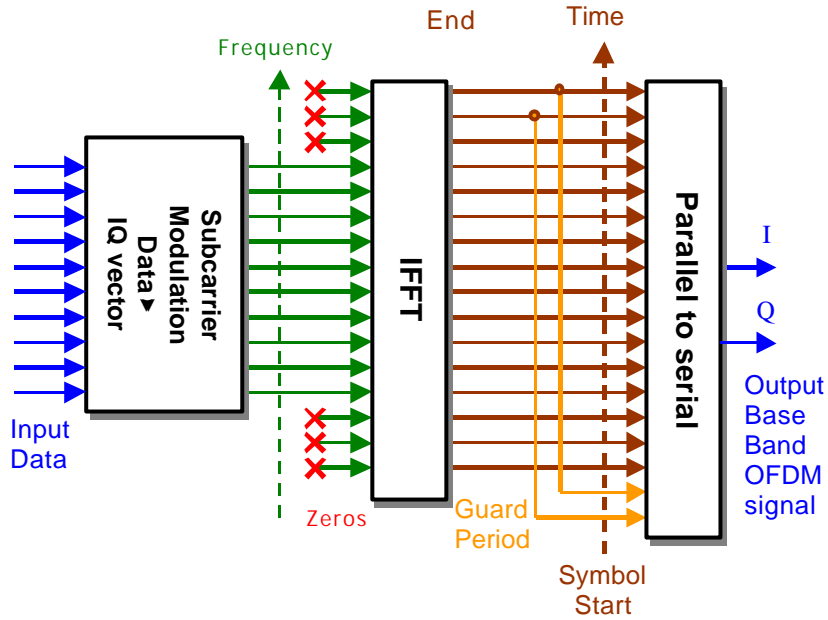


Figure 2-6, OFDM generation, IFFT stage

2.2.4 RF MODULATION

The output of the OFDM modulator generates a base band signal, which must be mixed up to the required transmission frequency. This can be implemented using analog techniques as shown in Figure 2-7 or using a Digital Up Converter as shown in Figure 2-8. Both techniques perform the same operation, however the performance of the digital modulation will tend to be more accurate due to improved matching between the processing of the I and Q channels, and the phase accuracy of the digital IQ modulator.

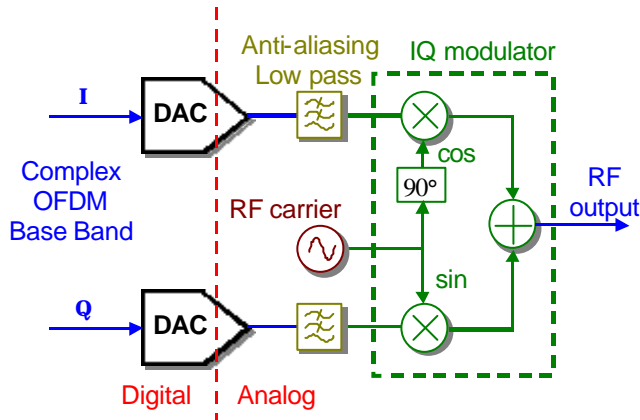


Figure 2-7, RF modulation of complex base band OFDM signal, using analog techniques.

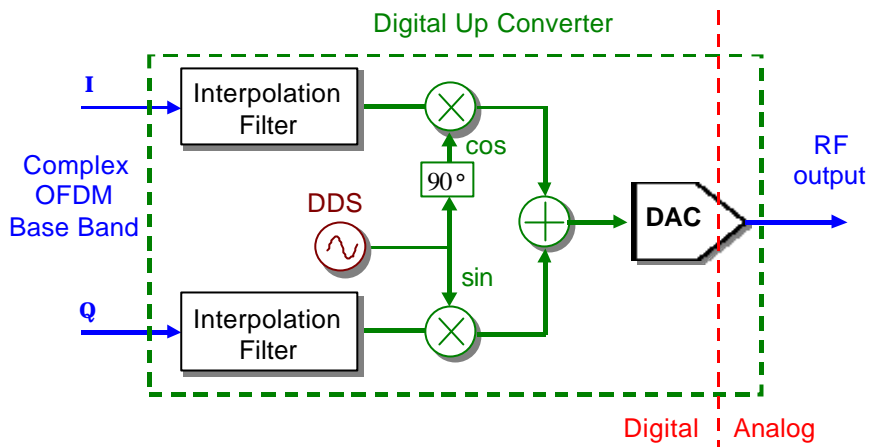


Figure 2-8, RF modulation of complex base band OFDM signal, using digital techniques. (DDS = Direct Digital Synthesis)

2.2.5 REAL VERSUS COMPLEX OFDM GENERATION

For most wireless applications the OFDM signal is generated at base band using complex samples, then modulated up to the required frequency using an IQ modulator, as shown in Figure 2-7 and Figure 2-8. The IQ modulator frequency shifts the OFDM signal from DC to the required RF frequency, and converts the complex signal into a real signal. A transmitted RF signal is always a real signal as it is just a variation in field intensity. It is however possible to directly generate a real OFDM signal. This is useful in wired applications, such as ADSL. In these applications the transmitted signal is generally from just above DC to an upper limit determined by the required signal bandwidth. The required transmission signal is a real signal as only a single cable is used. If a complex signal were used then two wires would be needed, one for the real signal and one for the imaginary signal.

A real signal is equivalent to a complex base band signal, centred on DC, mixed to the new centre frequency using an IQ modulator:

$$f_c = \frac{W}{2} + f_{off} \quad (2-3)$$

where f_c is the frequency translation required to shift the complex base band signal to form the real OFDM signal, W is the signal bandwidth and f_{off} is the offset from DC, also see Figure 2-9. In wired applications such as ASDL, the lower most subcarrier is offset from DC by a small amount compared with the signal bandwidth. This

means that the real signal can be generated directly using the IFFT stage instead of requiring the use of an IQ modulator for frequency translation.

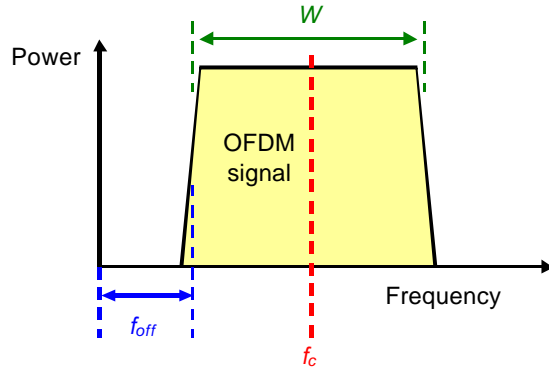


Figure 2-9, DC offset OFDM signal, W - bandwidth, f_{off} - frequency offset from DC, f_c centre frequency.

Figure 2-10 shows the set up of the OFDM signal in the frequency domain for the generation of a real waveform. With a real waveform the useable bandwidth of the signal is only half the sampling frequency, and so to generate a real OFDM signal only one half of the available subcarriers can be used for data modulation. To create a real waveform the upper frequency bins of the IFFT must be set to the complex conjugate of the mirror of the lower half.

This can be contrasted with the construction of a complex base band OFDM signal as shown in Figure 2-11. In this case all of the frequency bins can be used for subcarrier modulation, with the main limitation being that the outer bins must be kept as zero to allow reconstruction of the analog signal, without aliasing occurring. In most applications the subcarrier corresponding to DC is not used. Its removal simplifies the implementation hardware. Most OFDM system currently using an analog base band the same as shown in Figure 2-7. In order for the DC subcarrier to be used it requires that the IQ outputs are DC coupled to the IQ mixer. This is difficult to achieve in hardware as offset errors result in large errors in the generated IQ vector. Using AC coupling reduces the complexity of the implementation and so the DC subcarrier is usually not used. If digital modulation is used as shown in Figure 2-8 then the DC subcarrier can be used.

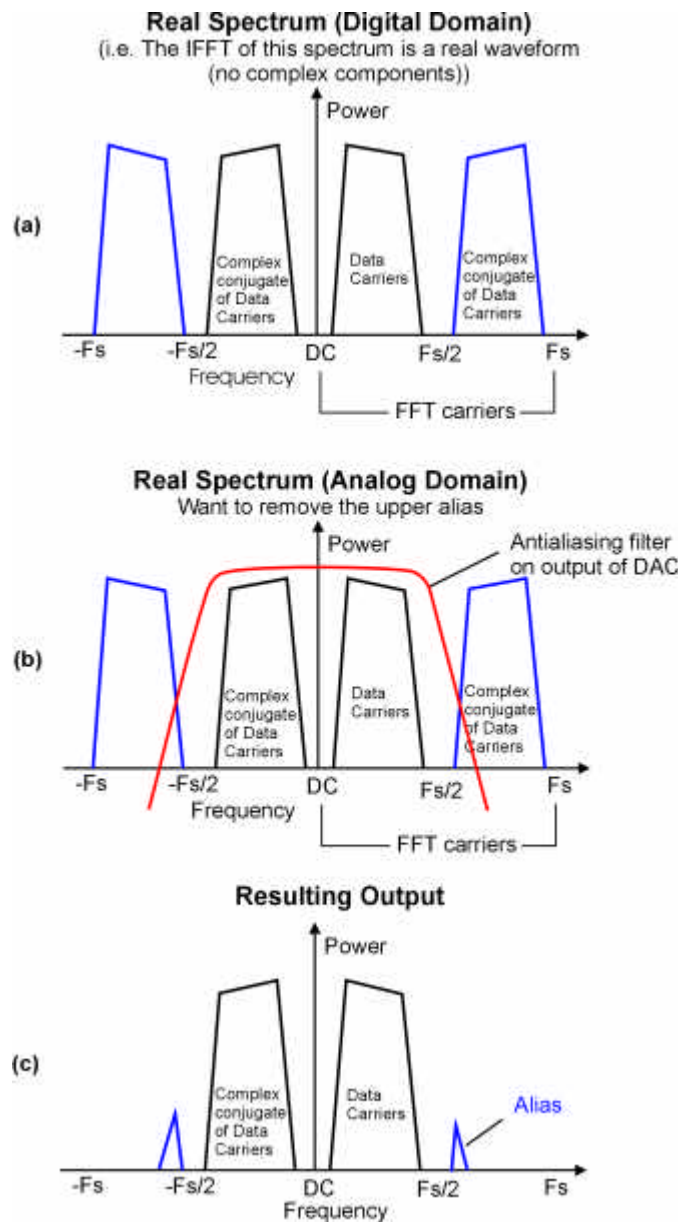


Figure 2-10, Construction of the subcarriers for generating a real output time domain waveform.

(The slope on the top of the signal block is to show spectral reversing of the signal)

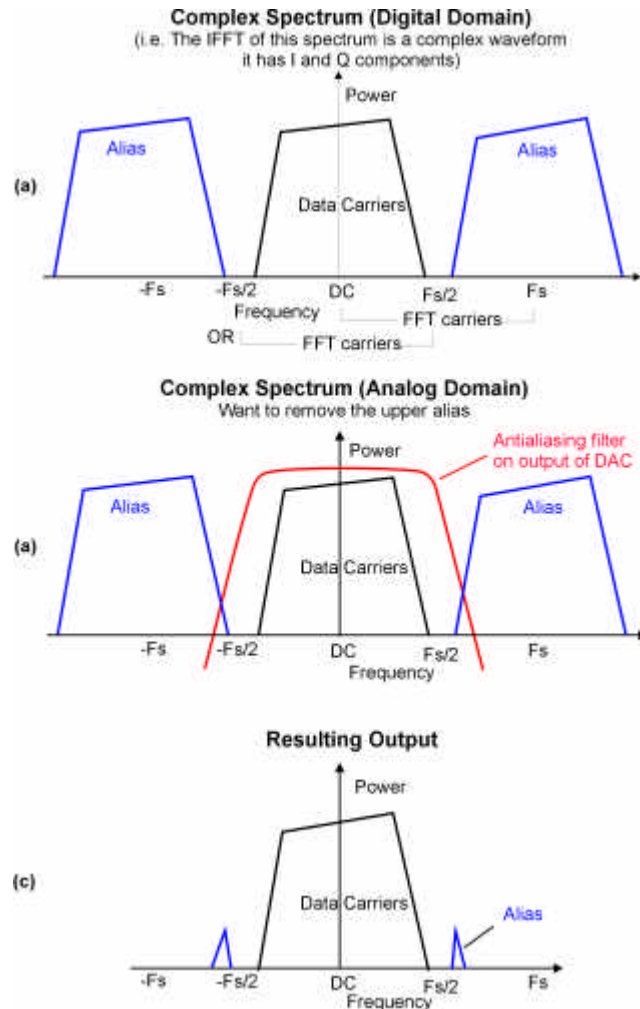


Figure 2-11, Construction of the subcarriers for complex signal representation of OFDM signals

2.3 GUARD PERIOD

For a given system bandwidth the symbol rate for an OFDM signal is much lower than a single carrier transmission scheme. For example for a single carrier BPSK modulation, the symbol rate corresponds to the bit rate of the transmission. However for OFDM the system bandwidth is broken up into N_c subcarriers, resulting in a symbol rate that is N_c times lower than the single carrier transmission. This low symbol rate makes OFDM naturally resistant to effects of Inter-Symbol Interference (ISI) caused by multipath propagation.

Multipath propagation is caused by the radio transmission signal reflecting off

objects in the propagation environment, such as walls, buildings, mountains, etc. These multiple signals arrive at the receiver at different times due to the transmission distances being different. This spreads the symbol boundaries causing energy leakage between them. Multipath propagation is discussed in more detail in Chapter 3.

The effect of ISI on an OFDM signal can be further improved by the addition of a guard period to the start of each symbol. This guard period is a cyclic copy that extends the length of the symbol waveform. Each subcarrier, in the data section of the symbol, (i.e. the OFDM symbol with no guard period added, which is equal to the length of the IFFT size used to generate the signal) has an integer number of cycles. Because of this, placing copies of the symbol end-to-end results in a continuous signal, with no discontinuities at the joins. Thus by copying the end of a symbol and appending this to the start results in a longer symbol time. Figure 2-12 shows the insertion of a guard period.

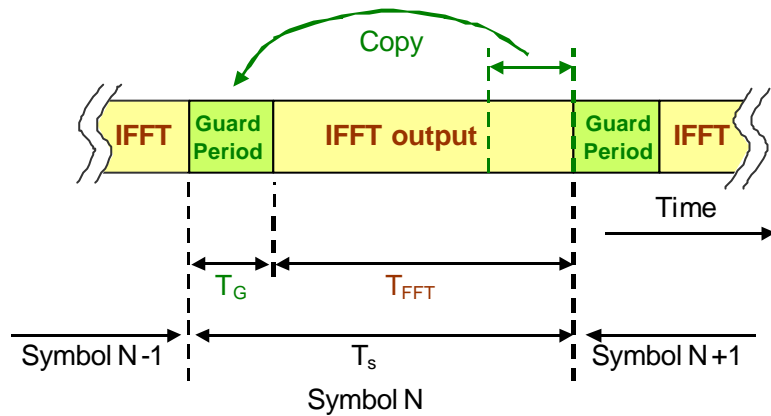


Figure 2-12, Addition of a guard period to an OFDM signal

The total length of the symbol is $T_s = T_G + T_{FFT}$, where T_s is the total length of the symbol in samples, T_G is the length of the guard period in samples, and T_{FFT} is the size of the IFFT used to generate the OFDM signal.

In addition to protecting the OFDM from ISI, the guard period also provides protection against time-offset errors in the receiver.

2.3.1 PROTECTION AGAINST TIME OFFSET

To decode the OFDM signal the receiver has to take the FFT of each received symbol, to work out the phase and amplitude of the subcarriers. For an OFDM system that has the same sample rate for both the transmitter and receiver, it must use the same FFT size at both the receiver and transmitted signal in order to maintain subcarrier orthogonality. Each received symbol has $T_G + T_{FFT}$ samples due to the added guard period. The receiver only needs T_{FFT} samples of the received symbol to decode the signal. The remaining T_G samples are redundant and are not needed. For an ideal channel with no delay spread (see section 3.4 for a description of delay spread) the receiver can pick any time offset, up to the length of the guard period, and still get the correct number of samples, without crossing a symbol boundary. Because of the cyclic nature of the guard period changing the time offset simply results in a phase rotation of all the subcarriers in the signal. The amount of this phase rotation is proportional to the subcarrier frequency, with a subcarrier at the nyquist frequency changing by 180° for each sample time offset. Provided the time offset is held constant from symbol to symbol, the phase rotation due to a time offset can be removed out as part of the channel equalisation. In multipath environments ISI reduces the effective length of the guard period leading to a corresponding reduction in the allowable time offset error.

2.3.2 PROTECTION AGAINST ISI

In an OFDM signal the amplitude and phase of the subcarrier must remain constant over the period of the symbol in order for the subcarriers to maintain orthogonality. If they are not constant it means that the spectral shape of the subcarriers will not have the correct *sinc* shape, and thus the nulls will not be at the correct frequencies, resulting in Inter-Carrier Interference. At the symbol boundary the amplitude and phase change suddenly to the new value required for the next data symbol. In multipath environments ISI causes spreading of the energy between the symbols, resulting in transient changes in the amplitude and phase of the subcarrier at the start of the symbol. The length of these transient effects corresponds to the delay spread of the radio channel. The transient signal is a result of each multipath component

arriving at slightly different times, changing the received subcarrier vector. Figure 2-13 shows this effect. Adding a guard period allows time for the transient part of the signal to decay, so that the FFT is taken from a steady state portion of the symbol. This eliminates the effect of ISI provided that the guard period is longer than the delay spread of the radio channel. The remaining effects caused by the multipath, such as amplitude scaling and phase rotation are corrected for by channel equalisation.

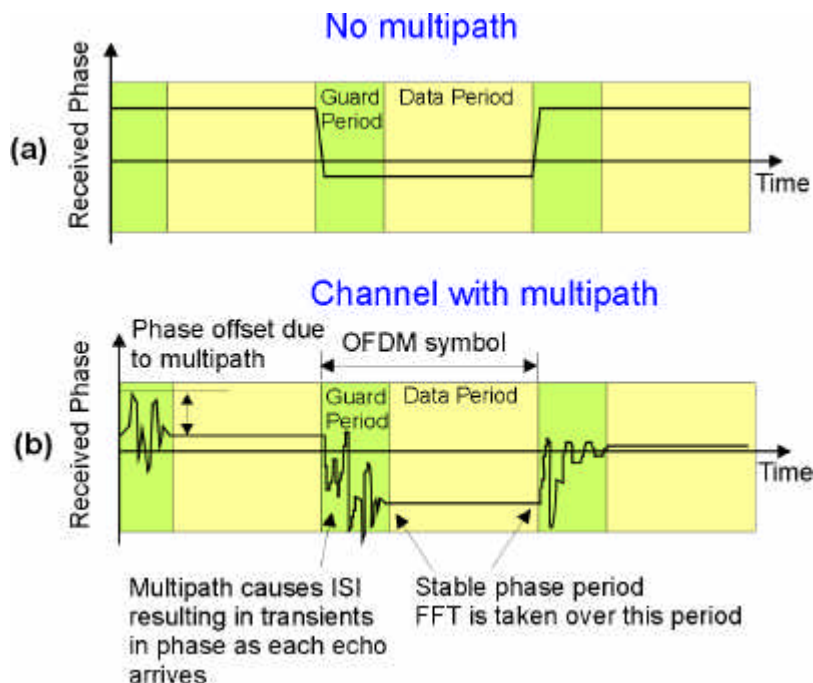


Figure 2-13, Function of the guard period for protecting against ISI.

The guard period protects against transient effects due to multipath, removing the effects of ISI, provided it is longer than the channel delay spread. This example shows the instantaneous phase of a single carrier for 3 symbols.

The addition of guard period removes most of the effects of ISI; however in practice, multipath components tend to decay slowly with time, resulting in some ISI even when a relatively long guard period is used.

Figure 2-14 shows the simulated performance of an OFDM system in the presence of static multipath. In this case the multipath impulse response (see section 3.3 for more detail) followed an exponential decay with a time constant of 8 samples, resulting in an RMS delay spread of 3.5 samples. Each sample in the impulse response was complex and Gaussian distributed. The RMS delay spread is a common parameter to

estimate the spread of the multipath energy in time, and used to estimate the level of ISI in single carrier communications. Section 3.4 provides a more detailed description of RMS delay spread with typical values for a range of environments. A more appropriate measure is the time over which 99% of the total accumulated impulse energy arrived, which in this simulation was 16 samples.

The results shown in Figure 2-14 plot the effective SNR of the demodulated OFDM signal as a function of the channel SNR. Effective SNR is used extensively throughout this thesis as a measure of the performance of the communications link. It is a measure of the signal to noise ratio as seen by the OFDM receiver after demodulation, where the signal power is the magnitude of the wanted signal, and the noise is the combined error in the received signal due to all the detrimental effects in the system including channel noise, IMD, filtering, ISI, ICI, frequency errors, time offset errors, channel equalisation errors, etc. The effective SNR provides a measure of the OFDM performance, independent of the modulation scheme. Traditionally the BER is used to measure the performance of a link, however in this thesis OFDM is considered the work with a large number of modulation schemes making BER a poor method of measurement. The BER of any particular modulation scheme can be estimated from the effective SNR by finding the BER of the modulation scheme in an AWGN channel with a SNR equal to the effective SNR (see section 2.6.9)

Figure 2-14 shows the effect of multipath on the OFDM transmission. Ideally the effective SNR should follow the channel SNR, however detrimental effects such as ISI lead to degraded performance. We can see from the results that as the length of the guard period is increased the maximum effective SNR improves. For example, the effective SNR of the OFDM signal only reaches a maximum of 15 dB when the guard period length is 4 samples in length, but reaches 25 dB when a guard period of 16 samples is used. This is a result of more of the ISI energy being removed by the guard period. This shows that having a guard period (16 samples) that is more than four times the multipath RMS delay spread (3.5 samples) still results in significant ISI.

The low effective SNR for when the guard period was a similar length to the channel RMS delay spread is fine for robust modulation schemes such as BPSK and QPSK, but is insufficient for higher spectral efficiency modulation schemes such as 64-

QAM and 256-QAM. Traditionally the RMS delay spread has been used as a measure of ISI and the allowable symbol rate in a multipath environment [68], [69], [70]. However if a higher spectral efficiency is required a more appropriate measure is needed. To achieve very high spectral efficiencies an effective SNR of greater than 35 dB must be able to be reached. In this case it required a guard period of at least 64 samples in length. This length of the guard period corresponds to the time it took for the impulse energy to decay to -35 dBc. Thus if we require a SNR of 25 dB then we have a guard period that is at least long enough to remove all impulse reflections that are stronger than -25 dBc.

The last two results in the simulation show the performance when using a guard period of 64 samples, with an IFFT size of 128, and 512. In the 128-point IFFT simulation, 80 subcarriers were used while in the 512-point simulation, 320 subcarriers were used, making the bandwidth of both systems the same. In order for the OFDM carriers to remain orthogonal to each other, the channel response must be approximately flat over the bandwidth of each subcarrier (see section 3.7.1). The simulation using 320 subcarriers divides the channel response using finer subcarriers, and hence the variation of the channel fading over their bandwidth of each subcarrier is more constant, improving the performance. The effective SNR for the 128 IFFT size is not limited by the guard period, but instead by poor channel equalisation caused by an insufficient number of subcarriers. For OFDM to operate effectively, the frequency response must be approximately flat over the bandwidth of a subcarrier. If insufficient subcarriers are used then the frequency response changes too rapidly, leading to degraded performance.

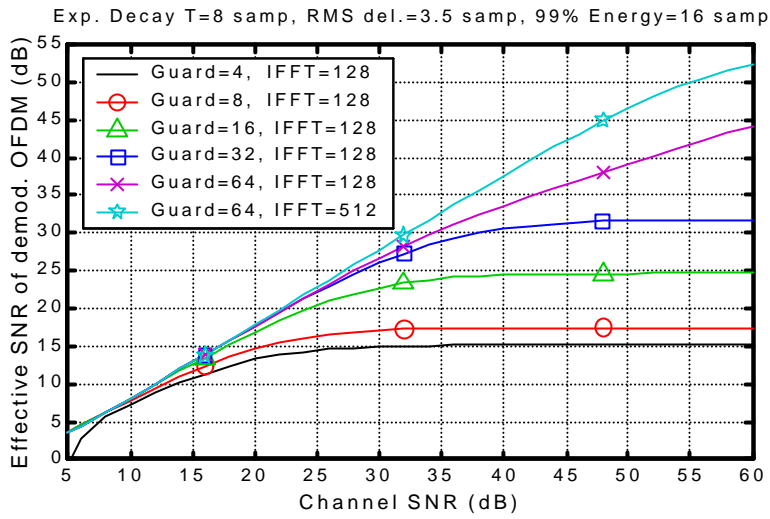


Figure 2-14, Effectiveness of adding a guard period for removal of ISI. (script s0082)

2.3.3 GUARD PERIOD OVERHEAD AND SUBCARRIER SPACING

Adding a guard period lowers the symbol rate, however it does not affect the subcarrier spacing seen by the receiver. The subcarrier spacing is determined by the sample rate and the FFT size used to analyse the received signal.

$$\Delta f = \frac{F_s}{N_{FFT}} \quad (2-4)$$

In Equation (2-4), Δf is the subcarrier spacing in Hz, F_s is the sample rate in Hz, and N_{FFT} is the size of the FFT. The guard period adds time overhead, decreasing the overall spectral efficiency of the system.

2.4 BANDLIMITING OF OFDM AND WINDOWING

OFDM in the time domain is equivalent to a sum of modulated sinusoidal carriers that are each windowed in time with a rectangular window function, also known as a boxcar window function (see Appendix A for more details). This window defines the boundary of each OFDM symbol, and determines the frequency response of the generated OFDM signal. Figure 2-15 shows an example time waveform for a single carrier OFDM transmission using Phase Shift Keying (PSK). The amplitude of the subcarrier is fixed and the phase is varied from symbol to symbol to transmit the data information. The subcarrier phase is constant for the entire symbol, resulting in a step in phase between symbols. These sharp transitions between symbols result in spreading in the frequency domain. Figure 2-16 shows the spectrum of a 52 subcarrier OFDM signal (same as HiperLAN2, or IEEE802.11a) with no band-pass limiting. The out of band components only fall off slowly due to the *sinc* roll off of each subcarrier. Figure 2-17 shows the spectrum of a 1536 subcarrier OFDM signal (same as Type I DAB). The side-lobes roll off faster than the 52-subcarrier case, as a fraction of the system bandwidth. However the side-lobes are still significant (> -40 dBc) even far away from the edge of the OFDM main signal block. These side-lobes increase the effective bandwidth of the OFDM signal, degrading the spectral efficiency. There are two common techniques for reducing the level of the side-lobes to acceptable limits; these are band pass filtering the signal, or adding a RC guard period.

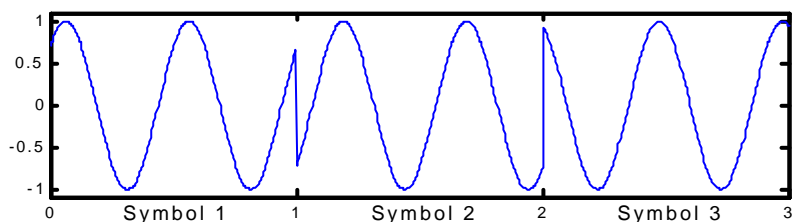


Figure 2-15, Time waveform of a single carrier OFDM signal, showing 3 symbols.

Note: Each symbol has an integer number of cycles per symbol, which is required for orthogonality. Also there are sharp phase transients between symbols. (script s0037)

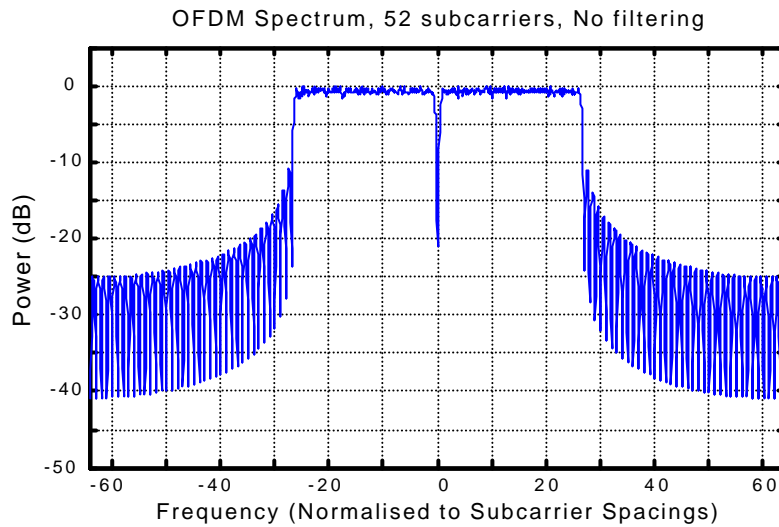


Figure 2-16, Spectrum of a 52 subcarrier OFDM signal with no band-limiting.
(script s0050)

This is the same frequency response as an un-filtered HiperLAN2 signal. For HiperLAN2 the subcarrier spacing corresponds to 312.5 kHz. The DC subcarrier has not been used, making the signal symmetrical around DC.

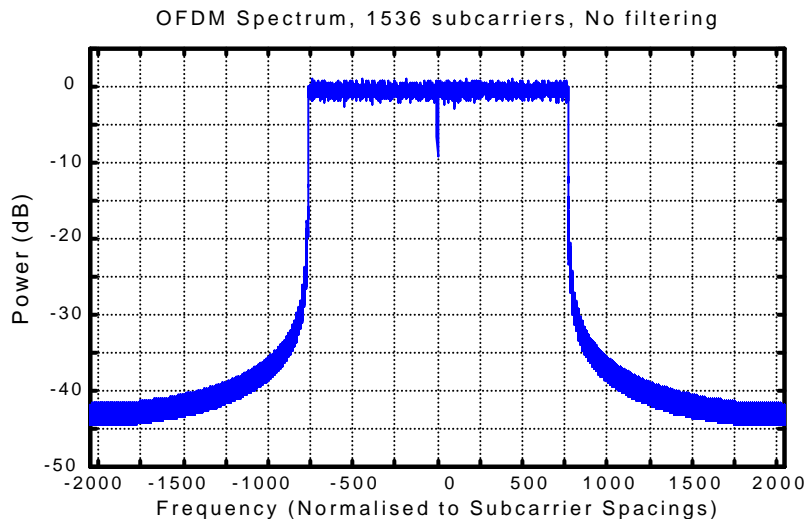


Figure 2-17, Spectrum of a 1536 subcarrier OFDM signal with no band-limiting. (script s0050)

This is the same frequency response as an un-filtered Type I DAB signal. For DAB the subcarrier spacing corresponds to 1 kHz.

2.4.1 BAND PASS FILTERING

Whenever signals are converted from the digital domain to an analog waveform for transmission, filtering is used to prevent aliasing occurring [120]. This effectively band pass filters the signal, removing some of the OFDM side-lobes. The amount of side-lobe removal depends on the sharpness of the filters used. In general digital filtering provides a much greater flexibility, accuracy and cut off rate than analog filters, making them especially useful for band limiting of an OFDM signal.

Figure 2-18 (a) shows the frequency response of the OFDM signal with no filtering. Figure 2-18 (b) - (e) shows examples of a band pass filtered OFDM signal. These signals have been filtered with a Finite Impulse Response (FIR) filter [120] developed using the windowing method (see Appendix A). A low number of subcarriers were used in these plots so that the roll off of the FIR filtering could be seen. The filtering removes virtually all of the side lobes, but does so at the cost of the computational expense of implementing the FIR filtering, and it reduces the effective SNR of the OFDM channel (see section 2.6 for calculating the BER for a given modulation scheme and effective SNR). The act of filtering the OFDM signal, chops off significant energy from the outer subcarriers, distorting their shape and causing ICI.

No publications to date could be found studying the effects of band pass filtering of OFDM signals, looking at the reduction in the effective SNR caused by the filtering. Very sharp cut off filters allow separate blocks of OFDM signals to be packed very closely in the frequency domain, improving the spectral efficiency. But this tight filtering can result in a degraded effective SNR, and so its effects must be taken into consideration when designing a system.

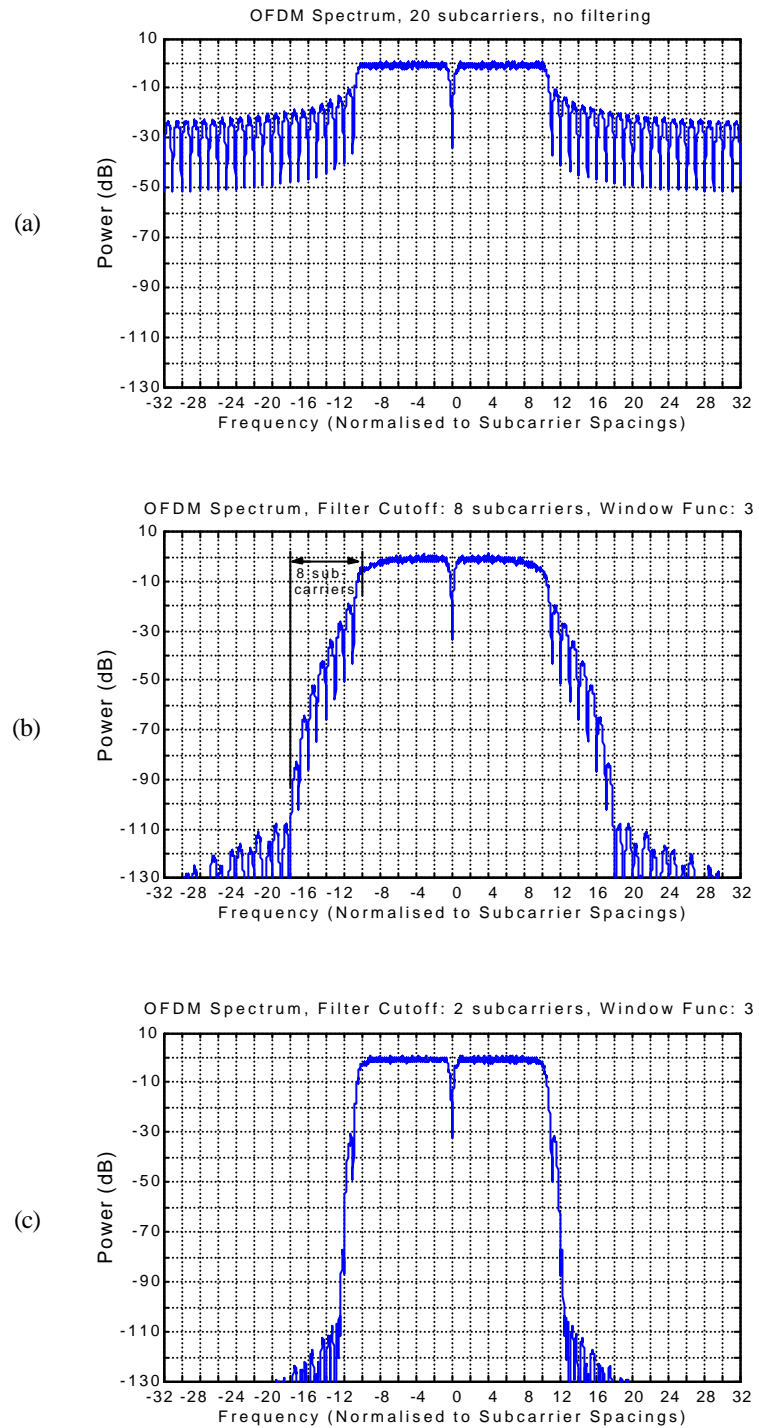


Figure 2-18 continued next page

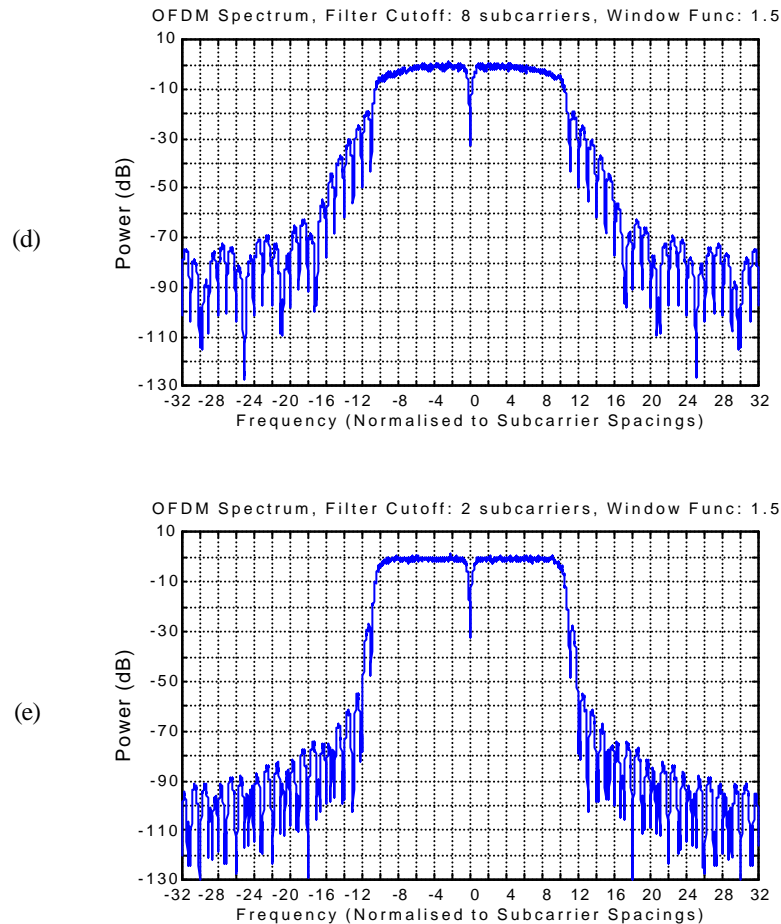


Figure 2-18, Spectrum of a 20 subcarrier OFDM, with and without band pass filtering. Centre subcarrier was not used. (script s0050)

(a) OFDM spectrum with no band pass filtering.

Filtered results were band pass filtered using an FIR filter, which was developed using the windowing method with a Kaiser window function. See Appendix A. (script s0050)

- (b) Kaiser window width of 3 (Side lobe attenuation of 89 dB). The transition width of the filter was 8 subcarrier spacings (24 tap FIR filter)
- (c) Kaiser window width of 3 (Side lobe attenuation of 89 dB). The transition width of the filter was 2 subcarrier spacings (96 tap FIR filter)
- (d) Kaiser window width of 1.5 (Side lobe attenuation of 40 dB). The transition width of the filter was 8 subcarrier spacings (12 tap FIR filter)
- (e) Kaiser window width of 1.5 (Side lobe attenuation of 40 dB). The transition width of the filter was 2 subcarrier spacings (48 tap FIR filter)

2.4.2 COMPUTATIONAL COMPLEXITY OF FIR BAND PASS FILTERING

Using digital band pass filtering is a very successful method for removing the side-lobes generated by OFDM signals. The problem with digital filtering is the high computational overhead. To implement an FIR band pass filter the number of taps required corresponds to:

$$N_{\text{taps}} = \text{ceil}\left(\frac{W_T \cdot \text{IFFT}}{F_T}\right) \quad (2-5)$$

where N_{taps} is the number of taps in the FIR filter, W_T is the transition width of the window function used to generate the FIR filter (see section A.2 in the appendix for a description of window functions), IFFT is the size of the IFFT used to generate the signal, and F_T is the transition width of the filter normalised for subcarrier spacings. Ceil is a rounding toward infinity, i.e. $\text{ceil}(1.1) = 2$.

For example, to generate the signal shown in Figure 2-18 (b) requires filtering with a 24 tap FIR filter. This can be calculated from the signal specifications. The signal was generated using an IFFT size of 64 and so $\text{IFFT} = 64$. A Kaiser window function with a transition width of 3 was used. This results in a stop band attenuation of 89 dB (see Figure A - 5 in the appendix). The side-lobe power of the unfiltered OFDM signal is -20 dBc and so after filtering it should be -109 dBc. This matches the results shown in Figure 2-18 (b). The transition width of the window function used was 3.0 and so the number of taps would be:

$$N_{\text{taps}} = \text{ceil}\left(\frac{3.0 \times 64}{8}\right) = 24 \quad (2-6)$$

Each tap of the FIR filter requires two Multiply and ACcumulate operations (MAC) as a result of the complex samples, and so for a sample rate of 20 MHz the number of calculations would be $20 \times 10^6 \times 24 \times 2 = 960$ MMAC (Million MACs).

In applications where the required number of taps in the filter is high (> 100), it is probably more efficient to implement it using an FFT implementation of an FIR filter. Another method for reducing the number of calculations is to implement the filtering using an IIR filter, however a review of the amount of ISI caused by the

non-linear phase of the filter would need further investigation.

2.4.3 EFFECT OF BAND PASS FILTERING ON OFDM PERFORMANCE

In the time domain, an OFDM symbol is rectangular in shape, which corresponds to a *sinc* decay in the frequency domain, as shown in Figure 2-16. If we were to band pass filter an OFDM signal with a brick wall filter then the signal would become rectangular in the frequency domain, causing the time domain waveform to have a *sinc* decay between symbols. This in turn results in ISI degrading the performance. The ISI caused by the filtering can be removed by using a guard period of sufficient length, and by choosing the time offset to synchronise in the middle of the guard period, so that most of the ISI energy is removed.

Figure 2-19 shows the simulated performance of a band pass filtered OFDM signal, with different transition widths for the filter, in a channel with no channel noise. This plot shows the performance of the OFDM transmission when the time synchronisation offset was varied. The guard period used in this simulation was of the same length as the IFFT section of the symbol. This very long guard period was used so that the effect of the time offset could be varied over a large range, while still maintaining a time offset within the guard period. The effective SNR was calculated by averaging effective SNR over all the subcarriers in the transmission. When the time offset is 0 this corresponds to the receiver taking the FFT of the IFFT section of the transmitted signal. When the time offset is negative this corresponds to the receiver taking the FFT over the IFFT section and part of the symbol guard period (see Figure 2-20).

The lowest ISI is achieved when the time offset is negative and half the guard period length. The sharper the filter cuts off the signal (in the figure the sharpest filter removes the side-lobes down to below -100 dBc within 2 carrier spacings), the longer the ISI. The residual capping of the SNR at 85 dB is caused by ICI, and distortion of the subcarriers at the edges of the signal.

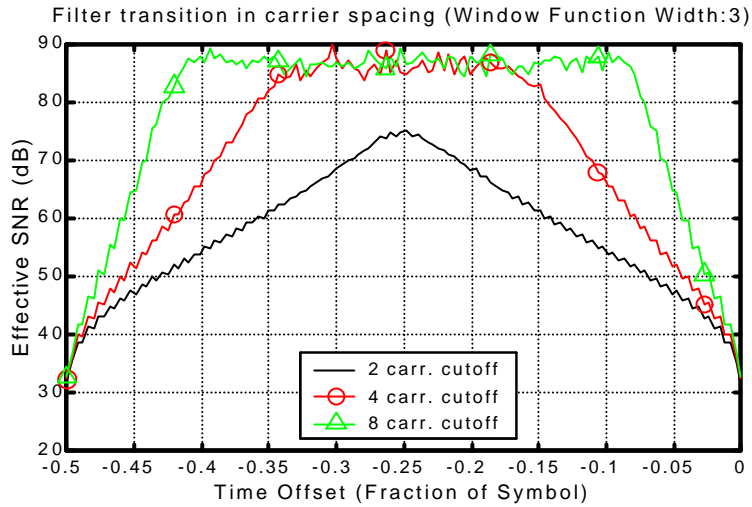


Figure 2-19, Effective SNR as a function of the time offset for a band pass filtered 52 subcarrier OFDM signal. (script s0057)

The guard period in this test was 50% of total symbol time, thus guard period length = useful symbol time. *Carr. cutoff* corresponds to the transition width of the filter in subcarrier spacings.

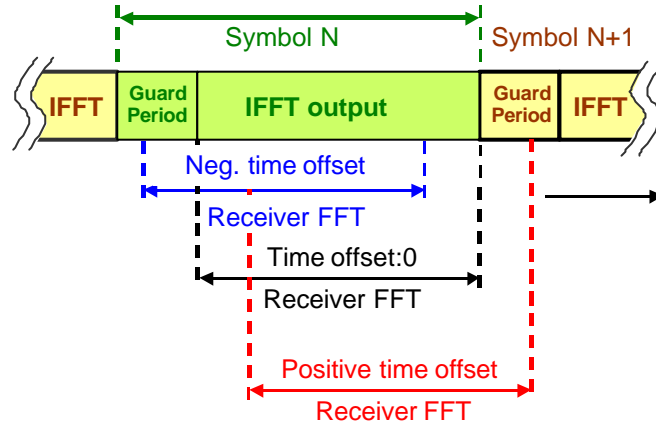


Figure 2-20, Section of the waveform that the receiver FFT is taken from depending on the time offset.

The effective SNR of a band pass filtered OFDM signal depends on the effects of both ISI and ICI. Figure 2-21 shows the performance of an OFDM system matching the specifications of HiperLAN2 or IEEE802.11a. In this case 52 carriers are used, and the guard period is 20% of the total symbol time. The effective SNR varies with subcarrier number as the filter distorts the response of the outer subcarriers the most. The highest modulation scheme used in HiperLAN2 and IEEE802.11a systems is 64-

QAM, which requires an effective SNR of greater than 26 dB. We can see from the results in Figure 2-21 that the effective SNR exceeds 26 dB for all carriers even when using a very sharp band pass filter that cuts off within one half of a subcarrier spacing.

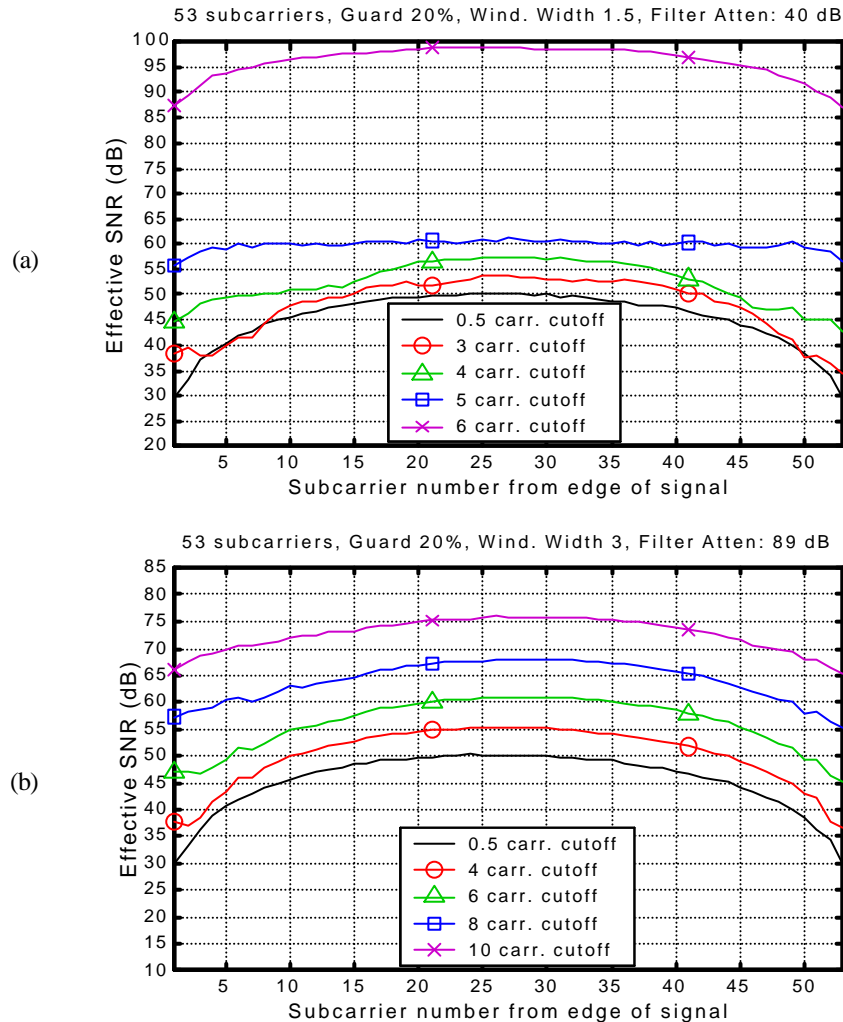


Figure 2-21, Effective SNR for each subcarrier as a result of band pass filtering.
(script s0057)

An odd number of subcarriers (53) were simulated to make the signal symmetrical about DC. The band pass filtering was implemented using an FIR filter based one the windowing method using a Kaiser window. Each result shows five different sharpness of the filter (carr. cutoff).

- (a) Kaiser window width of 1.5 (Side lobe attenuation of 40 dB).
- (b) Kaiser window width of 3 (Side lobe attenuation of 89 dB).

Signals with a larger number of carriers than the one shown in Figure 2-21, still have the effective SNR limited by the band pass filtering. Figure 2-22 shows the effective SNR for a signal with many subcarriers. Only the lower section is shown, as the SNR is symmetrical about the centre subcarrier. These results can be used to estimate the subcarrier effective SNR for any sized OFDM signal. In this simulation the only source of noise is the ISI caused by the band pass filtering of the signal.

For example: let us assume that we wanted to know the effective SNR of the 26th subcarrier from the edge of a HiperLAN2 signal when it is band pass filtered using a transition width of 6 subcarriers and we use a Kaiser window with a window width of 3, and a guard period of 20% is used. From Figure 2-22 (g) we can estimate the effective SNR to be 64 dB. In a HiperLAN2 signal the 26th carrier corresponds to the middle of the signal bandwidth and so it suffers from degradation from the filtering of both edges of the signal in the frequency domain. This degrades the effective SNR of the 26th subcarrier by 3 dB, thus the resulting in an effective SNR of 61 dB. This matches the direct simulated results shown in Figure 2-21 (b).

We can see that for each halving of the guard period length the transition width of the band pass filter must be approximately doubled in order to maintain the same effective SNR. Subcarriers more than 10 subcarrier spacings from the signal boundary have an effective SNR of greater than 30 dB regardless of the sharpness of the filtering provided some guard period is present. This effective SNR is sufficiently high to support a modulation scheme up to 128-QAM with a low error rate (see Figure 2-31), providing that there are no other detrimental effects. For subcarriers on the edge of the OFDM signal, their effective SNR can be as low as 20 dB, which may pose a small problem for modulation schemes above 32-QAM.

Band pass filtering of OFDM signals allows the side-lobes to be removed from an OFDM signal, effectively reducing its bandwidth, and improving the spectral efficiency. It does this with little or no extra overheads in the time domain, as the guard period is needed for protection from multipath delay spread.

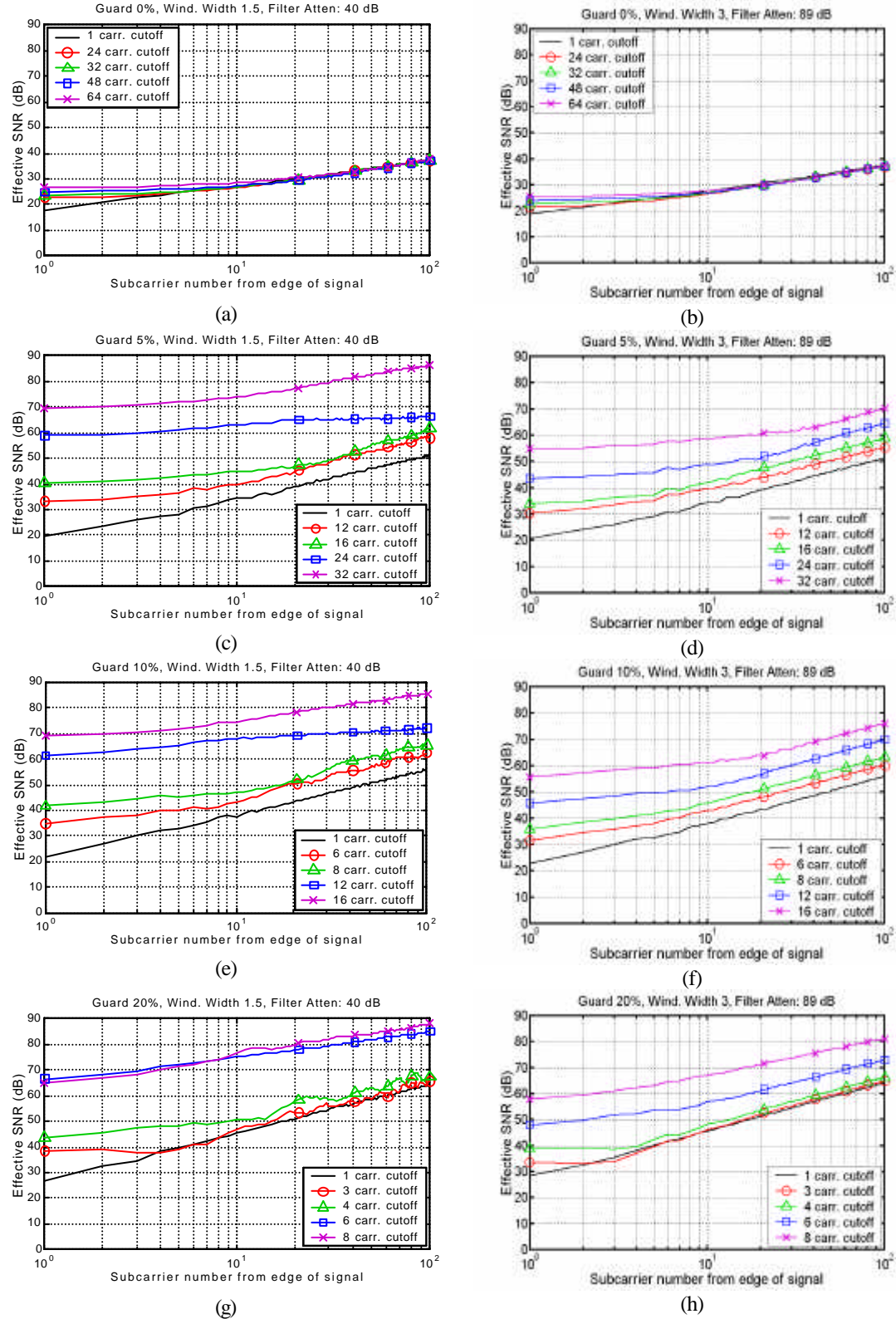


Figure 2-22, Subcarrier effective SNR, due to band pass filtering. (script s0085)

An OFDM signal with a large number of subcarriers (701) was simulated and only the lower 100 subcarriers is show. The guard period is specified as a percentage of the total symbol time (IFFT and the guard period)

2.5 RAISED COSINE GUARD PERIOD

One of the simplest methods for suppressing the side-lobes of an OFDM signal is to round the guard period of the OFDM signal, tapering it smoothly to zero before the next symbol. This tapering smooths the transition between symbols, resulting in reduced side-lobe power. Figure 2-23 shows the make up of a single OFDM symbol with a Raised Cosine (RC) guard period. This section of the guard period is windowed with a squared cosine shape ($\cos(\frac{\pi}{2}f)^2$), hence the name raised cosine.

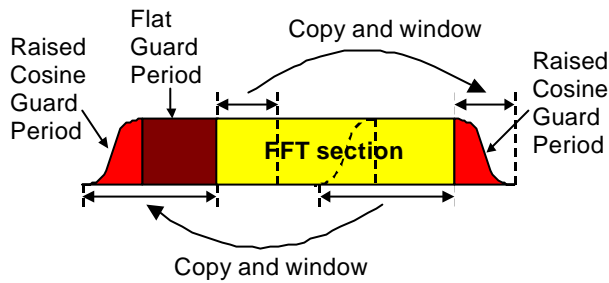


Figure 2-23, Construction of a RC guard period.

The raised cosine section of a guard period can be overlapped with the previous and next symbol as this section of the guard period only provides minimal protection against multipath and timing errors, and is ignored at the receiver. Because this section tapers to zero it results in minimal additional ISI. The main advantage of overlapping is that the length of the raise cosine section can be made double in length without incurring additional time overhead. Figure 2-24 shows a diagram of overlapping symbols.

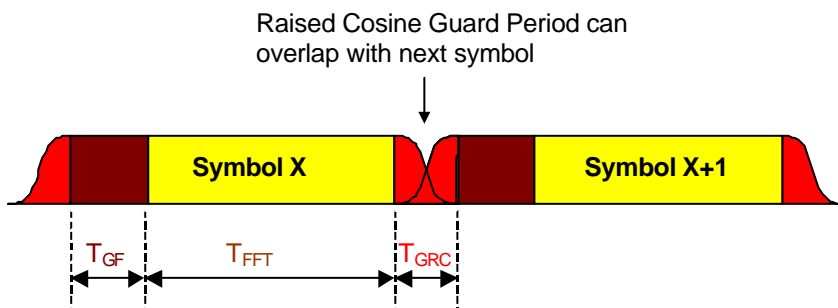


Figure 2-24, Envelope of OFDM symbols with a flat guard period and an overlapping raised cosine guard period.

The effect of adding a RC guard period to an OFDM signal was simulated to determine the level of the out of band side-lobes. Figure 2-25, Figure 2-26 and Figure 2-27 shows the spectrum of OFDM signals with an RC guard period. The spectrum shown has been shifted to the left so that just the upper edge of the OFDM signal is shown. The results were presented in this manner to normalise them so that the side-lobes could be compared regardless of the number of subcarriers used in the signal. In Figure 2-25 the lower edge of the OFDM signal can also be seen. The frequency axis has been normalised to units of subcarrier spacings.

The spectrum of an OFDM signal only varies slightly as the number of subcarriers is increased. The main difference occurs for the side-lobe level when little or no RC guard period is used. It can be seen in the simulations that as the number of subcarriers is increased from 20 (Figure 2-25) to 4000 (Figure 2-27) the level of the side-lobes, 200 subcarrier spacings from the edge of the signal, increases by about 8 dB. The increase is a result of the combined effect of all the subcarriers in the signal.

In Figure 2-25 through to Figure 2-27 the RC guard period length has been specified as a percentage of the flat section of the OFDM symbol, that is:

$$RC = 100 \cdot \frac{T_{GRC}}{T_{FFT} + T_{GF}} \% \quad (2-7)$$

Where RC is the raised cosine percentage, T_{GRC} is the length of the RC guard period, T_{FFT} is the length of the FFT section of the symbol and T_{GF} is the length of the flat guard period, see Figure 2-24. For example: The IEEE802.11a standard recommends a RC guard period of 100 ns. The useful symbol period (T_{FFT}) is 3.2 µs and the total guard period is 800 ns. The flat section of the guard period is the total guard period (800 ns) minus the RC section of the symbol (100 ns), thus $T_{GF} = 700$ ns. The RC section is thus:

$$RC = 100 \cdot \frac{100}{700 + 3200} = 2.56\% \quad (2-8)$$

From Figure 2-25 and Figure 2-26 we can estimate that the side-lobes will be -40 dBc approximately 30 subcarriers from the edge of the signal. Since HiperLAN2 uses 52 signal subcarriers (spaced at intervals of 312.5 kHz) the total system bandwidth using a threshold of -40 dBc is $(2 \times 30 + 52) \times 312.5$ kHz = 35 MHz. The

spacing of the HiperLAN2 channels is 20 MHz, and so a bandwidth of 35 MHz is too high. This indicates that the addition of the RC guard period is insufficient to reduce the side-lobes sufficiently, thus additional band pass filtering is required.

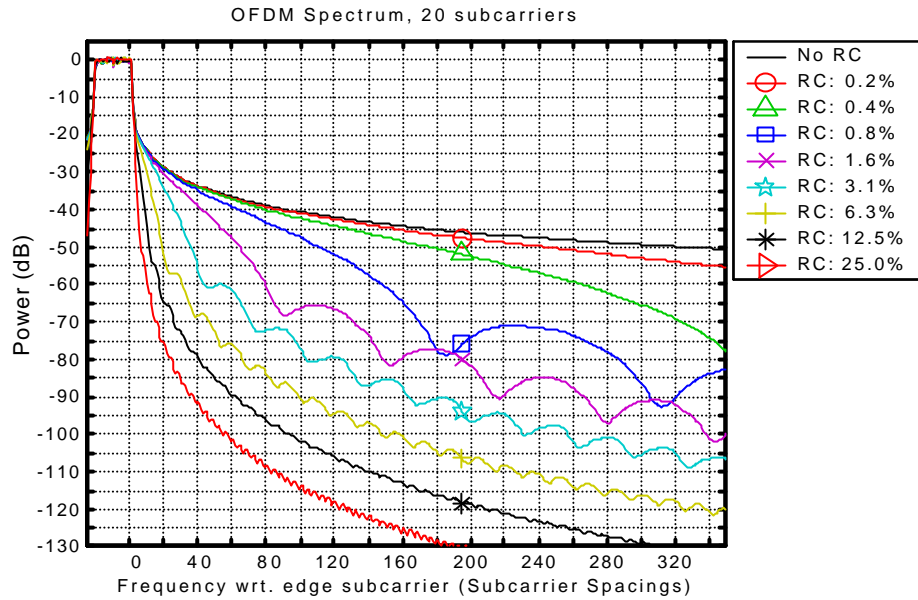


Figure 2-25, Side-lobe power for an OFDM signal with 20 subcarriers as the length of the RC guard period is varied. (script s0050)

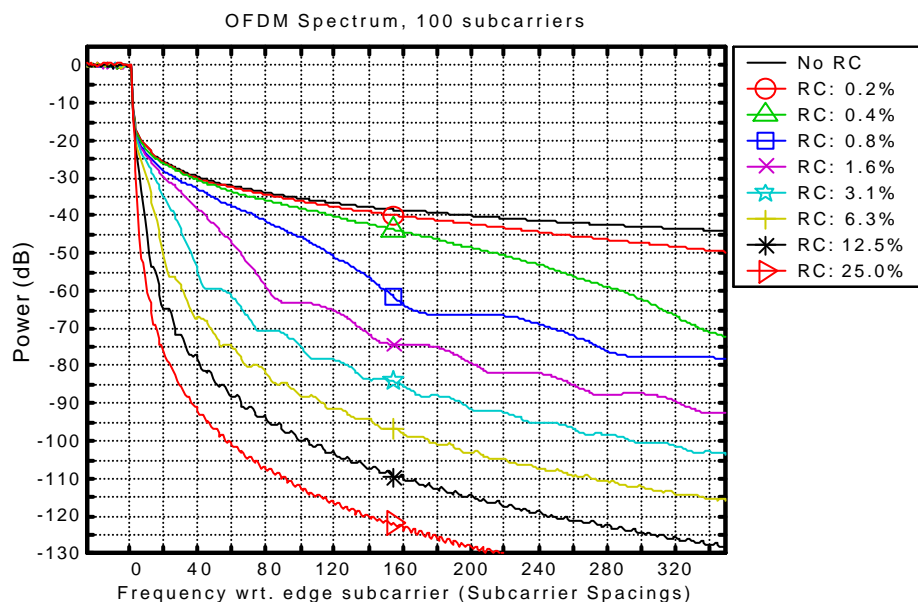


Figure 2-26, Side-lobe power for an OFDM signal with 100 subcarriers as the length of the RC guard period is varied. (script s0050)

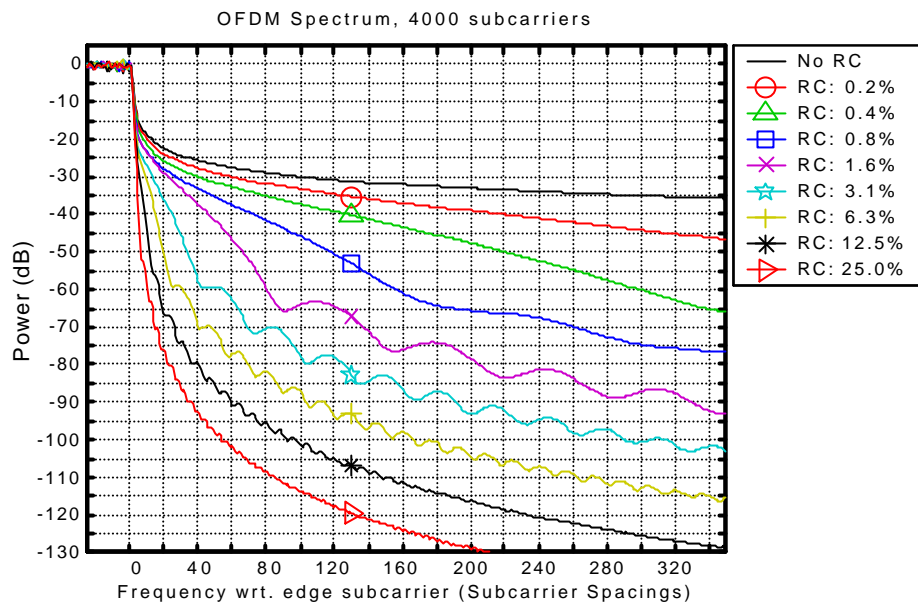


Figure 2-27, Side-lobe power for an OFDM signal with 4000 subcarriers as the length of the RC guard period is varied. (script s0050)

2.6 EFFECT OF ADDITIVE WHITE GAUSSIAN NOISE ON OFDM

Noise exists in all communications systems operating over an analog physical channel, such as radio. The main sources are thermal background noise, electrical noise in the receiver amplifiers, and inter-cellular interference. In addition to this noise can also be generated internally to the communications system as a result of Inter-Symbol Interference (ISI), Inter-Carrier Interference (ICI), and Inter-Modulation Distortion (IMD). These sources of noise decrease the Signal to Noise Ratio (SNR), ultimately limiting the spectral efficiency of the system. Noise, in all its forms, is the main detrimental effect in most radio communication systems. It is therefore important to study the effects of noise on the communications error rate and some of the trade offs that exists between the level of noise and system spectral efficiency.

Most types of noise present in radio communication systems can be modelled accurately using Additive White Gaussian Noise (AWGN). This noise has a uniform spectral density (making it white), and a Gaussian distribution in amplitude (this is also referred to as a normal distribution or bell curve). Thermal and electrical noise

from amplification, primarily have white Gaussian noise properties, allowing them to be modelled accurately with AWGN. Also most other noise sources have AWGN properties due to the transmission being OFDM. OFDM signals have a flat spectral density and a Gaussian amplitude distribution provided that the number of carriers is large (greater than about 20 subcarriers), because of this the inter-cellular interference from other OFDM systems have AWGN properties. For the same reason ICI, ISI, and IMD also have AWGN properties for OFDM signals.

2.6.1 MODULATION SCHEMES

Digital data is transferred in an OFDM link by using a modulation scheme on each subcarrier. A modulation scheme is a mapping of data words to a real (In phase) and imaginary (Quadrature) constellation, also known as an IQ constellation. For example 256-QAM (Quadrature Amplitude Modulation) has 256 IQ points in the constellation (see Table 2-2(h)), constructed in a square with 16 evenly spaced columns in the real axis and 16 rows in the imaginary axis. The number of bits that can be transferred using a single symbol corresponds to $\log_2(M)$, where M is the number of points in the constellation, thus 256-QAM transfers 8 bits per symbol. Each data word is mapped to one unique IQ location in the constellation. The resulting complex vector $I + j \cdot Q$, corresponds to an amplitude of $\sqrt{I^2 + Q^2}$ and a phase of $\angle(I + j \cdot Q)$ where $j = \sqrt{-1}$.

Increasing the number of points in the constellation does not change the bandwidth of the transmission, thus using a modulation scheme with a large number of constellation points, allows for improved spectral efficiency. For example 256-QAM has a spectral efficiency of 8 b/s/Hz, compared with only 1 b/s/Hz for BPSK. However, the greater the number of points in the modulation constellation, the harder they are to resolve at the receiver. As the IQ locations become spaced closer together, it only requires a small amount of noise to cause errors in the transmission. This results in a direct trade off between noise tolerance and the spectral efficiency of the modulation scheme and was summarised by Shannon's Information Theory [53], which states that the maximum capacity of a channel of bandwidth W , with a signal power of S , perturbed by white noise of average power N , is given by

$$C = W \log_2 \left(1 + \frac{S}{N} \right) \quad (2-9)$$

The spectral efficiency of a channel is a measure of the number of bits transferred per second for each Hz of bandwidth and thus the spectral efficiency S_E is given by

$$S_E = \frac{C}{W} = \log_2 \left(1 + \frac{S}{N} \right) \quad (2-10)$$

where both the signal and noise is linear scale, and the spectral efficiency is measured in b/s/Hz. If the SNR is significantly higher than one then each doubling of the signal power (a 3 dB increase) the ideal spectral efficiency increases by 1 b/s/Hz

2.6.2 OFDM VERSUS SINGLE CARRIER TRANSMISSION

The BER of an OFDM system is dependent on several factors, such as the modulation scheme used, the amount of multipath, and the level of noise in the signal. However if we look at the performance of OFDM with just AWGN then the performance of OFDM is exactly the same as that of a single carrier coherent transmission using the same modulation scheme.

If we look at just a single OFDM subcarrier (since the subcarriers are orthogonal to each other, this does not effect the performance in any way) then this is exactly the same as a single carrier transmission that is quadrature modulated with no band pass filtering. The transmitted amplitude and phase is held constant over the period of the symbol and is set based on the modulation scheme and the transmitted data. This transmitted vector is then updated at the start of each symbol. This results in a *sinc* frequency response, which is the required response for OFDM.

The optimal receiver for such a single carrier transmission is to use a coherent matched receiver, which can be implemented by mixing the signal to DC using an IQ mixer. This results in an IQ output that describes the amplitude and phase of the received modulated carrier. The amplitude and phase of the transmitted signal is constant over the symbol period, and so the optimal method of removing the most noise from the signal is to use an integrate-and-dump filter. This filter averages the received IQ vector over the entire symbol, then performs IQ demodulation on the average.

The demodulation of an OFDM signal is performed in exactly the same manner. In the receiver a FFT is used to estimate the amplitude and phase of each subcarrier. The FFT operation is exactly equivalent to IQ mixing each of the subcarriers to DC then applying an integrate-and-dump over the number of samples in the FFT. From this we can see that the FFT performs the same operation as the matched receiver for the single carrier transmission, except now for a bank of subcarriers.

From this we can conclude that in AWGN, OFDM will have the same performance as a single carrier transmission with no band limiting.

However, most propagation environments suffer from the effects of multipath propagation. For a given fixed transmission bandwidth, the symbol rate for a single carrier transmission is very high, whereas for an OFDM signal it is N times lower, where N is the number of subcarriers used. This lower symbol rate results in a lowering of the ISI. In addition to lowering of the symbol rate, OFDM systems can also use a guard period at the start of each symbol. This guard period removes any ISI shorter than its length. If the guard period is sufficiently long, then all the ISI can be removed.

Multipath propagation results in frequency selective fading (see section 3.6 for more details) that leads to fading of individual subcarriers. Most OFDM systems use Forward Error Correction to compensate for the subcarriers that suffer from severe fading. The adaptive modulation scheme proposed in section 4.2 matches the modulation scheme of each subcarrier to its SNR. The additional spectral efficiency of those subcarriers that have a SNR greater than the average (due to constructive interference) tends to compensate for subcarriers that are subjected to fading (destructive interference). As a result of this the performance of such an OFDM system in a multipath environment is similar to its performance in an AWGN channel. The performance of the OFDM system will be primarily determined by the noise seen at the receiver. However, the performance of a single carrier transmission will degrade rapidly in the presence of multipath.

2.6.3 MODULATION LIMITATIONS OF SYSTEMS

Most current mobile communication systems, specifically GSM, IS-95, and 3rd Generation Systems, only use modulation schemes with a high noise tolerance, such as BPSK, QPSK or similar. This results in a low spectral efficiency, but gives improved robustness. These systems use fixed modulation schemes due to the problems with obtaining a high SNR.

The symbol rate of single carrier systems has to be high if they are to obtain a high bit rate, and as a result, systems such as GSM require complex equalisation (up to 4 symbol periods) to cope with multipath propagation. GSM systems are designed to cope with a maximum delay spread of 15 μ s, which corresponds to the typical delay spread experienced at a transmission distance of 30 - 35 km. The symbol rate for GSM is 270 kHz corresponding to a symbol period of 3.7 μ s, thus ISI caused by the multipath spans over 4 symbol periods. This would normally completely destroy the transmitted information, but is recovered in practice by using complex adaptive equalisation. Although this works for robust modulation schemes such as Gaussian Minimum Shift Keying (GMSK) [22], [23] as used in the GSM system, it is difficult to successfully apply to higher modulation schemes, as the residual errors in the equalisation will cause a high error rate.

In DS-CDMA systems the problem is not primarily limited by multipath, but instead inter-user interference. DS-CDMA systems utilise the fact that by spreading the user information over a wide bandwidth it allows multiple users to transmit at the same frequency [26], [27]. Each of these users spread the information signal by multiplying it by a unique higher speed Pseudo Random Sequence (PRS). At the receiver the signal from each user is extracted by multiplying by the same PRS and integrating over the period of an information symbol. This process is however non-orthogonal in the reverse link, resulting in users appearing as noise to each other. The system capacity is maximised when the number of users is maximised, resulting in very high levels of noise. This results in the system typically operating at an Energy per Bit to Noise Ratio (EBNR) of around 5 - 8 dB after demodulation. This rules out the use of high spectral efficiency modulation schemes since the SNR is too low.

OFDM on the other hand, minimises both of these effects. Multipath is minimised by using a low symbol rate and the use of a guard period. Equalisation of the channel can be easily achieved through the use of pilot symbols and or pilot tones. This type of equalisation is accurate and results in minimal residual error, thus allowing a high average SNR. Additionally, users in OFDM are kept orthogonal to each other, by use of time division multiplexing or synchronised frequency division multiplexing, minimising inter-user interference. Both these advantages mean that a high effective channel SNR can be maintained even in a multiuser, multipath environment. This potential for a high SNR means that high modulation schemes can be used in OFDM systems, allowing for improved system spectral efficiency.

Additionally each subcarrier can be allocated a different modulation scheme based on the measured channel conditions. These measurements can be easily obtained as part of the channel equalisation step, allowing subcarriers to be dynamically allocated modulation schemes based on the SNR of each subcarrier. These variations in SNR arise due to interference, transmission distance, frequency selective fading, etc. This technique is known as adaptive modulation and is presented in section 4.2. Those subcarriers with a low SNR can be allocated to use BPSK (1 b/s/Hz) or to transmit no data at all. Subcarriers with a high SNR can transmit higher modulation schemes such as 256-QAM (8 b/s/Hz) allowing a higher system throughput. The modulation allocation is flexible in OFDM systems allowing them to be optimised to local current conditions, rather than having to always use a low modulation scheme just to ensure the system operates during worst-case conditions.

2.6.4 SIMULATION SET UP

The effect of AWGN on OFDM was simulated for a wide range of subcarrier modulation schemes. The IQ diagrams are shown in Table 2-2. The lower density modulation schemes show the data mapping used.

The results presented show the BER performance as a function of the channel SNR. Other simulations in this thesis, present the performance of OFDM under a range of detrimental effects. These simulations measure the performance by finding the effective SNR of the channel instead of the BER. These simulations show the communication performance that corresponds to an equivalent AWGN SNR. The

results presented in this section can then be used to predict the BER for the particular modulation scheme used.

The symbol error rate of most common modulation schemes has been derived in algebraic form [117]. However, the derivation of the BER is difficult due to possibility of multiple bit errors per symbol. Additionally the BER for only square QAM modulation schemes, such as 16-QAM, 64-QAM, 256-QAM, etc, can be calculated directly. To overcome this problem the BER performance of OFDM was obtained by using simulation. There are four main categories of modulation presented, which are, coherent QAM, coherent PSK, differential QAM, and differential PSK.

2.6.5 GRAY CODING

The IQ plot for a modulation scheme shows the transmitted vector for all data word combinations. Each data word combination must be allocated a unique IQ vector. Gray coding is a method for this allocation so that neighbouring points in the constellation only differ by a single bit. This coding helps to minimise the overall bit error rate as it reduces the chance of multiple bit errors occurring from a single symbol error. Figure 2-28 shows an example of gray coding for 16-PSK. Equation (2-11) shows the sequencing for gray coding in decimal format.

Gray coding can be used for all PSK modulation schemes (QPSK, 8-PSK, 16-PSK, etc), and square QAM (16-QAM, 64-QAM, 256-QAM, etc). For square QAM each axis is mapped separately using gray coding.

$$\begin{aligned}
 G_1 &= \{0, 1\} \\
 G_2 &= \{0, 1, 3, 2\} \\
 G_3 &= \{0, 1, 3, 2, 6, 7, 5, 4\} \\
 &\vdots \\
 G_{N+1} &= \left\{G_N(1, 2, 3, \dots, 2^N), G_N(2^N, 2^N - 1, 2^N - 2, \dots, 1) + 2^N\right\}
 \end{aligned} \tag{2-11}$$

Decimal	Gray Coding	Decimal	Gray Coding
0	0, 0, 0, 0	8	1, 1, 0, 0
1	0, 0, 0, 1	9	1, 1, 0, 1
2	0, 0, 1, 1	10	1, 1, 1, 1
3	0, 0, 1, 0	11	1, 1, 1, 0
4	0, 1, 1, 0	12	1, 0, 1, 0
5	0, 1, 1, 1	13	1, 0, 1, 1
6	0, 1, 0, 1	14	1, 0, 0, 1
7	0, 1, 0, 0	15	1, 0, 0, 0

Table 2-1, 4 bit Gray coding in binary

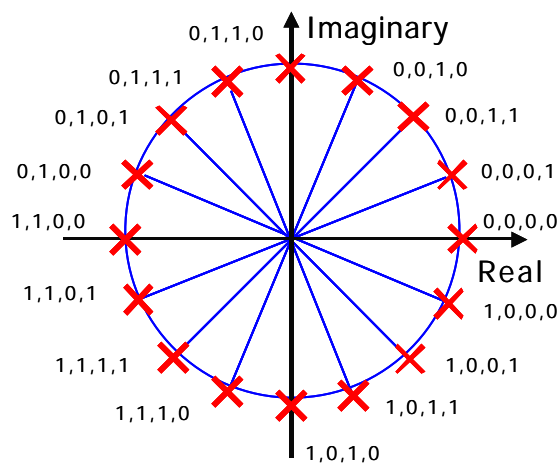


Figure 2-28, IQ plot of 16-PSK using gray coding. Note that each successive IQ location changes by only a single bit.

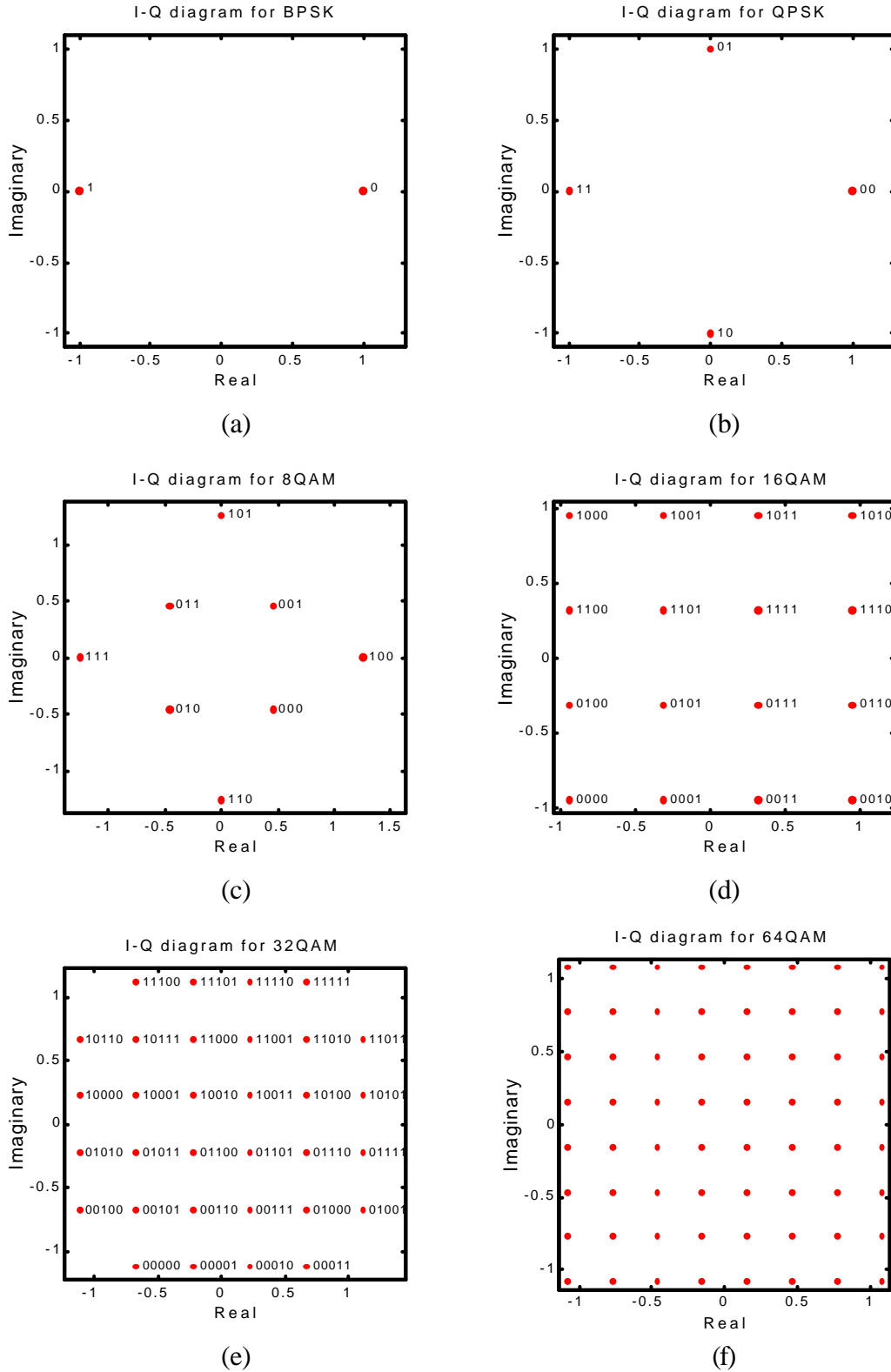


Table 2-2, IQ diagrams for modulations used in the OFDM simulations. (script s0045)

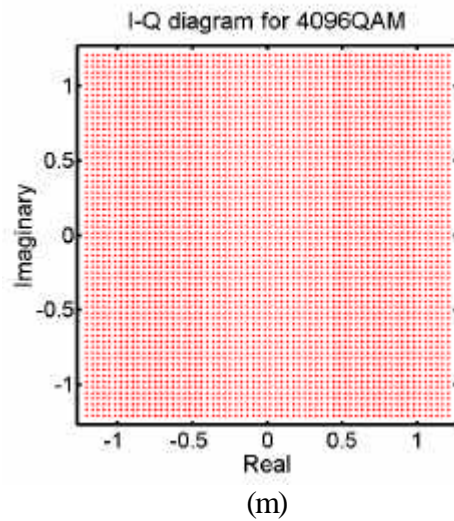
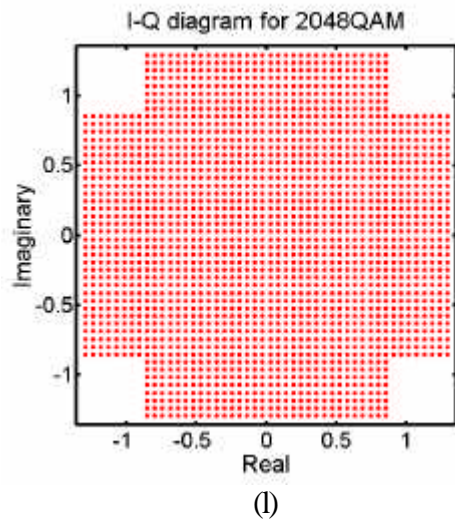
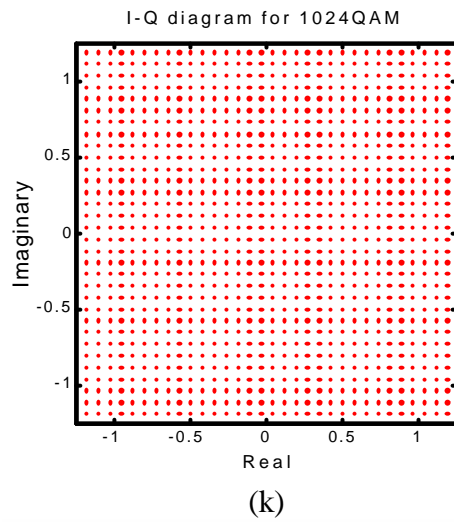
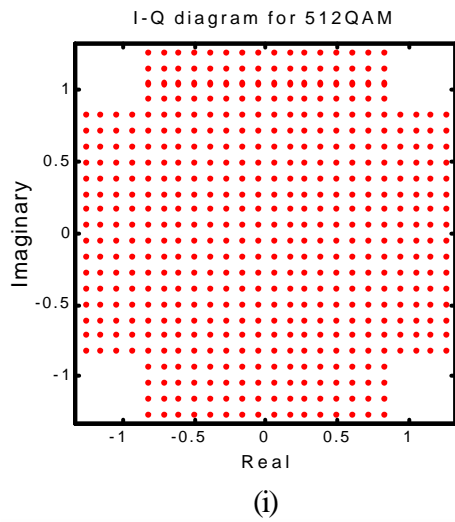
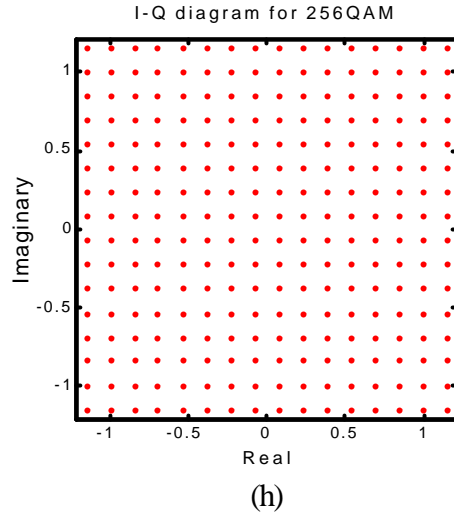
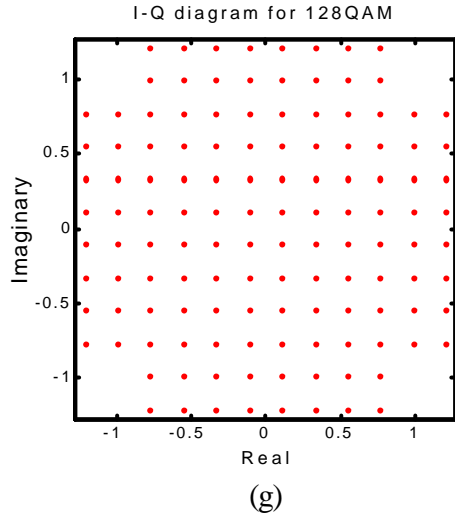


Table 2-2, continued

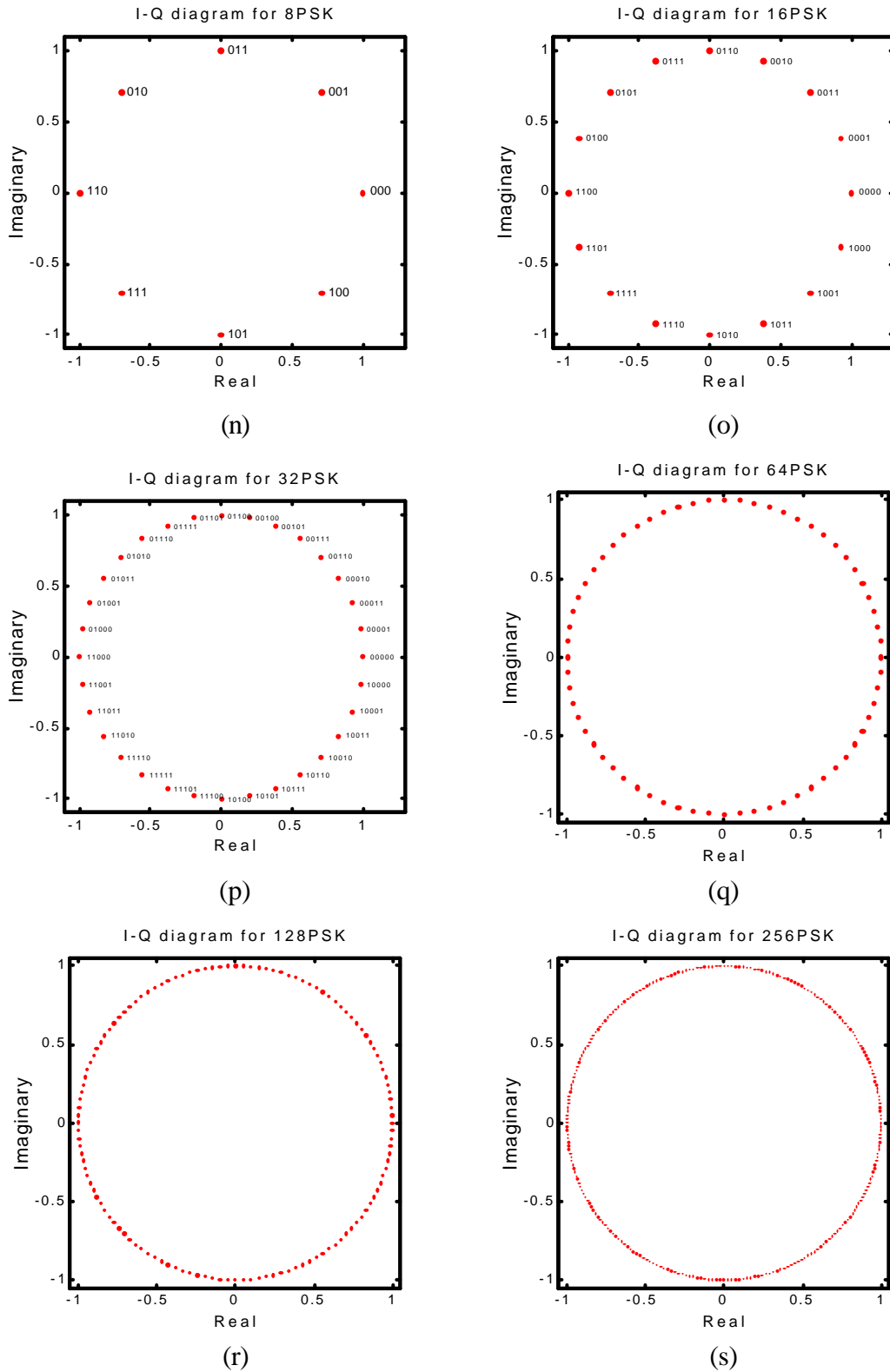


Table 2-2, continued.

2.6.6 COHERENT MODULATION

Coherent modulation is achieved by transmitting the IQ constellation data vectors with absolute phase angles, i.e. if BPSK was used then 0° or 180° would be transmitted. At the receiver it would compare the received phase to 0° or 180° . Phase rotations and amplitude scaling (important for QAM), greatly increase the error rate, or completely destroy all communications. This problem is however overcome by using channel equalisation to remove this scaling of the channel before demodulation. The phase rotation of the channel and the amplitude scaling is measured using pilot symbols and pilot tones, which contain a known IQ transmission vector. In a static channel with no movement, the response of the channel will be constant, and thus once measured and corrected for, data can be sent reliably. However in most applications radio channels are non-static. Frequency selective fading cause complete fades in the spectrum approximately once every wavelength of movement, causing the response of the channel to change rapidly during movement. Tracking of the channel requires continual updates in the channel equalisation, thus regular pilot symbols/tones must be inserted into the transmission. The greater the number of pilot signals the faster the channel tracking rate, however this also causes significant overhead. A more detailed analysis of the effectiveness of pilot tones in channels effected by AWGN can be found in section 2.7, page 69.

2.6.7 DIFFERENTIAL PHASE MODULATION

Another common method for subcarrier modulation is to send the data differentially. Instead of each symbol being independent of each other, the transmitted information is sent as a difference between symbols vectors. Differential Phase Shift Keying (DPSK) is the most common method of sending differential information. Instead of mapping data to an absolute phase angle, as in the case of coherent modulation, DPSK maps the data to a phase difference between symbols. The transmitted phase corresponds to the cumulative sum of the phase differences. For example, for differential QPSK each symbol transmits 2 bits of information, corresponding to 4 different phase differences. Table 2-2(b) shows the IQ diagram for coherent QPSK.

D-QPSK has the same IQ diagram except that each data combination corresponds to a phase difference. The most obvious method for allocating word combinations to phase differences, is to linearly map the binary word combinations to a linear phase difference, as shown in Table 2-3. For example, if the data to be transmitted is {1,0 1,1 0,0 0,1} then the differential phase would be {180°, 270°, 0°, 90°}, thus if the starting phase is 0° then the transmitted phase would be {180°, 180°+270° = 90°, (90°+0°) = 90°, (90°+90°) = 180°}.

In a noisy channel phase errors can result in the received phase being closer to the next or previous phase difference combinations, causing a symbol error. The number of bits in error depends on the data word mapping. Linear mapping is not optimal as a wrap around error from 270° to 0° causes a double bit error (1,1) to (0,0). By using gray coding, the number of bit errors can be reduced by ensuring that the phase-difference combinations that are closest to each other, only differ by a single bit in the data word.

Data Word	Phase Difference (linear mapping)	Phase Difference (gray coding)
0,0	0°	0°
0,1	90°	90°
1,0	180°	270°
1,1	270°	180°

Table 2-3, Phase mapping for differential QPSK.

This shows two options for allocating data word combinations to the transmitted phase difference.

Differential modulation has the advantage of cancelling out channel phase rotations, eliminating the need for additional channel equalisation. Additionally the phase tracking of the channel is effectively updated at the symbol rate, thus tracking the channel very quickly. Differential modulation is thus highly suited to mobile communication. The disadvantage of differential modulation is the limited range of modulation schemes, and that it requires about 3 dB higher SNR than coherent modulation. The output symbol phase corresponds to the phase difference between the present and previous symbols, and as a result the symbol noise is doubled (degrading the performance by 3 dB) compared with the phase noise of a single symbol (as used in coherent modulation).

2.6.8 DIFFERENTIAL QAM

Differential mapping can be applied to QAM modulation, with some limitations. For differential modulation to work, the mapping of the data to modulation domain must wrap. For example with differential PSK the transmitted phase is found by mapping each data word to a phase from 0 to 2π , then integrating this mapping from symbol to symbol. The phase wraps in a circular fashion as it is constrained to the range 0 to 2π . The receiver decodes the phase by taking the phase difference between symbols. To achieve this type of mapping with a QAM scheme the input data can be split into two data streams of $N/2$ bits each per symbol, where N is the number of bits per symbol. The number of bits per symbol must be even and so this mapping can only be done for square QAM mapping such as 16-QAM, 64-QAM, etc. Each $N/2$ bit data stream is mapped to the (I) real and (Q) imaginary axes to form the resulting transmitted vector. Because the signal is differentially modulated each axis is modulo integrated from symbol to symbol. Figure 2-29 shows an example of differential QAM. If we examine just one axis, then if the data to be transmitted was: {1, 2, 0, 3, 1}, and we started with a reference of 0, then the differentially encoded signal can be found by taking the cumulative sum of the data words {1, 3, 3, 6, 7} then modulo wrapping it to the bounds 0 to 3, resulting in {1, 3, 3, 2, 3}. The receiver decodes this by taking the difference, {1, 2, 0, -1, 1}, remembering that the reference at the start was 0, then wrapping from 0 to 3, resulting in {1, 2, 0, 3, 1}.

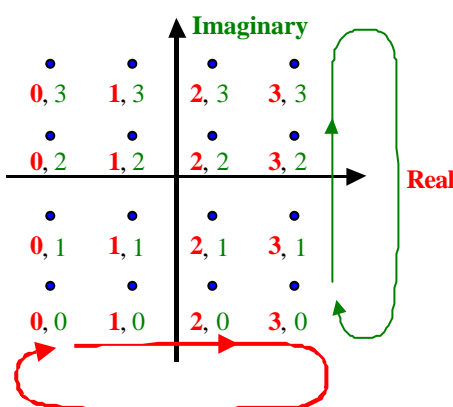
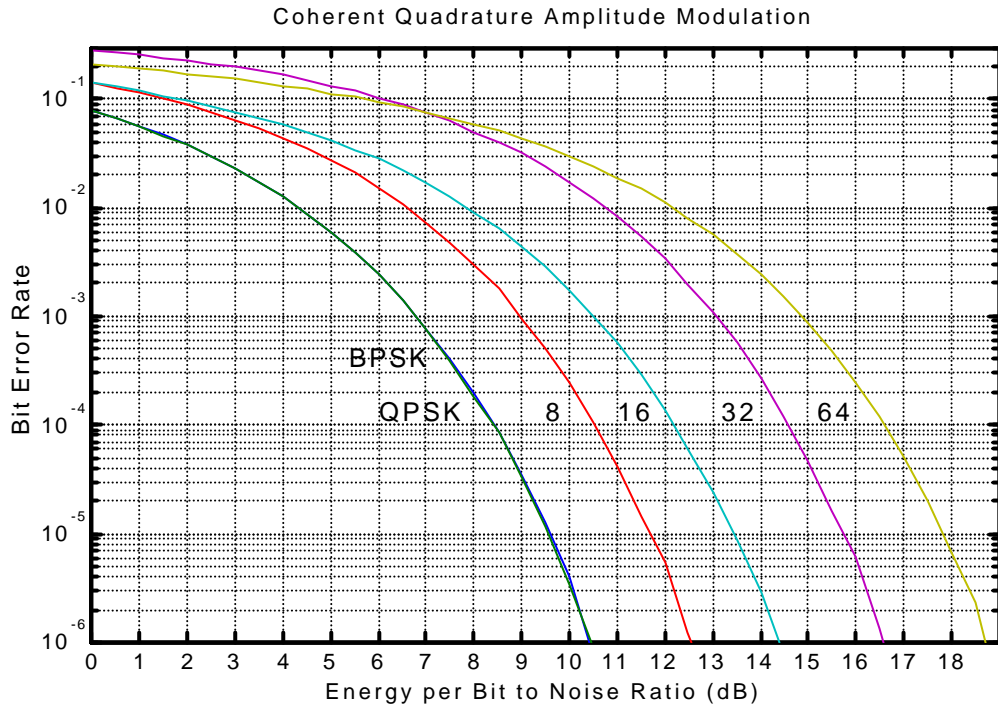
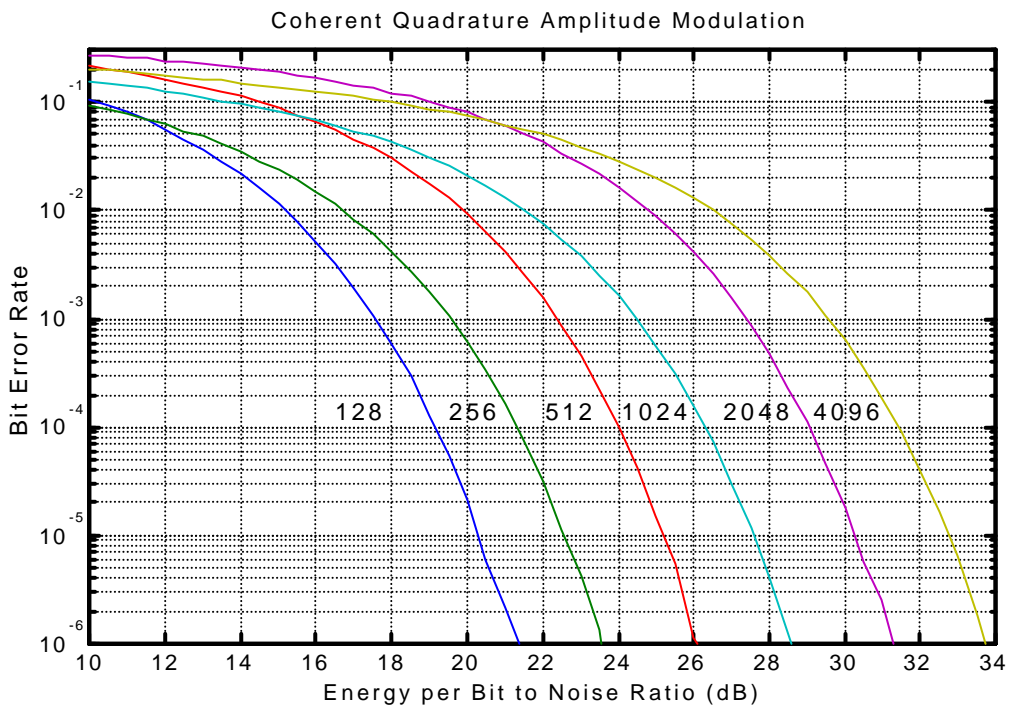


Figure 2-29, IQ data mapping for differential 16-QAM.

Data is split in two equal numbers of bits, then modulo integrated from symbol to symbol. Each number represents 2 bits (0 - 3) with each pair being 4 bits.

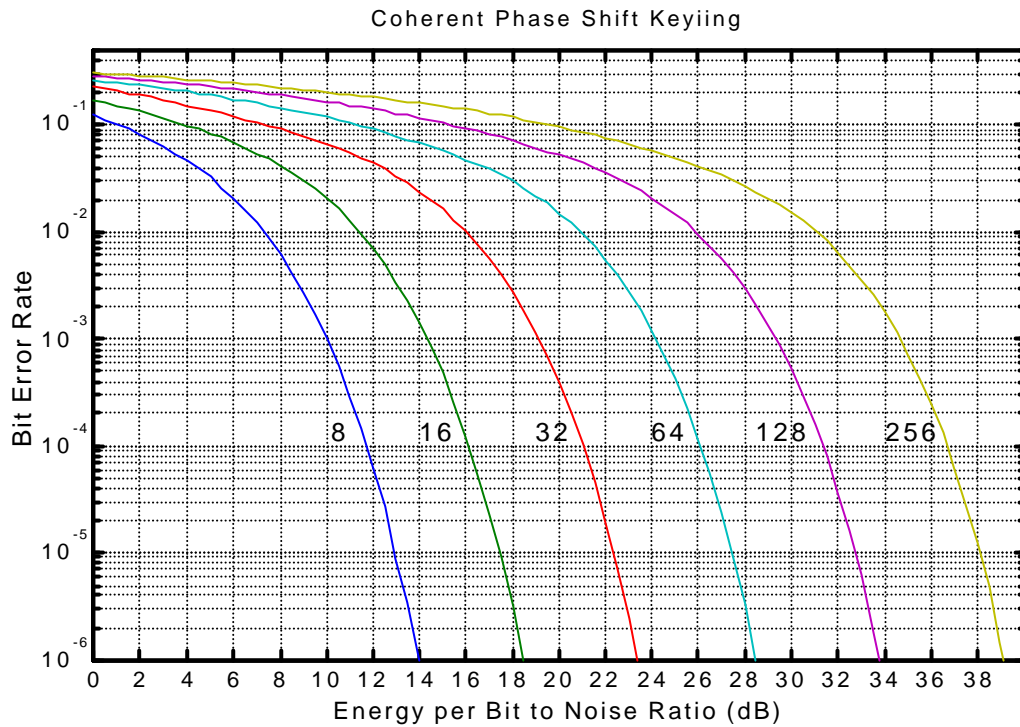


(a) BPSK, QPSK, 8-QAM, 16-QAM, 32-QAM, 64-QAM
Note: BPSK and QPSK have the same EBNR performance.

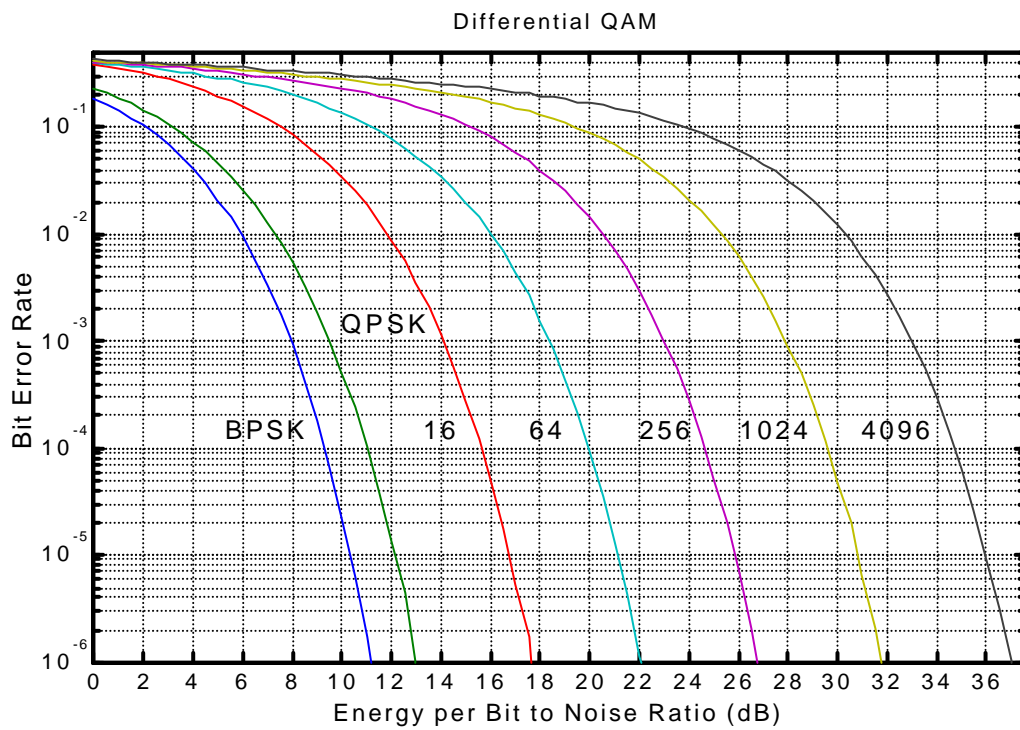


(b) 128-QAM, 256-QAM, 512-QAM, 1024-QAM, 2048-QAM, 4096-QAM

Figure 2-30 part 1 of 3. Note: Modulation schemes with an order number of bits per symbol (8-QAM, 32-QAM, 128-QAM, etc) don't use gray coding, resulting in a higher BER at a low EBNR.

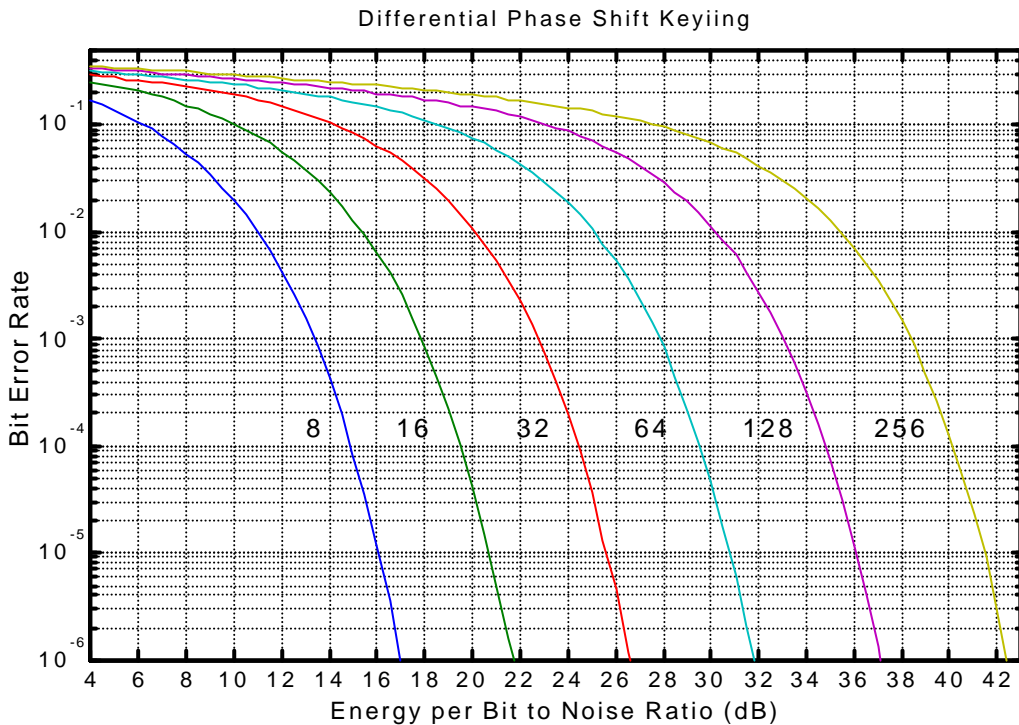


(c) 8-PSK, 16-PSK, 32-PSK, 64-PSK, 128-PSK, 256-PSK



(d) D-BPSK, D-QPSK, D-16QAM, D-64QAM, D-256QAM, D-1024QAM, D-4096QAM

Figure 2-30 part 2 of 3



(f) D-8PSK, D-16 PSK, D-32 PSK, D-64 PSK, D-128 PSK, D-256 PSK

Figure 2-30, Bit Error Rate verses the Energy per Bit to Noise Ratio for a selection of OFDM modulation schemes. (script s0041)

The number matching each line on the plot corresponds to the modulation scheme. For example, for part (e) the numbers 8, 16, 32, etc correspond to D-8PSK, D-16PSK, and D-32PSK, where D means differential.

2.6.9 SIMULATION RESULTS

The simulated performance for the modulation schemes tested is shown in Figure 2-30. These show the BER as a function of the Energy per Bit to Noise Ratio (EBNR). This is a measure of the energy efficiency of a modulation scheme. If a higher EBNR is needed to transfer data for a given modulation scheme, then it means that more energy is required for each bit transfer. Low spectral efficiency modulation schemes, such as BPSK and QPSK, require a lower EBNR, and hence are more energy efficient. For a power limited system, with unbounded bandwidth, the maximum data rate could be achieved using BPSK or QPSK. However, in most applications the available bandwidth is the limiting factor and so the data rate is maximised by using a more spectrally efficient modulation schemes such as 256-

QAM. The BER verses the SNR can be calculated from EBNR shown on the plots in Figure 2-30. The SNR for each modulation takes into account the number of bits per symbol, and so the signal power corresponds to the energy per bit times the number of bits per symbol. In log scale the SNR for a given EBNR can be found with:

$$SNR = 10 \cdot \log_{10}(N_b) + EBNR_{dB}$$

where SNR is in dB, N_b is the number of bits per symbol for the modulation scheme and $EBNR_{dB}$ is the EBNR in dB. For example, for 256-PSK the number of bits transferred per symbol is 8 bits/symbol and thus the SNR is $10\log_{10}(8)+EBNR$, thus for an EBNR of 40 dB, the SNR is 49 dB.

Figure 2-31 shows a comparison between all of the modulation schemes simulated. It shows the required SNR for a fixed BER of 1×10^{-5} . Coherent QAM performs best requiring the least SNR, while differential PSK is the worst. Also shown is Shannon's limit, which represents the lowest possible SNR for a given spectral efficiency over which zero error communications can occur. In order for a communication system to approach Shannon's limit powerful forward error correction coding techniques must be used. For the BER shown coherent QAM is approximately 7.5 dB worse than Shannon's limit. For QAM the required SNR for a fixed BER increases by approximately 3 dB for each additional 1 b/s/Hz in spectral efficiency, which matches the same slope as Shannon's limit. In comparison, for PSK the required SNR increases by 6 dB for each addition 1 b/s/Hz resulting in the capacity of PSK modulation techniques being approximately half that of QAM for the same SNR. The low efficiency of PSK is a result of under utilisation of the IQ vector space. PSK only uses the phase angle to convey information, with amplitude being ignored. QAM uses both amplitude and phase for information transfer and so is more efficient.

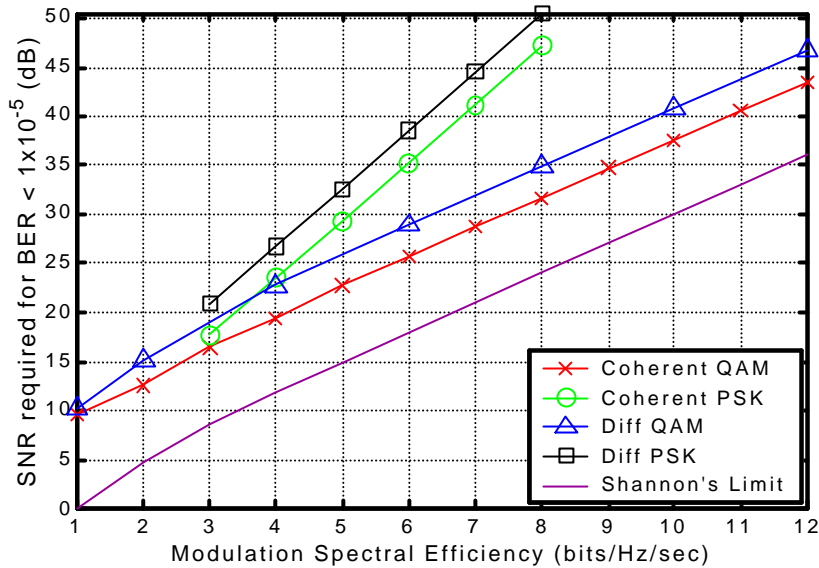


Figure 2-31, SNR required to maintain a BER of $< 1 \times 10^{-5}$, for all the simulated modulation schemes. (script s0046)

Also shown is Shannon's Limit. Note that the slope for QAM is 3 dB per bit/Hz/sec, whereas for PSK it is 6 dB per bit/Hz/sec.

2.7 EFFECT OF PILOT SYMBOL CHANNEL EQUALISATION IN COHERENT MODULATION

Coherent modulation schemes rely on channel equalisation to compensate for phase rotations and amplitude scaling. Without equalisation, the error rate is excessively large making communications impossible. The effectiveness of the channel equalisation depends on the accuracy of the channel characterisation measurements. However, these measurements are subjected to the same channel noise as the data transmission, resulting in measurement noise. This noise can be minimised by allocating more energy to the pilot tones / symbols, which can be achieved by increasing the relative power of the pilot tones / symbols, or by averaging multiple pilot symbols.

Averaging multiple pilot symbols allows the noise on the channel measurements to be made arbitrarily small, by increasing the number of symbols averaged over. However the greater the amount of averaging the larger the overhead used by the channel characterisation. This limits the allowable characterisation rate for a fixed

amount of overhead, effectively determining the maximum velocity of movement that the system can handle.

A better method for minimising the noise on the channel characterisation is to increase the transmitted power for the pilot symbols. However care must be taken when increasing the power of the pilot symbols, as it can result in excessive distortion. This will lead to inter-modulation distortion products limiting the effective SNR, defeating the original purpose. This problem can be minimised by using pilot symbols that have a low Crest Factor (CF). See section 6.1 for information about the CF of signals. The CF of random data words is very high, typically 8 - 10 dB, with a worst case of $10\log_{10}(N)$ where N is the number of subcarriers (see Figure 6-4). Because of this the average transmitted power is usually 8 - 10 dB lower than the peak output power of the transmitter to prevent clipping (see section 2.8). This can be exploited as it allows a low CF pilot symbol to be boosted in power without causing any clipping. Chapter 6 outlines several methods for generating low CF pilot symbols, and shows that Genetic Algorithms (GA) can be used to produce pilot symbols with a CF of less than 1 dB. This allows the pilot symbol to be boosted in power by 3 - 6 dB, compared with data symbols. This will give the same performance as sending 2 - 4 pilot symbols, with a symbol power equal to the data symbols.

Table 2-4 shows the detrimental effects of channel measurement noise on the BER for different modulation schemes. The noise in the channel characterisation means that to achieve the same BER performance as with perfect characterisation, the SNR must be higher. When only a single pilot symbol is used the noise performance is about 3 dB worse, which is almost exactly the same as the performance loss when using differential modulation. The SNR performance loss reduces almost proportionally with the number of pilot tones, thus the loss when using 4 pilot tones is 4 times lower (in dB). For example from Table 2-4(b) at a BER of 1×10^{-4} the performance loss when using only a single pilot symbol is 2.4 dB, when four symbols are used the loss reduces to 0.6 dB.

From the simulated results a single low CF pilot symbol with a boosted power of 6 dB would result in the performance loss due to imperfect channel characterisation of 0.1 dB to 0.9 dB depending on the modulation scheme.

Number of Pilot Symbols	BER $1 \cdot 10^{-2}$	BER $1 \cdot 10^{-3}$	BER $1 \cdot 10^{-4}$	BER $1 \cdot 10^{-5}$
1	1.55	1.2	1	0.8
2	0.6	0.35	0.2	0.15
3	0.3	0.2	0.15	0.15
4	0.2	0.15	0.1	0.1

(a) BPSK

Number of Pilot Symbols	BER $1 \cdot 10^{-2}$	BER $1 \cdot 10^{-3}$	BER $1 \cdot 10^{-4}$	BER $1 \cdot 10^{-5}$
1	2.5	2.4	2.4	2.35
2	1.3	1.3	1.2	1.2
3	0.85	0.8	0.8	0.7
4	0.65	0.6	0.6	0.45
8	0.35	0.3	0.3	0.2

(b) QPSK

Number of Pilot Symbols	BER $1 \cdot 10^{-2}$	BER $1 \cdot 10^{-3}$	BER $1 \cdot 10^{-4}$	BER $1 \cdot 10^{-5}$
1	2.7	2.95	3.05	3.2
2	1.5	1.65	1.7	1.75
3	1.05	1.1	1.15	1.15
4	0.8	0.85	0.85	0.85
8	0.4	0.45	0.4	0.4

(c) 16-QAM

Number of Pilot Symbols	BER $1 \cdot 10^{-2}$	BER $1 \cdot 10^{-3}$	BER $1 \cdot 10^{-4}$	BER $1 \cdot 10^{-5}$
1	2.85	3.15	3.4	3.6
2	1.6	1.7	1.9	2.05
3	1.1	1.2	1.3	1.4
4	0.85	0.9	0.95	1
8	0.45	0.45	0.5	0.45

(d) 64-QAM

Number of Pilot Symbols	BER $1 \cdot 10^{-2}$	BER $1 \cdot 10^{-3}$	BER $1 \cdot 10^{-4}$	BER $1 \cdot 10^{-5}$
1	2.95	3.3	3.6	3.75
2	1.7	1.85	2.05	2.25
3	1.25	1.3	1.35	1.5
4	0.9	0.95	1.05	1.1
8	0.45	0.5	0.5	0.55

(e) 256-QAM

Table 2-4, SNR degradation in dB due to imperfect channel estimation.

Pilot symbols were used to perform channel estimation. These pilot symbols are subject to channel noise and thus result in imperfect channel estimation and an increase in the BER. The tables show degradation in SNR (i.e. need a higher SNR for the same error rate) as compared with perfect channel estimation.

These results were obtained by simulating the OFDM transmission using different number of reference symbols. The total number of bits simulated was 7×10^9 . (BER simulations were performed using script s0041_ofdmber, and the tables generated using s0042_ref_degradation)

2.8 EFFECT OF DISTORTION ON OFDM

One of the problems with OFDM is that the signal has a high peak power compared with its average power. When an RF carrier is modulated with an OFDM signal it results in a similar variation in power of the carrier envelope. This results in the requirement that the signal is amplified and transmitted in a linear way. It is very difficult to maintain a high degree of linearity at high power levels, and so most of the distortion in a radio transmission usually occurs in the power amplifier of the transmitter. Some additional distortion can occur in the receiver if it is not designed properly, but in general it is relatively easy to keep the level of distortion in the receiver significantly lower than the transmitter. Distortion in the transmitter causes the most problems in the transmission chain, as it can result in spectral spreading, which can cause interference to neighbouring systems in RF frequency. For this reason we will focus on the effects of distortion in the transmitter.

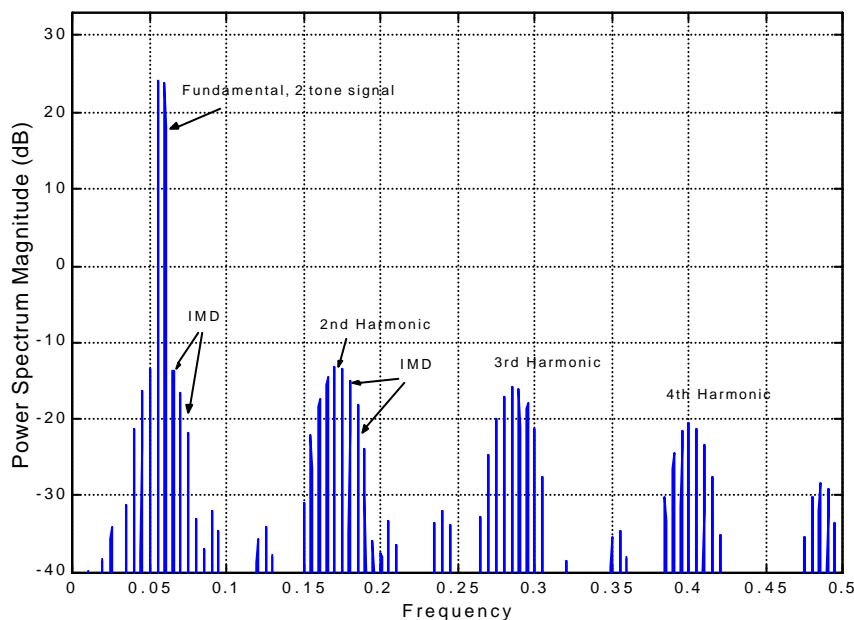


Figure 2-32, Effect of distortion on a 2 tone signal, showing harmonics and IMD. (script s0049)

Non-linearities in the transmission result in two main distortion products, Inter-Modulation Distortion (IMD) and harmonics. Figure 2-32 shows the effect of clipping distortion on a 2-tone signal. OFDM signals are made up from a large number of subcarriers resulting in many distortion products.

Harmonics result in frequency components at X times the RF carrier frequency, where X is an integer. Thus if we have a 900 MHz RF carrier the harmonics will occur at 1800 MHz, 2.7 GHz, etc. Harmonics can easily be removed using a relatively simple low pass filter on the output of the transmitter.

IMD is much more of a problem as it results in distortion components, which are in-band and out of band but close to the main transmission. These components are a result of mixing between each of the harmonics of the system, and subsequent mixing between the IMD products. In-band components result in added noise to the OFDM signal at the receiver, effectively limiting the SNR of the system, even in the absence of other sources of noise. Out of band components spread the signal in bandwidth, resulting in potential interference with other radio communications in neighbouring frequency bands. Even if the signal is perfectly band-limited before going to the transmitter power amplifier, spectral spreading will occur if the power amplifier is non-linear. Spectral spreading can be slightly reduced by using analog band pass filters after the power amplifier, however these will generally not have a sharp roll off because they are operating at the RF frequency.

The effect of distortion on OFDM transmissions has previously been studied by [54]-[56]. In [54] the effect of three different amplifier distortion models on the performance of DAB transmission is compared. The amplifier models compared are a Solid State Power Amplifier (SSPA), a Travelling Wave Tube Amplifier (TWTA) and a perfectly linearised amplifier. The results show that the optimal Output power Back Off (OBO) (see next section for explanation of OBO) for DAB is approximately 2 - 3 dB, with only a small difference of 0.6 dB due to the different amplifier models. These results are however limited to OFDM transmissions using QPSK, which is a very robust modulation scheme, and hence robust against effects of distortion. Modulation schemes that have a higher spectral efficiency (such as 16-QAM, 256-QAM, etc) are more susceptible to the effects of distortion due to the requirement of a higher effective SNR. In [55] the performance of both a QPSK and

a 16-QAM OFDM system was investigated. The optimal OBO for QPSK transmissions were found to be 3 dB in this study, which compare well with results presented in [54]. For 16-QAM the optimal OBO was found to be higher, approximately 6 dB. The performance of a 64-QAM modulated OFDM signal was investigated in [56], which showed that the optimal OBO is 6 dB for clipping distortion, and closer to 10 dB for a smooth limiter. Each of these papers show the performance of a fixed system, limiting the usefulness of the results. A more general study is presented showing the performance of an OFDM system as a function of clipping distortion. The effect of distortion causes in-band noise due to IMD, resulting in a lowering of the effective SNR of the channel. The results are presented as an effective SNR of the OFDM channel, and so are independent of any particular modulation scheme. The BER for a particular modulation scheme can be found from the effective SNR by using the results shown in section 2.6.

2.8.1 DISTORTION MODELLING

Distortion results from any non-linearity in the system. It is also dependent on the actual signal waveform and its power level. A signal with a high peak to average power ratio will tend to have peaks which operate much closer to the maximum range of the amplifier than say a sine wave, for the same average power. The amount of distortion is dependent on the signal envelope distribution as well as shape of the non-linearity of the amplifier. It is therefore difficult to compare the distortion analysis of one signal type to another.

Figure 2-33 shows the input verses output for a real amplifier. This result shows that the amplifier is not perfectly linear up to the clipping power, but tends to roll off as it becomes saturated. Additionally it shows that the response is not symmetrical in that the positive half of the output clips at a lower level than the negative side.

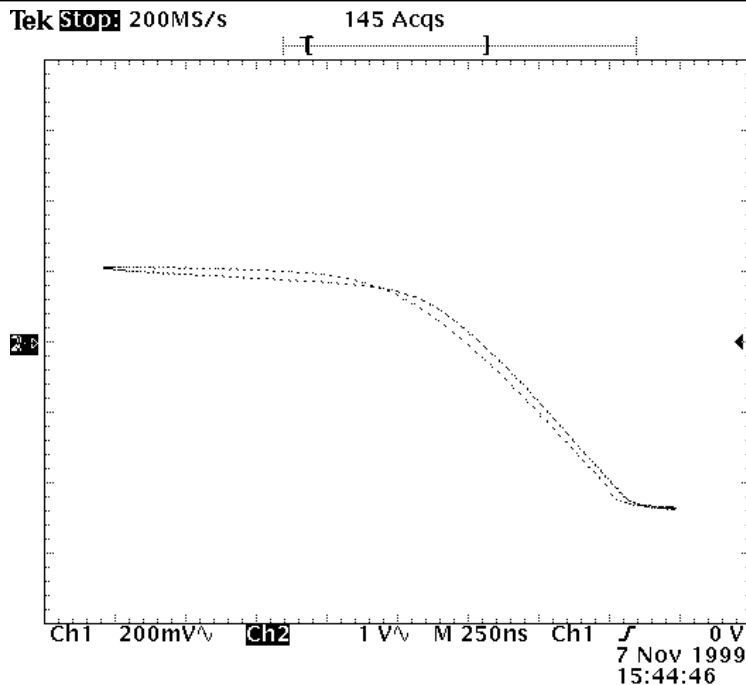


Figure 2-33, Measured Input verses Output for an MAR6 amplifier, showing distortion.

This amplifier is a class A MMIC RF amplifier. This is an inverting amplifier resulting in the linear slope being negative. Also the signals are AC coupled, resulting in the plot not passing through 0.

One way to reduce the effects of non-linearities in the transmitter power amplifier is the use of predistortion [57]-[61]. This involves predistorting the signal before the power amplifier in such a way as to cancel the distortion caused by the power amplifier. This predistortion is typically done at base band by changing the amplitude and phase of the time waveform. The most general form of predistortion uses feedback from the power amplifier output to achieve an accurate linearisation.

Predistortion can reduce distortion from non-linearities of the transmitter power amplifiers. It however cannot prevent distortion from clipping of the signal at high power levels, due to the limited peak power of any real amplifier.

Figure 2-34 shows the input verses output of the distortion model used for the simulations. In fact this is a model of a perfectly linear, but power limited amplifier, which is the best result that could be obtained. Distortion is a result of clipping of the signal power.

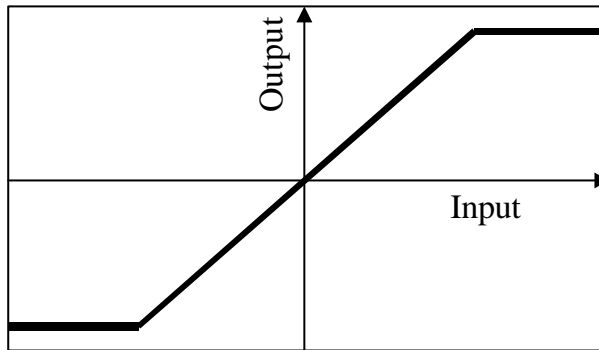


Figure 2-34, Input verses Output for a power limited linear amplifier.

This is the distortion model used for the simulations.

One method for estimating the efficient use of the output power amplifier is the Output power Back Off (OBO), which is defined as

$$OBO = 10 \cdot \log_{10} \frac{P_{sat}}{P_o} \quad (2-12)$$

where P_{sat} is the saturation power of the amplifier and P_o is the average output signal power. It is desirable to operate at a low OBO to allow high utilisation of the available power. This however tends to result in excessive distortion degrading the signal, and generating out of band spectral spreading.

The OBO is measured based on the average power of the signal after clipping, making it difficult to directly determine the required amount of clipping to be applied to the input signal. The amount of clipping required varies depending on the signal amplitude distribution. To overcome this difficulty, an iterative solution was used to determine this level to meet the required OBO.

The simulation results show the effect of clipping distortion on the performance of OFDM. For real amplifiers the onset of distortion is not as abrupt as clipping, and so the performance of the system will be degraded even before the signal power reaches the clipping power. This must be taken into account when studying the results of the simulations.

2.8.2 SPECTRAL SPREADING FROM DISTORTION CLIPPING

Figure 2-35 shows the spectrum of an OFDM signal that is clipped in power. The OFDM signal was band pass limited using an FIR filter, before being subjected to clipping distortion. This was done to remove the OFDM side lobes so that the spectral spreading caused by the clipping could be easily seen. The out of band interference increases as the OBO is reduced, resulting in significant out of band noise for OBOs below 8 dB. It can also be seen that the out of band interference slowly decays with frequency. Figure 2-36 shows the strength of the spectral spreading as a function of the OBO for an OFDM signal with 100 subcarriers. This shows that for an OBO of greater than 10 dB there is virtually no spectral spreading. This plot shows two results, the first being the level of out of band noise 100 subcarrier-spacings away from the signal centre (100% of system bandwidth), and the other 200 subcarriers away from the centre (200% of the system bandwidth). Several other tests were done to find the effect of changing the number of subcarriers, however it was found that the results were almost independent of the number of system subcarriers.

The worst case CF for an OFDM signal is $10 \times \log_{10}(N)$ where N is the number of subcarriers, and so for a 100 subcarrier signal the worst case CF is 20 dB. This would tend to suggest that significant distortion should occur for an OBO all the way up to 20 dB. This is not the case due to the CF distribution of OFDM signals. Even though the worst case CF is very high, the probability of it occurring is incredibly small. Figure 2-37 shows the CF distribution for OFDM signals. This shows that for signals with 100 subcarriers, only 1% of the symbols have a CF greater than 10 dB. Even these symbols will only have a very small fraction of the total symbol energy above 10 dB, and so clipping at 10 dB OBO has little effect.

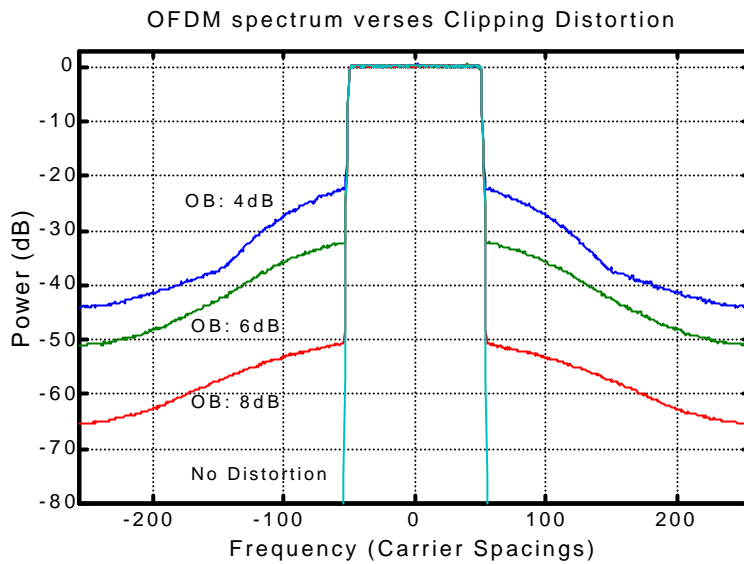


Figure 2-35, Spectrum of OFDM signal with clipping distortion. (script s0048)

This is for a 100 subcarrier OFDM signal, which has been frequency band limited using an FIR (see section 2.4.1) before the distortion was applied.

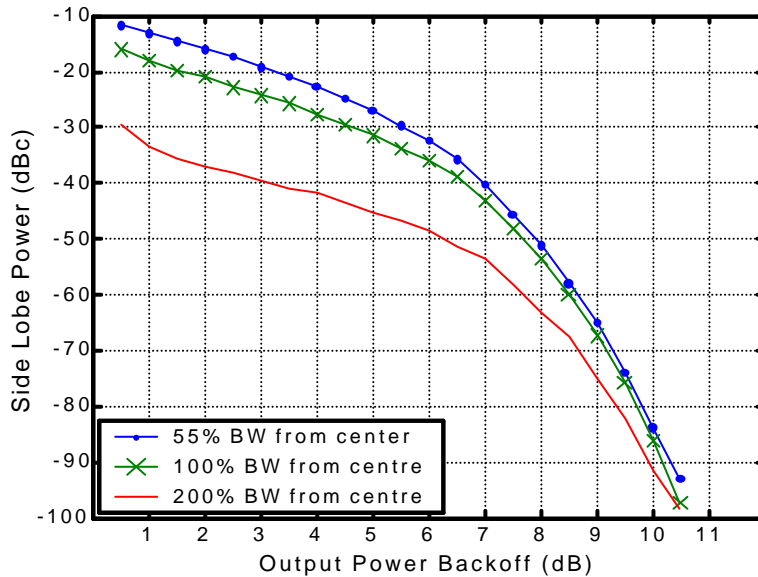


Figure 2-36, Strength of the spectral spreading as a function of the Output Power Backoff. (script s0048)

The distortion is caused by dipping of the signal. The spectrum of the OFDM signal goes up to 50% of the signal bandwidth (BW) from centre and so the 55% BW from the centre result corresponds to the out of band energy just outside the pass band.

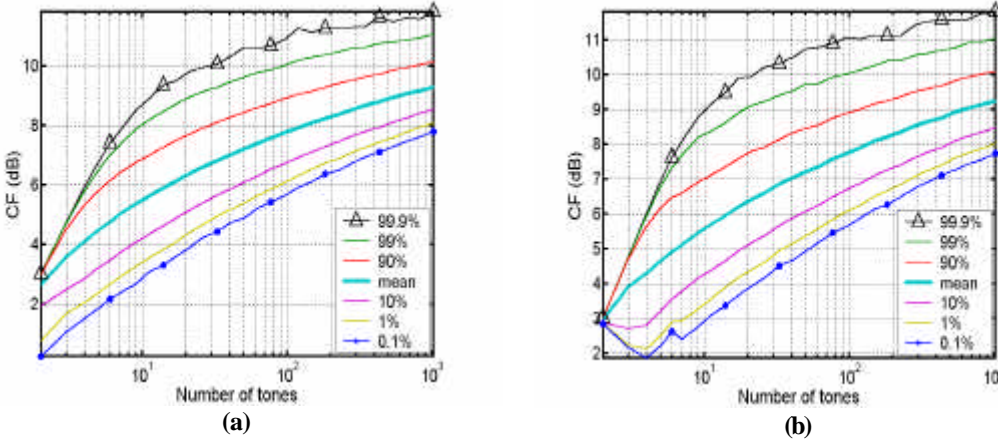


Figure 2-37, Crest Factor distribution verses number of subcarriers for an OFDM signal. (script s0032)

(a) Random phase modulation. **(b)** Random QAM modulation.

2.8.3 EFFECTIVE SNR FROM CLIPPING DISTORTION

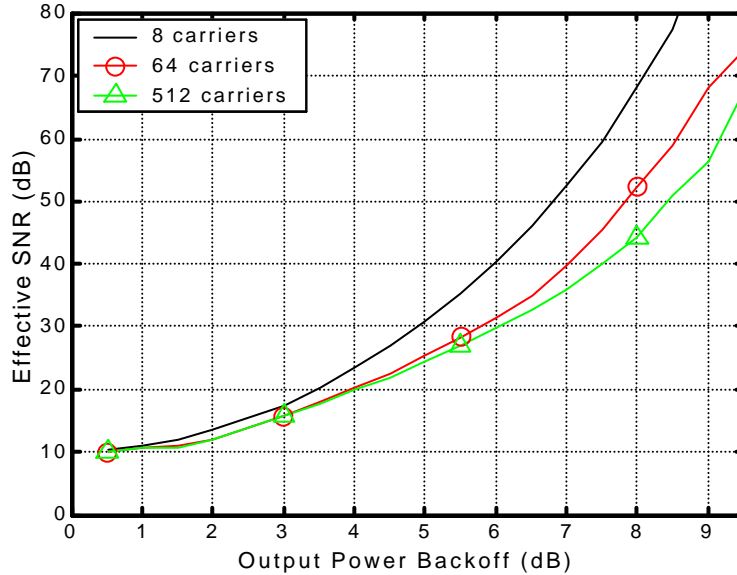


Figure 2-38, Effective SNR of an OFDM transmission verses the Output Power Backoff for 8, 64 and 512 transmission subcarriers. (script s0052)

Figure 2-38 shows the effective SNR of an OFDM transmission subjected to clipping distortion. The number of carriers has relatively little effect on the results. The CF of most OFDM signals is around 8 - 12 dB, and so we would expect clipping distortion to start to have a detrimental effect on the signal for an OBO of 8 - 12 dB. Figure 2-37 shows the distribution of the CF for random OFDM signals as a function of the number of subcarriers. This shows that the CF levels out at about 10 - 12 dB even for

large numbers of subcarriers. In addition to this, even if the CF is greater than the OBO, the peaks in the signal are only a small fraction of the total symbol period and thus clipping them result in only minor distortion to the overall symbol. This means that the effect of clipping distortion is almost independent of the number of subcarriers in the OFDM signal.

Figure 2-31 shows that for QPSK an effective SNR of 12 dB is needed to maintain a BER lower than 1×10^{-5} . From Figure 2-38 an OBO of as low as 2.5 dB can be used while still maintaining a sufficient effective SNR for QPSK. This matches closely with published results in [54] and [55], which showed an optimal OBO for QPSK of 2 - 3 dB. For 64-QAM, Figure 2-31 shows that an effective SNR of 26 dB is needed, which corresponds to a minimum OBO of 5.5 dB from Figure 2-38. This is slightly lower than the result published in [56] of 6 dB. This slight difference is due to the lower BER used and the increased number of subcarriers used in the simulations in [56].

2.8.4 EFFECT OF PILOT SYMBOL TYPE ON THE BER WITH DISTORTION

Coherent carrier modulation requires channel equalisation in order to work correctly. If the pilot symbols used for this are effected by distortion or noise then the overall system BER greatly increases. Pilot symbols consist of an OFDM symbol with a known amplitude and phase, allowing channel characteristics to be calculated. Preferably the phasing of the subcarriers should be chosen in such a way as to minimise the pilot symbol CF. This will help to prevent distortion from effecting the symbol. Additionally if a low CF symbol is used, its power can be boosted compared with the data symbols without causing clipping. This helps to improve the accuracy of the channel equalisation, minimising the BER in the presence of noise. (see section 2.7).

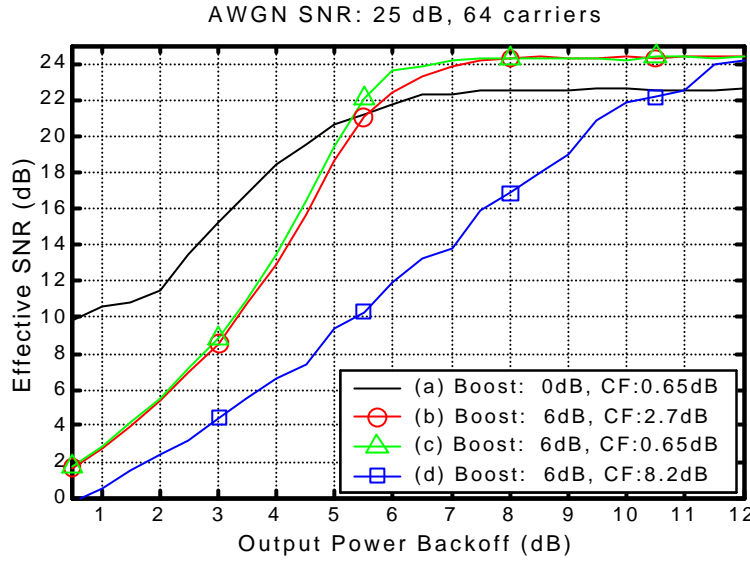


Figure 2-39, Effective SNR verses output power backoff using different pilot symbols. (script s0054)

- (a) Genetic Algorithm Optimised phasing scheme (average power equal to data power), (b) Quadratic Phasing Scheme [106], boosted by 6 dB in power, (c) GA Optimised phasing scheme boosted by 6dB, (d) random phase angle symbol boosted by 6 dB.

Figure 2-39 shows the effective SNR verses OBO for four different pilot symbol schemes. As well as distortion, AWGN was added to assess the effectiveness of the pilot symbol for estimating the channel response. The SNR of the simulation was set to 25 dB. As the OBO is increased the effective SNR of the OFDM channel also increases, approaching the upper limit of 25 dB. Figure 2-39 (a) shows the result for a single pilot symbol that has a CF of 0.65 dB (see section 6.2 for more detail on the phasing scheme used). From an OBO of 1 to 4 dB the effective SNR follows the same performance as that simulated in Figure 2-38. Even though the CF of the pilot symbol is 0.65 dB the data symbols are not, resulting in the degradation shown in the simulation. Above 4 dB the effect of the AWGN begins to limit the effective SNR. Above an OBO of 7 dB the effective SNR is capped at 22.5 dB. This is a degradation of 2.5 dB compared with the ideal performance of 25 dB, and is a result of noise on the channel characterisation, which is estimated from the pilot symbol.

Figure 2-39 (c) shows the performance with the same pilot symbol boosted by 6 dB. The resulting cap on effective SNR is 24.1 dB, reducing the degradation to only 0.9

dB. This improvement in the degradation is due to the improved channel estimation from the boosted pilot symbol power. The disadvantage of this boosted power is that clipping of the pilot symbol occurs when the OBO is below 6 dB. This results in rapid degradation of the effective SNR as the channel estimation is degraded.

Figure 2-39 (b) shows a similar result to (c) except that a different low CF pilot symbol was used. See section 6.2.3 for details on generation of this pilot symbol. The CF of this pilot symbol was 2.7 dB, making it 2.05 dB higher than the ultra low CF used in (c). Despite the higher CF, the performance was only slightly worse by approximately 0.8 dB, which is due to the small percentage of symbol power in the peaks.

Figure 2-39 (d) shows the performance when a boosted random pilot symbol was used. The CF of this symbol was 8.2 dB and so its performance was significantly worse than the other pilot symbols used.

This simulation has shown that the pilot symbol power can be boosted above the average power, provided that it has a low CF. This boosting of the power increases the effectiveness of the pilot symbol, improving channel characterisation.

2.9 REDUCTION OF SPECTRAL SPREADING BY PRE-FILTER CLIPPING

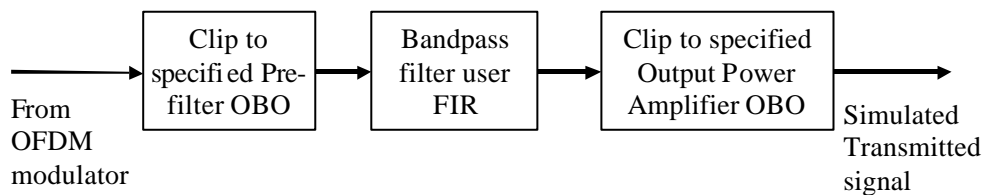


Figure 2-40, Pre-filter clipping is to reduce spectral spreading due to clipping in the power amplifier.

OFDM without any output filtering has a broad spectrum, as discussed in Section 2.4 page 37. One method for reducing this problem is to filter the output of the OFDM transmission. This filtering can also be used to reduce the amount of output spectral spreading caused by clipping in the output power amplifier.

Applying clipping to the OFDM signal in a digital form before the power amplifier,

allows the CF to be reduced, minimising the distortion and spectral spreading. However, clipping the signal in the digital domain also causes spectral spreading, eliminating the effectiveness of such a technique. However if the clipped signal is band pass filtered before being sent to the power amplifier, then this will remove the spectral spreading from the first clipping stage. The reduction in the CF reduces the amount of subsequent clipping in the power amplifier, and consequently the spectral spreading. This is a very simple method for reducing the CF of OFDM signals. The main problem with this technique is that IMD caused by the clipping limits the effective SNR, reducing the capacity of the system.

Numerous other techniques for crest factor minimisation have been published [108] - [113]. Section Chapter 7 provides a description of these techniques and presents a new method for CF minimisation of OFDM signals. This investigation into pre-filter clipping is to show the effectiveness of such a simple technique for spectral spreading minimisation.

If we were designing an OFDM system with 64 subcarriers and had decided that we needed an effective SNR of 35 dB, then by looking at Figure 2-38 we can see that the lowest OBO that can be used is 6.5 dB. At this OBO the spectral spreading due to IMD, 64 subcarriers from the system centre frequency, is -36 dBc (see Figure 2-36, 100% system BW at OBO of 6.5 dB). However if we know that the power amplifier in the transmitter is going to clip the waveform, then why not clip the signal before sending the signal to the power amplifier. Most of the spectral spreading can then be removed by digitally band-pass filtering the signal before transmission. This reduces the CF of the signal, reducing the amount of subsequent clipping in the PA, and spectral spreading in the broadcast signal. This eases the requirements on the analog band-pass filter after the PA.

Figure 2-41 shows the effect of pre-filter clipping on the output spectrum. This spectrum also shows the filtering of the OFDM signal. In this simulation the IFFT size used to generate the signal was 128 points, the transition width of the filter was 8 subcarrier spacings and the window function used to generate the filter had a window width of 2 (similar to hamming window function, see Appendix A). The resulting filter required $128/8 \times 2 = 32$ taps. A guard period of 16 samples was used to remove the ISI caused by the filtering.

When no pre-filter clipping is applied, the out of band side-lobes are exactly as predicted by Figure 2-36. However as pre-filter clipping is applied to the signal the side-lobe energy is reduced, with a 10 dB improvement for pre-filter clipping OBO of 6 dB, and a 34 dB improvement with a pre-filter clipping OBO of 5 dB. Clearly by clipping and filtering the signal before the PA can significantly reduce the broadcast spectral spreading. The question is how much has the pre-filter clipping reduced the effective SNR of the OFDM transmission.

Pre-filter clipping reduces the output spectral spreading, however it does not remove the in-band IMD products. Additionally for the pre-filter clipping to be effective the OBO used must be lower than the OBO used at the power amplifier. Typically it must be 0.5 - 1.5 dB lower to have a significant effect. This consequently increases the in-band distortion products reducing the effective SNR. Figure 2-43 shows the resulting effective SNR of the OFDM transmission for different levels of pre-filter clipping, and the OBO used in the power amplifier. We can see that for our example system earlier, that if we used a per-filter clipping of 6 dB, and an OBO in the power amplifier of 6.5 dB, that effective SNR drops to 31 dB. Thus we gain 10 dB side-lobe suppression for a loss in effective SNR of 4 dB (35 dB to 31 dB). Alternatively we can increase the pre-filter clipping OBO to 7 dB and the output power amplifier OBO to 8 dB, the effective SNR increases by 3 dB to 38 dB, and the side-lobe suppression increased by 37 dB to -77 dBc, all for the cost of only 1.5 dB reduced output power. To achieve this level of out of band suppression without using pre-filter clipping the power amplifier OBO would have needed to be increased to 9.7 dB, compared with 8 dB with the pre-filter clipping.

Pre-filter clipping can be used to trade off between the effective SNR of the transmission and the out of band suppression. Its use in practice will depend on the amount of distortion the system can tolerate. Also it can only be used in a system that uses digital filtering before the power amplifier. In a multiuser OFDM system, filtering removes the orthogonal nature between users which are using neighbouring subcarriers in the spectrum, thus limiting its use to system wide filtering.

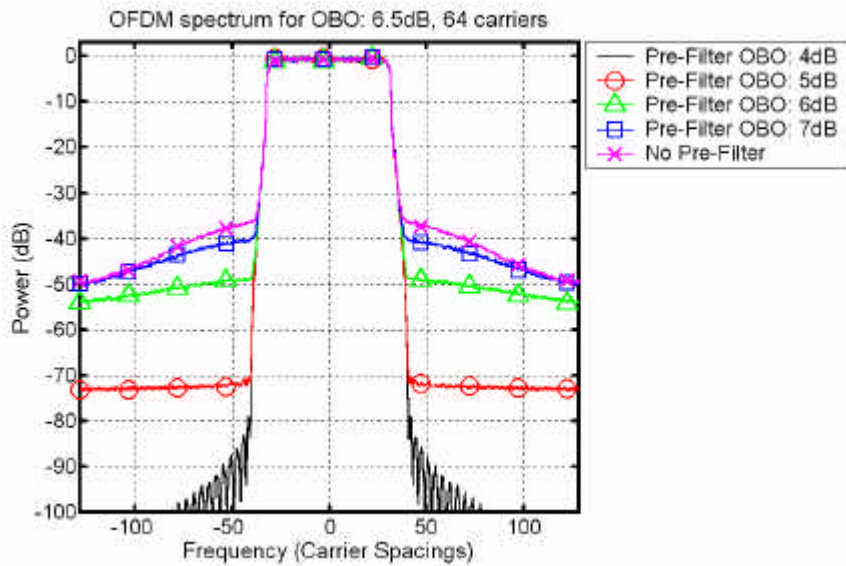


Figure 2-41, Spectrum of a 64 subcarrier OFDM signal with pre-filter clipping.
(script s0063)

The signal was clipped, digitally band pass filtered then re-clipped in the PA to an OBO of 6.5 dB.

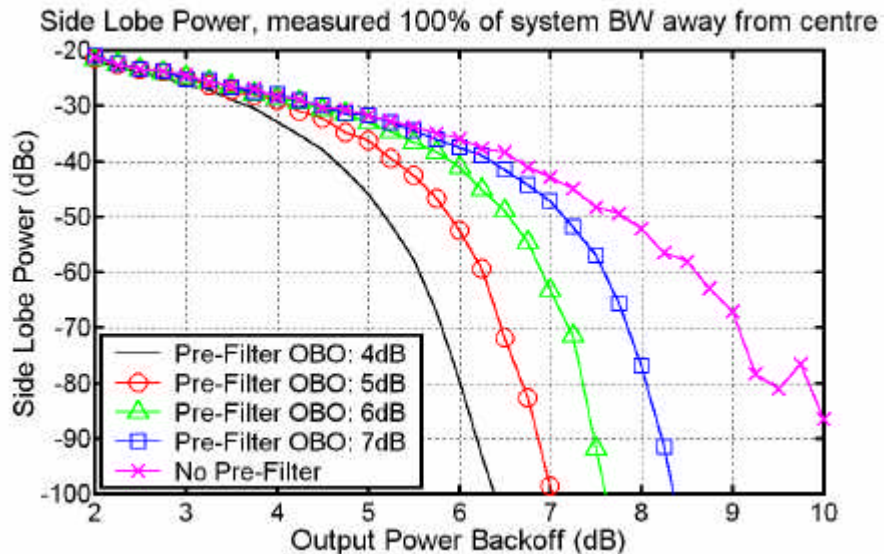


Figure 2-42, Side-lobe power caused by IMD as a result of clipping in the power amplifier, for different levels of pre-filter clipping. (script s0063)

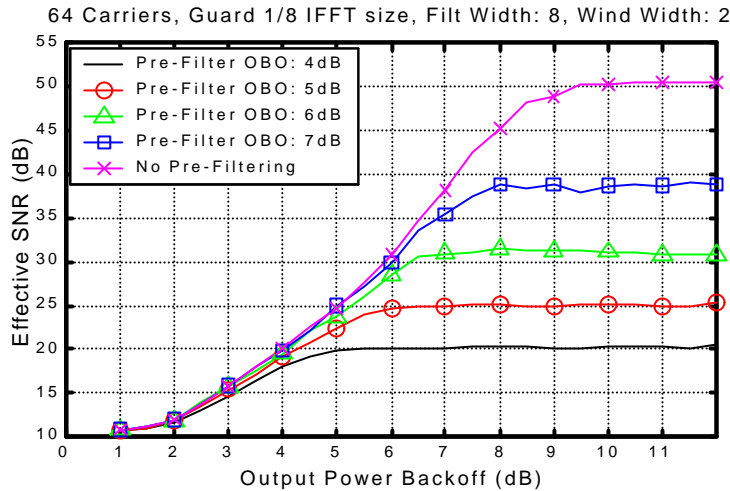


Figure 2-43, Effective SNR of the OFDM transmission as a function of the OBO in the Power Amplifier, and the Pre-filter clipping used. (script s0062)

2.10 EFFECT OF TIME SYNCHRONISATION ERROR

OFDM is relatively tolerant against timing errors, due to the inclusion of the guard period between symbols. For a channel with no multipath delay spread, the time offset error can be as much as the length of the guard period with no loss of orthogonality results, only a phase rotation in the subcarriers. The phase rotation is corrected as part of the channel characterisation, hence resulting in no degradation in performance. Time offset errors greater than the guard period result in a rapid loss in performance, as the section of the symbol that the FFT is applied to will contain some of the neighbouring symbol, leading to Inter-Symbol Interference.

Figure 2-44 shows the effective SNR of an OFDM transmission as a function of the time offset error. The zero point in time is taken with respect to the FFT section of the symbol. A positive time offset results in some of the next symbol being captured in the FFT, thus lowering the effective SNR. A negative time offset results in part of the guard period being used in the FFT. Since this is a cyclic extension of the symbol no ISI occurs. In a dispersive channel the effective length of the guard period is reduced by the delay spread of the channel resulting in a corresponding reduction in the allowable time offset error.

Figure 2-45 shows the effect of using an overlapping raised cosine guard period (see

Figure 2-24) on the timing error tolerance of the system. In this simulation the raise cosine section of the guard period was 50% of the total guard period time. This shows that the raised cosine section of the guard period only provides partial protection against time offsets, compared with a flat guard period. The effective length of the raised cosine guard period is shorter than its actual length. For a cut off of 30 dB effective SNR, the raised cosine guard period provides time offset tolerance equivalent to one quarter (5 samples) its actual length (20 samples).

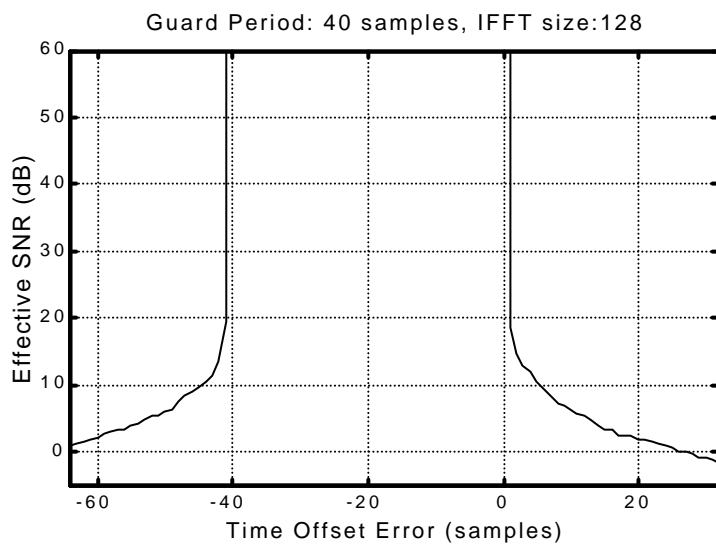


Figure 2-44, Effective SNR of an OFDM signal with a time offset error, using a flat guard period of 40 samples. (script s0053)

The time origin is with respect to the start of the IFFT section of the symbol, just after the guard period. A positive time error means the FFT in the receiver is capturing some of the next symbol; a negative time error results in the receiver getting the guard period.

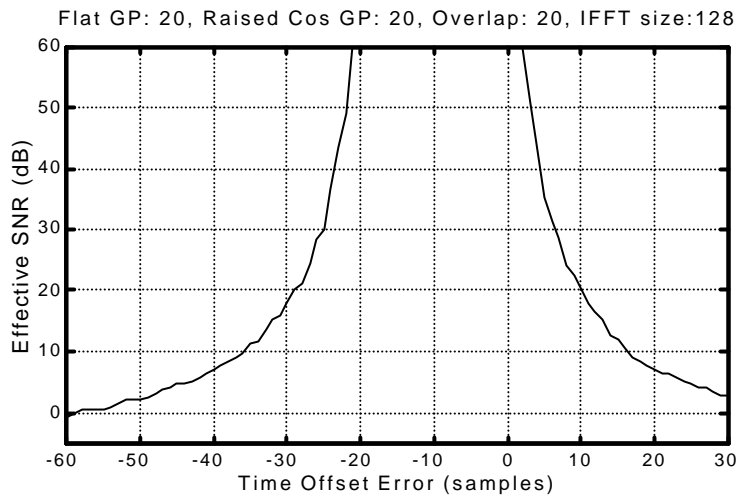


Figure 2-45, Effective SNR of an OFDM signal with a time offset error, using a raised cosine guard period. (script s0069)

The length of the flat guard period is 20 samples, with an overlapping raised cosine guard period of 20 samples.

2.11 EFFECT OF FREQUENCY SYNCHRONISATION ERROR

One significant problem with OFDM is its sensitivity to frequency offsets affecting the performance. The demodulation of an OFDM signal with an offset in the frequency can lead to a high bit error rate. This is caused by the loss of orthogonality between the subcarriers resulting in inter-carrier interference (ICI), and a lack of correction for phase rotation of the received data vectors.

Frequency errors will tend to occur from two main sources. These are local oscillator errors and Doppler spread. Any difference between transmitter and receiver local oscillators will result in a frequency offset. This offset is usually compensated for by using frequency tracking, however any residual errors result in a degraded system performance.

Movement of the transmitter or receiver results in Doppler shift in the signal. This appears as a frequency offset for free space propagation. This offset is usually corrected for as part of the local oscillator compensation. A much more serious

problem is that of Doppler spread, which is caused by movement of the transmitter or receiver in a multipath environment. Doppler spread is caused by the different relative velocity of each of the reflected multipath components, resulting in the signal being Frequency Modulated. This FM modulation on the subcarriers tends to be random due to the large number of multipath reflections that occur in typical environments. This Doppler spread is typically poorly compensated for and results in degradation of the signal.

Figure 2-46 shows the effect of frequency errors on the effective SNR of an OFDM transmission using coherent QAM. Any frequency offset results in a continual phase rotation of all the received subcarrier vectors. The greater the frequency offset, the greater the phase rotation. If the channel characterisation is only performed at the start of each frame then the unresolved frequency errors will lead to degradation in the performance with time. The first symbol after the channel compensation will have the maximum effective SNR, which will degrade to a low effective SNR by the end of the frame. Figure 2-46 shows the effective SNR of the 1st, 4th, 16th, and 64th symbol in an OFDM transmission with only channel compensation at the start of a frame. The spikes in the response for a frequency offset error $> 10^{-2}$, are caused by full rotations of the received vector.

The performance of differential phase modulation will be similar to that of the SNR of the first symbol after characterisation, as phase rotations will be corrected for every symbol.

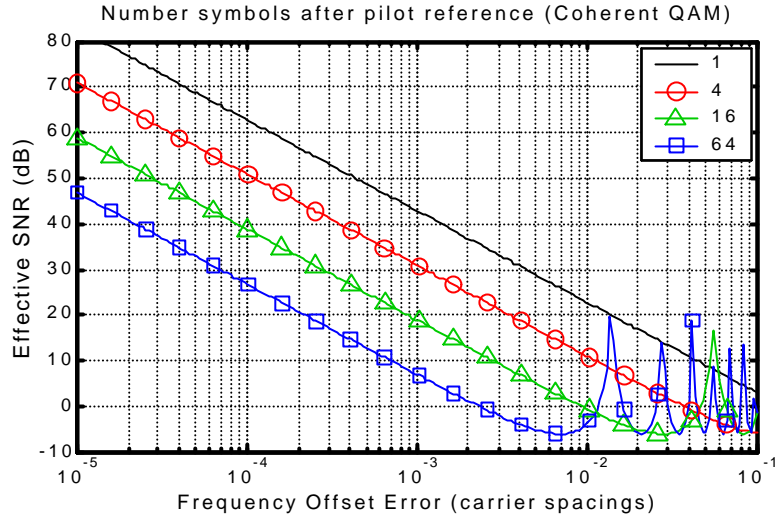


Figure 2-46, Effective SNR for Coherent QAM with frequency offset error.
(script s0068)

The effective SNR for the 1st, 4th, 16th, and 64th, symbol in an OFDM frame with channel equalisation, only at the start of the frame.

There have been numerous techniques developed to measure and track the frequency offset [35] - [52]. Also it has been stated that the frequency accuracy must be maintained to within 2 - 4% to prevent significant performance loss [35] - [37]. In a mobile multi-user environment the problem is worse, as the transmission from each user can have a different frequency offset. Even if each user is synchronized to the base station perfectly, there will still be significant different frequency offsets for each user due to Doppler shift. Frequency offset in a single user OFDM link isn't a significant problem as it can be compensated for with minimal increased receiver complexity. However in a multi-user case there is no easy way of correcting the frequency errors.

CHAPTER 3 RADIO PROPAGATION

This chapter provides a brief review of the major characteristics of radio propagation, and the problems these cause in transmitting digital information.

Radio propagation effects such as path loss, frequency selective fading, Doppler spread and multipath delay-spread limit the effectiveness of wireless communications. An understanding of radio propagation is needed before different forms of multiuser OFDM can be discussed. This chapter provides a review of well-known propagation effects and extends these to look at the effects on wide bandwidth transmissions. This chapter includes an experimental investigation of small-scale frequency selective fading of multipath environments. It looks at the variation of the multipath fading with small changes in space. This work was needed to allow different user allocation schemes, such as adaptive subcarrier modulation, to be investigated. This work provides insight into how fast radio channels change with space and time. Although there has been extensive work done on narrow band radio modelling, not much work has been done on wide band modelling (10 - 100 MHz bandwidth). Most models in literature are based on statistical results, making them of little use for investigating user allocation schemes in an OFDM system. For this the clustering of the frequency fading and change with space is needed to decide how subcarrier hopping systems will work. This work is very important for OFDM systems development because it provides a deterministic relationship between frequency selective fading and space (movement).

3.1 PATH LOSS AND ATTENUATION

During propagation, radio signals weaken with distance. This is due to the wave front of the radio signal expanding and thus reducing in power density. In free space, the propagating wave expands as a sphere and thus the power density reduces in

proportion to the surface area of this sphere. If the signal is transmitted using a directional antenna, the signal still expands as a sphere, except that the energy density is concentrated to one or more areas (see Figure 3-1). If we transmitted the same energy from an omnidirectional as a direction antenna, the integrated energy over the surface area of the RF sphere, the energy would be the same. Figure 3-1 shows an expanding RF pulse, if we were to imagine a sinusoidal transmission (single frequency) it would be continuous stream of expanding spheres, with the power of these following a sinusoid waveform.

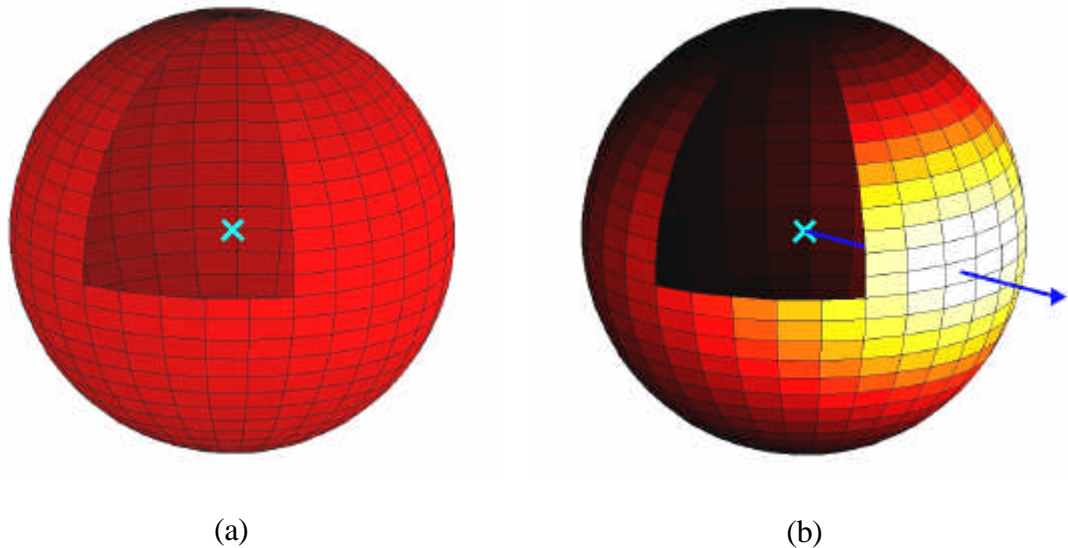


Figure 3-1, Expanding RF pulse from a central transmitter. (script s0029)

The transmitter is shown as an  in the cut away section. (a) For an omnidirectional antenna, the energy density is even in all directions. (b) For a high gain antenna, the energy is concentrated in one direction; it still however expands as a sphere.

The area of a sphere is proportional to the radius squared, and thus in free space the RF field strength reduces proportionally with distance squared. Equation (3-1) calculates the received power over transmission in free space.

$$P_R = P_T G_T G_R \left(\frac{I}{4\pi R} \right)^2 \quad (3-1)$$

Where P_R is the received signal power (watts), P_T is the transmitted power (watts), G_R gain of the receive antenna with respect to an isotropic antenna, G_T gain of the

transmitter antenna, λ wavelength of the RF carrier (m), and R is the transmission distance in metres.

Free space propagation is very predictable, and can be used to accurately model satellite communications and directional links with no obstructions, such as short-range microwave directional point-to-point links. However for most terrestrial communications such as mobile phones and wireless LAN systems, the environment is much more complex making propagation modelling much more difficult.

3.2 SHADOWING AND SLOW FADING

In most mobile radio applications, the environment through which the communication must occur is cluttered and has many obstructions such as buildings, hills, trees, walls, etc. These objects cause reflections off their surface and attenuation of signals passing through them, resulting in shadowing. These shadows can result in large areas with high path loss, causing problems with communication. The amount of shadowing is dependent on the size of the obstructing objects, the structure of the material, and the frequency of the RF signal. Most materials are highly transparency at RF frequencies compared with visible light, making non-Line Of Sight (LOS) propagation possible. Although many materials are transparent, metal objects act much like mirrors due to being good reflectors, making them opaque, resulting in wiring within walls, foil insulation, metal roofing, reinforcing in concrete, etc being opaque. In addition, large objects such as buildings and hills absorb much of the RF energy passing through, resulting in deep shadowing behind them. Under these conditions most of the received energy usually comes from reflections and diffraction around the object, rather than from the direct path.

Diffraction occurs at edges of obstructing objects in the transmission path. At the diffraction edge, the signal reradiates as a spherical wavefront originating from the diffracting edge. This allows it to bend partially around the object. Diffraction does not have any significant effect on shadowing for visible light due to the small wavelength of the light (0.4 - 0.7 μm) as compared with most object sizes (0.1 - 10 m). However, at microwave frequencies, the wavelength is relatively large (0.03 – 0.3 m) and thus diffraction significantly reduces shadowing.

The received signal is made up from a combination of direct path transmission, reflected signals and diffracted signals. The amount of received power is the resulting sum of transmission through these different signal paths. Moving the receiver, transmitter, or objects in the environment will result in a change in the path loss due to the transmission path changing, such as moving from a direct line of sight signal to behind a building (see Figure 3-2). This variation in the path loss occurs over large distances (typically 10 - 100 wavelengths) and is dependent on the size of the objects causing the shadowing, rather than the wavelength of the RF signal. Due to the slow changing nature of this variation, it is commonly referred to as slow fading.

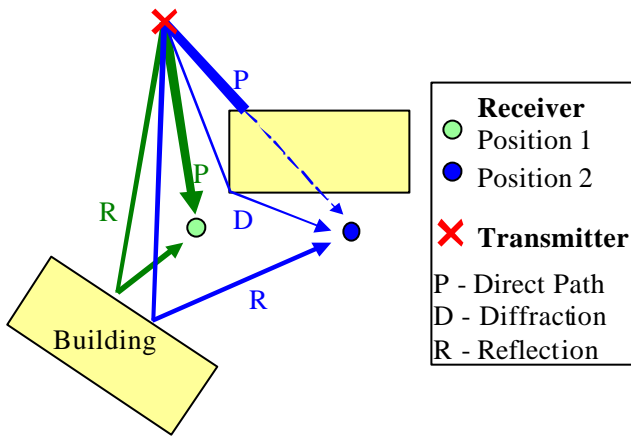


Figure 3-2, Effect of receiver position on the relative strength of the received direct, reflected and diffracted signals.

The path loss measured in terrestrial non-LOS links is higher than the predicted value when using the free space path loss equation (3-1). The signal power in cluttered environments typically falls off faster than free space. One common method to model this increased rate of decay is to change the distance dependent exponent from 2 (path loss is proportional to the distance squared) to a higher value. An adjusted path loss equation is shown in (3-2).

$$P_R = P_T G_T G_R \left(\frac{I}{4\pi R} \right)^{\alpha} \quad (3-2)$$

Where α is the path loss exponent, other terms are defined after Equation (3-1).

Environment	Frequency (MHz)	Path loss Exponent (α)	s (dB)
Retail stores	914	2.2	8.7
Grocery store	914	1.8	5.2
Office, hard partition	1500	3.0	7.0
Office, soft partition	900	2.4	9.6
Office, soft partition	1900	2.6	14.1
Indoor to street (Suburban Home)	900	3.0	7.0
Factory			
Textile/chemical (LOS)	1300	2.0	3.0
Textile/chemical (LOS)	4000	2.1	7.0
Textile/chemical (OBS)	4000	2.1	9.7
Metalworking (LOS)	1300	1.6	5.8
Metalworking (OBS)	1300	3.3	6.8
Paper/cereals	1300	1.8	6.0
Outdoor to indoor penetration of home *	5850	3.4	8.0

Table 3-1, Table of typical path loss exponent for different environments.

Also specified is the standard deviation (σ) measurements compared with the straight line predicted from the path loss exponent. LOS – Line Of Sight path, OSB – Obstructed path. Results obtained from [63] and * [64]

Using (3-2) only gives a rough estimate for the path loss, with no consideration of the actual environment and fine scale effects such as slow and fast fading.

3.3 MULTIPATH EFFECTS

In a radio link, the RF signal from the transmitter may be reflected off objects such as hills, buildings, vehicles, walls, etc. Some of these reflections will arrive at the receiver, effectively creating multiple transmission paths, commonly referred to as a multipath environment. The radio signal travels over a different distance for each of these paths, and thus takes a different amount of propagation time. If we were to transmit an RF pulse in a multipath environment we would receive a signal like the one shown in Figure 3-3 (a). Each impulse corresponds to one path, with the strength of each impulse dependent on the path loss for that path. For a fixed frequency signal, (i.e. a sine wave) the propagation delay results in a phase rotation of the signal. The amount of phase rotation corresponds to 360° for each wavelength of path length travelled. Each of the multipath signals will have a different propagation distance and thus a different phase rotation. These signals add at the receiver,

resulting in constructive or destructive interference. Each of the multipath signals can be represented as a phasor, which has vector length corresponding to signal power and the angle corresponding to the phase. The received signal corresponds to the vector sum of the multipath phasors (see Figure 3-3 (b)). Destructive interference occurs when the vector sum adds to zero. This is also referred to as a ‘null’. Constructive interference occurs when all the signals have a similar phase, reinforcing each other.

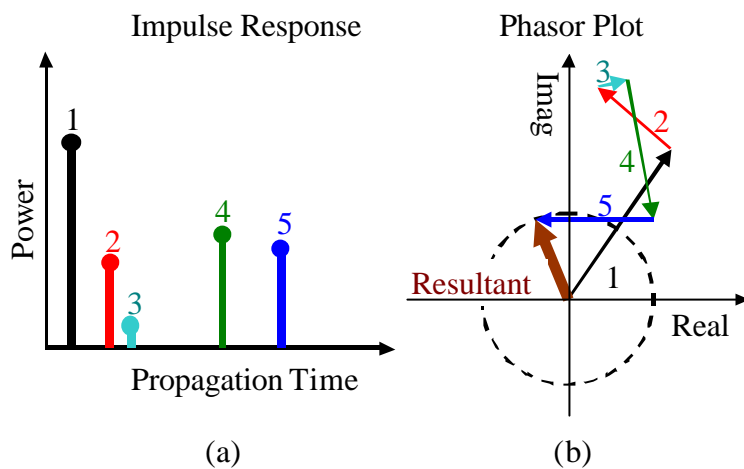


Figure 3-3, Impulse response and phasor plot for multipath channel.

(a) Impulse response of a radio channel with 5 significant paths. **(b)** Phasor plot of the same channel for a particular RF frequency. The length of each vector corresponds to the power and the angle of the vector corresponds to the phase of the RF signal at the receiver for that path. The receiver sees the vector addition of all the multipath signals.

Figure 3-4 shows an example of a channel impulse response. This is for an urban link over 2.4 km. This signal has a strong direct path signal (0 μ s) and two large reflections at 4.5 μ s and 7.5 μ s.

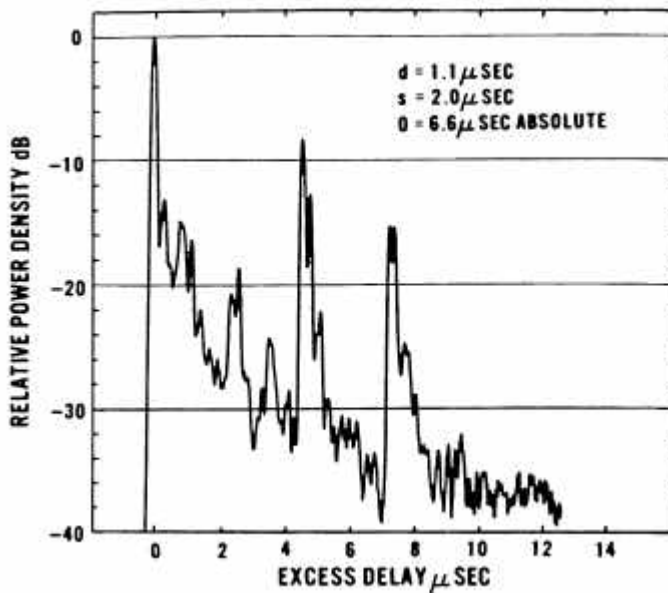


Figure 3-4, Example channel impulse response for a 2.4 km transmission at 910 MHz on Manhattan Island, New York City [71].

Transmitter height of 120 m, receiver height 2 m. ‘d’ is the average excess delay (centre of gravity with respect to first arrival delay), ‘s’ is the RMS delay spread, and ‘o’ is the absolute transmission delay.

3.4 DELAY SPREAD

Delay spread is a measure of the spread in the time over which the multipath signals arrive. It is a measure of the time dispersion of a channel, and is very important in determining how fast the symbol rate can be in digital communications.

A symbol is a period over which one or more groups of bits of information are sent. For a single carrier transmission, using Binary Phase Shift Keying (BPSK) as the modulation scheme, each symbol carries one bit of information. The symbol corresponds to the period required to send the phase information as 0° or 180° , which corresponds to the digital information of zero or one respectively. The faster the phase is varied the faster the symbol rate and the higher the data rate and bandwidth. For OFDM transmission, each symbol corresponds to a parallel transmission of many low bandwidth carriers. The symbol time in this case corresponds to the period over which the amplitude and phase of the data carriers is remained fixed corresponding to one data vector.

The impulse response of a multipath channel can be modelled by

$$H(t) = \sum_{k=1}^m A_k \cdot \delta(t - T_k) \quad (3-3)$$

where A_k is the complex amplitude and T_k is the time delay of each impulse; m is the number of received multipath components, and δ is the dirac delta function.

The RMS delay spread is one of the most widely used measurements for characterising the delay spread of a multipath channel and was originally used by Cox [72].

$$T_{rms} = \left[\frac{\sum_{k=1}^m (T_k - D)^2 \cdot P_k}{\sum_{k=1}^m P_k} \right]^{0.5} \quad (3-4)$$

where T_{rms} is the rms delay spread, and D is the average excess time delay, which is equivalent to the centre of energy for the impulse response.

$$D = \frac{\sum_{k=1}^m T_k \cdot P_k}{\sum_{k=1}^m P_k} \quad (3-5)$$

where P is the power of each impulse and is the magnitude of the complex impulse squared:

$$P_k = |A_k|^2 \quad (3-6)$$

Delay spread results in time blurring, where energy from previous data symbols becomes mixed in with current symbols. This causes interference, known as Inter-Symbol Interference (ISI), because previous symbols are uncorrelated, effectively adding noise to the signal. Single carrier transmissions are particularly prone to problems caused by delay spread as it normally sets the upper limit on symbol rate. This is because the bit error rate (BER) increases as the delay spread time becomes a significant fraction of the symbol time. Simple modulation schemes such as BPSK can tolerate a delay spread of approximately 10 - 20% of the symbol period; any more and the BER is too high. However, higher modulation schemes such as 16-

QAM, 256-QAM, etc, which have a higher spectral efficiency, are much more sensitive to ISI and thus the delay spread must be less than several percent of the symbol period.

Table 3-2 shows the RMS delay spread for a range of propagation environments. For small indoor environments (< 10 m) the RMS delay spread ranges from 8 – 22 ns, whereas it is higher in larger buildings (up to 100 m) with the RMS delay spread varying from 20 – 100 ns.

Description	Frequency (MHz)	Mean RMS Delay Spread	RMS delay spread range (10% - 90%)
Empty Conference Room (13.5 x 7.8 x 2.6 m) LOS, 7 m Tx – Rx separation [66]	Omni	60 GHz	18.1 ns
	Wide (60°)	60 GHz	13.6 ns
	Standard (10°)	60 GHz	4.7 ns
	Narrow (5°)	60 GHz	1.1 ns
Residential Room, LOS, (4.6m) [68]	5200	–	8 – 12 ns
Business Room, LOS, (14 m) [68]	5200	–	30 – 50 ns
University Building, LOS, (Average Room Dim: 11 x 5 m) 4 m Avg Tx – Rx separation [67]	37.2 GHz	10 ns	8.5 – 15.5 ns
Engineering Building, (60 x 44 m) (Mixed LOS and NLOS) [69]	2400	50 ns	21 – 79 ns
Retail Store, (100 x 108 m) (Mixed LOS and NLOS) [69]	2400	64 ns	30 – 98 ns
Office Building, (cubicles, offices and laboratory space) 5 m Tx – Rx separation [73]	1100	17 ns	12 – 22 ns
Office Building, (cubicles, offices and laboratory space) 30 m Tx – Rx separation [73]	1100	32 ns	17 – 45 ns
City streets in New York, NLOS, (2 x 2.5 km) [70]	910	1.2 μ s	0.5 – 2.5 μ s

Table 3-2, Measured delay spread for a variety of environments.

3.5 SHORT TERM FADING

In a multipath environment, the received signal fades with distance due to the changing phase of the multipath components. Short term fading is caused by the interference (constructive or destructive) that result from the combination of multiple received waves. As the receiver or transmitter are moved in space the relative phase between the different multipath components change, causing the interference to also change, resulting in fades in the received signal power. At certain locations, the signal can suffer almost complete cancellation of the signal, resulting in a deep null in

the signal. These nulls can be as much as 30 dB. Nulls occur approximately at intervals of the RF wavelength (30 cm for 1 GHz transmission). The rate of fading with distance is usually measured using the coherence distance. This is a measure of the distance over which the radio channel experiences comparable or correlated fading.

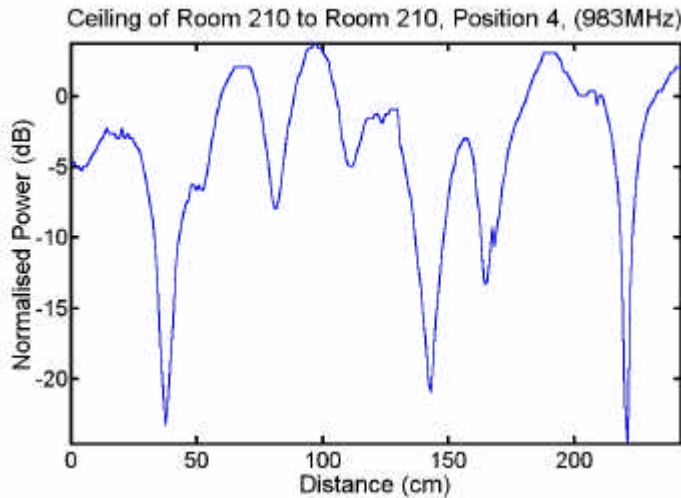


Figure 3-5, Plot of fast fading with distance. This is measured data for a short indoor link. (script s0030)

See section 3.8.1 for the location of the link. The spacing between fades is approximately one wavelength, in this case 30cm.

3.6 FREQUENCY SELECTIVE FADING

Multipath also causes fading changes with frequency. This is due to the phase response of the multipath components varying with frequency. The received phase, relative to the transmitter, of a multipath component corresponds to the number of wavelengths the signal has travelled from the transmitter. The wavelength is inversely proportional to frequency and so for a fixed transmission path the phase will change with frequency. The path distances of each of the multipath component is different and so results in a different phase change. Figure 3-6 shows an example two-path transmission. Path 1 is a direct signal and has a transmission distance of 10 m, while the second path is a reflection with a longer transmission distance of 25 m. For a wavelength of 1 m each path is an integer number of wavelengths hence the phase change from transmitter to receiver will be 0° for each path. At this frequency,

the two paths will reinforce each other. If we change the frequency to have a wavelength of 0.9 m then path 1 will be $10/0.9 = 11.111\lambda$, or a phase of $0.111 \times 360^\circ = 40^\circ$, while second path will be $25/0.9 = 27.778\lambda$, a phase of $0.778 \times 360^\circ = 280^\circ$. This makes the two paths out of phase, which results in a reduction in the signal amplitude at this frequency.

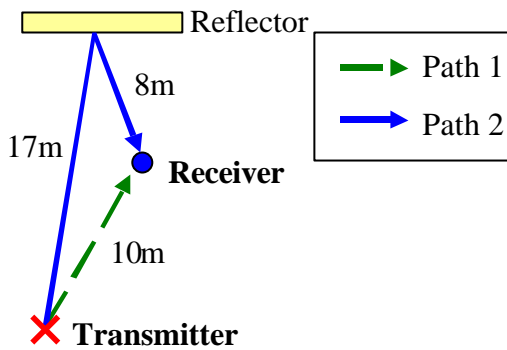


Figure 3-6, Two path transmission to demonstrate frequency selective fading.
(see text)

If we look in terms of the phasors of the multipath components as in Figure 3-3 (b), each phasor rotates in phase at a different rate, with changes in frequency. The rate of phase rotation is proportional to the path distance of each multipath component. For environments with a large number of multipath components, this results in complex variations in the fading versus frequency. Figure 3-7 shows an example of measured frequency selective fading within an indoor environment. The signal power varies by more than 25 dB with frequency, showing that at certain frequencies near complete signal cancellation is occurring. The frequency selective fading characteristics of a channel can be summarised by the correlation bandwidth of the channel. This is the approximate maximum bandwidth or frequency interval over which the fading is similar and correlated. The exact correlation bandwidth depends on the required level of correlation. The correlation bandwidth is inversely proportional to the channel delay spread.

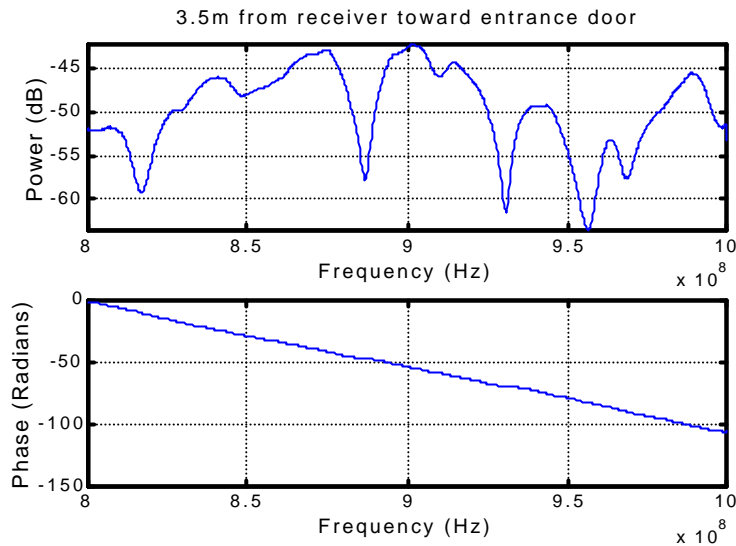


Figure 3-7, Frequency selective fading for a short indoor link. (script s0028)

3.7 FREQUENCY-SPACE FADING

As we have seen previously, in multipath environments, the signal fades with changes in distance (short term fading) and with frequency (frequency selective fading). In practice, these effects will always occur simultaneously. Figure 3-8 and Figure 3-12 show the measured channel response of a short indoor link, as a function of distance and frequency. From this it can be seen that fading patterns in frequency-space are very similar. In fact the scaling of the fading rates over both dimensions are dual problems. The coherence bandwidth (inverse of the fading rate in frequency) is approximately inversely proportional to the transmission distance, while the coherence distance (inverse of the fading rate in distance) is approximately inversely proportional to the carrier frequency. Doubling the transmission distance within a given transmission environment will approximately double the channel delay spread and consequently halve the correlation bandwidth. Similarly, doubling the carrier frequency will approximately halve the correlation distance. These comparisons are only approximate as they are dependent on the locations and reflective nature of the objects in the radio channel.

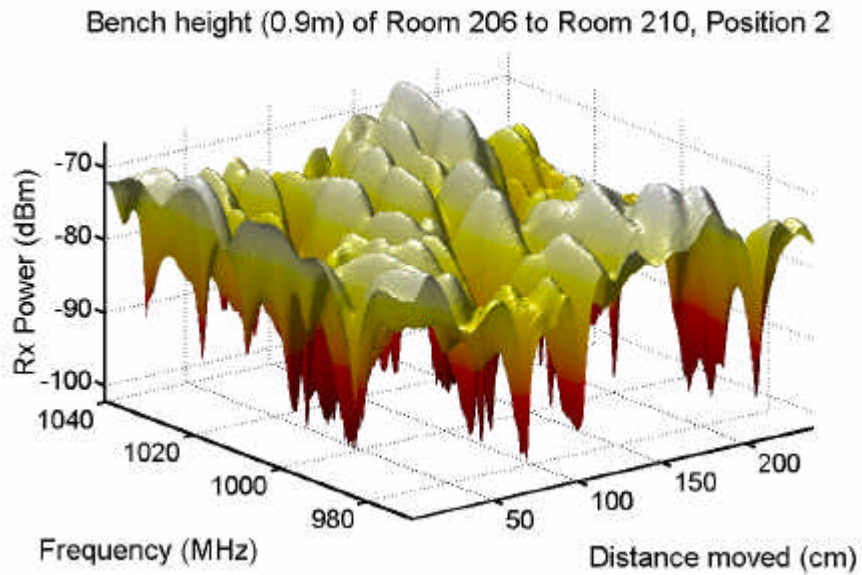


Figure 3-8, Short term fading, showing fading dependence on distance and frequency. (script s0030)

3.7.1 EQUALISATION

One method to overcome the limitations of delay spread for single carrier transmission is to use equalisation. The aim of equalisation is to find an inverse filter that compensates for the ISI so that all the multipath signals become shifted and aligned in time, rather than being spread out. For example, the GSM phone system, which uses 270 k symbols/s (3.7 μ s symbol period), can tolerate a delay spread of up to 15 μ s. This is a delay spread of over four symbol periods. The problem with equalisation is that it becomes increasing difficult, as the ISI is spread over more symbols. Errors in equalisation, particularly for delay spreads over more than one symbol, make it difficult to use higher modulation schemes in multipath environments.

OFDM systems work by resolving the frequency domain so that the width of the subcarriers is much narrower than frequency selective fading of the radio channel. This makes the frequency response over the bandwidth of each subcarrier effectively flat. Only simple equalisation is required for each subcarrier for data transmission as the flat fading on each subcarrier only results in an amplitude scaling and a phase rotation.

For coherent transmissions, equalisation is implemented by transmitting reference pilot symbols or tones, which are set to an amplitude and phase known by both the transmitter and receiver. The channel response is then estimated by dividing the received subcarrier IQ vector of the pilot symbol or tone by the known transmitted vector. This measured channel response is then used to equalise the transmitted data.

No equalisation is needed for transmissions using differential phase modulation. With this method, the amplitude of the subcarrier is not used for carrying information and so its value is not important. With differential phase modulation the data is transferred as a phase difference between successive symbols. This compensates for any phase offset caused by the propagation channel.

3.8 FREQUENCY SPACE FADING MEASUREMENTS

Equalisation of each of the OFDM subcarriers provides a large amount of information about the radio channel. It indicates which subcarriers have a high signal power, and those that are in nulls in the spectrum. This allows the allocation of subcarriers to users to be optimised, to maximise the performance of the system. These allocation schemes are outlined in detail in section 4.2, however in order to study these user allocation schemes a detailed knowledge of the fading characteristics of radio channels is required. Most traditional methods for modelling radio channels, statistically describe the fading probabilities. However, to investigate the user allocation schemes, the direct relationships between frequency fading and changes in space are required.

An experiment was set up to measure the fading as a function of frequency and space for an indoor environment. The aim of this experiment was to measure changes in frequency selective fading as a function of distance.

3.8.1 MEASUREMENT LOCATIONS

These measurements were performed in the Electrical Engineering building at James Cook University. This building has a structure that is fairly typical of a medium sized office building. The building is three stores high and has outer walls constructed

from concrete block. The internal walls were constructed mainly from plasterboard, with support columns approximately every 6 m. Measurements were taken at six locations on the second floor, and two locations on the first floor (Rm120 and Rm122).

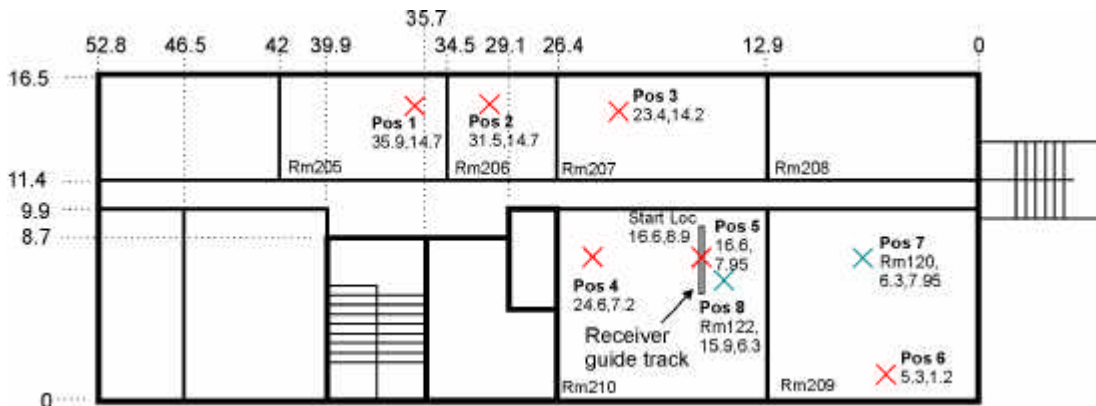


Figure 3-9, Plan of measurement locations for frequency space fading measurements.

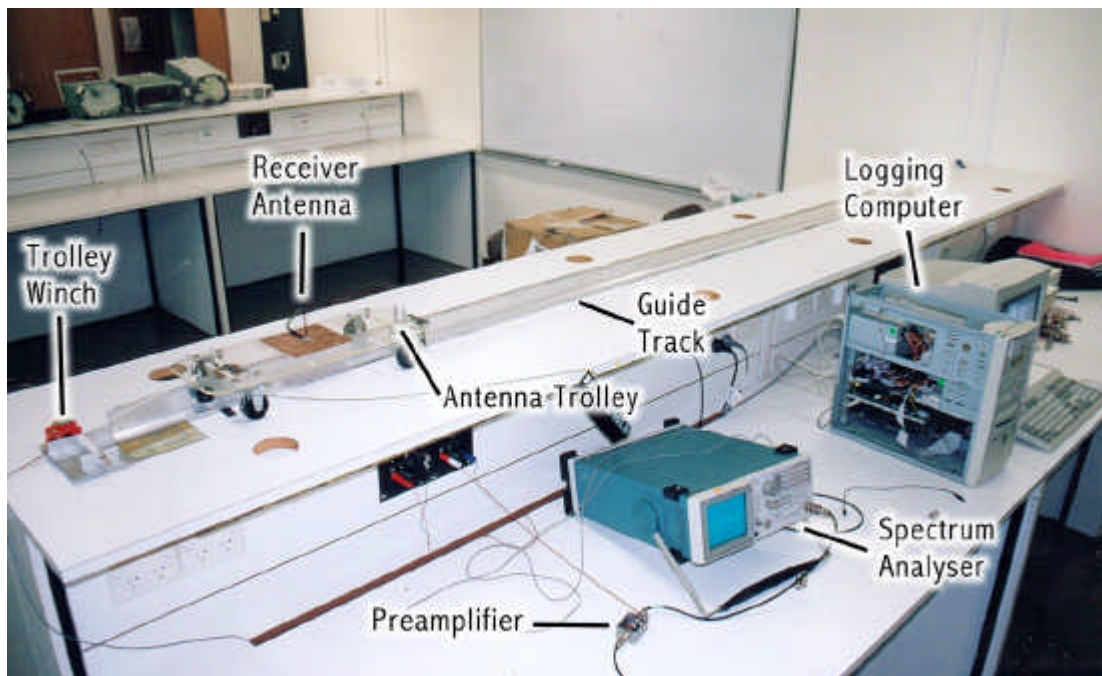


Figure 3-10, Set up of equipment for frequency space fading measurements.

Set of the receiver, showing the guide track in the middle of the raised section of the bench. On this track is the antenna trolley, which pulled along by the motor on the left. A spectrum analyser was used to measure the power frequency response at each location along the track, which were logged by a PC shown on the right.

The set up used in the experiment is shown below in Figure 3-11. The signal generator produced a slow sweep (approximately 3 min per sweep) across the frequency band of interest (970 - 1040 MHz). This signal appears as a slow moving continuous wave signal by the spectrum analyser. The maximum hold feature of the spectrum analyser was then used to trace out the received power at each frequency across the band. This trace corresponds to the power response of the radio channel transfer function. This channel response was then logged to a PC and after each sweep measurement the trolley was moved 1 cm and the process repeated. In all, 240 sweep measurements were done, taking a total time of about 12 hours. The measurements were very sensitive to any movement within the building and so the measurements were performed overnight.

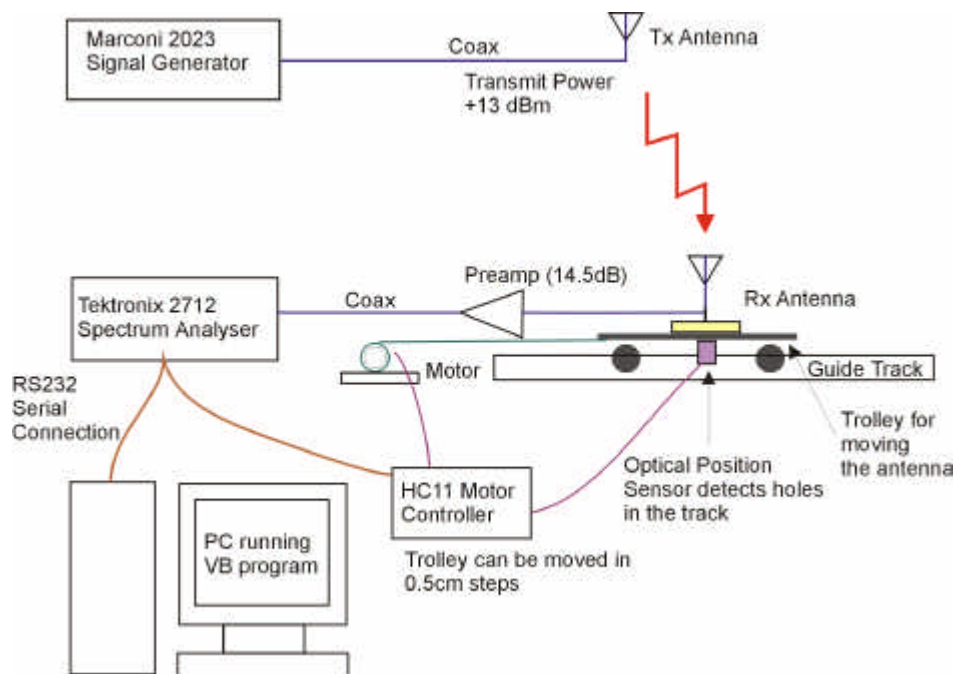


Figure 3-11, Experimental set up for measuring the radio channel response as a function of distance.

These measurements were used for simulating the performance of an adaptive modulation OFDM system in section 4.2. These measurements give a deterministic relationship between the fading in the frequency domain, and the fading in the spatial domain. This is extremely important for accurately determining the performance of multiuser OFDM systems using adaptive modulation.

3.8.2 MEASUREMENT RESULTS

Figure 3-12 shows an example of one of the measurements taken. The remainder of the results are shown in Appendix C. The result shown is for a non-LOS transmission over a distance of 14.9 m. The transmission signal passes through three walls, and as a result the average path loss (74.9 dB) is significantly higher than free space loss (55.9 dB) for this same distance.

The results of the measurements show that there is a strong correlation between fading as a function of distance and fading as a function of frequency. The fading pattern shows regions of strong constructive interference, with some of these peaks reaching 6 dB lower path loss than the mean. Nulls caused by destructive interference occur between these peaks, and are typically relatively small in distance and bandwidth. Although the nulls are small, they sometimes form clusters resulting in large suppressed regions.

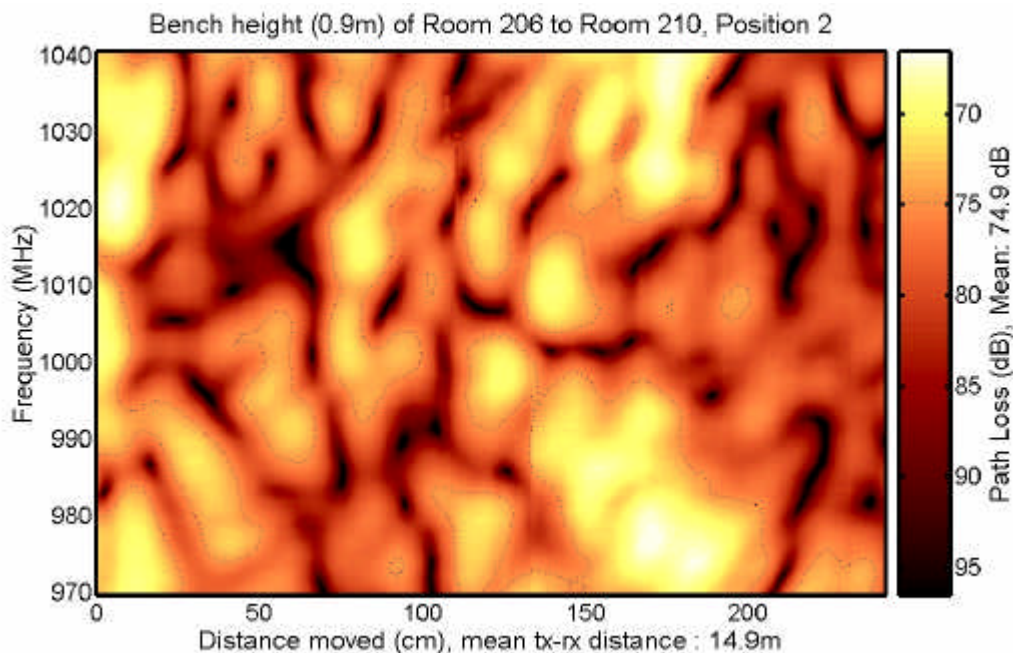


Figure 3-12, Measured frequency space measurement for a 14.9 m non-LOS indoor link. (script s0030)

Same data as in Figure 3-8 except as a 2D surface plot. The brightness indicates the received power for a particular position in space and frequency. Note the dotted contour shows the mean path loss.

Figure 3-13 shows the path loss for all the measurements taken. The path loss shown was taken as the average over the entire data set for each location. The path loss exceeds free space loss for all but one location. The best-fit path loss exponent (α) for all the measurement locations was 2.6, which compares well with previously published results for office buildings of 2.4 – 3.0, see Table 3-1. The variations in the path loss closely correlate with environment for each transmission. The LOS locations have a lower path loss, closely matching free space, with the exception of location 5. The path loss for this measurement was higher due to its location being directly above the measurement track, which corresponds to a null in the antenna pattern. This null is a result of the use of monopole antennas. Most of the other locations fall around the $\alpha = 2.5$ line, with the largest deviations occurring for location 7 and 8. These locations correspond to the next floor down in the building, resulting in an additional 6 - 9 dB of attenuation. Measurements that were taken at bench height have a higher path loss, due to the larger number of objects in the transmission path.

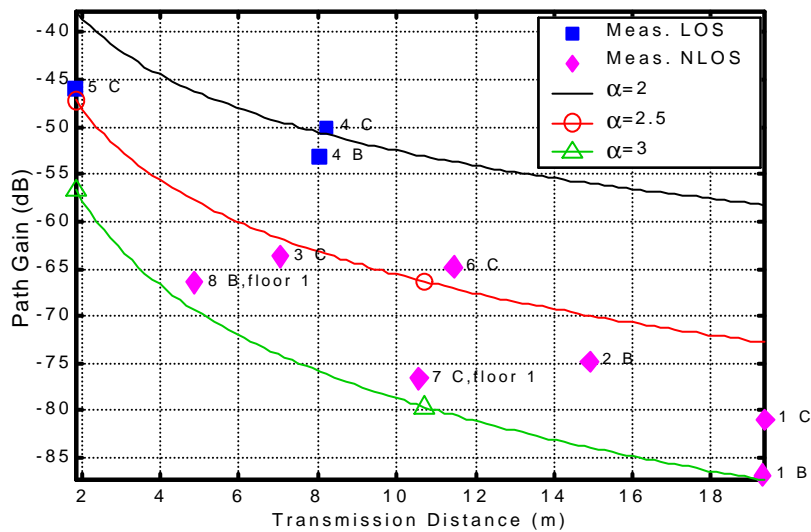


Figure 3-13, Path loss of the measurements taken. (script s0030)

The number beside each data location corresponds to the position number, while ‘B’ indicates that the measurement was taken at bench height, and ‘C’ corresponds to ceiling height. Two of the data points were taken on the next floor down show by the ‘floor 1’ tag. Lines shown represent the expected path gain for different path loss exponents.

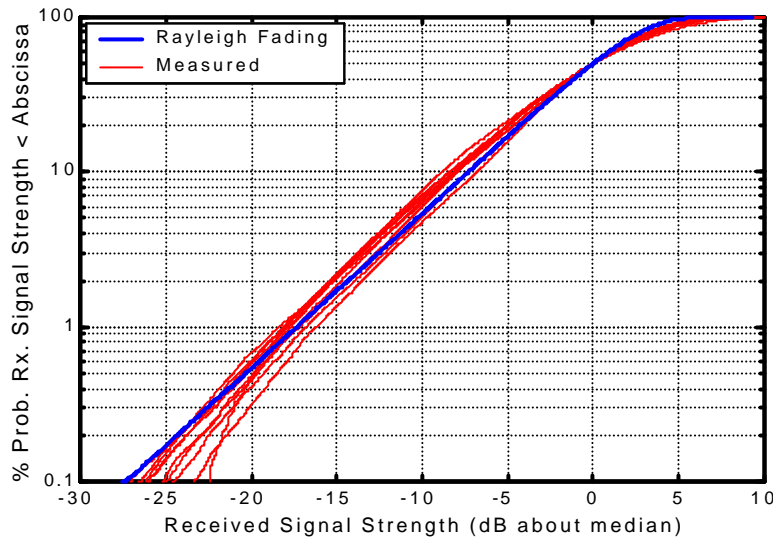


Figure 3-14, Fading probability distribution for each of the measurement locations. (script s0030)

Figure 3-14 shows the fading distribution for each of the measurement locations. They all closely follow a Rayleigh fading distribution [119], indicating that the direct signal energy is significantly smaller than the multipath energy. This was even true for LOS measurements.

3.9 RATE OF CHANGE OF RADIO CHANNELS

The aim of this set of experiments is to address the issue of how fast do the characteristics of indoor radio channels change, due to movement of people and movement of the transmitter. These measurements were performed to provide a guide to how fast radio channels change. Numerous studies have been performed to describe the statistical distribution of narrow band fading [62]. However, not many studies have been performed to investigate the effects of moving bodies around transmitter antennas [74]. This experiment simulates the variations in the channel response that would be experienced in a Wireless LAN application.

This thesis outlines several new adaptive schemes (see Chapter 4) for maximising the link capacity of an OFDM system. One of the reasons these techniques have not been used before in mobile applications is that, they must track the response of the radio channel continuously. This tracking adds complexity to the system and more

importantly, data overhead. An adaptive technique for maximising system capacity is not very useful if all the benefits are outweighed by the overheads. The overhead required for tracking of a changing channel depends primarily on how fast it changes and by how much. This experiment aims to address some of these questions.

In any radio channel the amount of disturbance an object makes to the channel response depends on several factors. These include, the size of the object, the distance it is from the transmitter and receiver, its reflectiveness, and how much fading the transmission was suffering from before moving the object. If the channel response is in a deep fade, only a very small change in the physical channel is required to cause a large change in channel response. For this reason the channel disturbance measurements were taken under two different conditions. The first test involved positioning the transmit antenna so that the overall channel response, before any object movement, was at a local maximum in the frequency fading spectrum. The other test was done when the position of the transmitter resulted in a local minimum (deep fade) in the channel response.

In this experiment, the complex propagation characteristics (magnitude and phase change due to the radio channel) of a short link were measured using a network analyser. Three sets of measurements were performed. The first test shows the effect of a person walking toward the transmitter antenna. The second test shows the effect of a person walking up to the transmitter antenna, sitting down and typing on a keyboard near the antenna. The third test shows the result of a person walking around in the same room as the transmitter and receiver.

All measurements were performed at 940MHz, which is lower in frequency to most wireless LAN systems (2.4GHz and 5.2GHz). However it was chosen due to limitations of the network analyser and the availability of a suitable filter for the pre-amplifier stage.

3.9.1 EXPERIMENTAL SET UP

The propagation characteristics across the room were measured using an analog network analyser. This set up is shown in Figure 3-15. The output sweep signal from the network analyser was feed back via a power splitter to the reference input. The

network analyser calculates the transfer function of the channel by comparing the received amplitude and phase to this reference signal. The channel measurement taken was the combined the transfer function of the coax, antennas, radio channel, preamplifiers and receiver band pass filter. The transfer function of these elements is however fixed, and since the aim of the experiment is to analyse the changing nature of the radio channel these static elements do not affect the results. A digital oscilloscope was used to capture the real and imaginary output waveforms from the network analyser. Before each measurement, a zero point measurement was made to ensure offsets in the IQ measurement taken by the Network Analyser were compensated for. The captured results were processed further on a PC using Matlab scripts².

The simulated performance of a channel response tracking system was performed on each of the measured responses. This was done to estimate the tracking error when an adaptive modulation system is utilised as outlined in section 4.2. The tracking error was measured by taking the time dependent power response of the channel, applying different sampling rates, then finding the error between the sample points and the signal in between the sample points. This information gives an indication of the amount of channel response error that can be expected for a given sample rate of the channel response.

If we assume that the received power level primarily determines the SNR of the channel, then from this data we can estimate how fast the modulation scheme must be updated in an adaptive modulation system. For example, for square QAM modulation schemes, the SNR threshold changes by 3 dB for each 1 b/s/Hz change in spectral efficiency. Thus if the channel power level changes by more than 3 dB then the modulation scheme should also change, otherwise the BER will become large if the SNR dropped, or the spectral efficiency should increase by 1 b/s/Hz if the SNR went up.

² Code\IQchannelmeas\s0028_plotdata.m

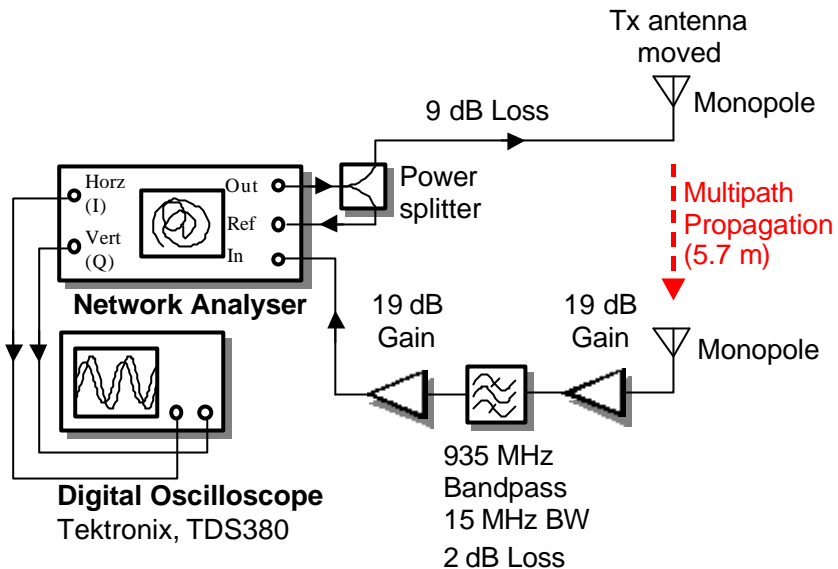


Figure 3-15, Experimental set up. The Network Analyser was used to measure the amplitude and phase of the channel. The Digital Oscilloscope was used to capture the results for further processing.

3.9.2 SCOPE AND SCALING OF THE RESULTS

The scope of this experiment is limited in that only one room was measured and at one radio frequency. However, these results do give a strong indication of the magnitude of effects.

The results can be roughly scaled in frequency by changing the time scale. Fading effects and multipath are proportional to the RF wavelength, and thus the higher frequency the shorter the distance between signal fades. The results shown here are measured in time and not distance, and so for a fixed velocity, changing the time scale will effectively give an indication of the fading rate for a different RF frequency. For example for HiperLAN2 that operates at 5.2 GHz, the time scale on the plots needs to be reduced by $5.2/0.94 = 5.53$ times. Thus tracking of fading at 5.2 GHz has to be 5.53 times faster than at 940 MHz to maintain the same performance. The actual effect of objects moving within the lab will vary slightly with frequency because of the size of the moving object relative to the wavelength of the radio carrier will be different.

3.9.3 MEASUREMENT LOCATION

The measurements were performed in one of the engineering labs at James Cook University. A photo of the lab is shown in Figure 3-16. The wall on the left is the outer wall of the building, which has embedded wire meshing, and thus would be a good reflector. The other three walls are made of plasterboard. The room contains a large number of objects, creating a scattering environment. Figure 3-17 shows a plan layout of the room, indicating the transmitter and receiver location.



Figure 3-16, Photo of the room where the propagation measurements were taken.

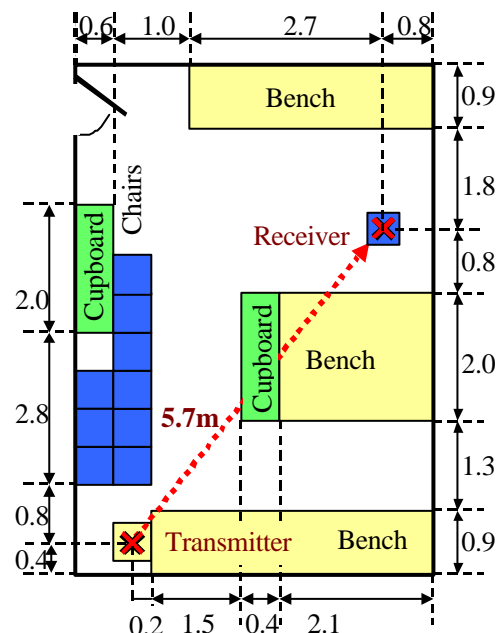


Figure 3-17, Plan view of the test room, showing the layout of the benches, and the position of the transmitter and receiver. Note: All lengths are in metres.

3.9.4 EFFECT OF WALKING TOWARD THE TRANSMITTER CHANNEL RESPONSE

This test involved walking toward the transmitter, pausing then returning to the start location. This test demonstrates the effect of a person walking around a room for a short range LAN system. The path of movement is shown in Figure 3-18. Two repeat measurements were performed. For the first measurement, the transmitter was moved to a location that resulted in the receiver being located in a local minimum (null in the spectrum). The second measurement was taken where the receiver was in a local maximum. The transmitter location was moved 30cm to achieve this. The walking pattern was the same in both tests.

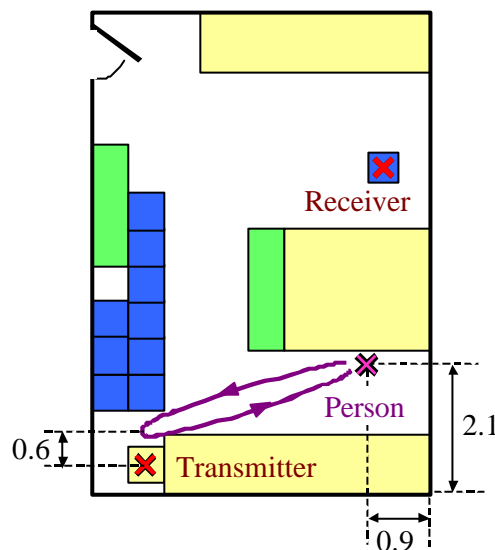


Figure 3-18, Movement of the person in the test room during the measurement period

Figure 3-19 shows the measured channel response during the movement of the person toward and away from the transmitter. The results show that the movement of the person has a significant effect on the channel response, particularly if the subcarrier signals are in a null in the spectrum. The magnitude of the disturbance from the person was about the same in both tests. The ripple in the measured IQ channel response caused by a person walking was about 2×10^{-4} (Unit-less due to the relative testing) in both cases. This disturbance had a much greater effect when the transmission was in a local minimum due to the disturbance being a large percentage

of the transmission power. The average power in the local minimum case is about 10 dB lower than the local maximum measurement. The Doppler shift was 10 times higher for the local minimum case and the disturbance to the power was about 14 dB compared with 2 dB for the local maximum.

These results show that the energy reflected from the person walking around was not sufficient to cause complete fading for frequencies that are at a local maximum. This means for an adaptive modulation system, which tracks the peaks in the spectrum, only small disturbances are caused by the movement of a person. Thus if the adaptive modulation system used a link margin of greater than 2 dB it would not have had to track the fine structure of the movement of the user. The link margin is difference between the channel SNR and the minimum SNR required for the modulation scheme used and the BER threshold chosen.

For the adaptive modulation scheme, as proposed in section 4.2, the modulation needs to be updated for each 3 dB change in the channel response. From Figure 3-19 (e) we can see that when the transmission is at a local maximum that a tracking rate of 4 Hz is sufficient to maintain a tracking error smaller than 1.2 dB for 99.9% of the time. Even when the transmission is in a null a tracking rate of 8 Hz will ensure that the tracking error is less than 3 dB for 98% of the time (Figure 3-19 (f)).

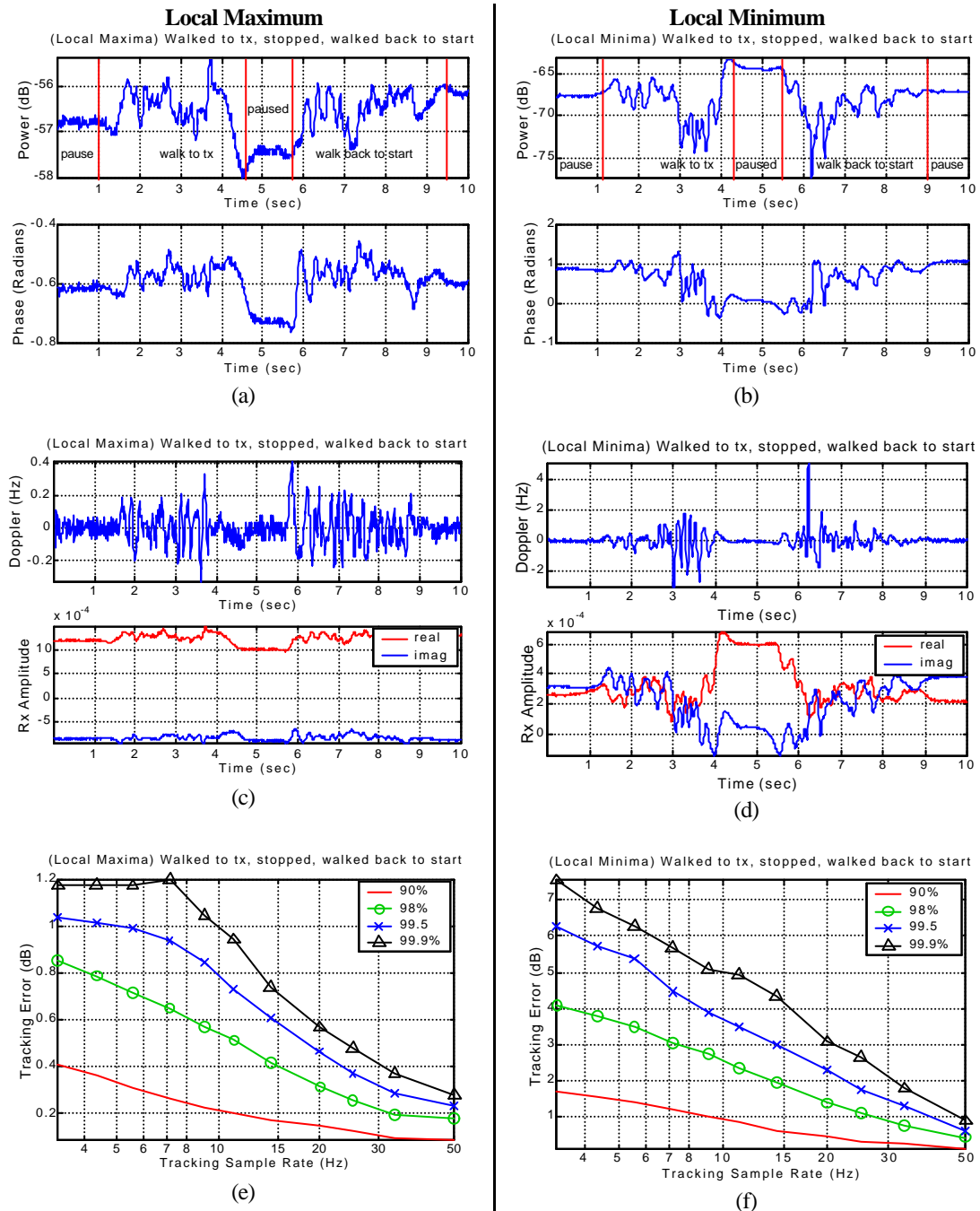


Figure 3-19, Radio channel response variation due to a person walking toward the transmitter. (At 940 MHz) (script s0028)

3.9.5 EFFECT OF TYPING ON A KEYBOARD NEAR THE TRANSMITTER ON THE CHANNEL RESPONSE

Figure 3-20 shows the effect of a person walking up to the transmitter antenna, sitting in front of it, and pretending to type (as though on a keyboard). This test was performed to simulate the effect of a WLAN transmitter attached to a notebook computer. The transmitter antenna was located 15 cm from the hands of the person typing. Figure 3-20 shows the results of this experiment. The measurement was performed twice, once with the transmitter located so that the transmission was in a local maximum in the channel response, and the other with it located in a local minimum.

The largest disturbance in the channel response occurred after the person sat down in front of the antenna and lent forward. This is a result of the large displacement of the body so close to the antenna. The typing in front of the antenna had very little effect on the channel response, resulting in only a 1 dB ripple for the antenna in a local maximum, and a 3 dB ripple for the antenna in a local minimum. From Figure 3-20 (e) we can see that only a very low tracking rate (> 4 Hz) is required for an adaptive modulation scheme, provided the signal is in a local maximum. However if the signal is in a local minimum the tracking rate needs to be 15 – 30 Hz to ensure that the tracking error is smaller than 3 dB.

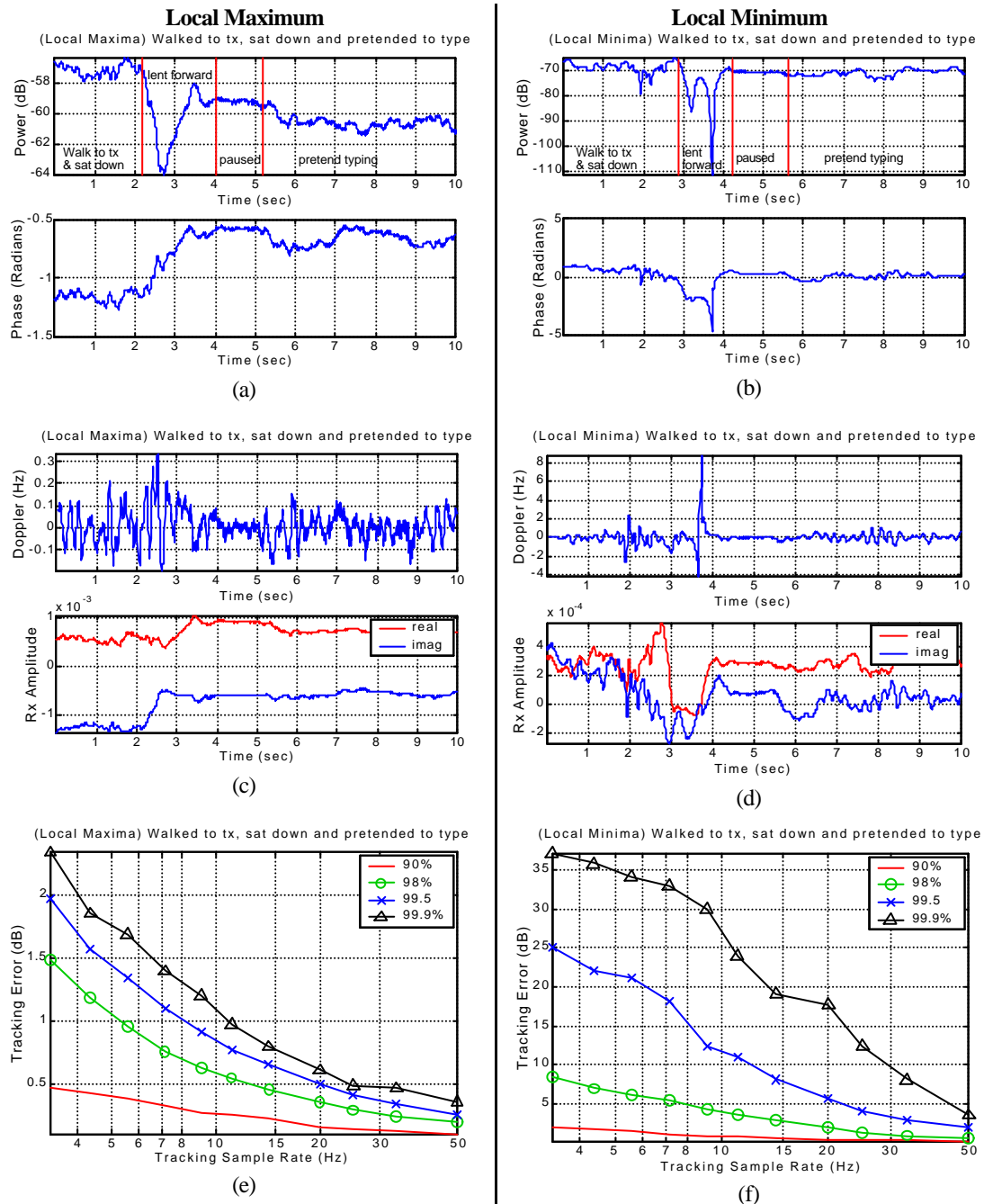


Figure 3-20, Fading causes by a person pretending to type on a keyboard 15 cm from the transmitter antenna. (script s0028)

3.9.6 EFFECT OF A MOVING PERSON ON THE CHANNEL RESPONSE

This test shows the effect on the channel response of a person walking through a lab, with a transmission across the room. The test was performed twice. One with the transmitter positioned so that the receiver was in a null for the person at the starting position (local minimum), and the other for the transmitter placed to have the transmission at a peak (local maximum). The magnitude of the ripple in the received amplitude was about the same in both tests, as expected. However, since the signal power for the transmission in the local minimum is low this disturbance ripple created a large variation in the received power. The power fluctuation for the local minimum case was 15 dB, as compared with only 4 dB for the local maximum.

From these results we can estimate the tracking rate required for implementation of adaptive modulation. If a passive user allocation scheme (FDMA, TDMA, Random, Comb, see section 4.2) than the user is just as likely to be allocated a local minimum as a local maximum. If we assume a maximum tracking error of 3 dB, and a 98% tracking probability then a tracking rate of 12 Hz is required in the local minimum to cope with the disturbance of the person moving in the lab.

If adaptive user allocation is used then users are allocated peaks in the channel response (local maximum) and so the disturbance is smaller and requires less tracking. From Figure 3-22 (e) we can see that for a local maximum the disturbance is small enough that only a very low tracking rate is required (< 4 Hz) in order to maintain a tracking error of less than 3 dB.

Although a tracking rate of 4 Hz will be sufficient when the receiver and transmitter are stationary, it will not be enough if the transmitter or receiver is moved. Section 4.4 shows that when the antenna (transmitter or receiver) is moving a tracking rate of around 100 Hz is needed for walking speed at 1 GHz.

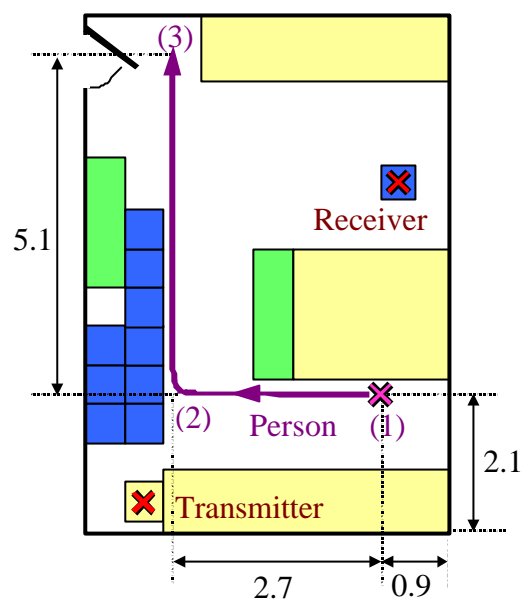


Figure 3-21, Movement of the person relative to the transmitter and receiver

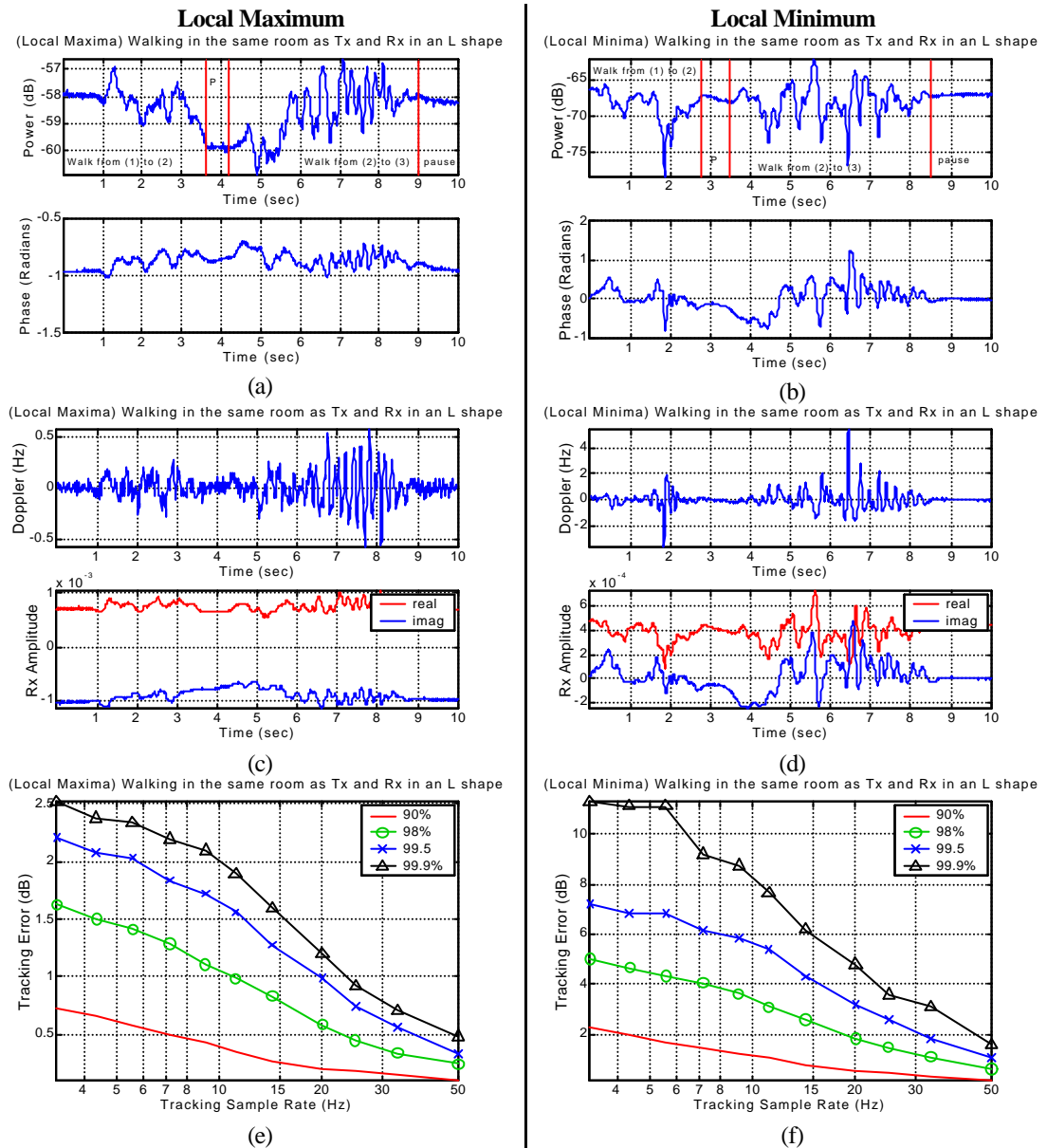


Figure 3-22, Fading caused by a person walking in the same room as the transmitter and receiver. (script s0028)

CHAPTER 4 MULTIUSER OFDM

OFDM has been used successfully in several broadcast systems, namely DAB and DVB, and for point-to-point communications [80]. However, its application in multiuser two-way communication systems has been limited. Only recently has it been applied to Wireless LAN applications, with the development of HiperLAN2 [97] and IEEE 802.11a [99].

OFDM is a good contender for the RF interface in 4th generation mobile systems, however not much work has been done to date in addressing the issues of applying OFDM in large scale multiuser applications. Multiuser OFDM provides a very flexible RF interface allowing users to be allocated using Frequency Division Multiplexing (FDM), by Time Division Multiplexing (TDM) or a hybrid of FDM/TDM. In addition to this, the multicarrier nature of OFDM allows the radio channel to be characterised and monitored quickly and easily, presenting numerous opportunities for optimising the overall system performance, such as:

- Allocating user subcarriers so as to minimise Signal to Interference Ratio (SIR) in cellular systems.
- Allocate subcarriers to minimise the effects of frequency selective fading.
- Dynamically allocate the modulation scheme on an individual subcarrier basis to match the current channel conditions.
- Dynamically change the bandwidth of each user based on the link quality. This allows the bandwidth of weak users to be reduced so that their energy spectral density remains sufficiently high to maintain communications.

4.1 NETWORK STRUCTURE

4.1.1 PEER-TO-PEER NETWORKING

Most current WLAN systems, such as networks using the IEEE 802.11b standard (11 Mbps DSSS), use peer-to-peer networking. This allows computers to communicate directly to each other. Computers on this type of network, typically connect to the rest of the world via a single computer connected via a wired Internet connection. This computer effectively acts as a virtual base station, as all external data traffic is routed through it. This type of networking is simple to set up and doesn't require any special hardware for the virtual base station. One problem with peer-to-peer networking is that some of the stations can become hidden from each other due to shadowing or distance, preventing communication. This problem can be overcome with various methods of multiple hopping of data packets, but this can cause system complexity to be greatly increased, especially if stations are mobile.

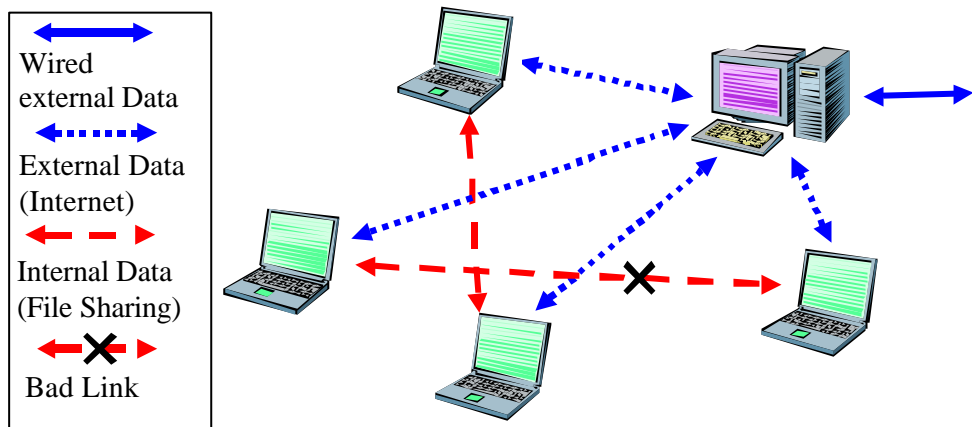


Figure 4-1, Peer-to-peer network. Users communicate directly to each other, with no centralised control.

Peer-to-peer networking requires that all stations can communicate with each other. As a result most systems use half duplex communications and transmit and receive at the same frequency.

4.1.2 SINGLE CELL BASE STATION

One subset of peer-to-peer networking is to use a fixed base station as shown in Figure 4-2. All data traffic is routed through the base station, simplifying routing as

mobiles always send data to the same computer. This set up is more suited to larger WLAN systems and has effectively the same structure as an isolated cell from a cellular network. One of the main advantages of having a base station is that additional resources can be added to it, such as improved antennas, diversity reception and multiple channel processing. These resources on the base station can significantly improve the performance of the entire network. Additionally due to the centralised control, resources such as time and frequency allocations can be optimised.

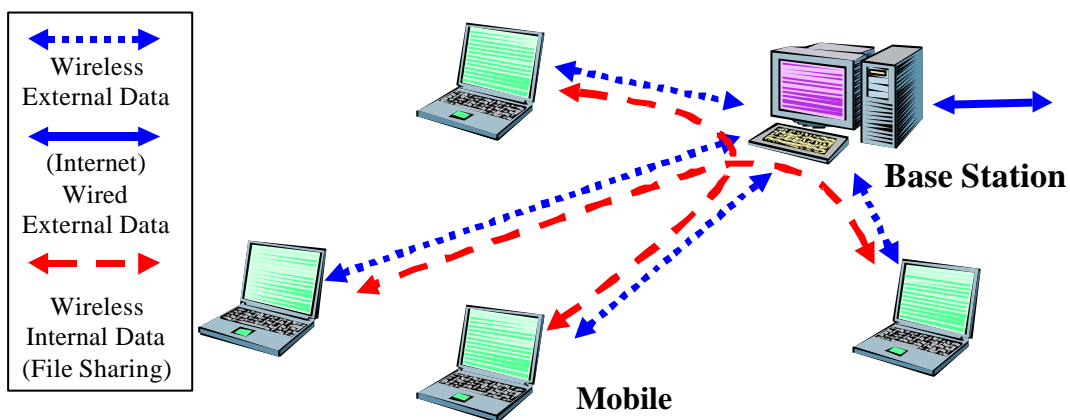


Figure 4-2, Base Station connected system. All data passes through the base station.

As all traffic passes through the Base Station (BS), the communication channel consists of a forward and reverse channel.

4.1.3 FORWARD CHANNEL

The forward channel corresponds to the signal transmitted from the BS to the remote users. The signal from the BS is received by all users, which then demodulate the proportion of the signal relevant to the user. Although the signal from the BS is common to each user, the propagation path to each user is different. The signal from the BS is subjected to the transfer function of the propagation channel. In a multipath environment this results in frequency selective fading, which will be different for each user.

One method for providing multiuser access is using Frequency Division Multiplexing (FDM) by allocating different subcarriers to each user. This however

requires that the signals for all users are time and frequency synchronised to each other.

In the forward link all user subcarriers are transmitted from the base station, and thus all subcarriers can be transmitted with perfect frequency and time synchronisation with respect to each other. However in the reverse link, subcarriers from each user are transmitted from different sources, leading to possible inter-user interference.

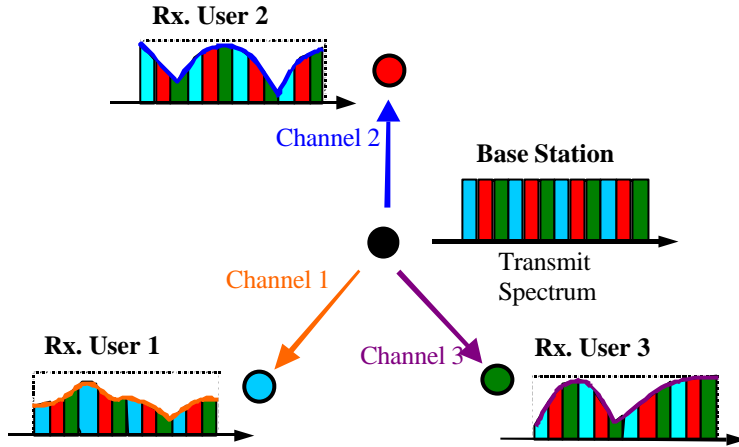


Figure 4-3, Forward Link in a single cell system.

4.1.4 REVERSE CHANNEL

The reverse channel corresponds to the transmission from the remote users to the base station. This link is more difficult than the forward link, as all the transmissions originate from multiple sources. It is therefore difficult to maintain orthogonality between all signals, as the propagation effects such as path loss, frequency selective fading, delay spread and Doppler shift are different for all users.

Due to the spectral overlapping nature of OFDM any loss of orthogonality can result in high levels of inter-carrier interference. Frequency and time synchronisation errors result in loss of orthogonality between subcarriers. A frequency offset error of 1 - 2 % of the subcarrier spacing results in a subcarrier power to interference ratio of 20 dB [85].

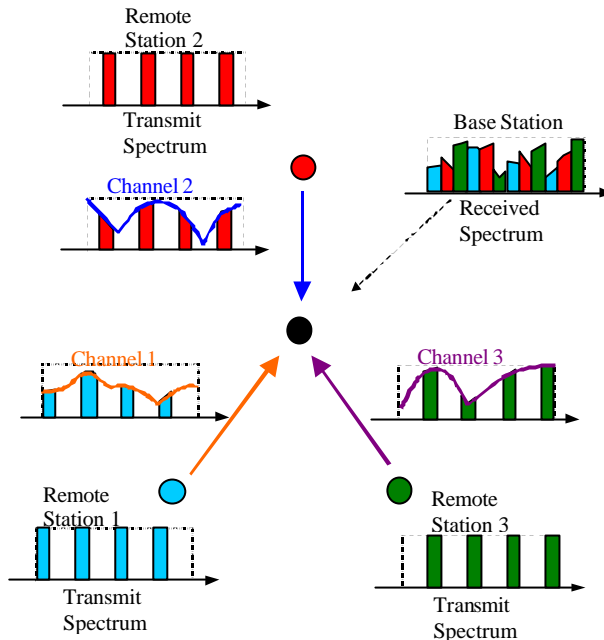


Figure 4-4, Reverse link of an OFDM system using a single cell network and FDM for user allocation.

Distortion in the transmission causes spectral spreading due to inter-modulation distortion. This can be a significant problem if users are of different received powers, as the distortion products from a strong user can swamp the signal from a weak user. This causes a problem known as near-far effect, as users that are close to the base station can swamp the signal from distant users. CDMA systems are very sensitive to near-far effects, requiring that all signals arrive at the base station with equal power to within 0.5 - 2 dB of each other. In the reverse link of a CDMA system, the users are not orthogonal to each other, and so appear as noise to each other. It is the level of this noise that sets the limit to the capacity of the system. If one user has a signal that is twice the power (3 dB) of the other users, it is equivalent to 2 users. This problem is overcome in CDMA systems by using very fast power control (typically 1500 updates per second). Multiuser OFDM systems are much less sensitive to this problem, as the power level difference between users is limited by spectral spreading, rather than inter-user interference as with CDMA. Therefore, if the transmission is free of distortion, then there are no near-far problems. In a typical system the power levels between users will need to be approximately 20 - 30 dB of each other.

4.2 ADAPTIVE MODULATION

Adaptive modulation is a powerful technique for maximising the data throughput of subcarriers allocated to a user. Adaptive modulation involves measuring the SNR of each subcarrier in the transmission, then selecting a modulation scheme that will maximise the spectral efficiency, while maintaining an acceptable BER. This technique has been used in Asymmetric Digital Subscriber Line (ADSL) [86], [87], [88], to maximise the system throughput. ADSL uses OFDM transmission over copper telephone cables. The channel frequency response of copper cables is relatively constant and so reallocation of the modulation scheme does not need to be performed very often, as a result the benefit greatly out ways the overhead required for measuring of the channel response. Using adaptive modulation in a wireless environment is much more difficult as the channel response and SNR can change very rapidly, requiring frequent updates to track these changes.

Adaptive modulation has not been used extensively in wireless applications due to the difficulty in tracking the radio channel effectively. Work has been done studying the use of adaptive modulation in single carrier systems [90] - [93], however not many works have been published on use of adaptive modulation in OFDM systems. BeamReach is a new communications company that formed in March 2000. They are utilising adaptive modulation in conjunction with OFDM and beam forming [95]. Unfortunately little information has been released due to the proprietary nature of the research. In [94] the effectiveness of a multiuser OFDM system using an adaptive subcarrier, bit and power allocation was investigated. Optimisation of the transmission was achieved by minimising the power requirement for a given transmission channel and user data rate. It was found that the use of adaptive modulation, and adaptive user allocation reduced the required transmitter power by 5 - 10 dB. The work in [94] didn't however investigate the effects of channel tracking errors on the BER performance.

This chapter outlines adaptive modulation and adaptive user allocation, with a focus on maximising the user data rate and the QOS (connection access probability). Section 4.3 shows the simulated performance of an adaptive multiuser OFDM

system. This research also investigates the effects of channel tracking errors on the BER performance.

Work in this chapter, demonstrates the effectiveness of using adaptive modulation in conjunction with different user allocation schemes. It also provides insight into the required tracking rate of the radio channel. Previous published work has shown the effectiveness of adaptive modulation using narrow bandwidth fading models. This chapter extends this to show simulations over wide bandwidth transmissions.

Most OFDM systems use a fixed modulation scheme over all subcarriers for simplicity. However each subcarrier in a multiuser OFDM system can potentially have a different modulation scheme depending on the channel conditions. Any coherent or differential, phase or amplitude modulation scheme can be used including BPSK, QPSK, 8-PSK, 16-QAM, 64-QAM, etc, each providing a trade off between spectral efficiency and the bit error rate. The spectral efficiency can be maximised by choosing the highest modulation scheme that will give an acceptable Bit Error Rate (BER).

In a multipath radio channel, frequency selective fading can result in large variations in the received power of each subcarrier. For a channel with no direct signal path this variation can be as much as 30 dB in the received power resulting in a similar variation in the SNR. In addition to this, interference from neighbouring cells can cause the SNR to vary significantly over the system bandwidth. To cope with this large variation in SNR over the system subcarriers, it is possible to adaptively allocate the subcarrier modulation scheme, so that the spectral efficiency is maximised while maintaining an acceptable BER.

Figure 4-5 shows an example of applying adaptive modulation to an individual subcarrier as the channel SNR varies with time.

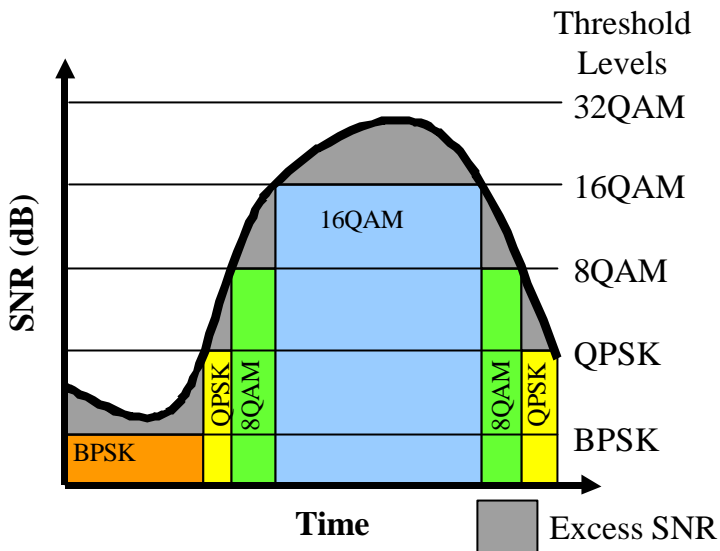


Figure 4-5, Adaptive Modulation. The modulation scheme is set based on the SNR of the channel.

The SNR must be greater than the threshold (chosen from Table 4-1) to maintain a maximum BER. Excess SNR results in the BER being lower than the BER threshold. This diagram assumes that the modulation scheme is updated continuously and with no delay.

Using adaptive modulation has a number of key advantages over using static modulation. In systems that use a fixed modulation scheme the subcarrier modulation must be designed to provide an acceptable BER under the worst channel conditions. This results in most systems using BPSK or QPSK. However these modulation schemes give a poor spectral efficiency (1 - 2 b/s/Hz) and result in an excess link margin most of the time. Using adaptive modulation, the remote stations can use a much higher modulation scheme when the radio channel is good. Thus as a remote station approaches the base station the modulation can be increased from 1 b/s/Hz (BPSK) up to 4 - 8 b/s/Hz (16-QAM – 256-QAM), significantly increasing the spectral efficiency of the overall system. Using adaptive modulation can effectively control the BER of the transmission, as subcarriers that have a poor SNR can be allocated a low modulation scheme such as BPSK, or none at all, rather than causing large amounts of errors with a fixed modulation scheme. This significantly reduces the need for Forward Error Correction.

4.2.1 LIMITATIONS OF ADAPTIVE MODULATION

There are several limitations with adaptive modulation. Overhead information needs to be transferred, as both the transmitter and receiver must know what modulation is currently being used. Also as the mobility of the remote station is increased, the adaptive modulation process requires regular updates, further increasing the overhead.

There is a trade off between power control and adaptive modulation. If a remote station has a good channel path the transmitted power can be maintained and a high modulation scheme used (i.e. 64-QAM), or the power can be reduced and the modulation scheme reduced accordingly (i.e. QPSK).

Distortion, frequency error and the maximum allowable power variation between users limit the maximum modulation scheme that can be used. The received power for neighbouring subcarriers must have no more than 20 - 30 dB variation at the base station, as large variations can result in strong signals swamping weaker subcarriers. Inter-modulation distortion results from any non-linear components in the transmission, and causes a higher noise floor in the transmission band, limiting the maximum SNR to typically 30 - 60 dB. Frequency errors in the transmission due to synchronisation errors and Doppler shift result in a loss of orthogonality between the subcarriers. A frequency offset of only 1 - 2 % of the subcarrier spacing results in the effective SNR being limited to 20 dB [85]. The limited SNR restricts the maximum spectral efficiency to approximately 5 - 10 b/s/Hz.

4.2.2 EFFECTIVE SNR MEASUREMENT

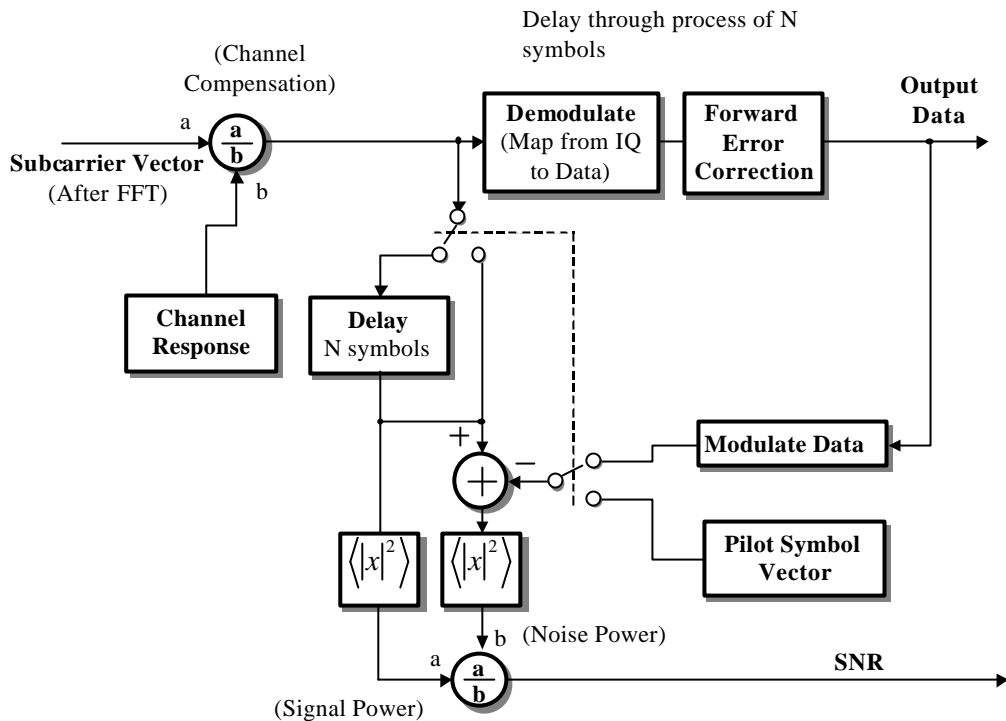


Figure 4-6, Algorithm for estimating the signal plus noise, to noise ratio ($(S+N)/N$) for a subcarrier. This approximates the SNR when the noise is significantly smaller than the signal power.

This is for coherent modulation schemes. The switch selects whether to use blind feed forward estimation, or to use a known pilot symbol. To use the pilot symbol, the SNR estimation must be synchronised with the received pilot symbol. $|x|$ is the absolute of the complex vector, $\langle x \rangle$ is the average.

Adaptive modulation requires accurate knowledge of the radio channel. Any errors in this knowledge can result in large increases in the BER, due to the small link margin used. The effective SNR of each subcarrier can be estimated by calculating the noise vector on the received signal after channel response compensation. Figure 4-6 shows a block diagram of an algorithm for estimating the SNR. The first step is to equalise the received data vector by dividing it by the measured channel response. This algorithm assumes that the noise on this channel response measurement is zero. In practice this is not the case as channel measurements will be subjected to the same noise as we are trying to measure. However the noise on the channel measurements can be minimised in several ways including boosting the power of the pilot tones or symbols, and combining results from multiple measurements.

After equalisation, the noise in the signal is found by taking the difference between the known reference IQ vector for each subcarrier and the received IQ vector. The SNR is then found by finding the ratio between the signal power and the noise power. These powers must be averaged over multiple symbols to smooth out the variations in the noise.

This type of measurement will treat any form of signal degradation as noise, such as AWGN, distortion, residual frequency errors, Doppler Spread, etc. Transmitting a symbol with known data allows the phase error to be estimated, giving the Signal to Interference, Noise and Distortion Ratio (SINADR) of each subcarrier. This SINADR can then be used to select the modulation scheme. The SINADR is referred to here as the effective SNR.

4.2.2.1 NOISE VECTOR ESTIMATION

To estimate the noise vector we need to know what the correct vector should have been. This can be achieved in two ways. One method is to use pilot symbols, which have a precisely known transmission vector, thus allowing the noise vector to be measured under all conditions. This method is the most reliable and fast method for characterisation.

Modulation Scheme (Coherent)	Spectral Efficiency (b/s/Hz)	Required SNR (dB)			
		BER < 1×10^{-2}	BER < 1×10^{-4}	BER < 1×10^{-5}	BER < 1×10^{-6}
BPSK	1	4.32	8.41	9.61	10.42
QPSK	2	7.33	11.41	12.58	13.48
8-QAM	3	11.38	15.30	16.45	17.35
16-QAM	4	13.90	18.22	19.46	20.43
32-QAM	5	17.75	21.58	22.74	23.58
64-QAM	6	19.94	24.39	25.60	26.52
128-QAM	7	23.62	27.60	28.76	29.83
256-QAM	8	25.74	30.34	31.60	32.61
512-QAM	9	29.44	33.54	34.75	35.65
1024-QAM	10	31.54	36.29	37.58	38.59
2048-QAM	11	35.23	39.49	40.67	41.75

Table 4-1, Required SNR to maintain a BER below a given threshold.

This is for an OFDM transmission with AWGN, using coherent modulation, with perfect channel characterisation. This table was derived from the results shown in Section 2.6. (script snrthresh.m)

Another method is to use the demodulated data as though it was known data, which is approximately true provided that the BER is low. The demodulated data is

remodulated to act as a reference allowing the noise vector to be estimated. Using this type of measurement allows the SNR to be tracked continuously without the need for pilot tones or symbols. There are however limitations to this method. The BER must be low in order for the SNR estimation to be correct, thus the minimum SNR that can be measured accurately depends on the modulation scheme being used. Table 4-1 shows the SNR to maintain the BER below three different thresholds, from this we can estimate the minimum SNR that can be measured for each modulation scheme. Each time there is a bit error in received signal, it will tend to make the noise level appear smaller than it really is. However, if averaging is used the chance of having more than one estimation error in the result is low, even if the BER is moderately high (around 10^{-2}). The lower limit to accurately estimating the SNR for a particular modulation scheme will depend on the required measurement accuracy, the amount of averaging used, and the forward error correction method. In a typical system the lower limit to estimating the SNR will be the SNR required to maintaining a BER of 1×10^{-2} , which can be found in Table 4-1.

Another method for estimating the subcarrier SNR is to measure the receiver power on each subcarrier. The channel equalisation information can be used to measure the received power on each subcarrier. The SNR can then be estimated by taking the ratio of the received power to the average noise floor. The level of noise in most transmissions will be relatively constant, and so a separate measurement of the noise floor can be made. This method can estimate the SNR very quickly as it does not require averaging over multiple symbols. The noise floor can be estimated by averaging the noise vector over many symbols, thus allowing it to roughly track the noise of the channel.

4.2.3 SINGLE USER ADAPTIVE MODULATION

The performance of a single user adaptive modulation system was simulated over a wide bandwidth fading channel. The path loss measurement used for the simulation was one of the measured channels shown in section 3.8. The power used in the transmission was set so that the average SNR was 17.41 dB. This SNR was iteratively chosen so that the average spectral efficiency of the adaptive modulation scheme was 2.0 b/s/Hz. This is so that it could be compared directly with a fixed

QPSK transmission. Figure 4-7 shows the resulting SNR of the channel, which varies from 0 dB up to 25 dB depending on the fading depth. The signal bandwidth of 65 MHz was divided into 200 subcarriers, and the adaptive modulation was updated every 1 cm, of travel. This corresponds to a velocity of 54 km/hr at an update rate of 1500 Hz. A delay of one update period (1 cm in distance travelled) in the adaptive modulation was used to simulate the time required for the measurement and reallocation of the subcarrier modulation schemes.

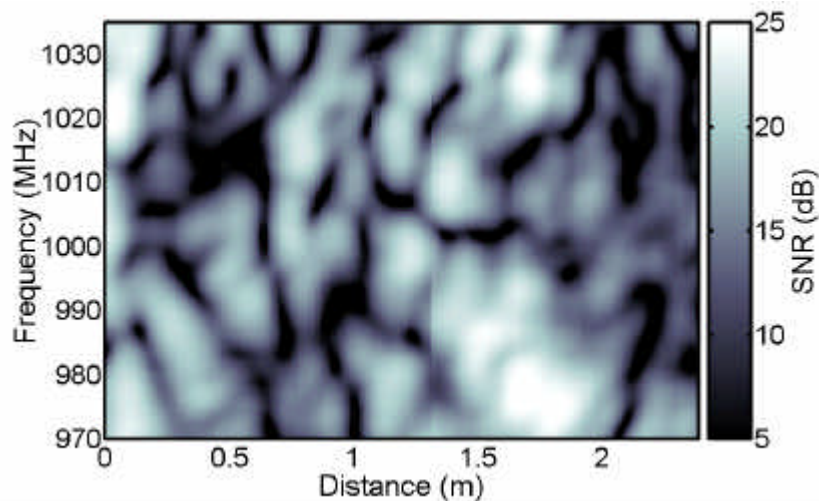


Figure 4-7, Signal to Noise Ratio of wide band radio channel used for single user adaptive modulation simulation. (script s0059)

In order to set up an adaptive modulation system an acceptable BER for the system must be decided. This BER threshold is used for deciding the SNR thresholds for each of the modulation schemes. To complicate the matter slightly, the overall BER of the system will be higher than the chosen BER threshold as a consequence of movement of the user and objects in the environment, and the delay between channel response measurement and the reallocation of the subcarrier modulation schemes.

For this experiment the system BER was chosen to be 1×10^{-4} as this was considered to be low enough for most forward error correction schemes to work effectively. The BER threshold used for the adaptive modulation allocation was chosen to be 2×10^{-6} to ensure that final BER of the system maintained a BER of below 1×10^{-4} . Figure 4-8 shows the resulting modulation scheme applied to each subcarrier as a function of the position moved by the user. The modulation scheme allocated varied from no modulation up to 5 b/s/Hz (32-QAM).

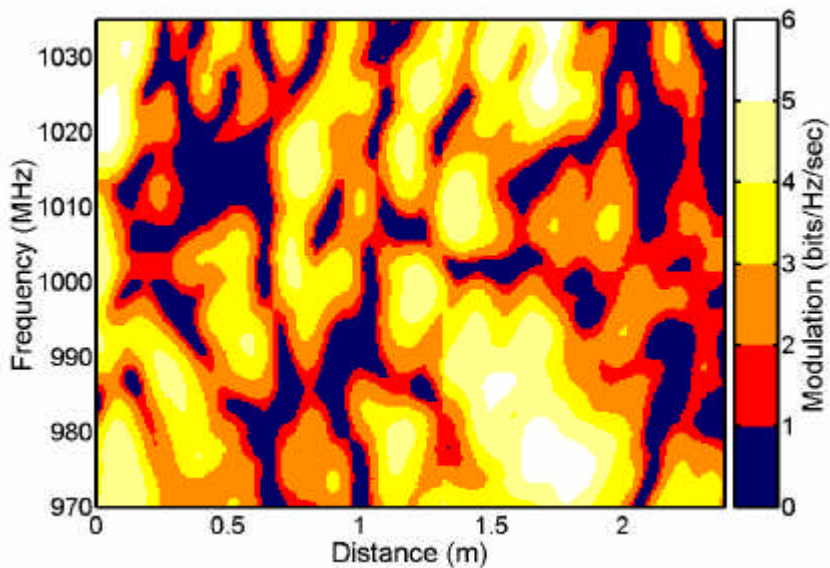


Figure 4-8, Modulation scheme allocated to each subcarrier. (script s0059)

Note: Dark blue means no allocation applied to that subcarrier.

The BER of the modulation allocation was estimated based on the delay in the allocation, and the SNR of the channel between the modulation updates. The BER was solely estimated based on the modulation scheme currently in use and the channel SNR. Other detrimental effects were not simulated, including Doppler spread, ISI, time and frequency sync errors and effects of distortion. This simplification, should however still give accurate results, as the above detrimental effects can be minimised with suitable system design. The BER as a function of modulation scheme and channel SNR was estimated using the simulated results in section 2.6. The channel SNR was calculated with a distance sample rate 10 times the update rate to ensure that fading between allocation updates was modelled accurately. Figure 4-9 shows the location of the bit errors as a function of frequency and space. This is very similar to a contour plot of the channel SNR, with more errors occurring around the transitions between modulation scheme allocations. The bit errors are also clustered around the falling edges of the channel SNR, where the modulation is being reduced from a high to a lower modulation scheme. The errors tend to occur here due to the delay in the allocation scheme. The BER threshold used for modulation allocation was 2×10^{-6} , which is 20 times lower than the resulting BER of 4.5×10^{-5} . This is also due to the delay in the allocation.

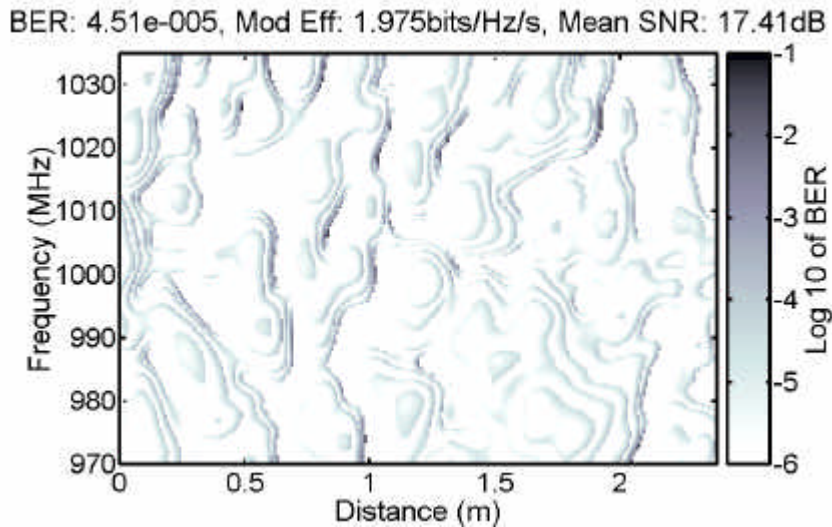


Figure 4-9, Location of the bit errors for the adaptive modulation simulation.
(script s0059)

In addition to the adaptive modulation simulation, the performance of a fixed modulation scheme was simulated under the same conditions. The average spectral efficiency of the adaptive modulation scheme was 2.0 b/s/Hz, and so the fixed modulation was simulated using QPSK, to give the same spectral efficiency. The location of the bit errors is shown in Figure 4-10. As expected we can see that most of the errors occur in the deep fades in the channel SNR, and any region where the SNR was less than 10 dB. Regions of high SNR have an error rate of virtually zero, showing that they are under-utilised. The overall BER corresponded to 0.011, which is extremely high, and approximately 250 times worse than the adaptive modulation scheme.

The fixed modulation simulation was repeated, but with a higher SNR. It was found that the SNR had to be raised to 34 dB before the BER dropped below the BER of the adaptive modulation scheme at a SNR of 17.4 dB. This shows that the adaptive modulation dramatically decreased the effects of fading, allowing the SNR to be lowered by 16.5 dB as compared with a fixed modulation scheme.

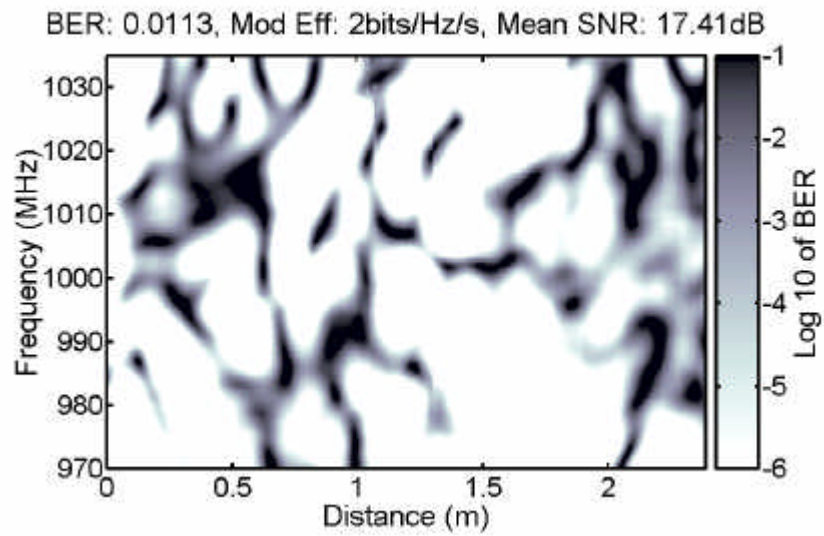


Figure 4-10, Location of bit errors for fixed modulation of QPSK, for the same channel as used for the adaptive modulation simulation (script s0059).

4.3 MULTIUSER SUBCARRIER ALLOCATION

There are several methods for allocating subcarriers to users in a multiuser OFDM system. The main five schemes are to use a group of subcarriers with a fixed frequency, randomly hopped subcarriers, using TDMA, spread out subcarriers in a comb pattern and adaptive user allocation.

The performance of these five different user allocation schemes were simulated using the wide band radio measurements presented in Chapter 3 section 3.8. These data sets are a measurement of the path loss to 10 locations within the Electrical and Computer Engineering building. The details of each measurement are shown in Appendix C. The path loss was measured as a function of frequency and distance, with it showing the dependence of frequency selective fading with space.

The multiuser allocation simulation was performed using 10 users. The propagation characteristics for each user were obtained by matching each user to one of the propagation measurements shown in Appendix C. The velocity of all the users was set to 3 m/s and the user allocation was performed over a movement path of 2 m. All five simulations used adaptive modulation in order to determine the modulation for each subcarrier in each time slot, with the only difference being the subcarrier frequencies allocated to each user. The adaptive modulation and the subcarrier frequency allocation was updated at a rate of 250 Hz, which corresponds to a distance travelled between updates of 4% of wavelength, for the carrier frequency of 1005 MHz used. The frequency allocations were subdivided into 100 subcarriers over the system bandwidth of 70 MHz. In practice the number of subcarriers would be more than this, however the number was kept reasonably low so that the frequency allocations could be seen in the simulation plots.

A BER threshold of 1×10^{-6} was used to decide on the SNR thresholds for the adaptive modulation allocation. The choice of this BER threshold is arbitrary and dependent on requirements of the final application of the system. Changing this threshold would result in a slight change in data throughput, however the general conclusions derived from the comparison of the different techniques would be the same. In this simulation the adaptive modulation, and user allocation were performed

with zero delay. The effect of adding delay to the allocation scheme is investigated in section 4.4.

Perfect channel estimation was assumed in this simulation. This would enhance the performance of the simulated system as compared with a practical system. In a practical system the effects of noise in the channel estimation can be minimised using several techniques discussed in section 2.7, and so the absolute error introduced by assuming perfect channel estimation will be less than 0.5 - 3 dB, depending on the system implementation. Since all the user allocation schemes will be affected in a similar manner the error in the comparison between these schemes will be much smaller (about 0.2 – 0.5 dB).

Two-dimensional quadratic interpolation was used to find the channel response at times matching the adaptive modulation tracking times. Finer interpolation was used to find the response of the channel between the tracking times. This was then used to estimate the BER due to channel response tracking errors of the system.

For each user allocation scheme simulation, two tests were performed. The first simulation measured the performance when all the transmitters in the system used a fixed transmitter power of -10 dBm. Since the path loss to each of the users varied by 40 dB the average received SNR also varied by about 40 dB. The second simulation measured the performance when power control was used to set the average SNR of all users to 20 dB. This power control was performed by calculating the average path loss of the channel from the base station to each user, then setting the transmitter power so that the average SNR at the base station was 20 dB. This calculated transmitter power was fixed over the 2 m path moved by each user.

In each of these simulations multiple users are transmitting at the same time in the same frequency band. These multiple transmissions form a single OFDM signal at the base station's receiver. In order for these signals to remain orthogonal to each other, they must all be frequency and time synchronised with each other. The time synchronisation must be accurate to within the effective guard period length (shorter than the actual guard period length due to channel delay spread), while frequency synchronisation must be sufficiently accurate as to maintain a sufficiently high effective SNR as to use the modulation schemes used in the simulation. The

maximum spectrum efficiency used in the adaptive modulation scheme used was 256-QAM, which requires an effective SNR of at least 32 dB (see Figure 2-31). If we assume that the period between channel characterisation pilot symbols is 16 symbols, then from Figure 2-46 we can estimate that a frequency offset accuracy of less than 0.02% of the subcarrier spacing is required to ensure that the SNR is not degraded by frequency errors. For a system with subcarrier spacings the same as HiperLAN2 (312.5 kHz) the maximum allowable frequency offset would be 62.5 Hz. At the transmission frequency of HiperLAN2 (5.2 GHz) a velocity of 3.6 m/s would result in a Doppler spread of 62.5 Hz. In order to use 256-QAM at higher velocities a multiuser Doppler spread correction technique would need to be implemented. The best method for implementing this is currently unknown. The frequency error tolerance of the system improves when the modulation scheme is lowered or the number of pilot symbols or tones is increased.

4.3.1 FIXED FREQUENCY GROUPED SUBCARRIERS

The simplest user subcarrier allocation scheme is to assign each user a group of fixed frequency subcarriers. Grouping the subcarriers will tend to minimise the level of inter-user interference due to distortion, power level variation and frequency errors. However, having a fixed group of subcarriers makes the transmission susceptible to fading, as the whole group of subcarriers can be lost in a null in the spectrum. Time interleaving with forward error correction can improve fading performance of a moving station. However for stationary applications, static nulls can greatly degrade performance. One method for overcoming the problems of fading is to use diversity reception. A study of diversity using the same propagation measurements is outlined in Appendix C.1.

Each user in this simulation was allocated a continuous block of spectrum, 7 MHz in bandwidth. The frequencies were fixed over the simulated path and show up as horizontal stripes in Figure 4-11.

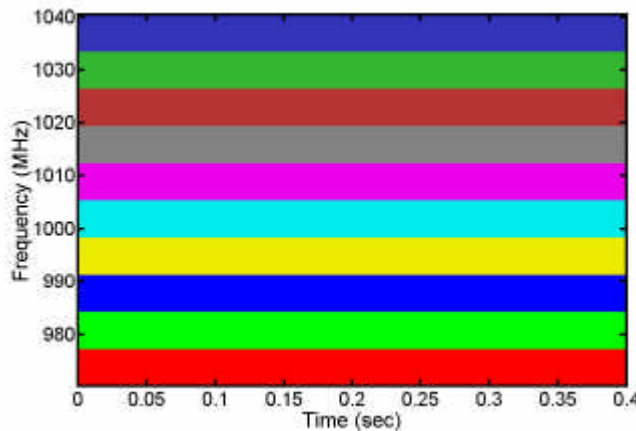


Figure 4-11, Frequency allocations for the fixed frequency group of subcarriers simulation. (script s0059)

Each of the 10 users was allocated 7 MHz bandwidth, shown as different colours and tones in the figure.

Figure 4-12 shows the simulated performance for the fixed user allocation scheme. For the simulation using a fixed transmitter power of -10 dBm, several of the users have insufficient power to support the bandwidth allocated, and so their SNR is insufficient to support even BPSK. These users have a data rate of 0 bps. Several of the users have a very high SNR and so end up continually operating at the maximum spectral efficiency, which in this simulation was set to 8 b/s/Hz.

The second simulation shows the performance when the path loss between the users is normalised using a rough power control. In this simulation the average SNR of each user was set to 20 dB. Each of the ten users suffers from frequency selective fading causing their data rate to vary significantly with time. Each of the users experienced fading of sufficient enough depth to interrupt the data transfer (modulation efficiency of 0 b/s/Hz). The length of these nulls was typically 5 cm in length.

It can be seen from Figure 4-12 (g) and (h) that the overall system throughput was higher for the slow power control experiment. This is simply due to a higher average SNR and does not imply that slow power control is better than a fixed transmitter power. The absolute throughput of the slow power control simulation was not intended to be compared directly with the fixed power simulation, but more to highlight the different properties of these techniques.

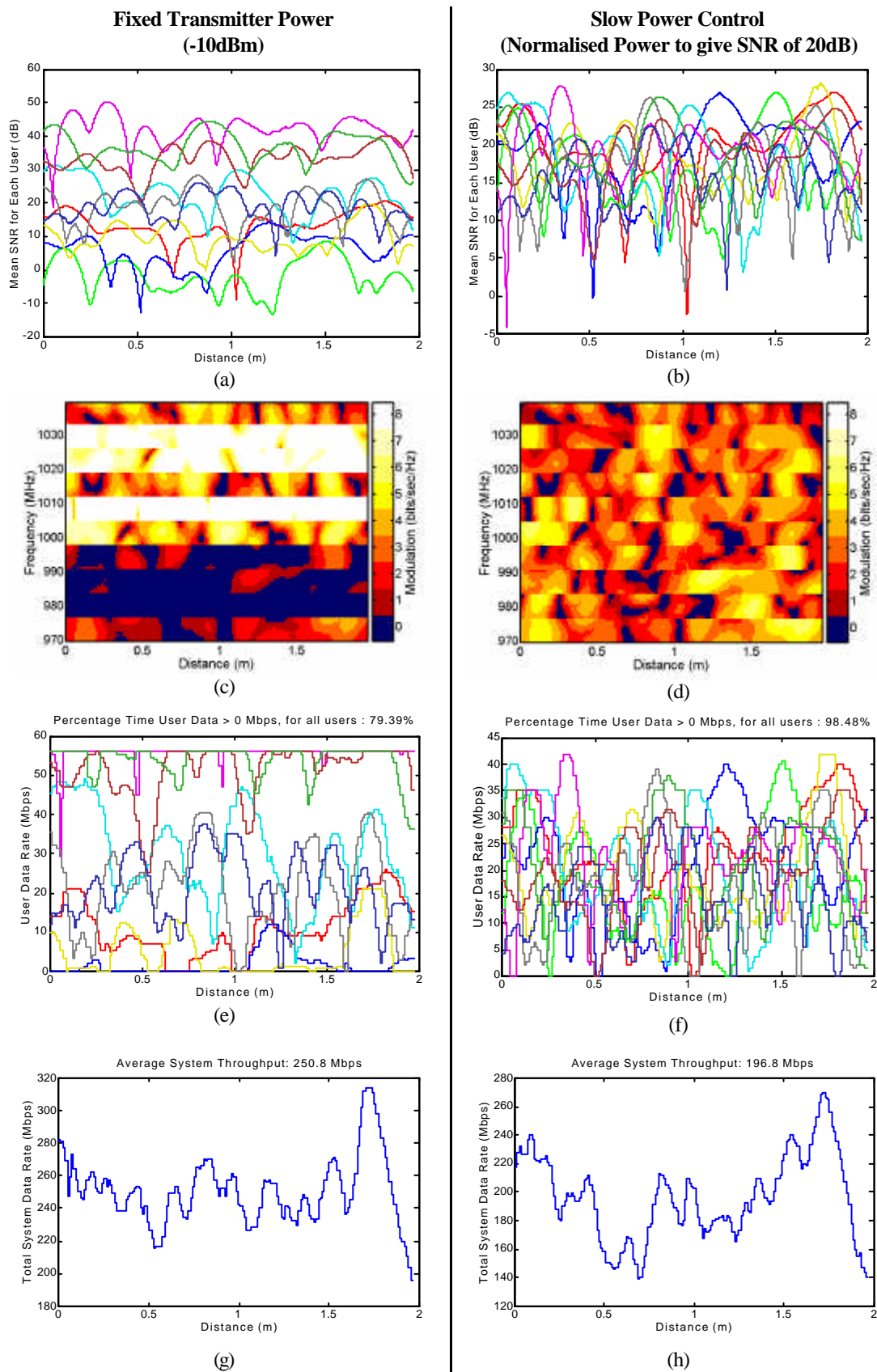


Figure 4-12, Simulated performance from allocating a fixed frequency group of subcarriers to each user. (script s0059)

4.3.2 RANDOM FREQUENCY HOPPING

Fixed wireless systems suffer from problems caused by static fading. In a static radio environment the frequency selective fading is constant resulting in static fading. In a mobile channel time interleaving can be used to cope with the brief periods when the entire signal is faded, however for a static channel the fading period becomes indefinitely long in time, making time interleaving ineffective.

This problem of static fading can be partly overcome by randomly frequency hopping the subcarriers over a wide bandwidth. In the user allocation scheme described by [84], groups of subcarriers are transmitted in short time blocks. These blocks are randomly frequency hopped to ensure that the time period spent in a null would be relatively short, approximately 11 symbols. To recover data lost during a null, time interleaving and forward error correction is used. These come at the cost of reduced system data capacity and increased delay. Grouping of the subcarriers allows the correlation between the subcarriers to be utilised.

A multiuser OFDM system using random hopping subcarrier allocation was simulated using the same conditions as the fixed frequency grouped carriers in section 4.3.1 . The performance of the random hopping system is shown in Figure 4-14. The quality of service for the random hopping is better than the fixed frequency group allocation. This is because the random allocation tended to spread the user allocation over the entire system bandwidth, minimising the probability of all the subcarriers suffering deep fading at the same time.

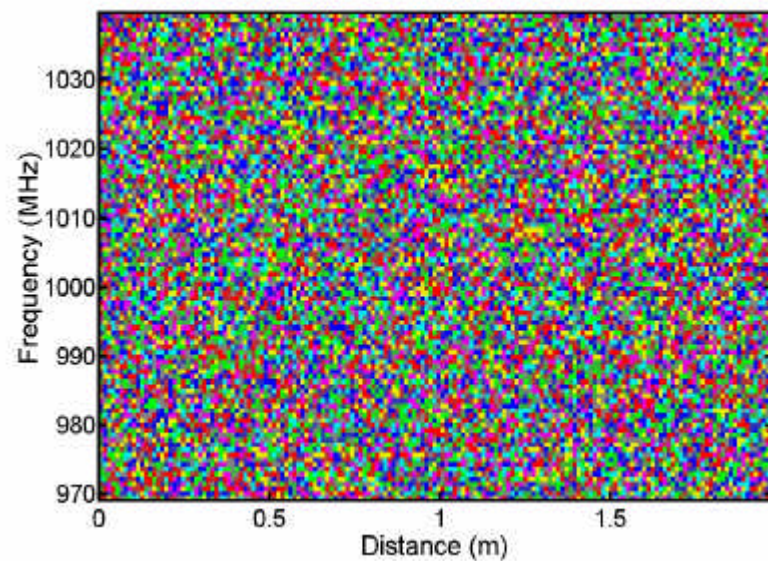
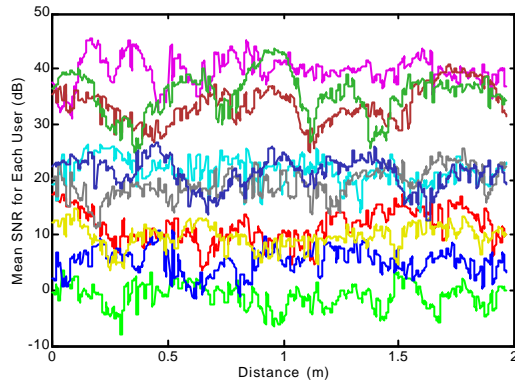
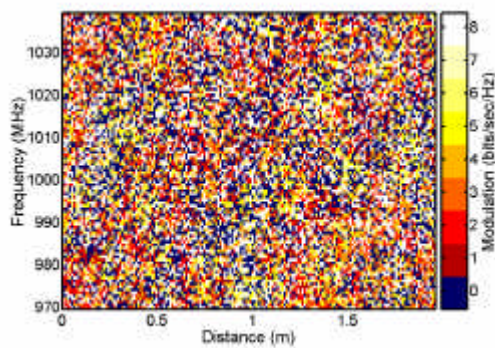


Figure 4-13, Frequency allocations for each user with random frequency hopping. (script s0059)

**Fixed Transmitter Power
(-10dBm)**

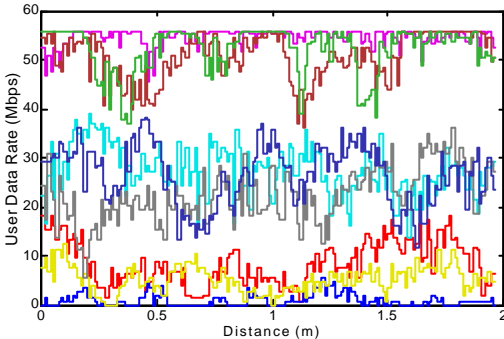


(a)



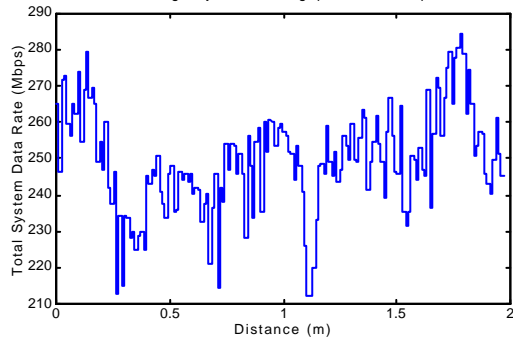
(c)

Percentage Time User Data > 0 Mbps, for all users : 85.55%



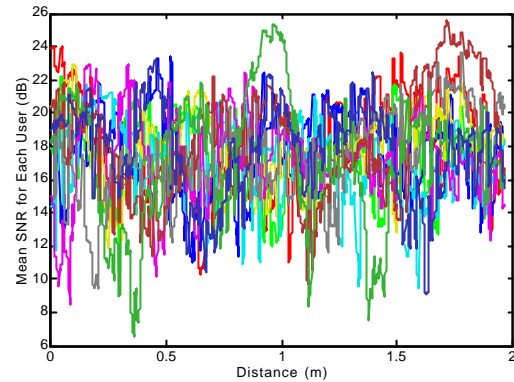
(e)

Average System Throughput: 249.3 Mbps

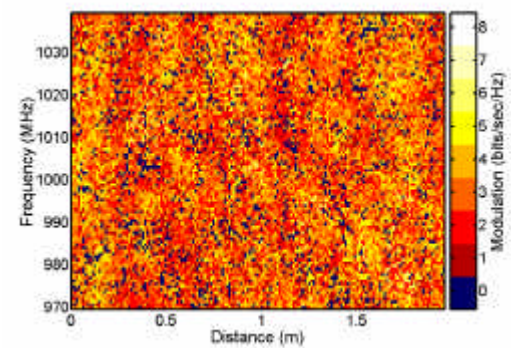


(g)

**Slow Power Control
(Normalised Power to give SNR of 20dB)**

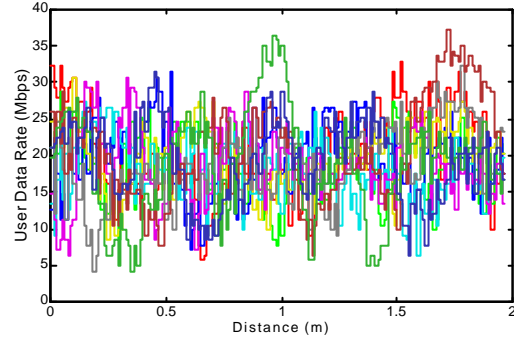


(b)



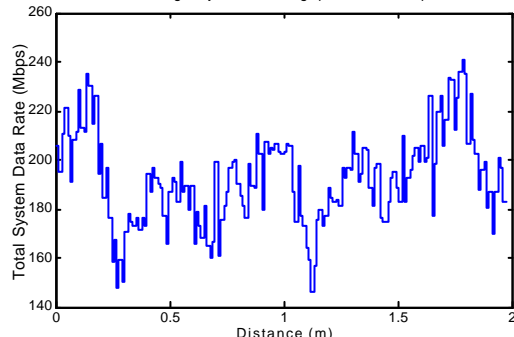
(d)

Percentage Time User Data > 0 Mbps, for all users : 100%



(f)

Average System Throughput: 192.6 Mbps



(h)

Figure 4-14, Simulated performance for randomly hopped groups of subcarriers.
(script s0059)

4.3.3 TIME DIVISION MULTIPLE ACCESS ALLOCATION

Using TDMA to separate users is one of the simplest methods for obtaining multiple user access. This is implemented by allocating each user unique time slots, during which only a single user accesses the channel. The allocation of time slots to individual users can be achieved in several ways, with the most suitable depending on the application and the type of data being transferred. With voice communications, video and other real time constant bit rate applications, it is better to pre-allocate users fixed time slots, then cycle between them in a round robin fashion. This ensures each user obtains the bit rate required and prevents collisions between transmissions. However for most applications the data traffic tends to arrive in random bursts. Data traffic tends to have similar statistical properties over a range of time scales, from milliseconds, seconds, minutes, hours, and even weeks. This means that data tends to cluster, and that these clusters also tend to cluster [89]. This can make pre-allocating of time slots inefficient, as most of the time no data is being transferred. To partly overcome these difficulties, it is likely that the most efficient allocation scheme would be a dynamic hybrid of pre-allocating users that have a constant bit rate and dynamically allocating users with a variable bit rate.

The performance of a round robin TDMA user allocation scheme is shown in Figure 4-16. In this simulation each user was allocated the full bandwidth of the channel. The 10 users were then allocated evenly spaced time slots in a round robin fashion. The peak transmitter power was boosted by 10 dB to ensure that the average power was the same as the other user allocation tests.

Figure 4-16 (a) shows the SNR verse distance travelled for all 10 users. The SNR is discontinuous due to the switching of time slots between users.

The synchronisation requirements for TDMA allocation is reduced compared with allocation schemes that allow multiple users to transmit at the same time. These include fixed frequency group allocation, random allocation, comb allocation, and adaptive user allocation. The overlapping of the subcarriers in the frequency domain requires very tight frequency synchronisation between multiple users transmitting at the same time. TDMA allocation removes the need for users to be frequency synchronised to each other.

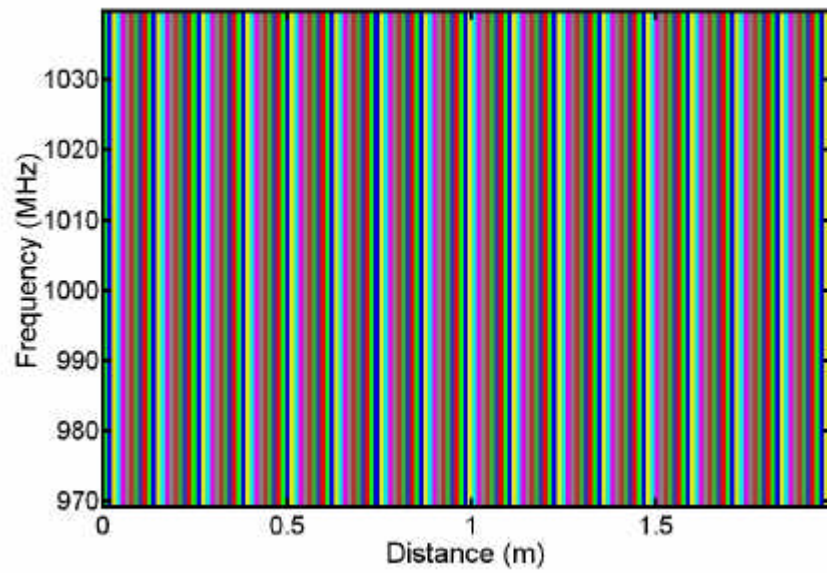


Figure 4-15, Frequency allocations for each user with TDMA. (script s0059)

Each user is shown as a different colour and tone. The users are allocated time slots in a round robin fashion, during which the single user allocated the time slot uses all the system subcarriers.

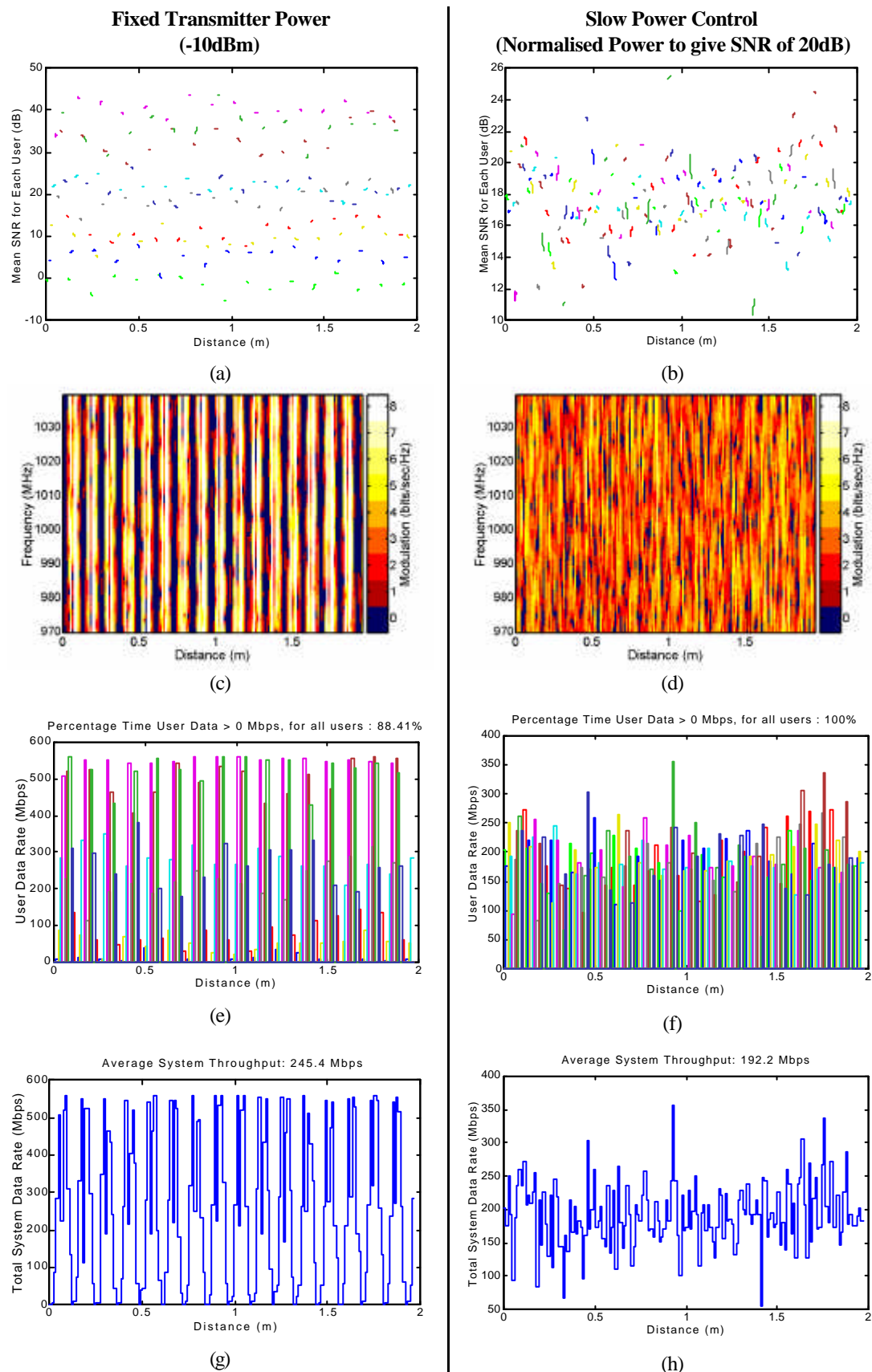


Figure 4-16, Simulated performance for TDMA allocation. (script s0059)

4.3.4 COMB SPREAD SUBCARRIERS

Static nulls can occur for fixed wireless applications causing problems if the transmission uses a single group of subcarriers with a fixed frequency. Instead, subcarriers can be allocated in a fixed comb pattern, spreading them over the entire system bandwidth. This improves the frequency diversity, preventing all the subcarriers used by a user being lost in a single null in the spectrum.

Transmitting as a comb pattern requires user subcarriers to be interleaved with one another, resulting in a large amount of overlapping energy between the users. Any slight loss of orthogonality due to frequency or timing errors can result in significant inter-user interference. By comparison, grouping the user subcarriers will slightly reduce the energy overlap between users, thus reducing inter-user interference. Despite these potential problems this type of user allocation is useful in applications that cannot use adaptive hopping or random hopping, due to the added complexity.

Figure 4-18 shows the simulated performance of a 10 user multiuser system using adaptive modulation and a frequency allocation using a comb pattern. The frequency allocation is shown in Figure 4-17. Using a comb pattern results in a high frequency diversity of the signal. The average SNR of the subcarriers allocated to each user (see Figure 4-18 (a)) is very small with relative small fading (< 10 dB).

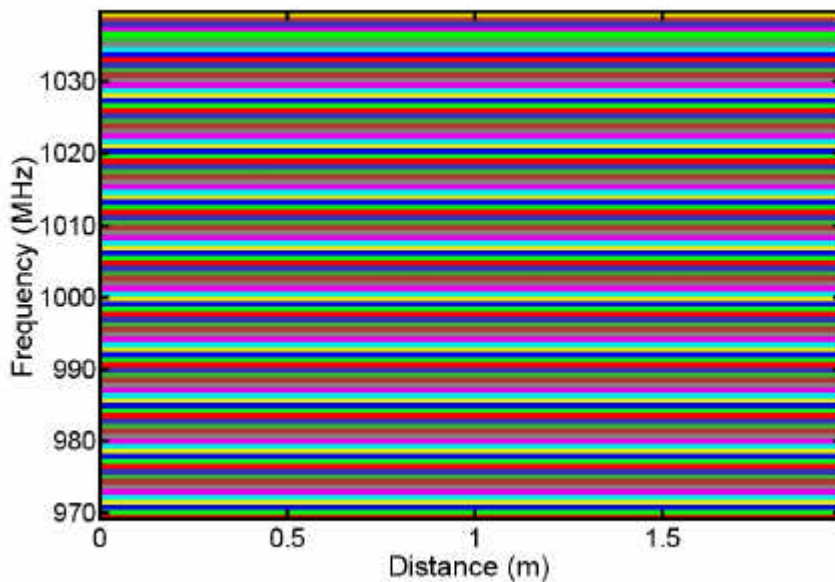


Figure 4-17, Frequency allocations for each user with a comb frequency pattern.
(script s0059)

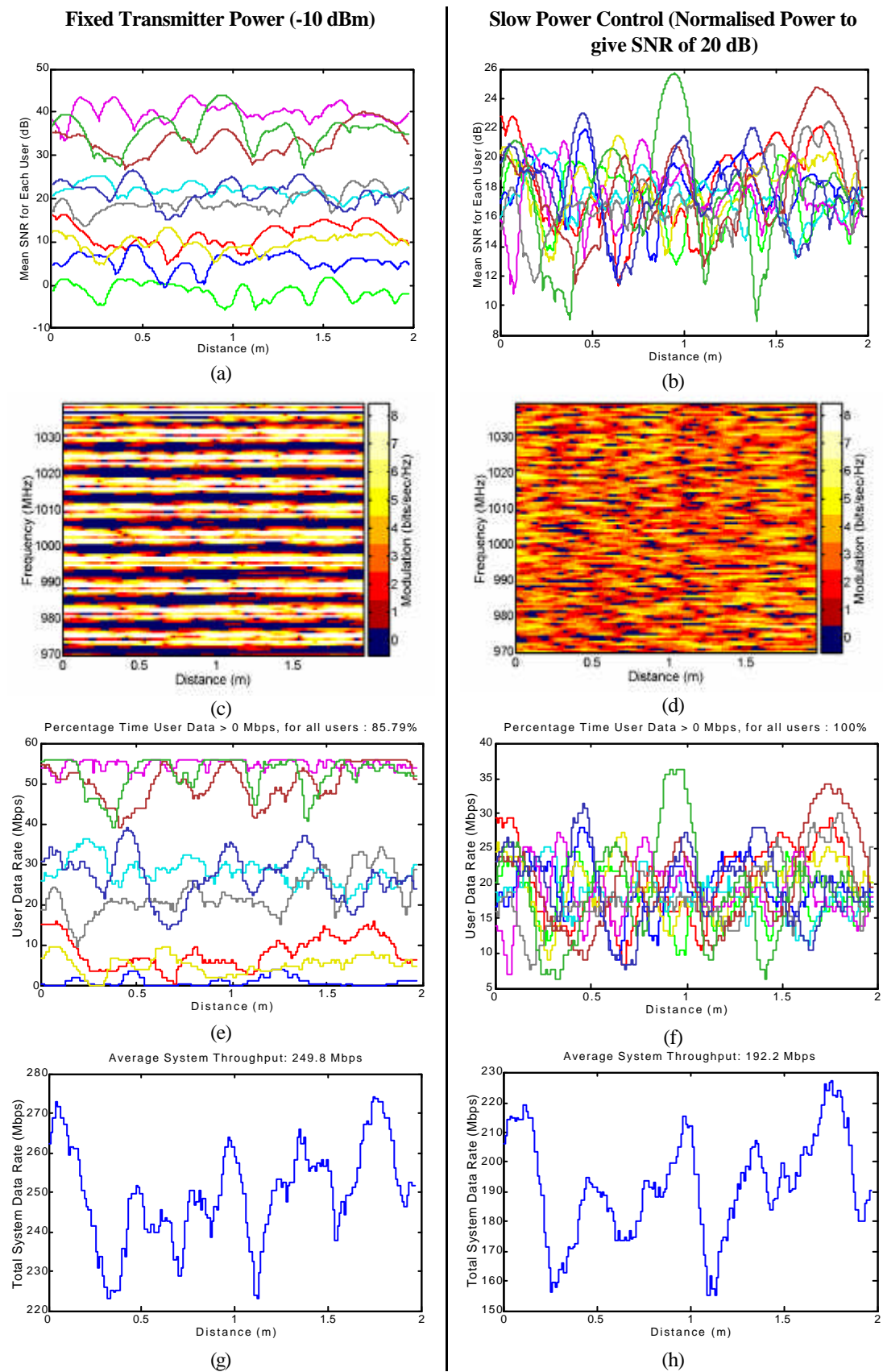


Figure 4-18, System performance when using adaptive modulation and comb frequency allocation. (script s0059)

4.3.5 ADAPTIVE USER ALLOCATION AND ADAPTIVE BANDWIDTH

A new adaptive frequency hopping technique is proposed for multiuser OFDM systems such that blocks of subcarriers are hopped based on the current channel conditions. After the radio channel has been characterised, each of the users is allocated subcarriers that have a high SNR for that user. Since each user will be in a different physical location their fading pattern will be different. The strongest subcarriers for one user are likely to be different from the other users. Similarly the subcarriers that are nulls for one user are likely to be strong in at least one other user in the system. Thus in most cases users can be allocated subcarriers with a high SNR, allowing the entire system bandwidth to be used without any nulls.

All the previous user allocation schemes outlined from section 4.3.1 - 4.3.4 have allocated a fixed amount of bandwidth to each user, regardless of the received signal power. This has led to problems for users that have low received signal strength. The SNR of these users was insufficient to support communications even using BPSK. The SNR seen at the receiver is dependent on the signal bandwidth, and so reducing the bandwidth while using the same transmitter power increases the SNR of the signal. For example, reducing the signal bandwidth by 10 times, allows the full transmitter power to be concentrated into one tenth the bandwidth, increasing the transmitted power spectral density by 10 fold, resulting in an improved received SNR of 10 dB.

The main aim of adaptive bandwidth allocation is to maintain communications with users that have low received signal strength. This is achieved by reducing their bandwidth to the point where the transmitted power spectral density is high enough to support communications at a low data rate. This can be used as a method for improving the quality of service (i.e. decreasing the outage probability).

Adaptive bandwidth by itself will not be suitable for all applications, especially those that required a fixed data rate such as streaming video and audio. In these applications a joint optimisation of bandwidth and modulation scheme could be performed to maintain a fixed data rate, while minimising the amount of bandwidth used at any one time. This could be achieved by allocating both the user bandwidth and modulation scheme so that the spectral efficiency multiplied by the user

bandwidth results in the required data rate. This way, as the signal strength becomes weaker, the amount of bandwidth allocated to that user increases to compensate. This fixed data rate optimisation is not included in the presented adaptive user allocation algorithm, and could be researched as future work.

In order for the adaptive techniques (adaptive user allocation, adaptive modulation and adaptive bandwidth) to work effectively all users in the system must be frequency and time synchronised to each other in order to maintain subcarrier orthogonality in the reverse link to the base station. In addition to this, the base station requires complete knowledge of the channel response to all the users in the system. This makes full implementation of such a technique difficult, as the overhead in requiring this information can be very high, particularly if the mobile users are moving or the system bandwidth is low. The principles involved in adaptive user allocation and adaptive bandwidth can however be reduced to fit various applications, while still providing some optimisation of system efficiency.

4.3.5.1 ADAPTIVE BANDWIDTH ALGORITHM

An algorithm for implementing adaptive bandwidth allocation was developed to investigate its possible benefits. While the algorithm developed performs reasonably well, it is not optimal. The joint optimisation of adaptive bandwidth allocation, adaptive user allocation and adaptive modulation allocation is reasonably complex. One method would be to check each combination of user allocations using brute force, however such a scheme would be extremely inefficient, especially when the number of users and subcarriers is large. The adaptive bandwidth algorithm presented uses an iterative process allocating users a given bandwidth; if this allocation results in the SNR being too low due to a low power spectral density, then the bandwidth to that user is decreased. The freed bandwidth is then re-allocated to other users. The algorithm is performed as follows:

Adaptive Bandwidth algorithm used in simulations:

- (1) Initially allocate all users an equal number of subcarriers, using the *adaptive user allocation* algorithm (see algorithm shown in section 4.3.5.2).
- (2) Calculate the SNR of all the subcarriers for a given user, based on the bandwidth allocated and the particular subcarriers that were allocated in step 1.

- (3) Find the minimum SNR of the subcarriers allocated to each user.
- (4) For each user check that every subcarrier allocated to that user, has a SNR greater than a given threshold. This is done to ensure that each subcarrier has a sufficiently high SNR to support at least BPSK modulation. A threshold of 12 dB was used in the simulations shown in Figure 4-19 and Figure 4-20. If a user has any subcarriers below this threshold then reduce the BW (number of subcarriers) allocated to that user. This frees up BW, making it available to other users. Make sure that each user is allocated at least one subcarrier. This prevents the degenerate case where a user is allocated zero subcarriers, which in turn makes the estimated SNR infinite (The SNR is inversely proportional to the signal bandwidth).

If all subcarriers meet the minimum SNR threshold, then the user allocation is complete, so apply adaptive modulation to each subcarrier and exit. If the SNR of one or more subcarriers is below the threshold then continue onto step 5.

- (5) Redistribute the free BW by allocating it to users that have a SNR significantly greater than the minimum SNR threshold. Transmitting over a wider BW results in a lower transmitted spectral density and received SNR. Thus there is no use reallocating the extra BW to a user that is just above the SNR threshold, as this would result in their SNR dropping below the threshold, defeating the purpose of the reallocation. In the simulations the extra BW was only allocated to users that were at least 3 dB above the minimum SNR threshold.

To help with data load levelling, the extra BW should be allocated to users that have a low SNR first, as users with a high SNR will already have a comparatively high data rate and thus shouldn't need more BW.

- (5) Based on the new user BW allocations, reallocate the subcarriers to users by repeating the *adaptive user allocation* algorithm (see algorithm shown in section 4.3.5.2).
- (6) Repeat from (2) until all allocated subcarriers have a SNR above the required threshold.

The exit for this algorithm is in step (4). It usually takes 3-5 iterations, however under certain channel conditions there will be no solution for meeting the minimum

SNR criteria, causing it to iterate infinitely, so limit the number of iterations to approximately 10 loops. No solution will be found when the received energy for one or more users is insufficient to support a SNR above the threshold, even when being allocated a single subcarrier.

4.3.5.2 ADAPTIVE USER ALLOCATION ALGORITHM

This algorithm allocates system subcarriers to each of the users based on the bandwidth allocated to each user, and the SNR of the user channels. Subcarriers are allocated to each user based on the frequency selective fading of the channel for that user. Ideally a system wide optimisation would result in all users being allocated subcarriers that correspond to peaks in the frequency response for each of the users. A fully optimised solution would however require an exhaustive search of all subcarrier-to-user allocation combinations, and thus would be very computationally intensive. A simple algorithm is proposed that allocates subcarriers to users with the lowest average SNR, thereby giving them first pick at the best subcarriers. This algorithm will tend to maximise the quality of service rather than maximise system spectral efficiency.

The algorithm outlined below performs relatively poorly if all of the users have a similar average SNR, as the user with the highest SNR (even if it is only 0.1 dB higher than the other users) will get last pick of the subcarriers. As a consequence it may end up with subcarriers that are all in nulls. A fairer algorithm in this case might be to allocate single subcarriers from each user in a round robin fashion. Optimisation of the algorithm is left to future research.

Adaptive User allocation algorithm used in simulations:

- (1) Find the mean SNR over the entire system BW for each user.
- (2) Perform allocation of subcarriers to users in-order, from, lowest mean SNR, to highest mean SNR. This helps to ensure that weak users get access to the best subcarriers.
- (3) Sort the SNR response for the user being allocated, removing any subcarriers that have already been allocated to other users. The SNR response is the SNR of each subcarrier as seen by that user. This will be different for each user, due to propagation variations.

- (4) Allocate from the sorted SNR response subcarriers in descending order from best SNR to worst SNR subcarriers to meet the BW required for the user. Repeat from step 2 until all users have been allocated.

4.3.5.3 COMBINED ADAPTIVE USER ALLOCATION, ADAPTIVE BANDWIDTH RESULTS

The simulated performance of a combined adaptive user allocation, adaptive modulation and adaptive bandwidth system was measured under the same channel conditions as previous simulations outlined in section 4.3.1 through to 4.3.4. In this simulation the adaptive modulation, adaptive bandwidth and adaptive user allocation scheme was updated for each 0.04λ of movement, where λ is the wavelength of the RF carrier. The performance of the system was measured at a finer spacing of 0.005λ in order to show the effect of channel change between modulation updates.

Figure 4-19 (a) and (c) show the performance of a system with a fixed user transmission power of (-10 dBm). From this we can see that the bandwidth allocated to each user varies due to the adaptive bandwidth scheme. In previous simulations several of the users could not support any data transmission due to an insufficient SNR. With adaptive bandwidth the weakest user was only allocated a bandwidth of less than 1 MHz, instead of the usual 7 MHz, (see Figure 4-20 (c)). From Figure 4-20 (e) we can see that the percentage time where the data rate is above 0 bps, is 100%, which is much better than other allocations schemes (fixed bandwidth group 79.4%, Random frequency hopping 85.6%, TDMA 88.4% and Comb 85.8). This is a direct result of the adaptive bandwidth allocation. A SNR threshold of 12 dB was used to determine the maximum bandwidth that could be supported by each user. If their SNR was below 12 dB then the user bandwidth was reduced until the SNR of their weakest subcarrier achieved a SNR above 12 dB. The effect of this algorithm can be seen in Figure 4-20 (a) where the SNR of the weaker users hovers around the threshold of 12 dB. Their SNR dips below the 12 dB threshold several times due to the slow tracking rate of the adaptive user allocation (0.04λ).

For the simulation using power control, Figure 4-19 (b) and (d), the modulation applied is very consistent, with little evidence of fading.

The system data rate with adaptive user allocation is much higher than that achieved

by any passive allocation scheme. For the fixed transmitter power the average system data rate was 348 Mbps, which is 40% higher than the passive allocation schemes that all achieved a data rate of approximately 250 Mbps.

Adaptive user allocation combined with adaptive bandwidth and adaptive modulation produces a system that has both a very high quality of service and a high spectral efficiency.

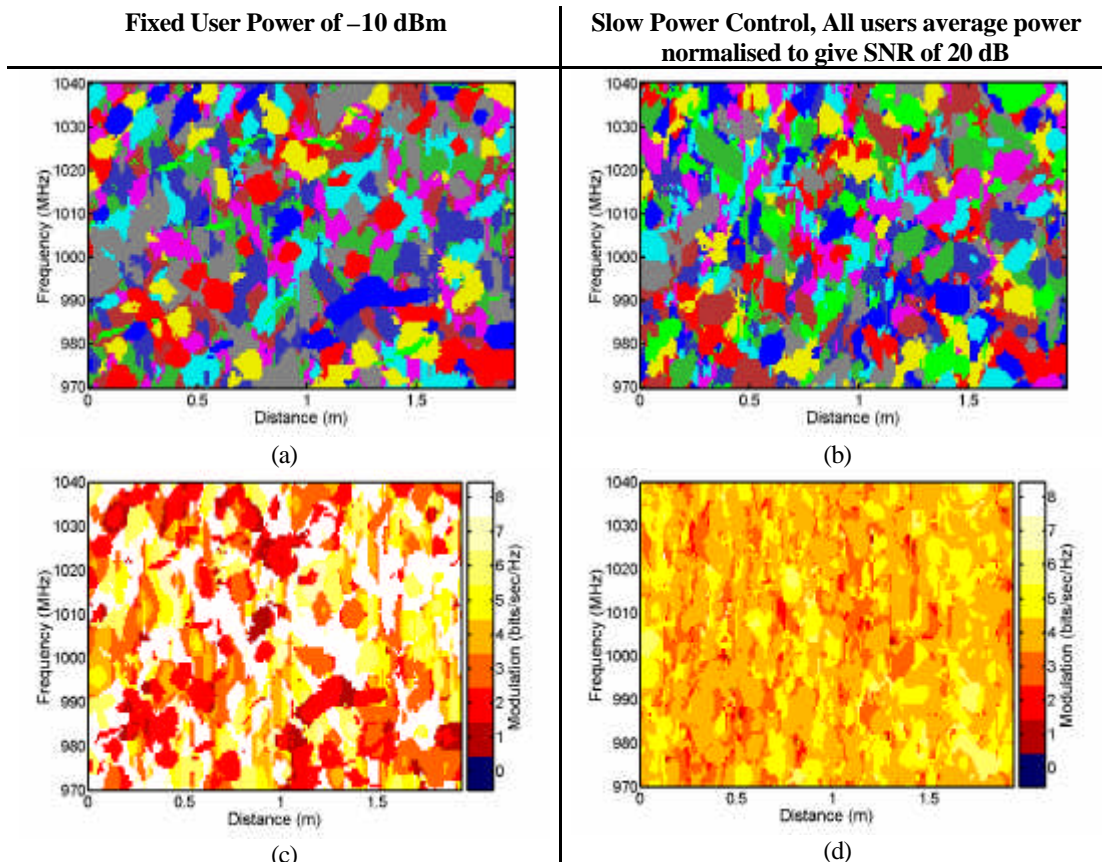


Figure 4-19, Simulated adaptive user allocation, utilising adaptive bandwidth, adaptive frequency, and adaptive modulation. (script s0059)

Results shown in (a) and (c) are for each user having a fixed transmission power. The transmitter power in (b) and (d) were set so that the average received power would result in an average SNR of 20 dB. (a) and (b) show the frequency allocations for each of the users. Each user is shown as a different colour. (c) and (d) show the modulation scheme used at each frequency. This simulation assumed perfect channel knowledge for each user.

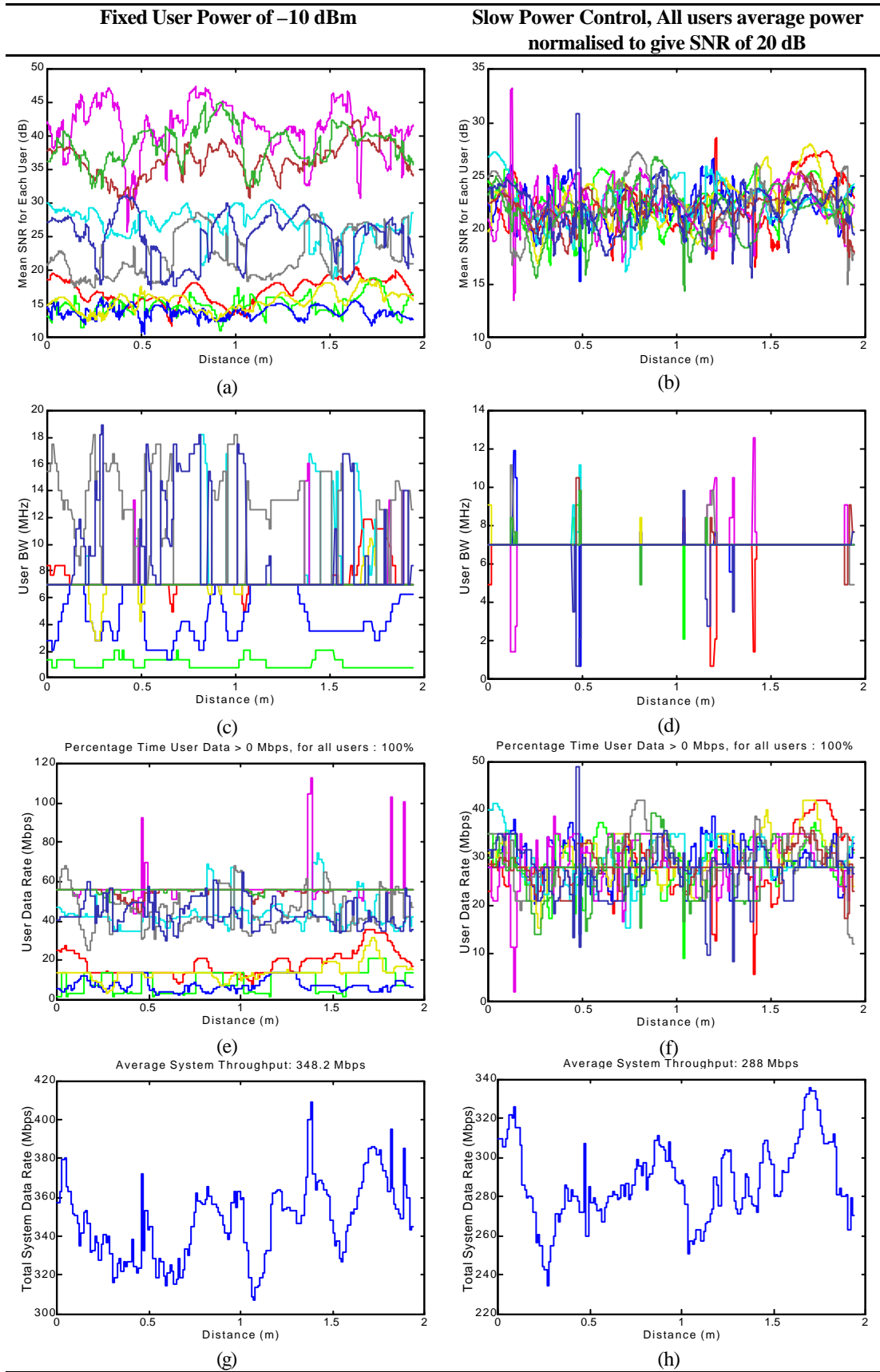


Figure 4-20, Continuation of results from Figure 4-19

(a) and (b) show the SNR for each user, (c) and (d) shows the bandwidth allocated to each user, (e) and (f) shows the resulting data rate for each user, and (g) and (h) showing the overall system data rate. (script s0059)

4.3.6 SUMMARY OF USER ALLOCATION SCHEME PERFORMANCE

The data throughput and QOS for a number of user allocation schemes were simulated. These schemes can be logically grouped into two types based on whether the user allocation was based on current channel conditions or not. Fixed frequency grouped allocation, TDMA allocation, Random allocation, and Comb allocation all assign the user subcarriers with no consideration of the current channel conditions, and so these can be grouped and are referred to as passive allocation. As a contrast to these schemes, adaptive user allocation allocates the frequency and time slots based on the current channel conditions, and so can be considered to be an active allocation scheme.

User Allocation	Fixed User Power (-10 dBm)			Slow Power Control (Avg. SNR 20 dB)		
	System Data Rate (Mbps)	QOS (% User Data > 0 Mbps)	BER ($\times 10^{-5}$)	System Data Rate (Mbps)	QOS (% User Data > 0 Mbps)	BER ($\times 10^{-5}$)
Fixed Group	250.8	79.4	0.95	196.8	98.5	0.61
TDMA	245.5	88.4	1.1	192.2	100	0.60
Random	249.3	85.6	1.4	192.6	100	0.59
Comb	249.8	85.8	1.3	192.2	100	0.62
Adapt. User	348.2	100.0	0.4	288.0	100	0.27

Table 4-2, Summary of system performance when using different user allocation schemes. Note: all schemes used adaptive modulation.

It can be seen from Table 4-2 that the system data rate for all of the passive user allocation schemes is approximately the same at around 250 Mbps. This is a result of the uniform probability distribution of all radio channels. All of the radio channels in the simulation had a Rayleigh fading probability distribution (see section 3.8). As a result any passive allocation scheme will also suffer from Rayleigh fading, regardless of how the frequency-time slots are allocated. This means that the system throughput of all passive allocation schemes will be approximately the same, as each of them will have approximately the same SNR distribution and corresponding spectral efficiency.

The only scheme that performed better is adaptive user allocation. It resulted in a higher system data rate, a higher QOS, and a lower BER, all of which can be attributed to the optimisation of the user frequency allocation. The higher data rate is a result of the users being allocated peaks in the channel response, which reduced the path loss and consequently resulted in a higher average SNR and data rate. The higher QOS was a result of the adaptive bandwidth algorithm used. The lower BER of adaptive user allocation as compared with passive allocation schemes is a result of the users being allocated peaks in the channel response. The channel response (magnitude of the channel response in log scale) changes slower at the peaks than the nulls and as a result the channel tracking for adaptive modulation is more accurate. This reduces tracking error and results in a reduction in the BER.

4.4 TRACKING RATE REQUIRED FOR ADAPTIVE MODULATION AND ADAPTIVE USER ALLOCATION

Adaptive modulation and adaptive user allocation are dynamic techniques that require continual tracking of the changing channel conditions in order to perform well. The reallocation of the modulation and the user subcarriers have to be refreshed many times per second in order to maintain a high performance.

Two different user allocation schemes were simulated (adaptive user allocation and fixed frequency group allocation) at different tracking rates, both using adaptive modulation.

Adaptive user allocation has a different performance to passive allocation schemes such as random frequency hopping, fixed group or comb allocation, as it aims to steer clear of nulls in the spectrum. This improves the SNR of the subcarriers and lowers the required tracking rate. This is because the rapid changes in the channel response occur around the nulls, thus by avoiding them the channel appears to change more slowly, consequently lowering the required tracking rate.

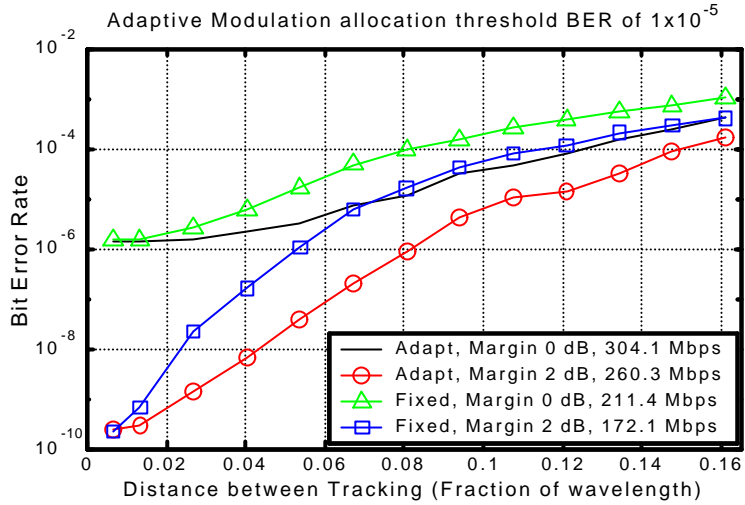


Figure 4-21, BER as a function of the distance between tracking points for a multiuser system using adaptive modulation and adaptive user allocation. (script s0061)

Figure 4-21 shows the BER as a function of the update rate. For adaptive user allocation both the subcarriers allocated to each user and the modulation scheme used were reallocated at each update. For the fixed group of subcarriers, only the modulation scheme was updated for each subcarrier. This simulation assumed that the BER of the link was determined only by the modulation scheme used and the current SNR of each subcarrier. Perfect channel knowledge was also assumed and that the delay between the channel response measurement and reallocation of the modulation scheme was zero.

Although the time between changing the modulation scheme was potentially large (up to 0.16λ) in this simulation it was assumed that the equalisation of OFDM receiver would be updated sufficiently fast to not cause a detrimental effect on the communication link. Also other detrimental effects such as distortion, frequency errors, Doppler spread, etc were not considered. Also overheads required implementing an adaptive user allocation scheme, or adaptive modulation was not included in the system data rate results. The main aim of this simulation was to focus on the potential effectiveness of both adaptive modulation and adaptive user allocation.

In Figure 4-21 the distance has been normalised as a fraction of the wavelength of the RF carrier.

$$D = \frac{VT}{\lambda} \quad (4-1)$$

Where D is the normalised distance as a fraction of the wavelength, V is the velocity of the user in m/s, T is the time between adaptive modulation tracking (sec), λ is the wavelength in m.

In the legend for Figure 4-21, the right most set of numbers shows the average system capacity for each simulation result. The system capacity was nearly constant as a function of update distance, with it varying by less than 1%. Adaptive user allocation, with a link margin of 0 dB, achieved the highest system data rate of 304.1 Mbps, (an average of 4.34 b/s/Hz). The fixed subcarrier allocation method only achieved 211.4 Mbps (3.02 b/s/Hz) for the same transmission power and communication channels. Adaptive user allocation achieves a higher capacity by exploiting the frequency selective fading so that users are allocated peaks in the frequency response, improving the average received power by about 4 dB. If the radio channels were completely flat with no fading, both fixed frequency allocation and adaptive user allocation would have performed equally well. In fact the adaptive user allocation would have been worse since it requires overhead to perform the adaptive allocation. Note however that the above simulation has not taken this overhead into account.

A link margin was added to the SNR thresholds determined by the BER. This link margin would increase the required SNR for each of the modulation schemes, resulting in the adaptive modulation erring on the side of caution. A positive link margin consequently results in a reduction in the BER and system spectral efficiency.

The SNR thresholds used to decide on the modulation allocations were chosen to give a maximum BER of 1×10^{-5} . These thresholds can be found in Table 4-1. However, at low speed, with a 0 dB link margin, the BER ends up being lower than this threshold (approx. 2×10^{-6}), which is a result of quantisation of the modulation allocation.

Another simulation was done showing the BER when a link margin of 2 dB was added to the SNR thresholds for a BER of 1×10^{-5} . This is also shown in Figure 4-21. The increased SNR threshold dramatically reduced the BER, but can at the cost of a

reduced overall system capacity. The system data rate for adaptive user allocation dropped from 304.1 Mbps (4.34 b/s/Hz) when no link margin was used, to 260.3 Mbps (3.71 b/s/Hz) for a 2 dB margin. This drop in the data rate is to be expected. For coherent QAM the spectral efficiency can be increased by 1 b/s/Hz for every 3 dB increased in SNR. Thus for a 2 dB margin we would expect $2/3 = 0.67$ b/s/Hz drop in the system spectral efficiency. The simulated results showed a drop of $4.34 - 3.71 = 0.63$ b/s/Hz, closely matching the expected value of 0.67 b/s/Hz. The advantage of this added link margin is that it allows the tracking rate to be lowered, while still maintaining the BER below the required threshold.

The lower limit on the BER that can be expected for adaptive modulation for a chosen BER threshold can be calculated. The easiest case is when the tracking rate is sufficiently high that it appears to be continuous. This is the case in Figure 4-21 where the distance between subsequent modulation updates is less than $0.01 \times \lambda$. If the adaptive modulation is updated on a continuous basis then SNR of the channel will always exceed the minimum SNR to achieve the chosen BER threshold. This excess in SNR, above the minimum threshold, results in the BER being lower than the chosen BER threshold.

If we assume that the SNR of the channel varies in a random manner, then the excess SNR will be approximately uniformly distributed between 0 and the SNR difference between the modulation scheme thresholds. For coherent QAM modulation this difference corresponds to 3 dB for each 1 bit/s/Hz increase. The average BER for a particular modulation scheme can be calculated by taking the average of the BER from the minimum SNR up to the threshold for the next modulation scheme. In most systems the SNR will vary sufficiently such that all modulation schemes will be used, thus the overall BER will be the average of average BER results for all modulation schemes.

BER Threshold	Theoretical Resulting BER (at high update rate)	Effective Margin (dB)
1×10^{-5}	1.4×10^{-6}	0.82
1×10^{-4}	1.7×10^{-5}	0.94
1×10^{-3}	2.4×10^{-4}	1.08
1×10^{-2}	3.8×10^{-3}	1.24

Figure 4-22, Calculated BER for adaptive modulation. (script s0065)

This is for a high update rate (distance between updates less than $\lambda/100$), using modulation schemes from BPSK through to 1024-QAM. The BER versus SNR for each modulation was found using simulation result shown in Section 2.6.

4.4.1 EFFECT OF DELAY ON THE PERFORMANCE OF ADAPTIVE MODULATION

The effect of delay on the performance of a single user adaptive modulation system was investigated. The set up of the system was the same as that in section 4.2.3 . The delay between the channel measurement and the modulation allocation update was varied and the resulting BER recorded. The adaptive modulation was updated 50 times for every wavelength of movement of the user. The simulation was performed twice, at an average SNR of 17 dB and 30 dB. Figure 4-23 shows the simulated performance. At 30 dB the BER is more susceptible to allocation delay than at 17 dB. The reason for this is that at a low SNR the nulls in the channel are not used due their low SNR, and consequently are not allocated data. As a result the subcarriers that are in nulls do not contribute any bit errors. However when the SNR is high enough (such as in the 30 dB simulation) all of the subcarriers have a high enough SNR to be allocated data, including the nulls in the channel. As a consequence of all the subcarriers being used, the system becomes most susceptible to allocation delay. The channel response changes very rapidly in the nulls and so even small delays in the allocation result in large errors in the channel tracking. This results in the majority of the errors occurring in these nulls. Figure 4-24 shows the location of the bit errors for the single user adaptive modulation scheme at a SNR of 42 dB. It can be seen that most of the errors occur as the channel is fading into nulls.

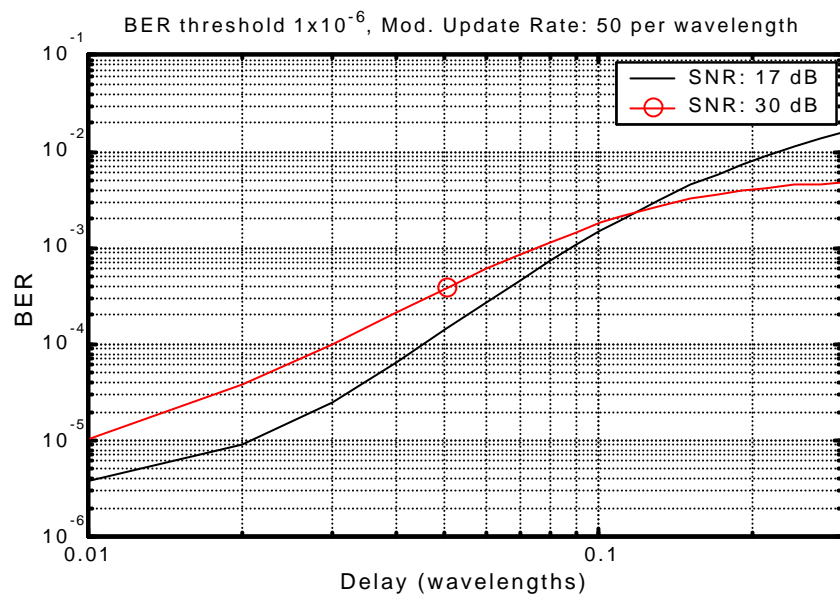


Figure 4-23, BER as a function of the delay between channel measurement and adaptive modulation allocation (script s0085)

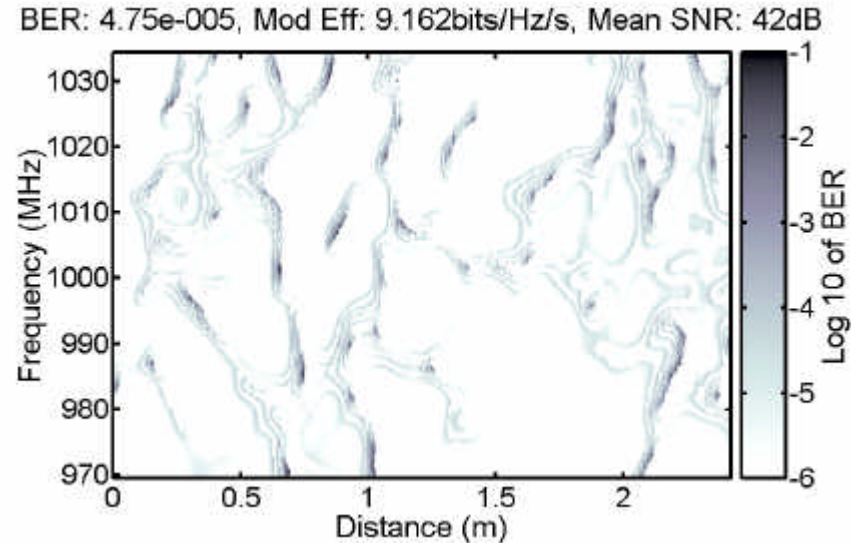


Figure 4-24, Location of the bit errors in a single user adaptive modulation scheme at a SNR of 42 dB. Channel measurement Figure A - 12 was used for this simulation. (script s0059)

CHAPTER 5 ACCESS POINT REPEATERS

Wireless networking is an emerging technology allowing users the freedom of movement. The aim of WLAN systems is to provide users with a data rate comparable with wired networks within a limited geographic area. Currently most WLAN products use Direct Sequence Spread Spectrum (DSSS) techniques, based on the IEEE 802.11b standard, providing a data rate of 11 Mbps in the 2.4 GHz ISM band [96]. The next generation of WLAN systems will be based on two similar WLAN standards known as: HiperLAN2 (Europe), and IEEE802.11a (US) [97]. These support a physical layer transmission rate of up to 54 Mbps and use OFDM for the physical layer implementation.

OFDM is a multi-carrier modulation scheme, which has a high immunity to multipath effects, and allows a wide range of carrier modulations schemes to be used. HiperLAN2 adaptively changes the forward error correcting coding rate and the carrier modulation scheme (BPSK, QPSK, 16-QAM, 64-QAM) allowing the data rate to be maximised based on the current radio channel characteristics. Using a higher spectral efficiency modulation scheme, such as 64-QAM, allows the data rate to be increased, but requires a higher Signal to Noise Ratio (SNR) for a fixed error rate. Minimising the path loss, allows the SNR and corresponding data rate to be maximised, as described in section 4.2.

Currently the number of WLAN systems is relatively low and thus interference between most systems is low. In addition to this, most operate within buildings, which provide significant interference shielding by the outer walls. This results in the SNR being primarily limited by transmission power not intercellular interference. If we can therefore minimise the path loss over the coverage area of the WLAN, we can therefore maximise the SNR, and the corresponding data rate.

In a free space environment, the path loss is proportional to the transmission distance squared. However, for indoor environments the path loss typically increases much faster with distance due of shadowing caused by absorption from obstructing objects, such as walls, cabinets, doors etc.

Shadowing can result in numerous regions of the building having an inadequate coverage, resulting in a poor Quality Of Service (QOS). This is a significant problem as the QOS of WLAN systems is very important if they are to replace wired networking. Shadowing also increases the average path loss compared with free space, requiring more transmission power, in order to maintain communications.

High quality coverage of a building can be obtained by using a cellular system as shown in Figure 5-1 (a). Each base station forms a cell, covering a small area of the building. These cells operate at different frequencies to prevent interference between them. The path loss is minimised, as the distance from the mobile station to the closest base station is minimised. Additionally if the transmission path to the closest base station is blocked, the mobile can connect to another cell. However, this type of implementation can be expensive, due to the requirement of a number of base stations. Additionally it requires multiple frequency bands for cellular implementation and hand-offs between cells, increasing the system complexity. A new method is proposed to augment the performance of a single cell. This technique is a simpler and cheaper method for obtaining reliable coverage, in an environment that suffers from shadowing.

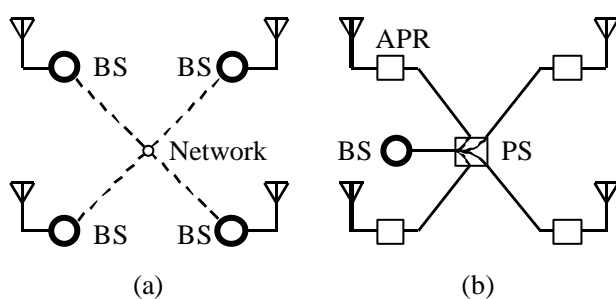


Figure 5-1, Methods for obtaining spatial diversity.

APR - Access Point Repeater, BS - Base Station, PS - Power Splitter / Combiner. **(a)** Cellular system with four cells controlled by four base stations, connected with a wired network for hand off between cells. **(b)** Single multiple transmission cell using Access Point Repeaters.

5.1 SPATIAL DIVERSITY BY MULTIPLE REPEAT TRANSMISSIONS

A form of spatial diversity can also be achieved by splitting the signal from a single central base station and transmitting the same signal from multiple locations around the building to be covered. This is shown in Figure 5-1 (b). Shadowing is reduced because there are multiple opportunities to receive the signal. Even if several paths are blocked by walls or buildings, others may have a reasonable transmission path. Using multiple transmitters effectively reduces the transmission distance, as the closest transmitter dominates the signal power.

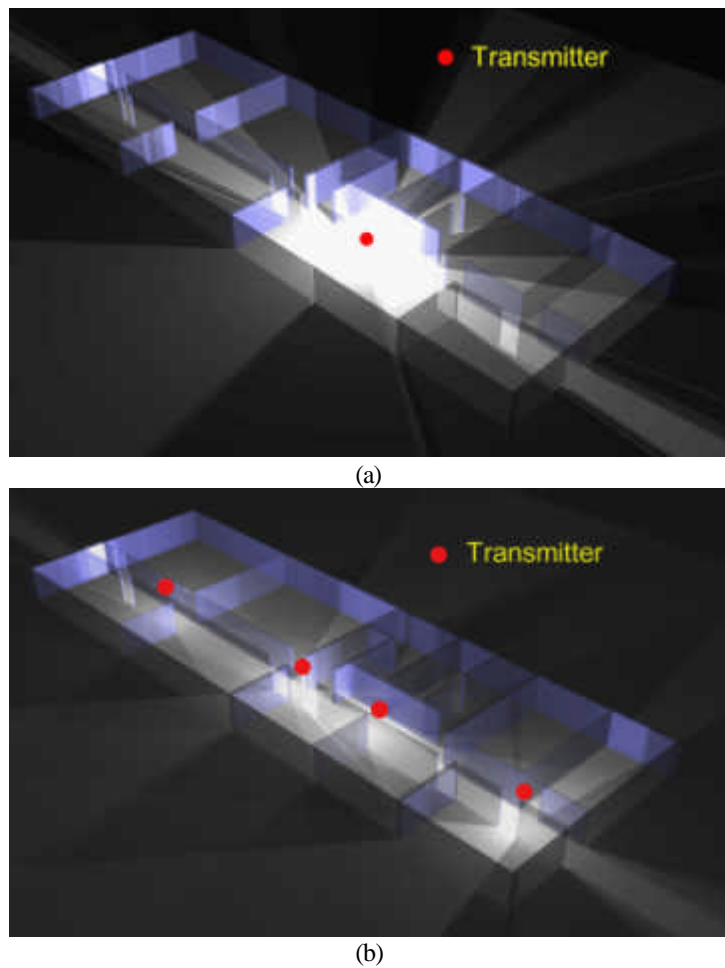


Figure 5-2, Pictorial demonstration showing the difference in shadowing when using a single transmitter (a), and 4 transmitters (b).

The total power in both cases is the same. With 4 transmitters the energy is spread more evenly. (Produced using Corel 3D Dream 6.0)

An example of how spatial diversity maximises power efficiency is lighting of a building. If you were trying to illuminate a typical large building with a single light bulb, the high opacity of the walls would result in many deep shadowed regions. The amount of power that would be required, for all parts of the building to be reasonably bright, would be extremely high, as shadowed regions would be lit solely from reflections and gaps in obstructing walls, such as doorways. However, by using one light per room, the illumination will be much more even, with minimal shadowing and a reduced total lighting power. The same is also true for radio signals, thus by using multiple transmitters spread over the area of a building we can reduce the average path loss.

Most communication systems need two-way communications using a forward and reverse link. Due to the reciprocal nature of radio propagation, the properties of the reverse link will be the same as the forward link. Thus, the path loss for the reverse link can also be minimised by using multiple receive antennas connected to a single central base station. The receive and transmit antennas can be combined into one unit, referred to here as an Access Point Repeater (APR). The use of APRs can provide a significant improvement with minimal expense.

The problem with using APRs is the mobile receiver will see signals from all APR transmitters. The propagation delay from each transmitter will be different, and so will arrive at the receiver with a different delay. This is equivalent to receiving the signal distorted by strong multipath. This causes frequency selective fading, and an increase in the delay spread of the transmission, which can result in Inter-Symbol Interference (ISI). This is particularly a problem for modulation schemes such as Frequency Shift Keying (FSK), as the maximum symbol rate is limited by ISI caused by delay spread.

Direct Sequence Spread Spectrum (DSSS) systems have a high multipath tolerance when a RAKE receiver is used [102]. A RAKE receiver uses correlation to resolve delayed copies of the signal caused by multipath propagation. These are then aligned in time and combined. This allows the signals from each of the transmitters to be resolved and combined. The maximum delay spread that can be tolerated by an IEEE802.11b DSSS WLAN system, using a 16-tap RAKE receiver, is 125 ns at 11 Mbps and 250 ns at 5.5 Mbps [103]. This level of multipath tolerance should allow

APRs to be spaced out with a maximum diameter of about 20 - 35 m, although problems might arise due to the increased delay spread. This small antenna spacing means that there would be little advantage in using multiple APR with an IEEE802.11b system as sufficient coverage can easily be obtained over 20 - 35 m with a single transmitter.

OFDM has a higher multipath tolerance than DSSS, and allows for a much greater range of modulation schemes to be used. Minimising the path loss allows the SNR to be increased, provided inter-cellular interference is low. This improved SNR can be utilised by adaptively setting the modulation scheme based on the SNR, allowing the throughput of the system to be increased.

The high multipath tolerance of OFDM is a result of the low symbol rate used, and the use of a guard period between symbols. The guard period is a cyclic extension of each OFDM symbol, giving protection against ISI, provided it is longer than the delay spread of the radio channel.

Multipath causes frequency selective fading, which can result in subcarriers of the OFDM signal being lost in nulls in the spectrum. These nulls are typically handled by including forward error correction to compensate for the lost data. Adding multiple transmitters will result in an increased delay spread, resulting in a decrease in the correlation bandwidth of the channel. This will not cause any detrimental effects on the OFDM transmission, provided that enough subcarriers are used.

Indoor propagation normally suffers from a combination of Rician and Rayleigh fading [74]. Using multiple APRs increases the level of multipath energy, as a result of the receiver seeing the direct signal from each APR and the reflections from each APR (see Figure 5-3). This increase will tend to result in more areas in the building suffering from Rayleigh fading. However this increase in fading should be more than compensated for by the decreased path loss due to the multiple APRs. More research is needed to establish the extent of the additional multipath when using APRs.

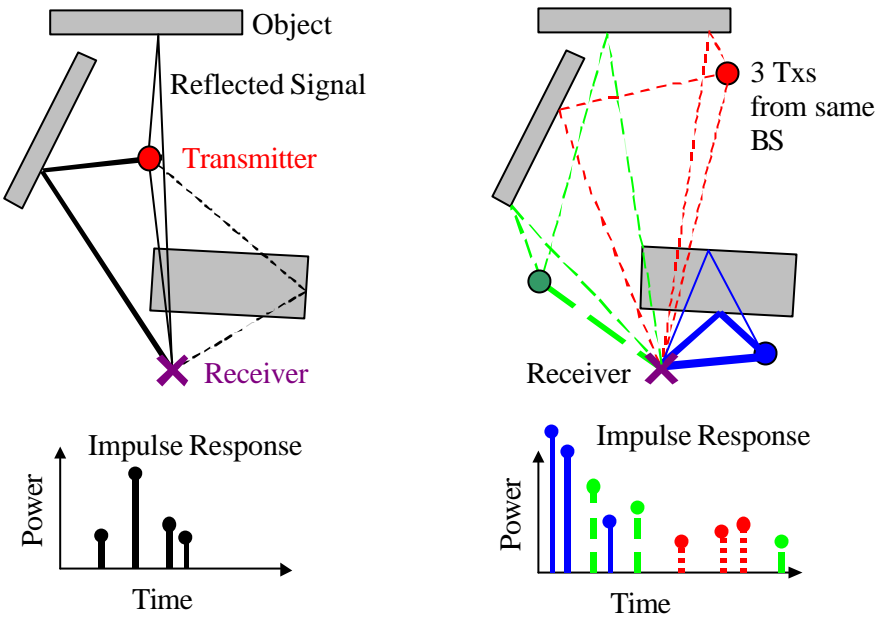


Figure 5-3, Increase in the multipath delay spread as a result of using Access Point Repeaters.

The overall impulse response with APRs corresponds to the sum of the impulse responses from each APR antenna.

The use of multiple transmitters to obtain improved coverage was first introduced in the Digital Audio Broadcasting (DAB) system [20]. DAB uses OFDM with a low symbol rate and a long guard period. With DAB, it is possible for all transmitters to use the same frequency and transmit copies of the same signal, referred to as a Single Frequency Network (SFN). For VHF band transmissions, DAB uses 1536 subcarriers with a symbol time of 1 ms, and a guard period of 246 μ s, allowing transmitters to be up to 96 km apart in a SFN, before the delay spread is too large.

5.1.1 APR SPACING FOR HIPERLAN2 SYSTEM

The maximum diameter for a HiperLAN2 system, using APRs, can be estimated based on the length of the guard period used in HiperLAN2. If we assume that there are two APRs in a uniform environment (uniform multipath scattering) the worst-case multipath will occur at a location approximately three quarters between the APR antennas. At this distance the signal power from both transmitters is reasonably similar, resulting in significant frequency selective fading. Also at this distance the time delay between the two paths is close to the maximum possible. If the receiver

moves much closer to either of the transmitters then the signal power will be dominated by just one of the transmitters reducing the multipath fading.

The guard period for HiperLAN2 is 800 ns, and so the first approximation for maximum spacing between the transmitters is:

$$D = \frac{T_{GF} \times c}{0.75} = \frac{800 \times 10^{-9} \times 3 \times 10^8}{0.75} = 320m$$

where D is the space between the transmitter antennas, T_{GF} is the length of the flat section of the guard period and c is the speed of light.

This estimate is however overly optimistic for several reasons. Some of the guard period is needed to allow for error in the accuracy of the time synchronisation, shortening the allowable delay spread. Also band pass filtering in the transmitter and receiver can introduce additional delay spread. In addition to this, the result would only be valid if we were only using BPSK or QPSK. These modulation schemes are robust and can tolerate a large amount of ISI energy. However, HiperLAN2 uses higher modulation schemes such as 16-QAM and 64-QAM, which are more sensitive to ISI caused by delay spread, and as a consequence the maximum antenna separation must be reduced. This will reduce the channel delay spread and the resulting ISI. In a typical building the RMS delay spread is in the order of 20 - 60 ns (see Table 3-2). This is much shorter than the length of the HiperLAN2 guard period, however the RMS delay spread is only a good indicator for robust modulation schemes such as BPSK and QPSK. The RMS delay spread can be thought of as approximately the time period over which half the channel impulse energy arrives. This means that the other 50% of the energy is spread over a longer period. For 64-QAM, it can only tolerate a very small amount of ISI energy. At a BER of $\times 10^{-5}$, 64-QAM requires an effective SNR of 25.6 dB. Channel noise, IMD, frequency and time synchronisation errors, Doppler spread, channel equalisation noise and ISI all degrade the effective SNR of the OFDM transmission, and so the degradation from just ISI must result in an effective SNR of significantly greater than 25.6 dB. For this reason it has been estimated that the level of ISI must be result in an effective SNR of greater than 30 dB.

In order to maintain an effective SNR of greater than 30 dB the level of ISI must be

less than 0.1% of the symbol power, thus the guard period must be sufficiently long so that it covers the period over which 99.9% of the multipath impulse energy arrives. Most publications on multipath characterisation have focused primarily on the RMS delay spread [69], [71], [73], [76], [77], however what is needed is the time period over which 99.9% of the energy arrives. This time spread can be estimated approximately by looking at the time spread over which the impulse reflections have died away to below 30 dB the normalised power. This type of measurement is known as the *profile width* and has been used in [77], [78], and [79]. Unfortunately all these papers are for urban radio propagation, making there results difficult to apply to indoor environments. However they do allow the relationship between the RMS delay spread and the profile width to be estimated. From these results it was estimated that the profile width with a cut off of 30 dB below the normalised power is approximately 6 - 8 times that of the RMS delay spread. Obviously this will vary based on the actual environment but it does allow an estimate of the guard period used up by multipath in a typical building environment. If the RMS delay spread is 20 - 60 ns than period over which 99.9% of the energy arrives will be about 160 - 480 ns.

As well as protecting against building multipath, the guard period in a HiperLAN2 system also protects against timing offset errors and allows for some side-lobe suppression by using a raised cosine windowing of 100 ns. Since the raised cosine section of the guard period overlaps with the previous symbol its effective guard period length is reduced. So if we assume that the effective Hiperlan/2 guard period for multipath protection is reduced by 150 ns due to these factors than we get an effective guard period of 650 ns. Taking into account the multipath spread of 480 ns we are left with $650-480 \text{ ns} = 170 \text{ ns}$. From this we can estimate the maximum spacing between the APRs to be approximately:

$$D = \frac{170 \times 10^{-9} \times 3 \times 10^8}{0.75} = 68m$$

Several other factors haven't been included in this estimate, such as the possible detrimental effect of the decreased channel coherence bandwidth on channel equalisation and degraded time synchronisation accuracy due to the larger delay spread. As a result of these degradations, it is estimated that the maximum allowable

range spacing for a HiperLAN2 network using APRs is 40 - 60 m. Additional research is needed to verify this.

5.2 IMPLEMENTATION OF AN ACCESS POINT REPEATER

All APRs within the same cell transmit and receive the same signal, thus only one base station (BS) is needed per cell. For transmission, the signal generated by a base station is split N ways, where N is the number of APRs. Coaxial cable or some other medium, such as optic fibre, is used to deliver the signal to each APR. The signal is then amplified at the APR to compensate for any losses in the coaxial cable transmission. For reception, the reverse process is used. Each APR has a Low Noise Amplifier (LNA) to compensate for losses in the coax, in order to maintain a low noise figure. The received signals from all APRs are combined and demodulated at the base station. Phase differences between the APRs have little or no effect as they are corrected for, in the OFDM demodulation process.

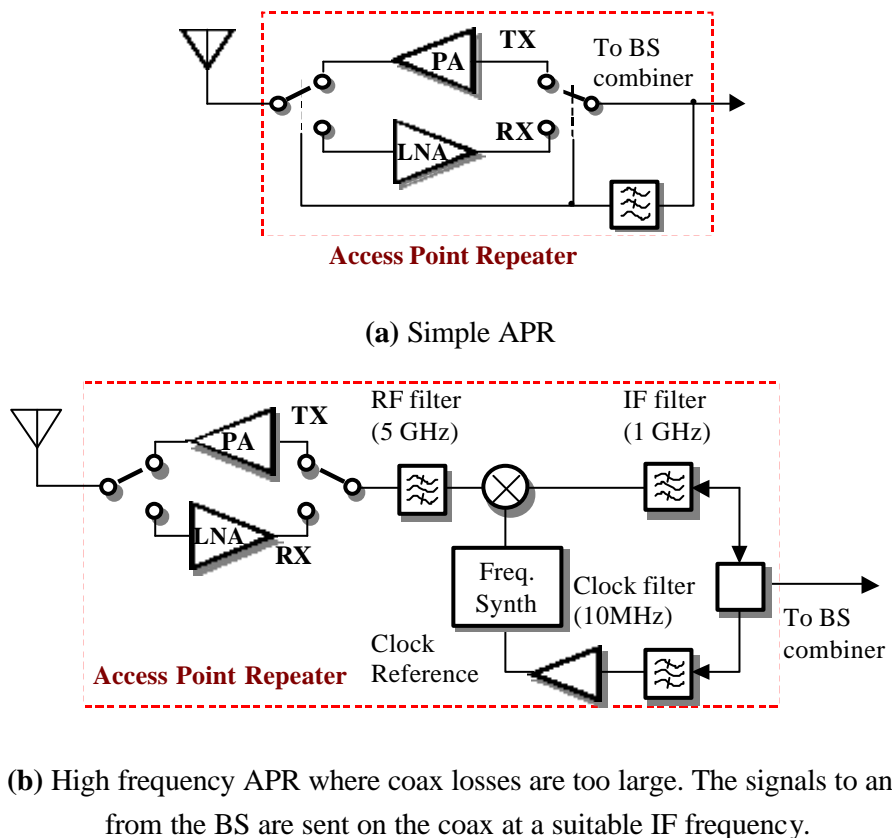


Figure 5-4, Possible implementation of an Access Point Repeater.

Figure 5-4 (a) shows a simple implementation of an APR, which can be used when the loss in the coaxial cable is low (< 20 dB). The mast-head amplifier operates at the RF frequency and so no frequency translation is required. A low frequency control signal can be used to select whether to transmit or receive. For a full duplex system, the RF switches can be replaced with diplexers.

In larger systems where the cable losses are too large, the signal can be transmitted on the cable at an IF frequency. Figure 5-4 (b) shows one possible implementation for an IF APR. A common clock reference must be used by all APRs to ensure frequency synchronisation, otherwise frequency errors will reduce the orthogonality of the OFDM, causing ICI. A suitable out of band clock reference must be transmitted from the base station. This common clock can then be frequency multiplied using a Phase Locked Loop (PLL) to generate the Local Oscillator (LO) for the IF-RF mixing. For such a design, care must be taken to ensure the phase noise of the clock reference is low and that the clock signal does not interfere with the received signal.

Another method for distributing high frequency RF signals is to use optic fibre. The RF signals can be converted to optical signals and transmitted over long distances with optic fibre. This type of technology is currently being developed for use in mobile phone applications as a method for producing pico sized cells [101].

5.3 EXPERIMENTAL SET UP

An experiment was set up to test the effectiveness of using multiple transmitters (APR) to minimise shadowing in an indoor environment. The forward link from the base station to the mobile stations was tested, by measuring the effective path loss from fixed transmitters to a mobile receiver. The path loss from a single transmitter (simulating a single Access Point) was compared with the path loss when using two transmitters (simulating two APRs).

The path loss was measured at 235 locations on the second floor of the Electrical and Computer Engineering (ECE) building at James Cook University. The measurement locations and the building layout are shown in Figure 5-5. The internal walls are shown as dark lines. The selection of the measurement locations, the position of the

transmitters, and the construction of the building can easily influence the overall path loss probability distribution. However, the results presented will be representative of the improvement that could be expected in a typical building of similar construction to the one the measurements were taken in.

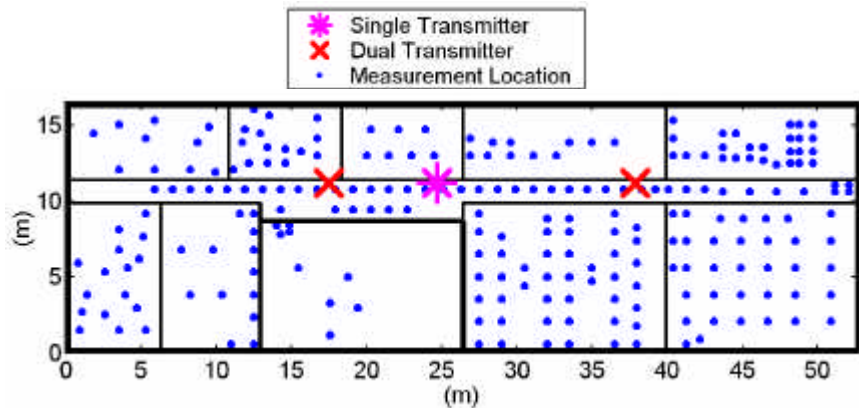


Figure 5-5, Path loss measurement locations in the ECE building for APR testing.

Lines represent internal walls. The thin lines are plaster board walls, and the thick ones are concrete walls.

The transmitter set up is shown in Figure 5-7. Simple monopole antennas were used and were assumed to have an effective gain of 0 dBi, including matching losses. The uncertainty in the gain of the antennas resulted in an absolute error in the path loss measurements of approximately 3 dB and a differential error between the single and dual transmitter measurements of 1 dB.

The signal strength at each location was measured using a spectrum analyser on a trolley, as shown in Figure 5-6, and converted to path loss by compensating for transmitter power and receiver gain. A slightly different frequency was used for the single and dual transmitters to allow simultaneous measurements of the path loss. The receiver antenna was placed on a rotating platform, as shown in Figure 5-8, which was turned during the received power measurement. Video averaging on the spectrum analyser was used to average the power over a 0.6 m circular path swept by the antenna. This was done to remove the effects of frequency selective fading, and obtain an accurate measure of the path loss. Even though the path loss was measured using a continuous wave transmission, the results are still valid for a wide bandwidth signal.



Figure 5-6, Photo of the mobile receiver trolley, showing the rotating antenna on top, spectrum analyser in the middle, and the battery for powering the pre-amp.

Due to limitations of the equipment available, the measurements were performed at 1 GHz, rather than 5 GHz. This will tend to reduce the effects of shadowing, as the opacity of most materials is lower at lower RF frequencies, thus we would expect the effectiveness of using APRs to improve at higher RF frequencies.

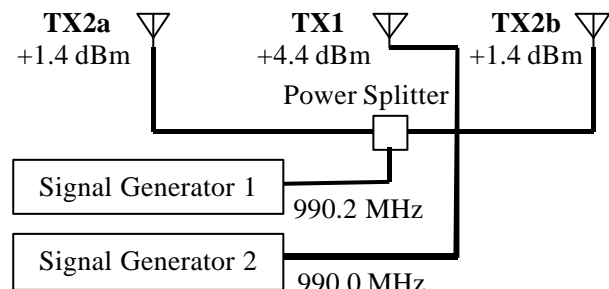


Figure 5-7, Transmitter set up simulating Access Point Repeaters. The total transmitter power from Tx2a and Tx2b were matched to the Tx1 power.

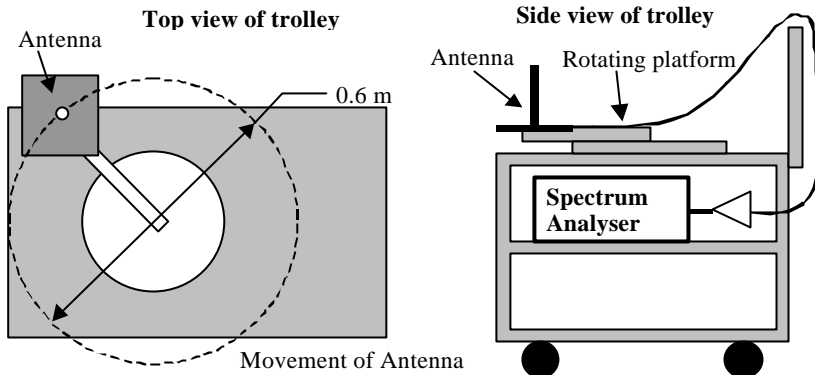


Figure 5-8, The receiver antenna was swept over a circle to average out effect of fading.

5.4 DISCUSSION OF MEASURED RESULTS

Figure 5-9 shows the path loss for the single transmitter. The path loss increases rapidly with distance from the transmitter. The path loss in the bottom left corner of Figure 5-9 at location 5 m, 5 m, has a high path loss of over 100 dB, which is equivalent to 1 km of free space loss, even though it is less than 20 m from the transmitter. Figure 5-10 shows the path loss when two transmitters were used. In this case the path loss is lower and much more evenly distributed.

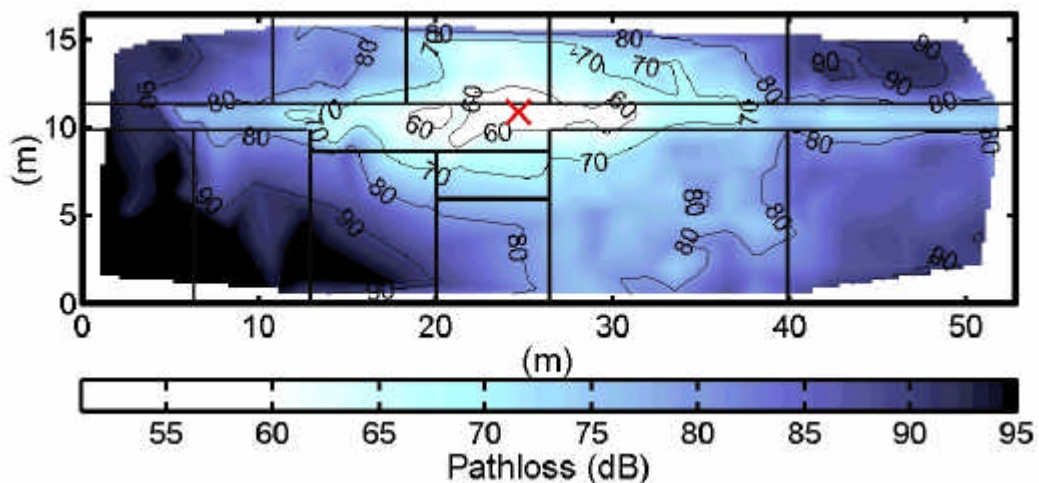


Figure 5-9, Measured path loss with one transmitter over the area of the ECE building at 990 MHz. (script s0011)

The dark lines are the internal walls. The shows the location of the transmitters. (script s0011)

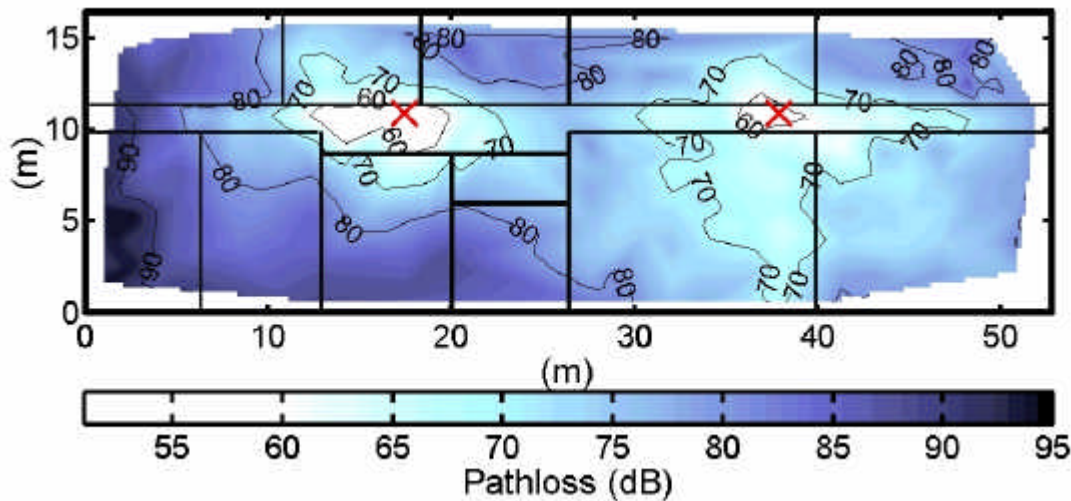


Figure 5-10, Measured path loss for two transmitters over the area of the ECE building at 990 MHz. (script s0011)

This simulates two APRs. Note the total transmitter power is the same as for the one transmitter measurements. The shows the location of the transmitters. (script s0011)

Figure 5-11 shows the measured and simulated probability distribution of the path loss. It shows that the measured path loss is more than 7 dB lower when using two transmitters as compared with one. This result is to be expected, as the longest distance to a transmitter was reduced by 1.62 times. The typical path loss exponent of an obstructed path within a building is 4 to 6 [119], as compared to a path loss exponent of 2 for free space loss. We would therefore expect the path loss to be reduced by 8.4 to 12.6 dB for a reduction in distance of 1.6 times. Since the transmission power is split over two transmitters this will reduce the received power by 3 dB, thus resulting in an overall improvement of 5.4 to 9.6 dB. This compares well with the measured improvement of 7 dB. Even though there are two transmitters, the received signal power tends to be dominated by the closest transmitter due to the rapid fall of power with distance. This is why the improvement in signal power can be estimated with reasonable accuracy by considering the reduction in distance to the transmitter.

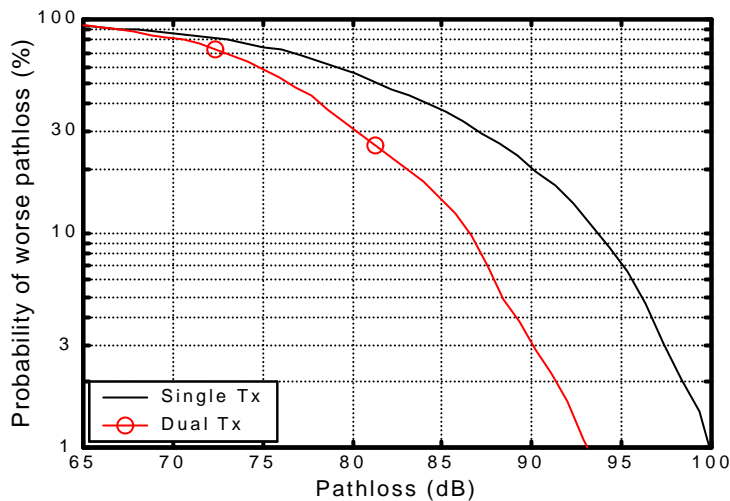


Figure 5-11, Probability of path loss over the measured area of the building.
(script s0011)

5.5 REDUCTION IN CELLULAR INTERFERENCE

At a large distance, multiple APRs appear as a point source and so the received power is the same as when using a single Access Point, where the total transmitted power is the same. This means that the interference to neighbouring systems is approximately the same regardless of the number of APRs used, for fixed total transmission power. The near field path loss can be reduced by 7 dB using two APRs, allowing the total transmitted power to be reduced by up to 7 dB for the same SNR. This will reduce the overall interference to distant (distance is greater than the diameter of the APR WLAN system) WLAN systems by 7 dB. Further improvements could be made using a higher number of APRs. Using one APR per room could potentially decrease the near field path loss by 20 - 30 dB, allowing a large reduction in external interference with suitable power control. The reduced interference will allow a better frequency reuse in a cellular system.

5.6 SHADOW MODELLING

A simple ray trace path loss model was developed to allow continued investigation into the use of multiple access point repeaters. This is similar to the model used in [75]. A 2D model was used instead of a 3D one for simplicity and to reduce the

amount of simulation time. The 2D model calculates the path loss along radial rays, which are converted to a fixed rectangular data grid using interpolation. The rectangular grid allows the signal power from multiple transmitter sources to be added together.

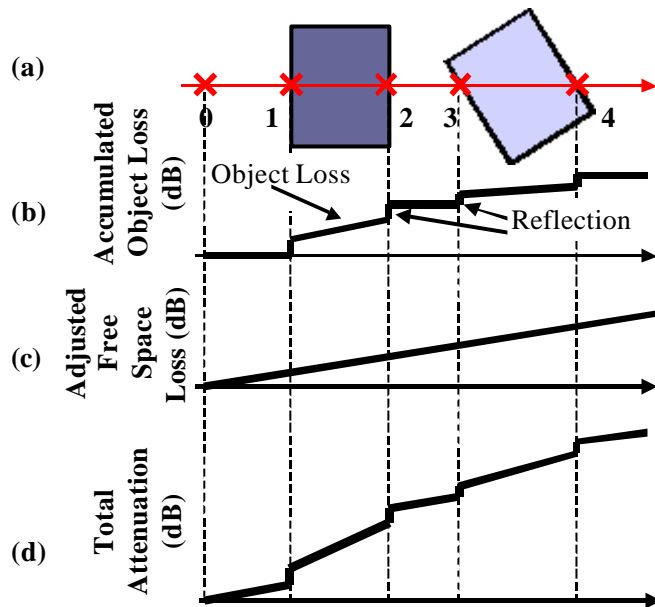


Figure 5-12, Attenuation calculations for a ray passing through two objects.

The path loss along each ray is found by calculating its intercept to each object in the environment. The loss through each object is calculated based on the reflection coefficient of the object surface and the distance through the object. Each surface the ray intercepts results in energy being reflected causing a jump in the accumulated attenuation. As shown in Figure 5-12 (a), surface 1, 2, 3, 4 result in jumps in the accumulated object loss shown in Figure 5-12 (b). In this model, the amount of reflected energy is constant regardless of the angle of the ray. This reflected energy is not calculated as another ray, and is ignored to simplify the model.

In addition to reflected losses, each object absorbs energy as the ray passes through it. This is calculated as a loss proportional, in dB, to the distance travelled through the object medium. The loss along the ray is accumulated as the ray passes through multiple objects. This loss is then added to the loss calculated by the standard free space radio path loss equation to obtain the overall attenuation with distance. The radio path loss equation is

$$P_L = -10\log_{10}\left(\left(\frac{\mathbf{I}}{4\pi R}\right)^a\right) \quad (5-1)$$

where P_L is the path loss (dB), \mathbf{I} is the wavelength of the radio signal (m), R is the distance from the transmitter (m), and a is the path loss exponent. For free space propagation, $a = 2$. The simulation calculates the path loss due to objects, and so ideally, the path loss exponent used in the simulation should be two. However due to the simplicity of the model, a path loss exponent of 2.65 was found to best match the measured results.

5.6.1 INTERCEPT CALCULATIONS

Figure 5-13 shows the method used for finding the intercepts between the ray being calculated, and the objects in the environment. Each object is represented as a set of vertices. The intercept points were found by calculating the intercept between in the line equations that join the object vertices and the line equation for the ray. If this intercept lies within the bounds of the two lines then this is taken as an object intercept. The process is repeated for each line that makes up the surface of each object and then for all objects in the environment. After all object intercepts have been found the attenuation along the ray is calculated in a piece wise manner. The ray is initially assumed to start on the outside of all objects, and so the first object intercept indicates the point where the ray enters into an object. Each pair of object intercepts represent the entering and exiting of objects. This model assumes that the objects do not overlap. The attenuation caused by each object is found by multiplying the object absorption coefficient (in dB/m) and the distance between the entry and exit points of the object. In addition to this a fixed amount of energy is also assumed to be reflected from each surface of the object.

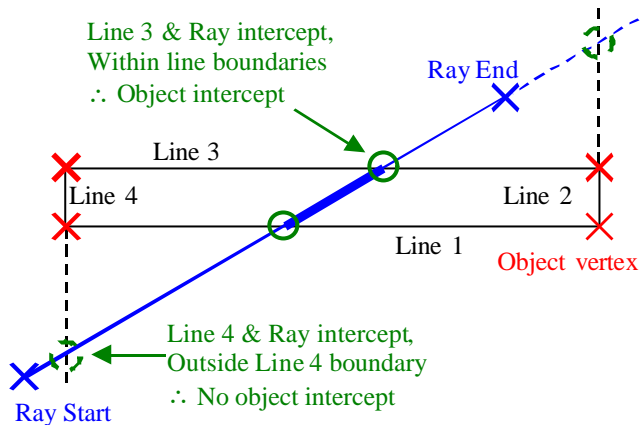


Figure 5-13, Diagram showing the method for find the intercepts between a ray and an object.

Once the path loss has been calculated along all rays, it is converted to a rectangular grid system using 2D cubic interpolation. This normalisation of the grid locations allows the signal power from multiple simulations to be combined. This allows for simulation of multiple transmitters, and the investigation of interference between transmitters in neighbouring cells. Figure 5-14 shows the conversion from the polar grid to rectangular.

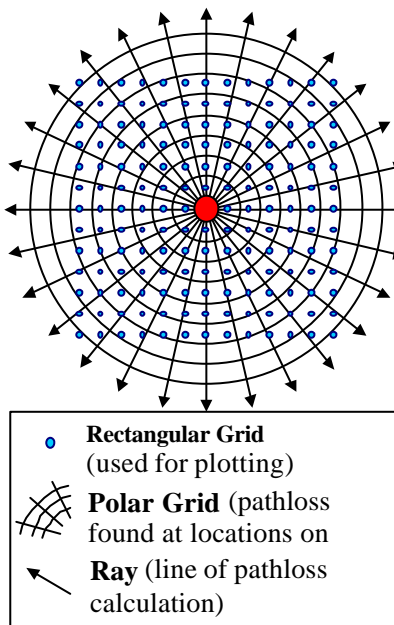


Figure 5-14, Polar to rectangular conversion used for plotting of simulated path loss.

The path loss is calculated along at each point on the polar grid. These results are then converted to a 2D rectangular grid using 2D cubic interpolation.

5.6.2 SPACIAL ANTI-ALIASING

Aliasing effects can occur in the path loss simulation due to the finite number of rays used. This problem becomes more acute when the number of rays is small. This problem is shown in Figure 5-15. Averaging multiple simulations, each with the transmitter moved slightly, can significantly reduce this problem. Good results were obtained by moving the transmitter in a circular area, with a radius equal to the wavelength. Averaging of the transmitter movement smoothes shadowing, reducing the fine shadows due to gaps and overlapping joins between objects. This also gives a crude approximation of diffraction for objects close to the transmitter.

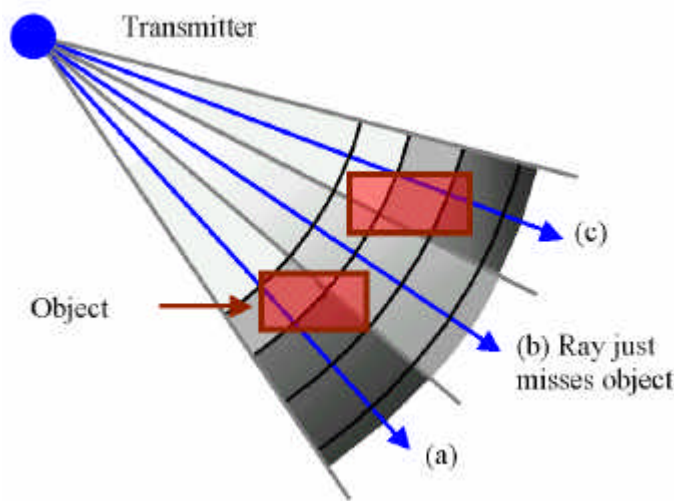


Figure 5-15, Example of spatial aliasing due to finite number of rays used.

A ray that just misses an object, or one that just intersects an object results in shadowing which is disproportionate to the objects.

5.6.3 MODEL VERIFICATION

The radio model was compared to the measured results to verify the model accuracy and to adjust the model parameters to give realistic results. The material properties of the walls were measured directly and are shown in Table 1. These values compare well with values measured in [75]. The walls were found to be non homogeneous, caused by wiring, reinforcing, studs, and nearby objects, making accurate measurements difficult.

In the simulation, the material properties of the walls were optimised to obtain a good match between the simulated and measured building path loss shown in Figure

5-9 and Figure 5-10. The resulting simulation parameters were found to closely match the direct wall loss measurements, as shown in Table 5-1. Figure 5-16 shows the resulting match between the measured and simulated results. This figure shows the percentage area of the building (Y-axis), which has a path loss worse than a specified path loss in the X-axis. For example, 20% of the building has a path loss of greater than 90dB when using a single transmitter, where as it is only 3% for two transmitters.

Wall Type	Thickness (m)	Total Attenuation (dB)	Direct Measurement of wall loss (dB)
Plaster Board	0.13	1.45	1.5 ± 1
Concrete	0.2	3.80	4 ± 1.5

Table 5-1, Material properties of the internal walls.

This shows direct measurements and wall loss found by simulation optimisation

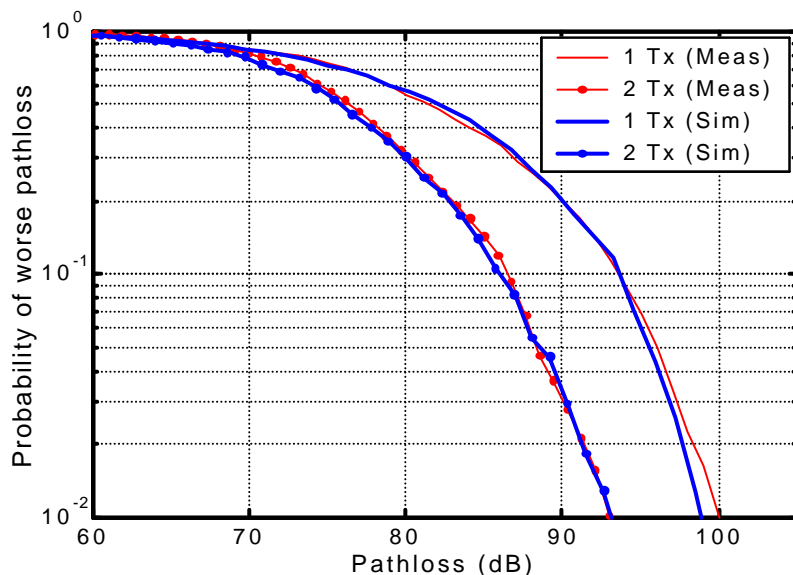


Figure 5-16, Cumulative Distribution Function of the path loss within the measured and simulated building. (script s0011)

5.6.4 SIMULATED RESULTS

Figure 5-17 and Figure 5-18 show the simulated path loss for a single and double transmitter respectively, for the same building and transmitter location as measured data shown in Figure 5-9 and Figure 5-10. The probability distribution of the path loss is shown in Figure 5-16. The main difference between the simulated and

measured results is that the simulated results are smoother, which is the result of the simple environment model.

In addition to simulating one and two transmitters, the path loss was simulated with four and eight transmitters. The transmitters were positioned in the simulation to approximately maximise their effectiveness. Figure 5-19 and Figure 5-20 shows the simulated results for 4 APR and 8 APR respectively. These show that the path loss continues to decrease significantly as the number of repeaters is increased. This is despite the fact that the energy being transmitted by each repeater becomes smaller and smaller, as the total transmission power is fixed. Figure 5-21 shows the path loss distribution for all the simulated results. The path loss for the worst 2% of the area of the building was improved by 7 dB when using two transmitters, 16 dB for four transmitters and 22 dB for eight transmitters.

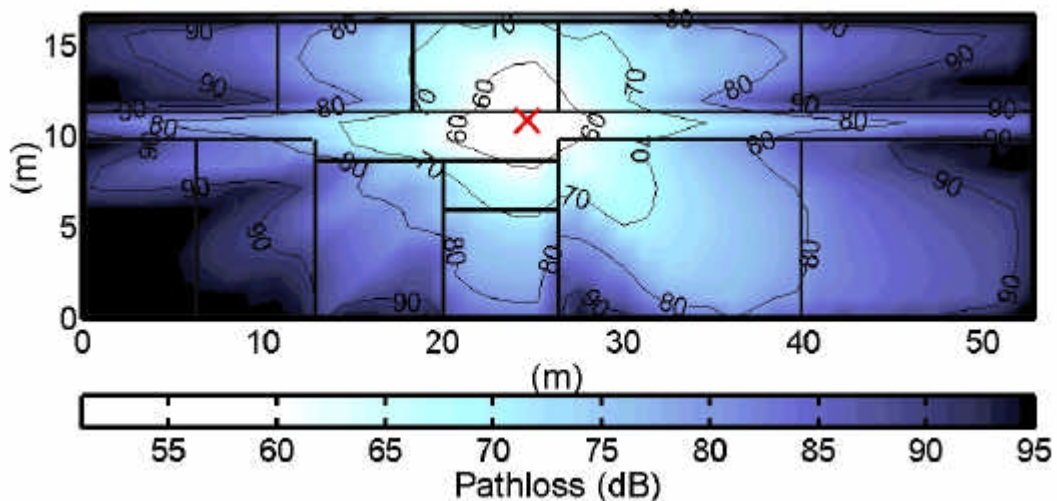


Figure 5-17, Simulated path loss for one transmitter at 990 MHz. (script s0011)

The shows the transmitter location.

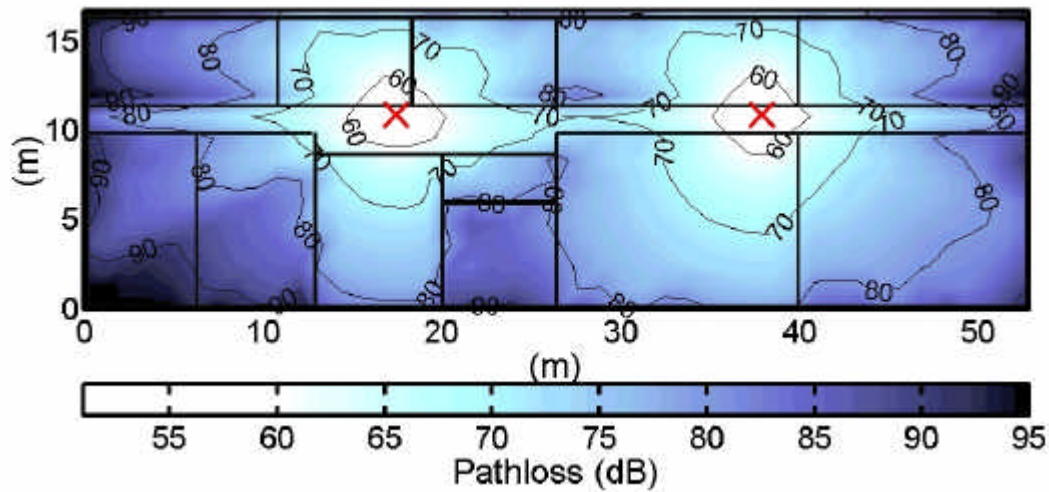


Figure 5-18, Simulated path loss for two transmitters at 990 MHz. (script s0011)

The ' shows the location of the transmitters.

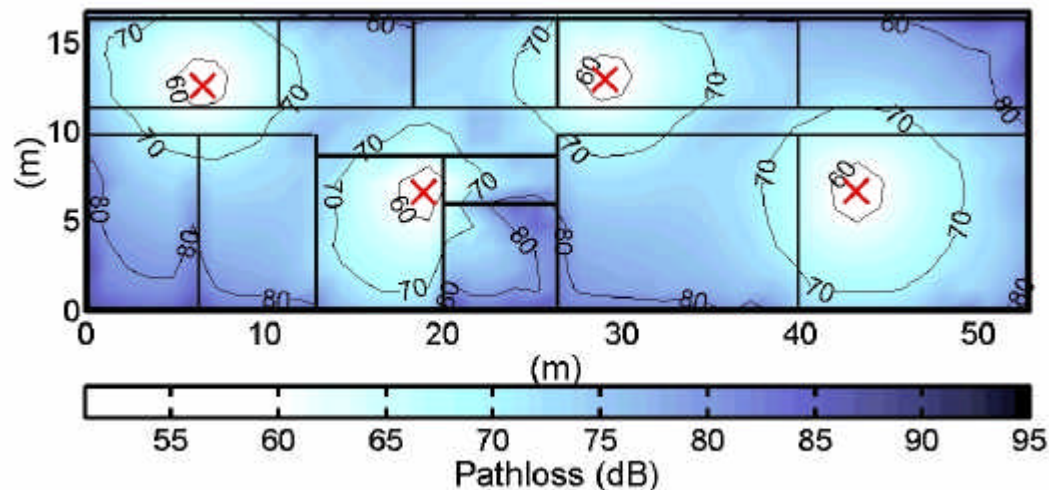


Figure 5-19, Simulated path loss for four transmitters for 990 MHz. (script s0011)

The ' shows the location of the transmitters.

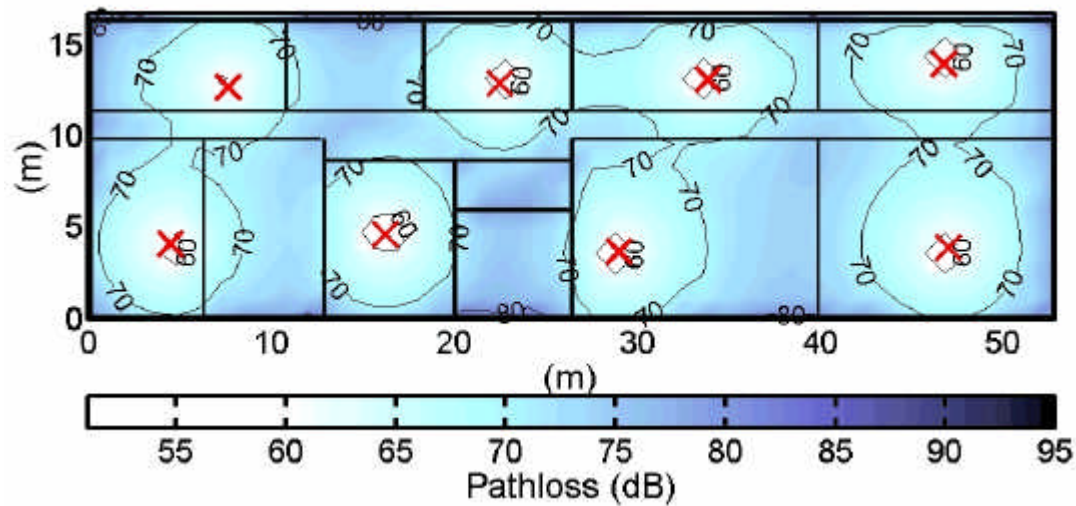


Figure 5-20, Simulated path loss for 8 transmitters for 990 MHz. (script s0011)

Note the total transmission power is the same as for one transmitter. The shows the location of the transmitters.

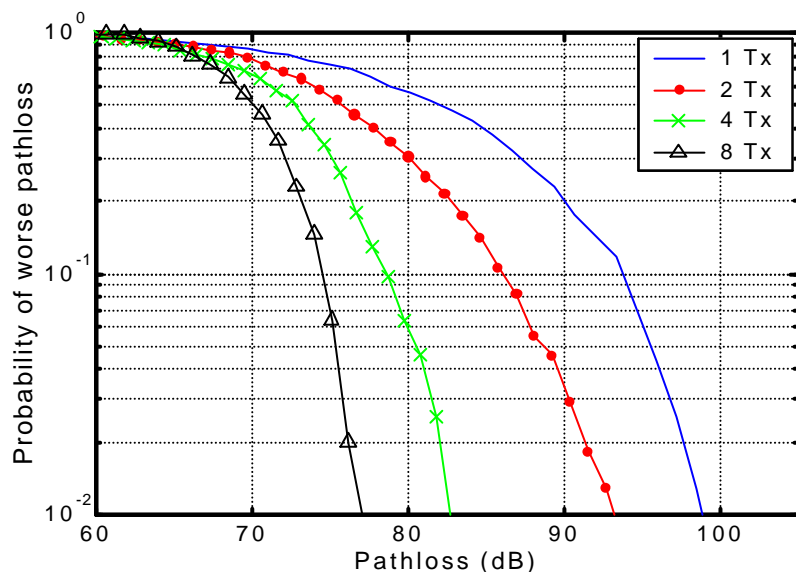


Figure 5-21, Cumulative Probability Distribution for simulated results, showing the result for 1, 2, 4 and 8 transmitters. (script s0011)

5.7 ACCESS POINT REPEATER PERFORMANCE WITH A MOVING INTERFERER

Previous simulations and measurements show that adding multiple transmitters significantly reduces the path loss within a building, improving the capacity and quality of service. This reduced path loss should also improve the tolerance to outside signals, caused by inter-cellular interference or a mobile station operating at the same frequency near by. To investigate this possibility a simulation was set up using the radio model developed in section 5.6.

Two buildings were set up side by side to simulate neighbouring buildings. Both buildings in the simulation used the same lay out as the Electrical and Computer Engineering building at JCU. This model was used as it has been previously verified with measurement. If a different building model were used, it would result in a different shadowing pattern and thus a different result, however the general results would be much the same.

The top building was set up as a fixed wireless LAN system using 1, 2, 4, or 8 APRs. The interference between this WLAN and a moving interferer was simulated. The interferer was moved from the outside of lower building then moved in a straight-line passing through the lower building and out the other side. The signal to noise ratio over the area of the top building was calculated for each movement of the interferer.

5.7.1 SNR CALCULATION

The Signal to Noise Ratio (SNR) at each point in space was calculated based on the transmission power of the APRs and mobile interferer, the path loss with shadowing from the buildings, and the thermal and electrical noise in the receivers based on the transmission bandwidth.

$$SNR = P_{LAN} - (P_I + N_p) \quad (5-2)$$

Where P_{LAN} is the power received from the fixed wireless LAN system (from the APRs) in dBm, P_I is the power from the interferer in dBm, and N_p is the noise power from thermal and electrical noise, also in dBm.

The received power for multiple APRs was calculated by adding the power received from each APR.

$$P_{LAN} = 10 \log_{10} \left(\sum_{k=1}^A (T_k \cdot H_k) \right) \text{ (dBm)} \quad (5-3)$$

Where A is the number of APRs, T_k is the transmitted power from each APR in mW, and H_k is the channel gain from the transmitter to the receiver. The channel gain is the ratio of the transmitted power to the received power and was found using the ray trace model, and is the inverse of the path loss.

For the interferer the calculation was the same except that there was only a single transmitter.

$$P_I = 10 \log_{10} (T_I \cdot H_I) \text{ (dBm)} \quad (5-4)$$

Where T_I is the transmitted power from the interferer in mW, and H_I is the channel gain from the interferer to the receiver.

In addition to interference noise, thermal and electrical noise was included in the SNR calculation:

$$N_P = 10 \log_{10} (KTB) + NF \text{ (dBm)} \quad (5-5)$$

Where K is Boltzmann's constant (1.38×10^{-23} J/K), T is the antenna temperature in K, and B is the bandwidth of the system in Hz. NF is the noise figure of the receiver (in dB), which is a measure of the added electrical noise by the receiver electronics.

For the simulations the bandwidth was set to 20 MHz, the NF set to 10 dB, the antenna temperature set to 300 K, the interferer power set to 100 mW, and the total APR transmitter power to 100 mW.

5.7.2 RESULTS

Figure 5-22 shows the signal power for the interferer and APRs, from which the SNR was calculated. The performance of the simulated WLAN system was measured by taking the average SNR over the area of the top building. From this calculated SNR the spectral efficiency of an OFDM system was estimated for a system using adaptive modulation. Coherent QAM from 1 b/s/Hz to 10 b/s/Hz were used and

allocated based on a BER threshold of 1×10^{-4} . Figure 5-23 shows the resulting spectral efficiency as the interferer moves through the lower building. The spectral efficiency is more than double for 8 transmitters compared with a single transmitter, corresponding to an improvement of 10 dB. The interferer has the most detrimental effect when it is outside the lower building, which is to be expected as the building will tend to shield and contain the interference.

As well as spectral efficiency, the QOS was estimated by measuring the percentage area of the building where the SNR was insufficient to support a spectral efficiency of at least 1 b/s/Hz (SNR > 8.4 dB). Figure 5-24 shows the QOS of the WLAN system in the top building as the interferer is moved. For the WLAN system using a single APR between 25 - 40 % of the building is not covered indicating a poor performance. However, increasing the number of APRs improves the performance considerably, with both 4 and 8 APRs resulting in an average outage of less than 1%.

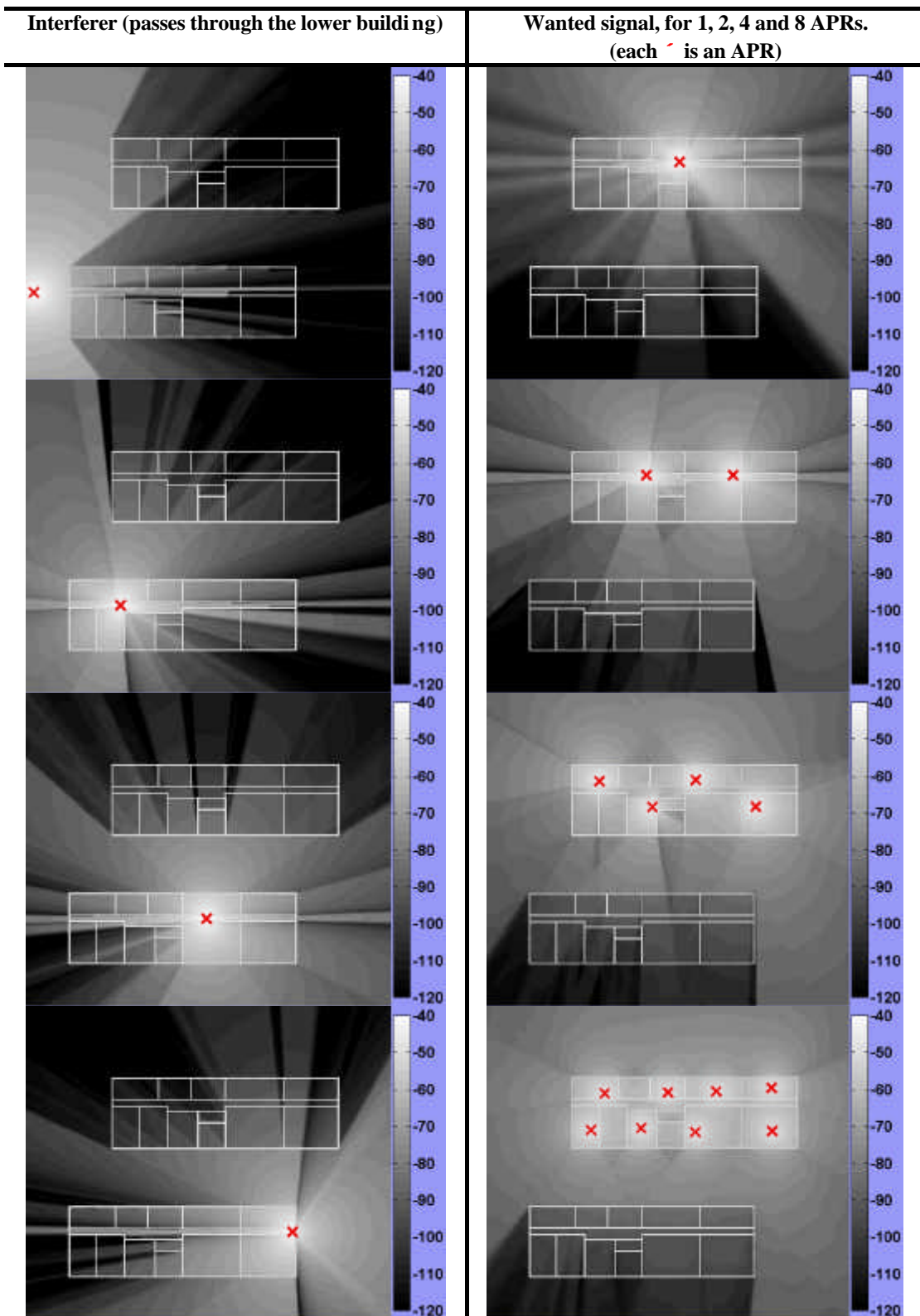


Figure 5-22, Received signal power for interferer and wanted signal. (script s0010)

The interferer column shows the results at four points in the simulation. The APR column shows the result for 4 separate simulations. (colourbar in dBm)

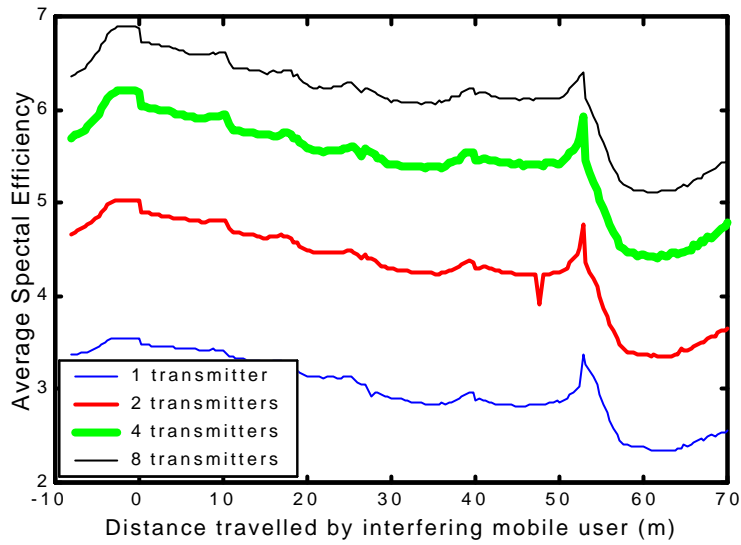


Figure 5-23, Average spectral efficiency over the area of the top building, as a function of the movement of the interferer. (script s0009)

The boundary of the building that the interferer passes through is from 0 m through to 53 m. (y-axis units are in b/s/Hz)

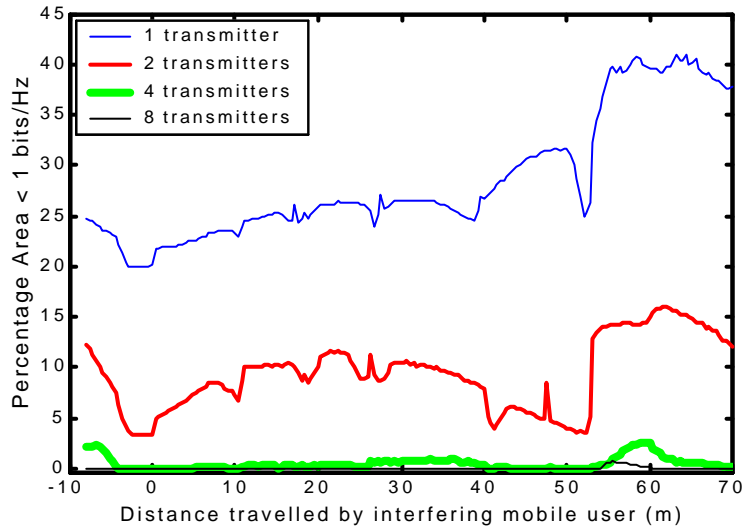


Figure 5-24, Quality of service provided in the top building in the simulation. (script s0009)

5.8 CONCLUSION

Using multiple Access Point Repeaters is a low cost method that can be used to reduce shadowing and near field path loss within a building. This allows a reduction in intercellular interference with suitable power control. It was shown experimentally to decrease the near field path loss by 7 dB @ 1 GHz within an indoor environment, using two repeaters as compared with a single transmitter. Simulated results show that the improvement can be as much as 20 dB for eight transmitters. Using multiple APRs will result in an increase in the received multipath, however OFDM systems, including HiperLAN2 and IEEE802.11a, should be able to tolerate this without detrimental effects. This tolerance should allow a maximum spacing of 40 - 60 m between any two APRs in a HiperLAN2 cell. Using APRs can be used to minimise the effects of interference, by improving the coverage within a building. This allows a reduction in the frequency reuse in cellular and neighbouring WLAN networks improving the overall spectral efficiency.

CHAPTER 6 GENERATION OF LOW CREST FACTOR MULTI-TONE SIGNALS

One disadvantage of OFDM is that the peak of the signal can be up to N times the average power (where N is the number of subcarriers). These large peaks increase the amount of inter-modulation distortion resulting in an increase in the error rate. The average signal power must be kept low in order to prevent the transmitter amplifier limiting. The variability of a signal is normally measured by its crest factor (CF), which corresponds to a measure of the peak to average envelope power of the modulated RF carrier. Minimising the CF allows a higher average power to be transmitted for a fixed peak power, improving the overall signal to noise ratio at the receiver.

This chapter describes how the CF of a sampled signal can be measured accurately, and outlines several techniques for minimising the crest factor of multi-tone signals. The term Discrete Multi-Tone (DMT) is used throughout this chapter to describe the OFDM signals under investigation. Although these terms refer to the same signals, OFDM implies data communications, while DMT simply describes the signal structure. The term DMT is used here to emphasise the focus on the multi-tone nature of the signals rather than the use for communications.

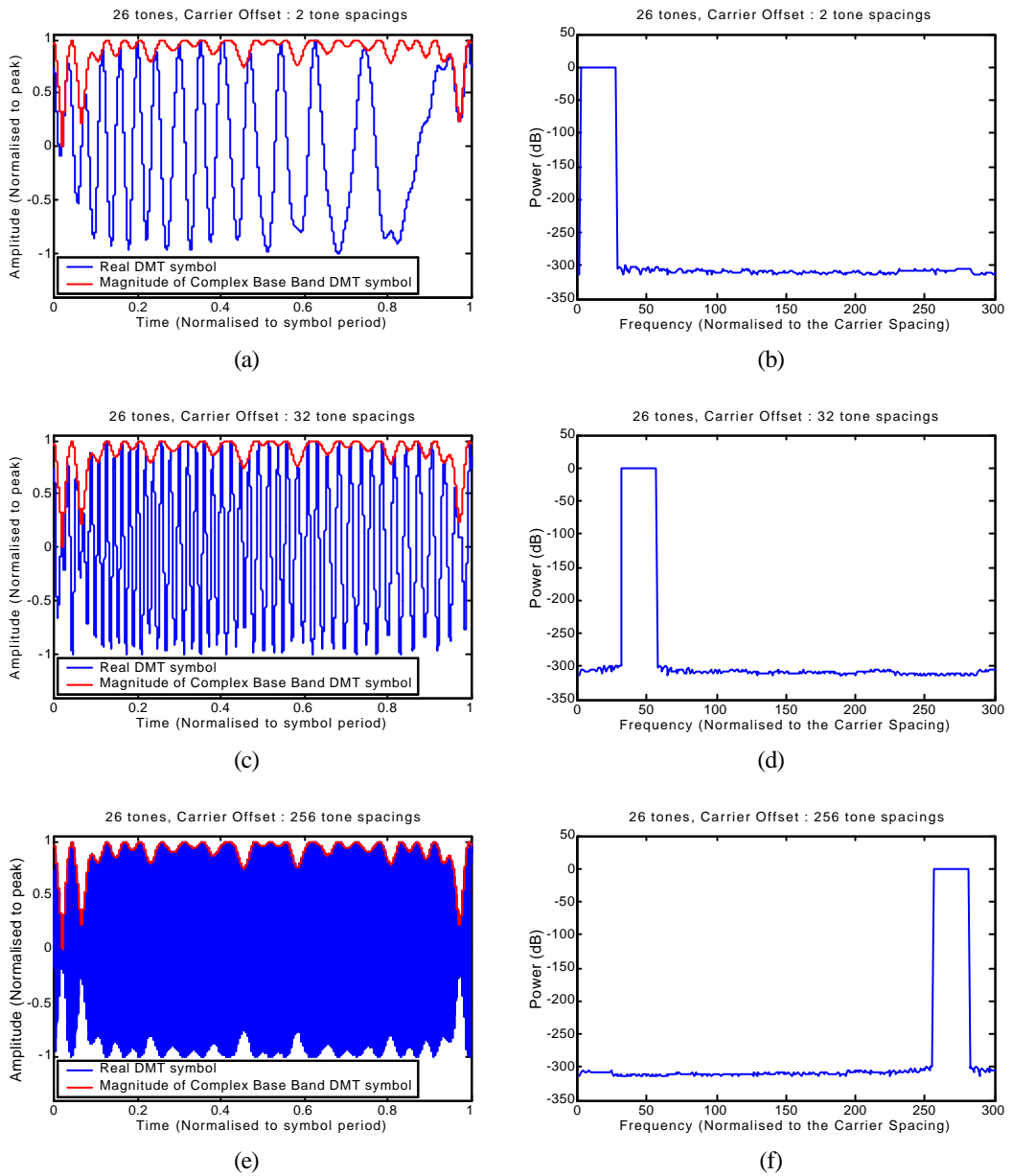


Figure 6-1, The magnitude of the complex base band DMT signal (shown in red) represents the envelope. (script s0001)

6.1 CREST FACTOR MEASUREMENT

The CF is a measure of the peak to average power ratio of the RF envelope. We however want to be able to calculate the CF from the base band signal, as simulating an RF waveform requires an extremely high sample rate, resulting in excessive computational overhead. Figure 6-1 shows the same DMT signal generated at different centre frequencies using a real waveform. As the centre frequency is increased, the envelope caused by DMT modulation can be clearly seen. Another method for finding the envelope accurately is to generate the DMT centred on DC, using a complex waveform rather than real waveform. Figure 6-1 also shows the magnitude of the DMT calculated at base band using complex waveform. It can clearly be seen that the magnitude of the complex waveform corresponds to the envelope of the carrier. Let the complex base band signal be defined as in.

$$\tilde{s}(t) = s_I(t) + j \cdot s_Q(t) \quad (6-1)$$

When this is quadrature modulated to RF the signal can be written in polar form as:

$$s_{rf}(t) = a(t) \cdot \cos(2\mathbf{p} \cdot \mathbf{f}_c t + \mathbf{q}(t)) \quad (6-2)$$

where $a(t)$ is the amplitude and $\mathbf{q}(t)$ is the phase of the signal. Thus:

$$a(t) = \sqrt{s_I^2(t) + s_Q^2(t)} \quad (6-3)$$

The CF is the ratio of the peak envelope power to the mean envelope power, taken over a given time period. Since we are interested in the CF of individual DMT symbols the time period is taken to be the symbol time of the DMT signal. The definition of the CF is shown in Equation (6-4), where T is the DMT symbol period [108].

$$CF_{dB} = 10 \log_{10} \left(\frac{\max_{0 < t < T} (a^2(t))}{\text{mean}_{0 < t < T} (a^2(t))} \right) \quad (6-4)$$

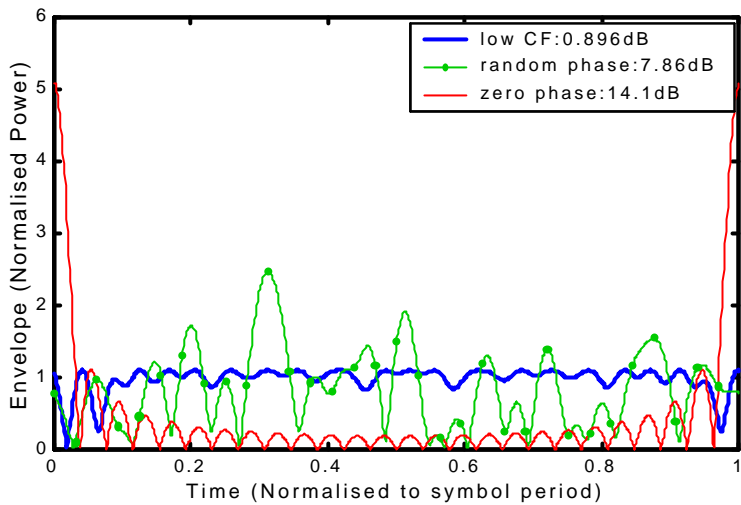


Figure 6-2, Envelope for 26 tone DMT symbol for different phasing schemes.
(script s0005)

Low CF uses the phasing method described later in this chapter (see section 6.2).

Figure 6-2 shows three DMT symbols. These symbols have equal power on each of their subcarriers. The difference between them is that the phase angle of the subcarriers is different. The CF of a DMT is dependent on the phase angle of the subcarriers. If the phase of the subcarriers is set to zero, or a linear ramp, the envelope will be the same as a band limited impulse. This has the worst case CF, which corresponds to N for N subcarriers, thus in dB, for the 26 subcarriers the CF will be:

$$CF = 10 \log_{10}(N) = 10 \log_{10}(26) = 14.14dB \quad (6-5)$$

6.1.1 RANDOM PHASE DMT SYMBOLS

Using a random phasing scheme results in a variable CF depending on the phase sequence. Some sequences result in a low CF while others give a high CF. The distribution of the CF follows approximately a lognormal Probability Distribution Function (PDF). This means that the PDF of the log of the CF (i.e. CF in dB) follows a normal distribution function (bell curve). This can be seen in Figure 6-3. This type of distribution results in most of the symbols having a moderate CF, typically around 7 - 10dB, with only a very small number having a very high or low CF. As the

number of tones is increased the mean CF also increases, however the standard deviation decreases, thus the spread of the CF distribution is decreased.

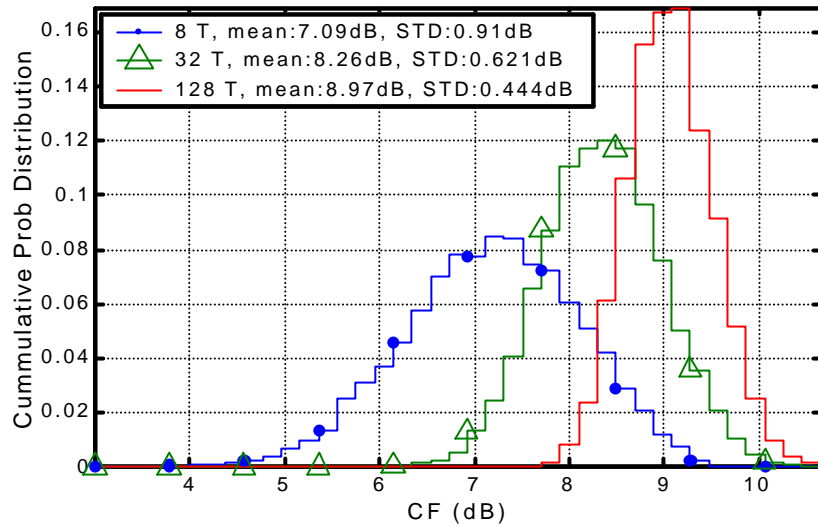


Figure 6-3, Crest Factor probability distribution function (split into 40 bins) for simulated random phase DMT signals, with 8, 32 and 128 tones (script s0032)

Studying random phase DMT symbols is also useful for analysing the CF distribution for digital data transmission using OFDM. If we assume that the data is random and that the transmission uses a phase modulation scheme such as QPSK, 16-PSK, etc, the distribution of the CF of the data symbols can be considered to be close to a random phase distribution. Figure 6-4 shows the distribution for random phase DMT symbols. This plots shows that for data transmissions the CF will only very rarely go over 11 dB (less than 0.1% of the time) even for a large number of subcarriers such as 1000. This CF is much lower than the worst-case CF of $10 \times \log_{10}(N)$, where N is the number of subcarriers. For 1000 subcarriers the worst-case CF is $10 \times \log_{10}(1000) = 30$ dB.

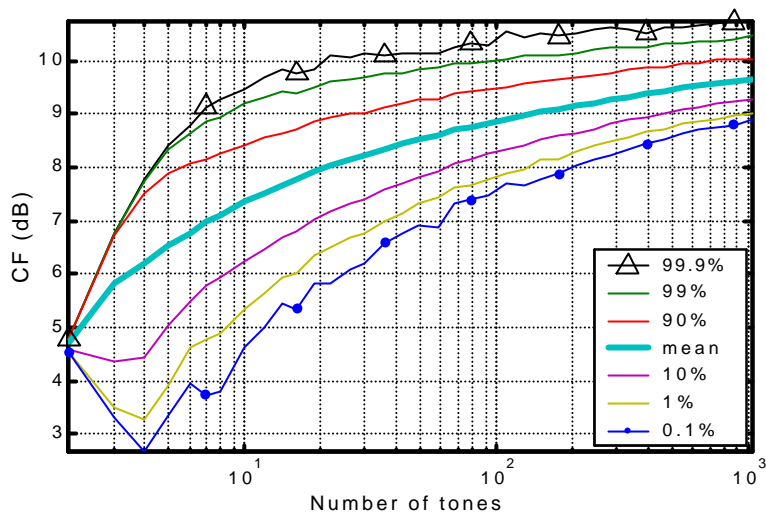


Figure 6-4, CF distribution of phase modulated OFDM signals verses the number of tones. (script s0032)

Note: most (99.9%) random phase DMT symbols have a CF much less than the worst case of $10 \log_{10}(\text{number of tones})$.

6.1.2 MEASUREMENT OF CREST FACTOR

Care must be taken when estimating the CF of a waveform, particularly for a discrete time signal. Accurate measurement of the CF requires that the true peak of the waveform be accurately measured. If the signal under investigation occupies close to the full nyquist bandwidth, then there will be few samples representing the fast transitions in the waveform. This can lead to large errors in peak estimation, as shown in Figure 6-5.

One method for measuring the peaks accurately is to interpolate the signal, and then measuring the peak of the resulting signal. The greater the signal is interpolated the better the estimate of the true peak and consequently the higher the accuracy of the CF measurement. This method assumes that the reconstructed signal will be perfectly frequency band limited. In practice when the signal is converted back to analogue, non-ideal reconstruction, such as aliasing non-linear amplification, and non-ideal frequency response, will result in slight variations in the peaks of the waveform, and consequently changes in the CF. This amount of deviation from ideal is however typically small (0.01 - 0.1 dB).

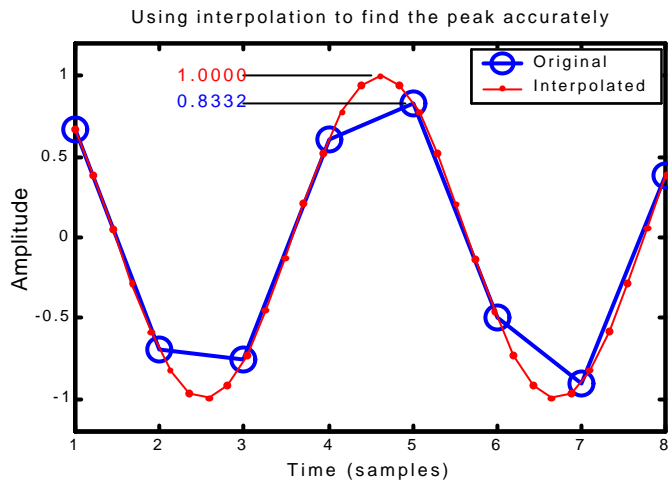


Figure 6-5, Accurate measurement of CF requires accurate measurement of the peaks in the waveform, which can be found using interpolation. (script s0004)

6.1.3 ESTIMATION OF ERROR IN CF MEASUREMENTS

The accuracy of the CF measurement of a waveform can be estimated theoretically. If we assume that the modulating waveform is a sine wave, then we can calculate the amount of error in the CF measurement as a function of the over-sampling of the waveform. Obviously, a multi-tone waveform is not the same as a sine wave. For an arbitrary phase modulated DMT signal the peak estimation will tend to be worst for sections of the waveform that are changing quickly. The higher the frequency of a signal, the faster it will change, thus a sine wave at the nyquist rate (frequency = half the sample rate) should approximate the fast changes in the DMT waveforms.

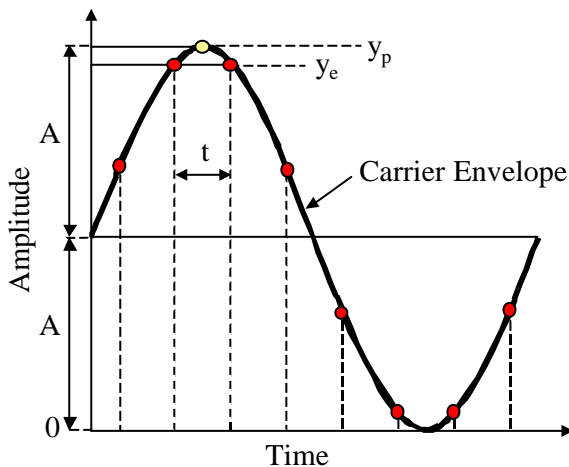


Figure 6-6, Worst case peak estimation sampling.

Figure 6-6 shows the waveform for the CF error estimation, which is a sine wave with amplitude the same as the carrier. The sampled locations are shown as red dots. The worst peak estimation will occur when the two sample locations around the true peak are the same in amplitude. Due to the symmetrical nature of the sine wave, this will occur when the true peak is exactly half way between samples. Let $y(t)$ be the modulating sine wave, with y_p the true peak of the waveform and y_e be the estimated peak, based on the sampled waveform. Let N be the number of samples per half cycle of the sine wave. This means that N is the interpolation rate. For the minimum interpolation rate of one ($N = 1$), there would be two samples per cycle of the sine wave, hence the frequency would correspond to the nyquist rate. t is the sample time, thus in terms of phase:

$$t = \frac{P}{N} \quad (6-6)$$

Since N is the number of samples per half cycle and there are π radians per half cycle.

The estimated peak can be found from the samples that are centred one either side of the true peak. The amplitude of these samples is equal, and so the estimated amplitude can be found using the sample to the left of the peak.

$$y_e = A + A \sin\left(\frac{P}{2} - \frac{t}{2}\right) \quad (6-7)$$

Thus the estimated peak, as a function of the over sampling rate N is,

$$y_e = A + A \sin\left(\frac{P}{2}\left(1 - \frac{1}{N}\right)\right) \quad (6-8)$$

To find the error in the CF measurement for the sample signal, we need to find the CF for the continuous signal and the sampled signal.

$$CF = \frac{\text{peak power}}{\text{mean power}} = \frac{\max(|y(t)|^2)}{\text{mean}(|y(t)|^2)} \quad (6-9)$$

The CF for the continuous waveform is:

$$\begin{aligned}
 CF_p &= \frac{\max(A + A \sin(\mathbf{q}))}{\text{mean}(A + A \sin(\mathbf{q}))} \Big|_{\mathbf{q}=0}^{\mathbf{q}=2\mathbf{P}} \\
 &= \frac{(2A)^2}{1.5A^2} = \frac{8}{3}
 \end{aligned} \tag{6-10}$$

The CF for the sampled signal will be:

$$\begin{aligned}
 CF_e &= \frac{y_e}{1.5A^2} \\
 &= \frac{\left[A + A \sin\left(\frac{\mathbf{P}}{2}\left(1 - \frac{1}{N}\right)\right) \right]^2}{1.5A^2}
 \end{aligned} \tag{6-11}$$

Cancelling out A and expanding the squared top term we get:

$$CF_e = \frac{1 + 2 \sin\left(\frac{\mathbf{P}}{2}\left[1 - \frac{1}{N}\right]\right) + \sin^2\left(\frac{\mathbf{P}}{2}\left[1 - \frac{1}{N}\right]\right)}{1.5} \tag{6-12}$$

Thus the error in the CF estimation can be determined by the difference between the CF of the continuous waveform and the sampled waveform. The CF calculated previously was in linear scale, however the error in dB is what is of interest, thus CF error can be found by difference between CF_p and CF_e after converting to dB. Thus the error in the CF estimation for the sampled system is:

$$CF_{error} = 10 \log_{10} CF_p - 10 \log_{10} CF_e \tag{6-13}$$

$$\begin{aligned}
 CF_{error} &= 10 \log_{10} \left(\frac{8}{3} \right) - 10 \log_{10} \left(\frac{1 + 2 \sin\left(\frac{\mathbf{P}}{2}\left[1 - \frac{1}{N}\right]\right) + \sin^2\left(\frac{\mathbf{P}}{2}\left[1 - \frac{1}{N}\right]\right)}{1.5} \right) \\
 &= 10 \log_{10} (4) - 10 \log_{10} \left(1 + 2 \sin\left(\frac{\mathbf{P}}{2}\left[1 - \frac{1}{N}\right]\right) + \sin^2\left(\frac{\mathbf{P}}{2}\left[1 - \frac{1}{N}\right]\right) \right)
 \end{aligned} \tag{6-14}$$

6.1.4 SIMULATED RESULTS

A simulation was set up to verify the theoretical error estimate, and to find how much effect having a DMT signal instead of a sine wave envelope has on the CF measurement. The simulation was performed by generating a large number of random phase, complex base-band, DMT signals. These were generated at different amounts of interpolation. The interpolation was done in the frequency domain by increasing the size of the IFFT used for transform from the frequency domain to the time waveform. The unused subcarriers were set to zero. The CF for each DMT symbol was measured at different amounts of interpolation, from 1 to 128. The interpolated result with the highest CF was assumed to be best estimate of the true CF for that waveform. The CF error was found by taking the difference between the highest CF and the CF found for all other rates of interpolation. This process was repeated with different random phase DMT symbols, and the highest error for each level of interpolation was recorded. Figure 6-7 shows the simulated results. The predicted results match the simulation results closely provided the number of carriers is greater than 2, and the interpolation rate is greater than 1.

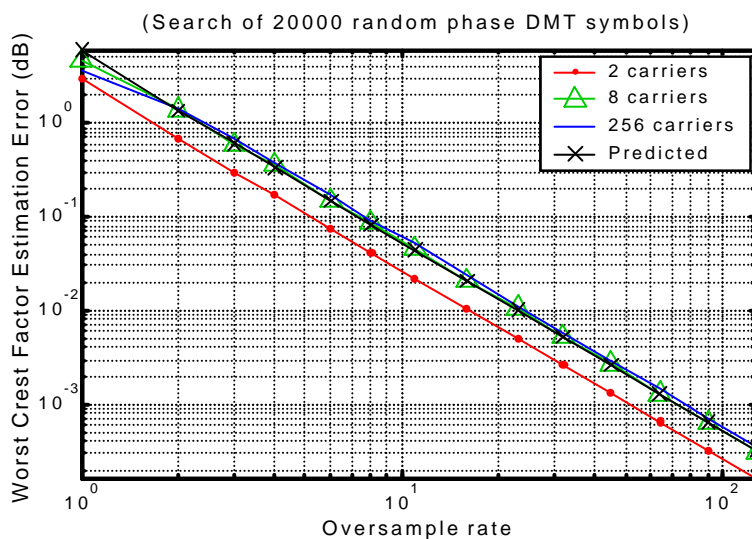


Figure 6-7, Maximum error in CF measurements as a function of over sampling of the DMT signals. (script s0002)

The over sampling is the simulated bandwidth used divided by the minimum nyquist bandwidth for the signal. This is a plot of simulated DMT results, and theoretical results for a sine wave modulated subcarrier.

6.1.5 CF ERRORS IN PRACTICE

The CF can be theoretically calculated very accurately for a waveform using interpolation. However, when it comes time to generate the signal in practice, several factors will make the CF different from the theoretical. The main two effects that significantly change the CF are the frequency response and distortion of the transmitter. Most low CF DMT generation algorithms assume that the amplitude of all subcarriers is equal, and that the phase angle of these subcarriers is used to generate a low CF. However in practice no system will have a perfectly flat frequency response, resulting in some of the subcarriers having more power than was assumed in the phasing scheme. This modifies the waveform and will typically result in a worse CF. Distortion will also change the CF, particularly clipping of the signal, which tends to reduce the CF of the signal.

6.2 CREST FACTOR MINIMISATION USING GENETIC ALGORITHMS

This section outlines a new phasing method for generating ultra low Crest Factor (CF) OFDM symbols. This phasing scheme uses genetic algorithms to optimise the phase of the subcarriers to minimise the CF of the waveform. The result of this process is that symbols with a CF as low as 0.65 dB are possible, which is 0.7 dB lower than any previously known algorithm. These ultra low CF symbols can be used for channel estimation due to the known phase angle of the subcarriers transmitted. This makes them useful for pilot symbols in coherent modulation or for adaptive modulation to allow tracking of the radio channel.

Because of their ultra low CF, the average power of these symbols can be boosted significantly (~6 dB) while still maintaining the same peak power as data symbols. This allows the channel estimation to have an improved SNR and thus improve channel estimation and speed.

Several phasing schemes have been previously developed, producing low overall CFs. We start out by looking at the performance of these techniques.

6.2.1 SHAPIRO-RUDIN PHASES

Shapiro and Rudin (1954) [104] showed that for multi-tone signal with N tones (N is a power of 2) that by setting the phase of the subcarriers to 0 or π , in a particular sequence, that this could yield a crest factor of 2 (3 dB). The sequence is defined as follows. We start with the string $p=11$, and repeatedly concatenate to p a copy of p with its second half negated. For example:

Length	Shapiro-Rudin Phase Sequence
2	$s = \{1\}$
4	$s = \{1\ 1\ 1\ -1\}$
8	$s = \{1\ 1\ 1\ -1\ 1\ 1\ -1\ 1\}$
16	$s = \{1\ 1\ 1\ -1\ 1\ 1\ -1\ 1\ 1\ 1\ 1\ -1\ 1\ -1\ 1\ 1\}$
32	$s = \{1\ 1\ 1\ -1\ 1\ 1\ 1\ -1\ 1\ 1\ 1\ -1\ 1\ -1\ 1\ 1\ 1\ 1\ -1\ 1\ 1\ -1\ 1\ 1\ 1\ 1\ -1\ 1\ 1\ 1\ -1\ 1\}$

Table 6-1, Shapiro-Rudin phase sequences for generating low CF DMT signals

The phase of the subcarriers is then set to 0 if $s_k = 1$, and π if $s_k = -1$.

$$\mathbf{q}_k = \begin{cases} 0, & s_k = 1 \\ \mathbf{p}, & s_k = -1 \end{cases} \quad (6-15)$$

If N is not a power of 2 the crest factor is still low, with it dipping to 2 when the number of tones is a power of two. To generate a non-power of two number of tones, the phase sequence is truncated from both directions. Figure 6-8 shows the crest factor as a function of the number of tones for Shaprio-Rudin's phasing scheme.

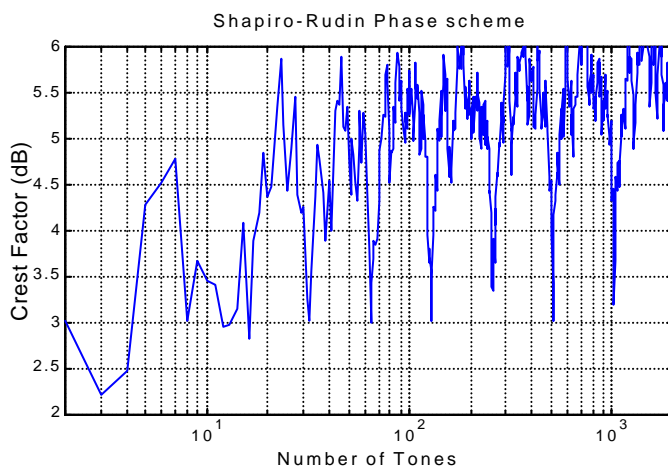


Figure 6-8, Crest Factor of a multitone signal when using Shaprio-Rudin's phasing scheme. (script s0067)

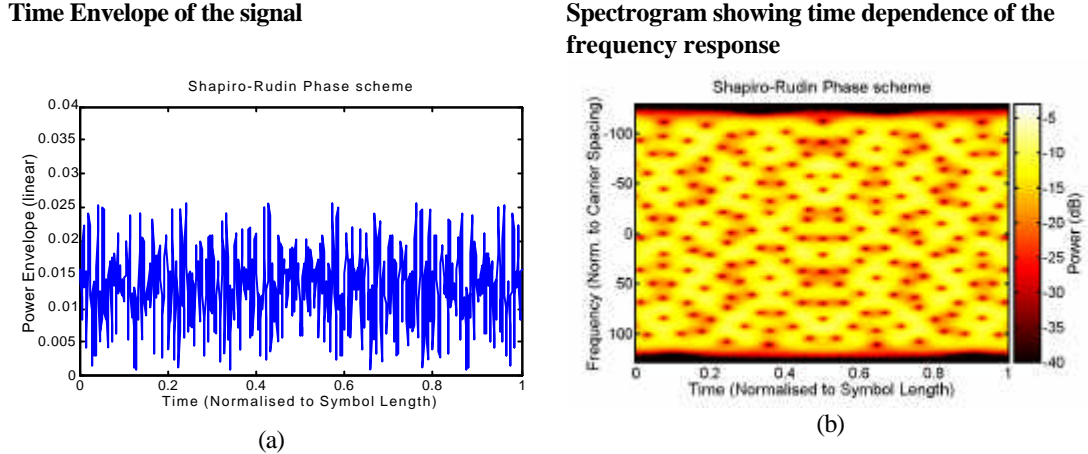


Figure 6-9, Time envelope and spectrogram for DMT based Shapiro-Rudin's phasing scheme. (script s0055)

This is for a 224-tone signal.

Shapiro and Rudin's scheme is interesting in that the phase angles used are discrete, and semi-random. This differs from the other schemes such as Newmann [105] and Narahashi [106] (as described later) as these schemes vary the phase continuously in a quadratic form.

6.2.2 NEWMANN PHASES

D. J. Newmann proposed varying the phase in a quadratic fashion in 1965 [105]. Equation (6-16) calculates Newmann phases where N is the number of subcarriers and k is the index of the particular subcarrier. Figure 6-10 shows the crest factor as the number of tones is varied. The worst case CF is 3.6 dB, which is for 3 tones. For greater than 10 tones the CF is less than 2.8 dB. The CF approaches an asymptote of 2.6 dB as the number of tones tends toward infinity.

$$\mathbf{q} = \frac{\mathbf{P}(k-1)^2}{N} \quad (6-16)$$

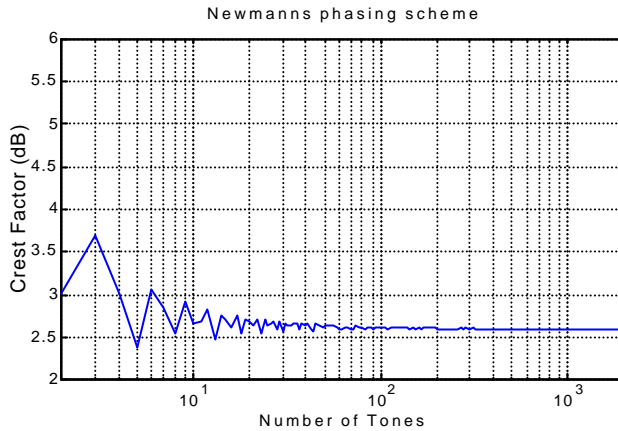
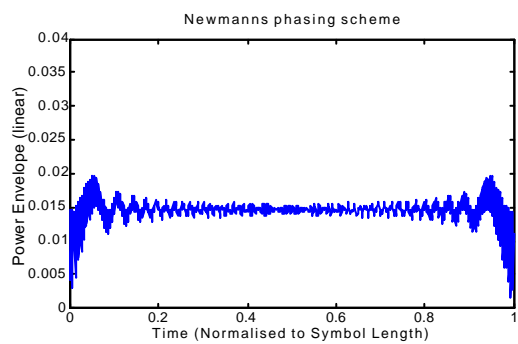


Figure 6-10, Crest Factor for Newmann's Phasing scheme. (script s0067)

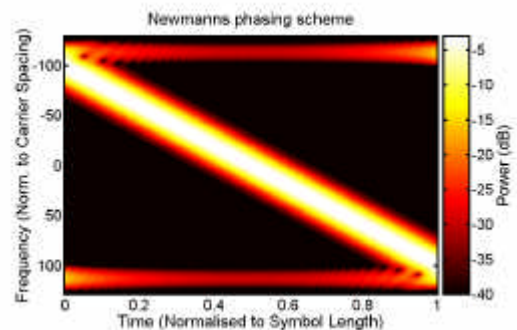
Figure 6-11 shows the time waveform and spectrograph of a 224-tone signal using Newmann's phasing scheme. From the spectrograph it can be seen that the signal is very similar to a linear frequency sweep. If we take a single continuous tone it will have a constant envelope power, resulting in a CF of 0 dB. If this tone is then swept slowly, then we end up with a signal similar to a DMT signal produced by Newmann's phasing scheme. The main difference is the transients at the start and end of the sweep. The FFT of the DMT will be perfectly flat in the frequency domain, and will have a small amount of ripple in the time domain, resulting in a CF of greater than 0 dB. Conversely, the linear frequency sweep will be perfectly flat in the time domain, but have a slight ripple in the frequency domain.

Time Envelope of the signal



(a)

Spectrogram showing time dependence of the frequency response



(b)

Figure 6-11, Time envelope and spectrogram for DMT based on Newmann's quadratic phasing scheme. (script s0055)

This is for a 224-tone signal.

6.2.3 S. NARAHASHI AND T. NOJIMA PHASING SCHEME

In 1994 S. Narahashi and T. Nojima [106] proposed a new phasing scheme based on a result similar to Newmann. The phase of each of the subcarriers is set as in equation (6-17). The resulting crest factor is very similar to Newmann's phasing scheme except that it performs slightly better than Newmann's method for small number of tones (< 6). However, Newmann's method is consistently better for $N > 24$.

$$\mathbf{q} = \frac{(k-1)(k-2)}{N-1} \mathbf{p} \quad (6-17)$$

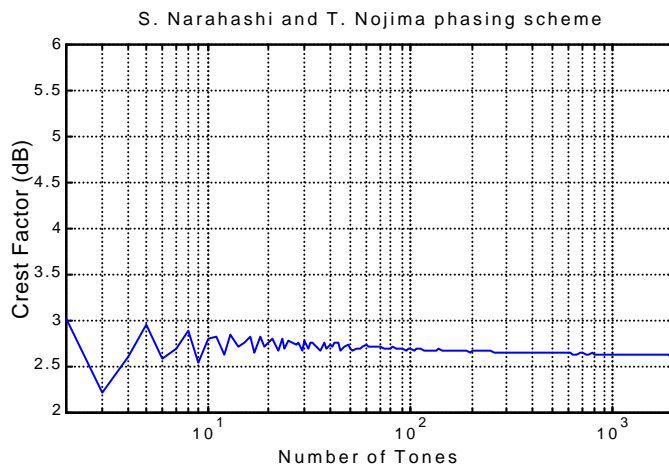


Figure 6-12, Crest Factor as a function of the number of tones for S. Narahashi and T. Nojima phasing scheme [106] (script s0067)

The time waveform and spectrograph of a 224-tone DMT signal generated using S. Narahashi and T. Nojima's phasing scheme is shown in Figure 6-13. Not surprisingly it is almost identical to that obtained using Newmann's method, as both schemes use a quadratic phase equation of approximately the same gain, and both give about the same CF.

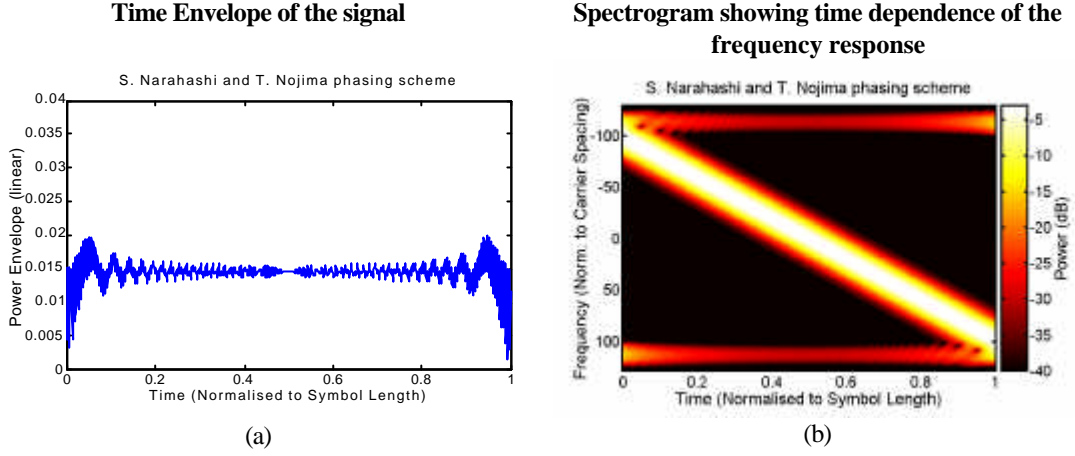


Figure 6-13, Time envelope and spectrogram for DMT based on S. Narahashi and T. Nojima's quadratic phasing scheme. (script s0055)

This is for a 224-tone signal.

In 1995, S. Narahashi presented a new method for producing low CF symbols [107]. Instead of developing an equation to minimise the CF, an iterative optimisation procedure was performed. The algorithm starts with a random phase sequence, and then uses steepest descent minimisation on the variance of the instantaneous envelope. This process is repeated for many random phase sequences and the best resulting sequence is kept. This algorithm results in a much lower CF symbols than previous methods. Figure 6-14 shows the resulting CF using this algorithm compared with the GA method presented in this chapter.

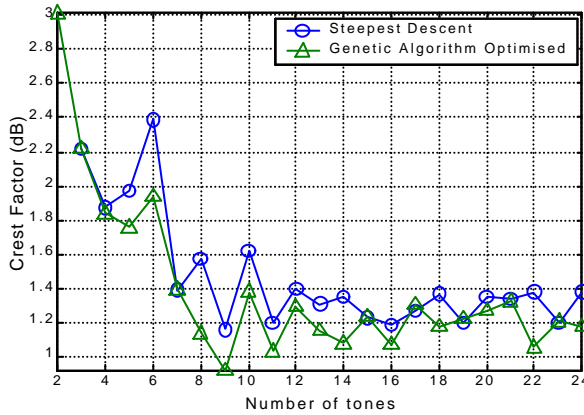


Figure 6-14, Crest Factor for the steepest descent optimised phasing scheme proposed in [107]. (script s0034)

Also shown is a comparison with the result obtained using the proposed technique presented in section 6.2.4 , using genetic algorithms to optimise the phase sequence.

6.2.4 GENETIC ALGORITHM PHASE OPTIMISATION

The envelope of a DMT signal is extremely complex as the phase angles of each of the tones in the signal interact to give constructive and destructive interference at different points along the resulting time domain signal. It is easy to obtain the resulting time domain waveform for any given subcarrier phase sequence, however it is not easy to obtain a method for optimising the phase sequence to minimise the CF of the resulting DMT waveform. The addition of each new subcarrier into a DMT signal, effectively adds another dimension to the problem, and so to optimise the CF, the searching must span a large multi-dimensional space to find the optimal solution. This makes it impossible to perform a brute force numerical optimisation, as the number of optimisation variable is too large. For example a 100-tone DMT signal has 100 variables that need optimising. To make this even worse, the space defining the relationship between the phase sequence and the resulting CF is fractal in nature. This means that there are many similar good solutions, making it difficult to ever find any global minimum.

There is no known direct analytical method for calculating a phase sequence that will result in the minimum CF possible [107], and so previous published research has focused obtaining a minimisation of the CF by using a mathematical approximation for the envelope of the DMT symbols [105], [106]. Two of the most important phasing schemes developed using this technique have been outlined in section 6.2.2 and 6.2.3 . CF minimisation was achieved by using analytical minimisation of envelope approximation. This method resulted in good solutions (CF of 2.6 dB), but does not approach the lowest CF possible.

This thesis presents a new method for obtaining phasing schemes that result in DMT signals with a very low CF. The method presented uses Genetic Algorithms (GA) to perform a searching algorithm to find low CF phase sequences. This method does not rely on any approximations for the signal envelope and so results in a much better end solution. The lowest CF obtained using this method was 0.65 dB, which was for 64-tone signal, making this 2 dB better than analytical techniques. This process uses numerical searching to obtain good solutions and so the performance of the end result is dependent on the amount of computer processing applied to the problem,

and so it is still an open question as to how low the CF can be made for a multi-tone signal.

Genetic Algorithms solve problems in a completely different manner to analytical minimisation. GA allows the optimisation of arbitrarily complex systems without requiring a mathematical understanding of how the optimisation is to be done. It is also very well suited to optimising problems that have a very large number of variables that require optimisation, as in this case. The use of GAs has gained popularity in the last few years as a method for optimising complex problems [114] - [116].

GAs are based on the principles of Darwinian evolution. To use genetic algorithms to solve a problem, the solution is represented as a sequence of variables known as a genome (or chromosome). In the case of optimising the phase scheme for generation of low CF DMT symbols, the genome corresponds to the sequence of phase angles applied to each tone in the DMT signal. Multiple genome sequences are used, making up a population. The genomes within a population are all different, representing genetic diversity. The actual problem domain to be optimised is defined by the transformation from each genome to its performance or fitness. For the case under investigation, the fitness corresponds to calculating the CF of the DMT for each of the phase sequences, where the lower the CF, the higher the fitness of the phase sequence. Optimisation occurs by selecting the highest performing phase sequences, then using these to create a new generation by mutating these sequences.

Figure 6-15 shows the algorithm used to perform the CF minimisation.

6.2.4.1 GENETIC ALGORITHM USED FOR CREST FACTOR MINIMISATION OF DMT SIGNALS

The simulation starts with an initial population of phase sequences. The length of each sequence corresponds to the number of tones being simulated. The fitness of each phase sequence is measured by calculating the crest factor of the DMT signal with subcarrier phase angles set to the phase sequence. The sequences are then sorted by fitness. A percentage of the best sequences are kept for reproduction to make the next generation, and rest removed, simulating death. The surviving sequences are paired up randomly, simulating sexual reproduction. Enough pairs are made to restore the population back to its original size. Each pair forms one resulting phase

sequence, by using a random splicing location. To this new sequence a small amount of random noise is added to simulate mutations in reproduction. The amount of random noise added is initially relatively large, but is decayed with the generations. This simulates a form of settled annealing. A large amount of mutation noise allows the problem domains to be widely searched; however it tends to prevent any settling into minima, resulting in a poor performance in the long run. Using a small amount of mutation noise results in a very slow progression, requiring a large number of generations to be simulated. In addition to this, it also tends to result in the process lodging in a local minima, leading to a poor performance. Starting with a large amount of mutation noise, then reducing it with the number of generations, results in good overall performance. In the simulations performed an exponential decay was used, with a decay time constant of 400 generations. In each of the simulations a population size of 1000 was used, and 200 of the best sequences were selected to create the next generation.

Figure 6-16 shows the CF as a function of the number of tones in the signal when using the GA outlined above. For symbols with more than 12 tones the CF is below 1.4 dB, and for 60 – 350 tones the CF is below 1.0 dB. For greater than 200 tones, the crest factor is artificially high due to insufficient number of generations simulated, as a result of the large number of computations required. For up to 56 tones the number of generations simulated was 5000. Above this, the number decreased gradually to 1200 generations for 512 tones. Most of the simulations were performed on the university supercomputer, with an approximate total simulation time of 10 CPU months (233 MHz processor). This large amount of simulation time was required due to the large number of generations and the large number of different test set as the number of tones in the signal was varied from 2 to 512. The number of generations needed to approach the minimum possible CF, varies as a function of the size of the population used, the amount of mutation noise, the starting phase sequence and the number of sequences kept to make the next generation. This simulation time could have been significantly reduced had the GA parameters been more optimised. This prompted the research on parameter optimisation shown in section 6.2.4.2.

Appendix D contains tables showing the optimised subcarrier phasing.

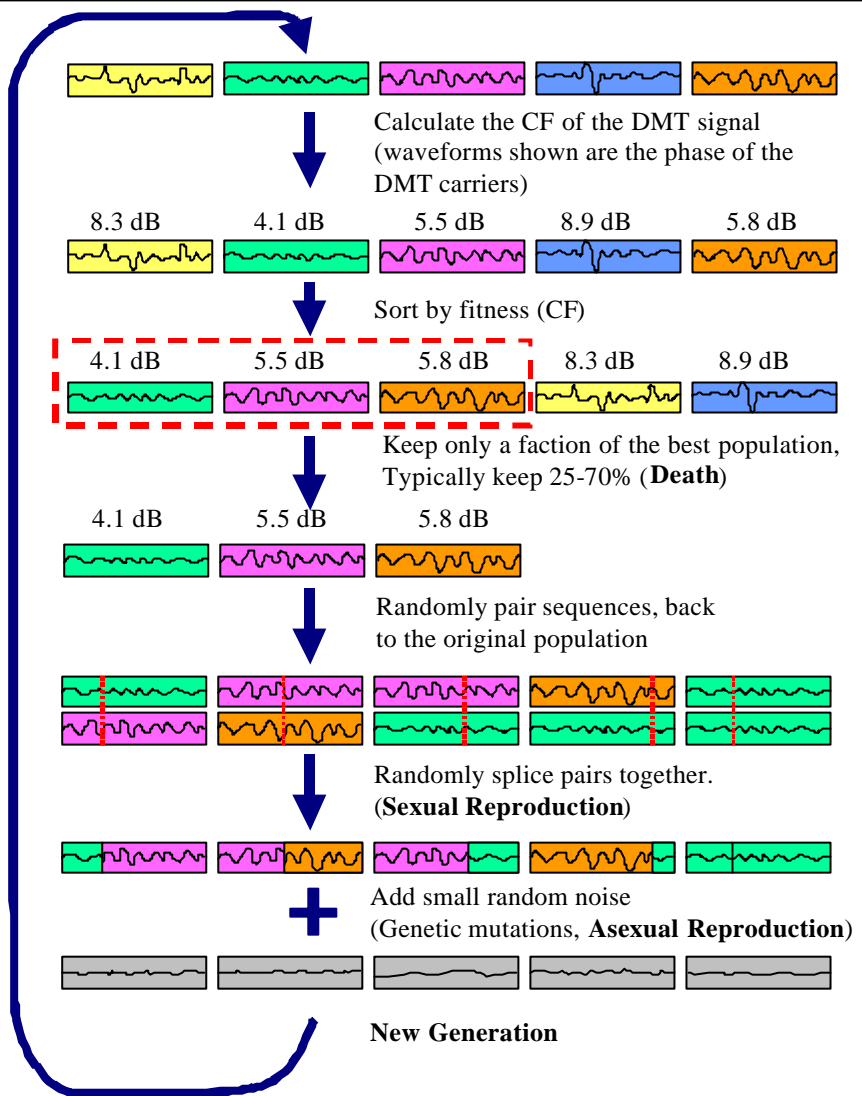


Figure 6-15, Genetic Algorithm used to minimise the CF of the DMT waveforms

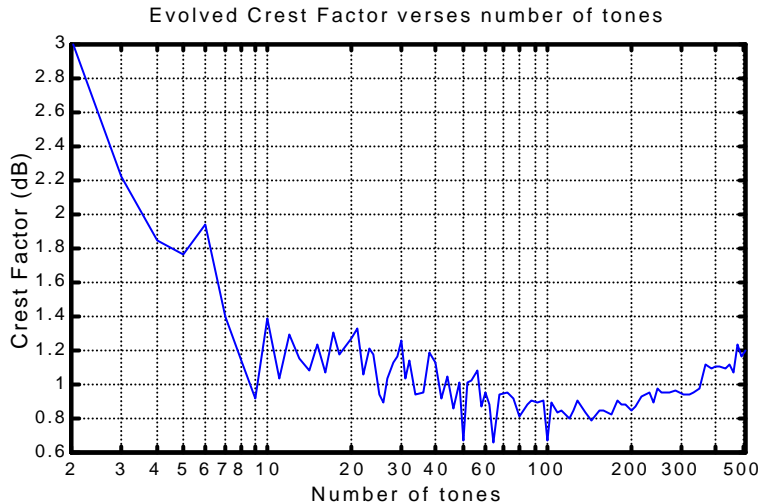


Figure 6-16, Best crest factor found using GA verses the number of tones in the signal. (script s0020)

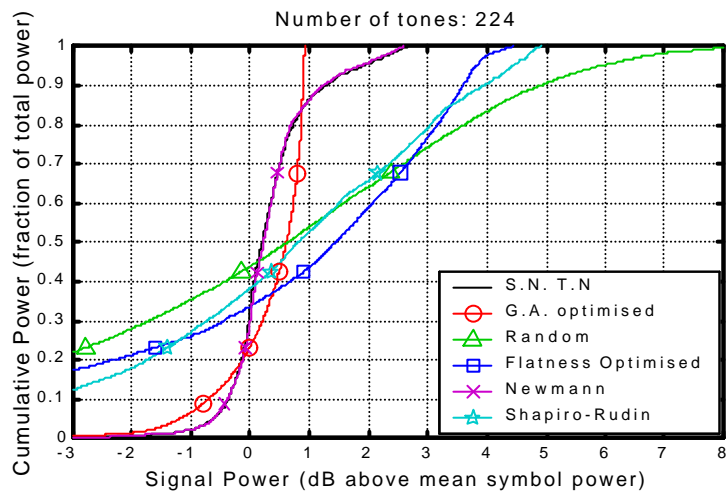


Figure 6-17, Power distribution of the time waveform for DMT signals generated using a range of phasing schemes. (script s0055)

S.N. T.N. quadratic phasing scheme (see section 6.2.3), Flatness Optimised details are outlined in section 6.3.

6.2.4.2 PARAMETRIC INVESTIGATION OF USING GENETIC ALGORITHMS FOR CREST FACTOR MINIMISATION

Using genetic algorithms is an effective optimisation technique for crest factor minimisation. However, there are many simulation parameters associated with the GA process that must be set in order to apply the genetic algorithm, such as the population size, the percentage to cull after each generation, the amount of mutation noise to add, etc. The choice of these parameters effects the number of generations required to achieve a good solution, and the quality of the ultimate solution. In order to address some of these uncertainties, an investigation into the effect of each simulation parameter was performed.

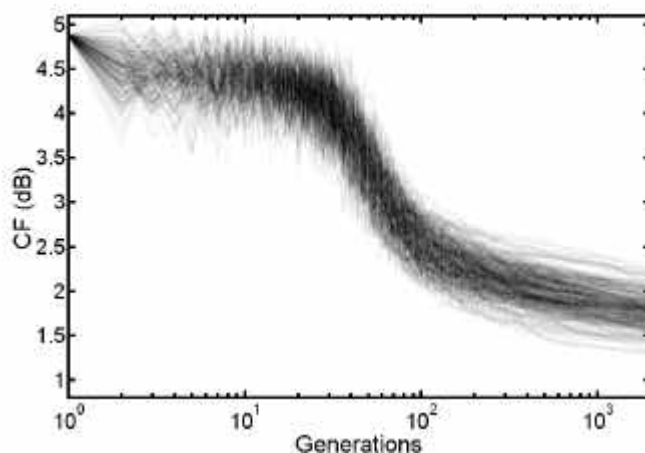


Figure 6-18, Crest factor distribution as a function of the simulated generations.
(script s0021)

This is for a 26 tone signal. The simulation was repeated 100 times, showing the variation in the evolution process.

Each generation consists of a population of phase sequences. These phase sequences are tested to find the crest factor of the resulting DMT signal. Within each generation the crest factor varies between individual sequences within the population. As the number of generations simulated increases the overall crest factor reduces due to the optimisation of the genetic algorithm. The performance of the genetic algorithm was tested by monitoring the crest factor of the best sequence in each generation, producing a plot of crest factor as a function of the number of generations simulated. Repeating the simulation restarts the evolution process, which can result in a different end solution. This is due to the random searching nature of genetic

algorithms. Figure 6-18 shows the crest factor verses the number of generations simulated. The solution obtained varies from simulation to simulation due to the random searching nature of genetic algorithms. Many of the simulations do not obtain a solution that is close to the global minimum. This is due to fact that the problem domain has many dimensions (1 dimension for each tone) and has many local minima. The search tends to get lodged in a local minima, thus rerunning the simulation multiple times tends to find a better solution.

Figure 6-19 shows the effect of changing the population on the performance of the GA. The results shown are the average of ten repetitions of the GA optimisation. As the population is increased the rate of optimisation is slower at the start of the GA optimisation, however after a sufficient number of generations is simulated a better end result is achieved. Using a large population improves the genetic diversity, which in turn improves the end solution.

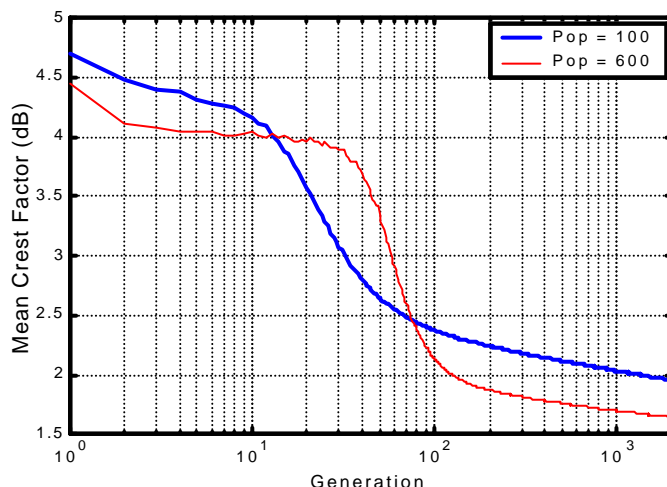


Figure 6-19, Effect of population size for genetic algorithm optimisation of CF, for 26 tone signal. (script s0021)

The mean CF was found by repeating the evolution simulation 10 times. (Keep = 50% for next generation)

Figure 6-20 shows the effect of changing the percentage number of the population to use for breeding of the next generation. Keeping the top 30% of the population for breeding the next generation results in the fastest progression to a good solution (CF < 3 dB), however it produced worst results than keeping 50% and 70% after 2000 generations. If too few of the sequences are used from one generation to the next

than genetic diversity is reduced resulting in the solution tending to get lodged in local minima in the optimisation space, rather than continually optimising to the global minimum.

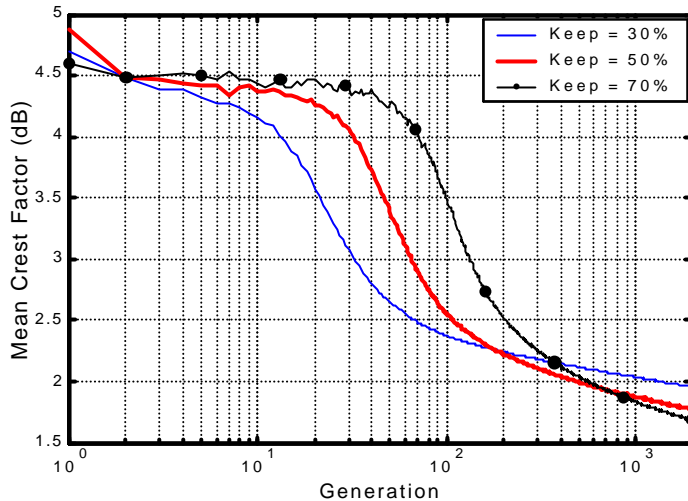


Figure 6-20, Effect of percentage population used to breed the next generation for genetic algorithm optimisation of CF. (population = 100). (script s0021)

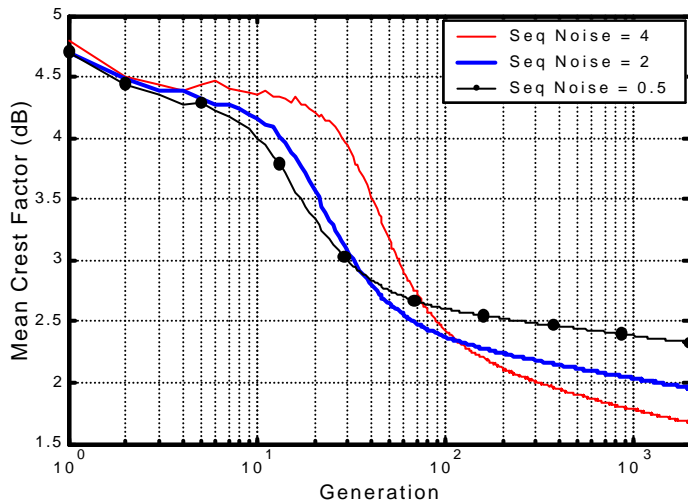


Figure 6-21, Effect of changing the amplitude of the mutation noise for genetic algorithm optimisation of CF. (script s0021)

Figure 6-21 shows the effect of changing the amount of mutation noise added to the phase sequences as part of calculating the next generation. For all the GA simulations performed the level of noise added to the sequences was decayed with the generation number, so that the level of noise was high at the start of the evolution and low toward the end of the simulation. In these simulations the level of the noise

added at each generation was calculated based on:

$$\text{Noise} = \text{SeqNoise} \times \text{Generation}^{-0.6}.$$

As the mutation noise is increased if increases the genetic diversity and hence the searching capability of the GA. It prevents the solution getting lodged in local minima, although too much noise tends to prevent any progression, as the solution never settles down.

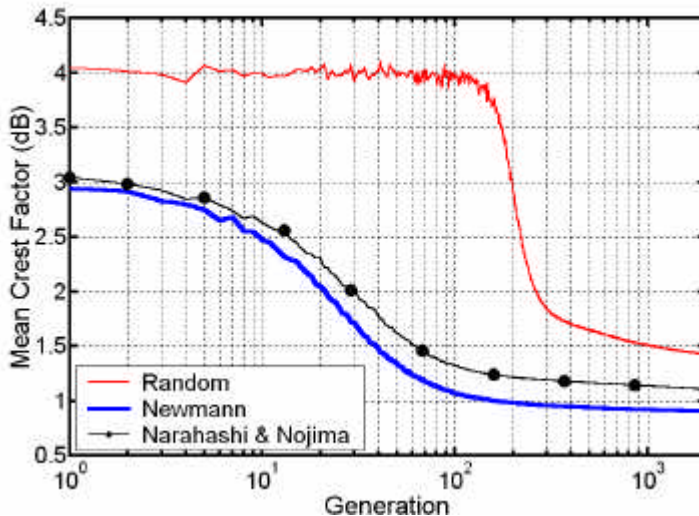


Figure 6-22, Effect of initial phase sequence used for genetic algorithm optimisation of the CF. (script s0021)

Figure 6-22 shows the effect of changing the initial population of phase sequences. The random simulation started with an initial population with purely random phase sequences. The other two tests started with the phase sequence calculated by Newmann's phasing scheme (see section 6.2.2) and Narahashi & Nojima's phasing scheme (see section 6.2.3). Newmann's and Narahashi phasing schemes generate low CF signals using a quadratic phase equation. Both these schemes perform much better than using a random phase sequence. This is probably due to the initial population starting with a result that is close to the global minimum (best solution), whereas when a random phase sequence is used a much larger solution space needs to be searched before the global minimum is found.

6.3 PHASING SCHEMES FOR NULL SYMBOL SYNCHRONISATION

One method for time synchronising an OFDM signal is to insert a null symbol (zero power transmitted for a complete symbol period) at the start of each frame. This null symbol can be detected at the receiver using a relatively simple envelope detector. This form of time synchronisation is used in the DAB system [20] for its simplicity. The best way to detect the null symbol is to measure the instantaneous power of the received signal, and then apply a moving average filter that averages over the null symbol length. The output of this detector is approximately constant when the OFDM signal is present, however when a null symbol is received the output drops will a minimum occurring at the start of the first OFDM symbol in the frame (Figure 6-28 (d) shows a good example of this). The first symbol in the OFDM frame is usually a reference symbol for channel equalisation for coherent modulation, or as a phase reference for differential modulation. This symbol contains a known (by the transmitter and receiver) phase reference on each of the subcarriers, allowing the receiver to measure the phase rotation and amplitude scaling of the radio channel. This phase reference does not transmit any data information due to its predetermined phase sequence.

When using a null symbol for synchronisation, the waveform of the first symbol in the frame determines the performance of the time synchroniser under fading conditions. The question is: how do we pick a suitable reference symbol? To make the reference symbol effective all of the subcarriers should have an equal transmission power. Ideally this symbol should have a low CF, so that it can be boosted in power without causing clipping distortion. It should also give a sharp time response when using a null symbol synchroniser. The synchroniser basically uses envelope detection, and so we want a symbol that has a consistently flat envelope, even over short periods of time (fraction of the symbol time). Thus a phasing scheme is required so that the CF is minimised and the time response is sharp.

One possible candidate is to use a low CF phasing scheme, such as those developed by S. Narahashi, T. Nojima [106] or by Newmann [105] or the Genetic Algorithm

Optimised low CF developed in Section 6.2. All these phasing schemes have very low CFs, and have a time response that is very similar to a frequency sweep. Although this type of phase reference has a low CF, its time domain response can cause a problem in a multipath environment. Frequency selective fading causes the filtering of the signal, resulting in some frequencies being boosted in power and others being reduced. The low CF symbols have a frequency sweep time domain waveform, and as a result the envelope follows the frequency response of the channel. This causes the envelope of the received symbol to be non-flat, degrading the performance of the null symbol time synchroniser. An example of this can be seen in Figure 6-28 (b).

Ideally the reference symbol should have a low CF, but be spectrally flat regardless of the time interval over which it is viewed. That way the detected envelope will be flat regardless of the frequency selective fading of the channel. As a starting place it would seem logical to start with a low CF phasing scheme. These schemes result in a single frequency sweep over the period of the symbol. If the rate of the sweep could be increased so that it repeats many times per symbol then the symbol would appear to be more spectrally flat, as taking a sub-section of the symbol would contain a complete sweep, covering all frequencies.

Both Newmann's (equation (6-16)) and S. Narahashi, T. Nojima's (equation (6-17)) phasing schemes set the phase angle as a quadratic of the subcarrier frequency. If we take a single carrier and vary the phase in a quadratic manner then the result is a frequency sweep. This is because the frequency of a carrier corresponds to the rate of change of the phase. If we take the differential of a quadratic the result is a linear sweep. The result is similar for a multicarrier signal.

We can approximate both Newmann's and Narahashi's phase schemes as a quadratic that is a function of subcarrier number, multiplied by a scaling coefficient, as shown in equation (6-18).

$$\mathbf{q} = Ak^2 \quad (6-18)$$

where A is a constant coefficient and k is the subcarrier number. For example for a 48-tone signal k would vary from 1 to 48. Varying the coefficient A changes the rate of the resulting frequency sweep in the generated OFDM signal.

6.3.1 SPECTRAL FLATNESS

To measure the effectiveness of the phasing scheme the time spectral flatness and CF of the resulting symbol was measured. Time spectral flatness was determined by taking a time overlapping spectrogram of the time waveform then measuring the peak to average ratio of the spectrogram. To ensure accurate time and frequency measurements four times interpolation was performed in both the time and frequency domain. The spectrogram breaks the input signal into time slices then performs an FFT of the slice to estimate the time varying frequency response. Interpolation in the time domain was performed generating the OFDM signal at a sample rate four times the amount required by the nyquist bandwidth of the signal. This was achieved by zero padding in the frequency domain by adding zeroed subcarriers to the outer edges of the OFDM signal. After the OFDM signal was converted to the time domain the signal was analysed using a spectrogram using a sliding FFT. Zero padding was added to each time slice before the FFT was performed. This resulted in interpolation in the frequency domain.

Measuring the spectral flatness by looking at the peak to average power ratio of the spectrogram is effective as it shows the variation in the frequencies generated in each subsection of the symbol. If the signal was perfectly flat over all time slices then the peak to average power ratio of the spectrogram would be 0 dB.

The aim of producing a low CF reference signal is so that the power of this symbol can be boosted without suffering significant additional distortion. The amount of interference caused by clipping of peaks in the signal is dependent on the height of the peak and the percentage time the clipping occurred for. For this reason the peak to average power ratio of the spectrogram was estimated using the 99% percentile of the waveform distribution instead of the true peak of the spectrogram. To improve the quality of the measurement, the length of the FFT used in the spectrogram was varied from half the symbol length to 1/16 the symbol length in four steps. This effectively changes the time/frequency resolution over a wide range, removing any assumptions about the time window used. The worst peak to average power ratio for these four different results was taken as the measured time spectral flatness.

In addition to measuring the time spectral flatness, the CF was measured as well, as the required symbol must perform well in the frequency domain and time domain. The results are shown in Figure 6-23. The crest factor function is an extremely complex function, with small changes in the gain coefficient A resulting in large variations in the crest factor. Both equations (6-16) and (6-17) divide the phase by the total number of tones in the signal (N). This scales the CF function so that all peaks align even for different number of tones and gain coefficients. By removing this division the CF function becomes more random, as can be seen in Figure 6-23(a). The problem with leaving this term in, is that it causes problems with the time spectral flatness. Leaving it in results in the time spectral flatness function varying with the number of tones used. By removing it, the function becomes normalised, making it less randomised. The spectral flatness is the most important part of the optimisation and so it is more important that the time spectral flatness is normalised. Although the CF is relatively randomised there are regions that have a generally lower crest factor. The time spectral flatness is more regular than the CF, but is also a complex function. The time spectral flatness is fractal in nature in that the structure is self-similar.

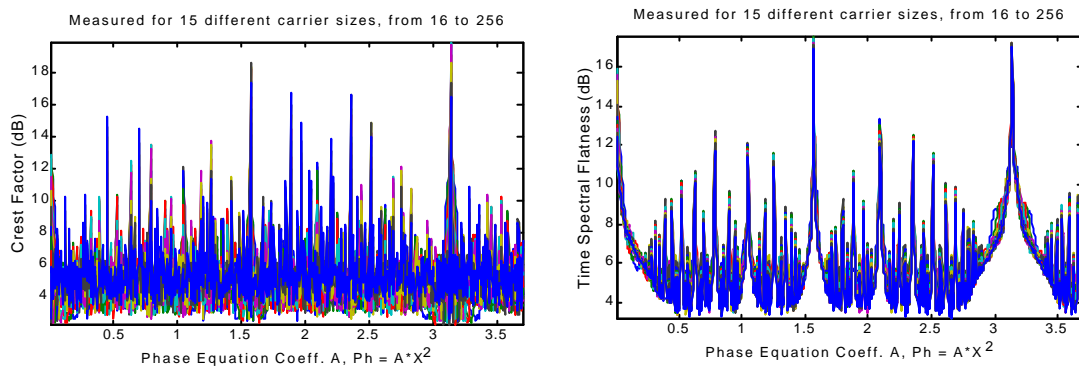


Figure 6-23, **(a)** Crest factor and **(b)** time spectral flatness as a function of the phase equation coefficient A . (script s0056)

The results are for 15 different number tones from 16 to 256. The final equation has to work effectively for any number of tones, hence the need to analyse range of combinations.

In order to choose a phasing scheme that would perform well over a wide range of tones, a fitness criteria was decided based on the CF and the time spectral flatness. For a particular number of tones the fitness criteria was based on adding one quarter

of the CF to the time spectral flatness, where both are in linear scale and not dB. This fitness was then calculated for a wide range in the number of tones. The mean fitness of all the tone tests was taken as the estimate of the fitness. Figure 6-24 shows the fitness criteria, from has a local minimum for A of 3.6315. The performance of the fitness approximately repeats every π .

To verify the effectiveness of the phasing scheme, the crest factor and time spectral flatness was measured as a function of the number of tones.

$$\mathbf{q} = 3.6315k^2 \quad (6-19)$$

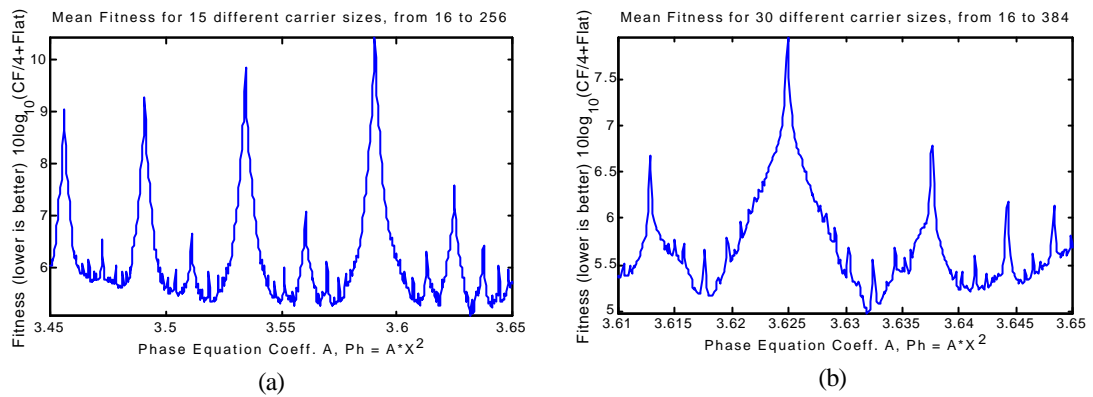


Figure 6-24, Fitness of the phase scheme for null symbol time synchronisation as a function of the phase gain coefficient A . (script s0056)

(a) shows a wide view of the fitness, while **(b)** shows a zoomed up section, indicating that the local minimum is at a value of 3.6315.

Figure 6-25 shows the CF and time spectral flatness as the number of tones is varied. The CF varies between 3.3 dB and 6.8 dB, which corresponds to a CF that is significantly lower than 99.9% of random phase symbols (see Figure 6-4). The time spectral flatness is very low for signals containing more than 40 tones, which remains below 3.6 dB up to the testing limit of 2000 tones.

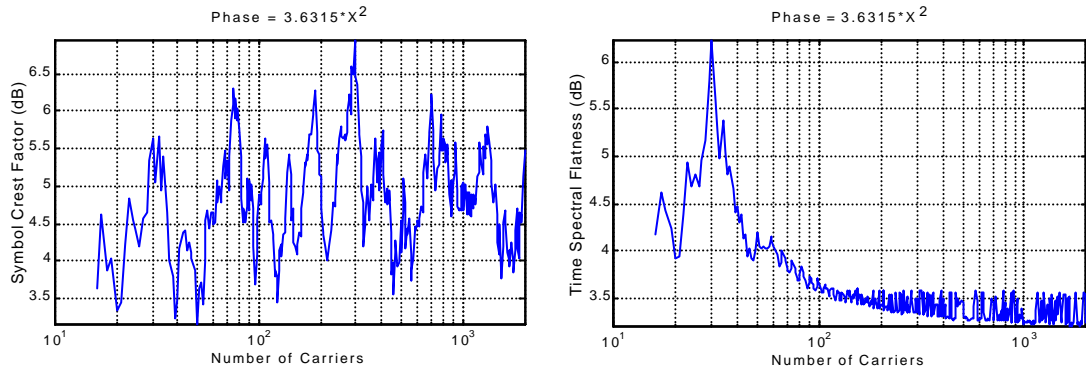


Figure 6-25, Crest Factor and Time spectral flatness as a function of the number of tones. (script s0056)

Figure 6-26 shows the time waveform and the spectrogram of a 256 tone OFDM signal using the time spectral flatness optimised phasing scheme. The spectrogram shows that the signal is very flat and consistent over the entire symbol period. The time waveform is semi-repetitive, with around 13 similar sections.

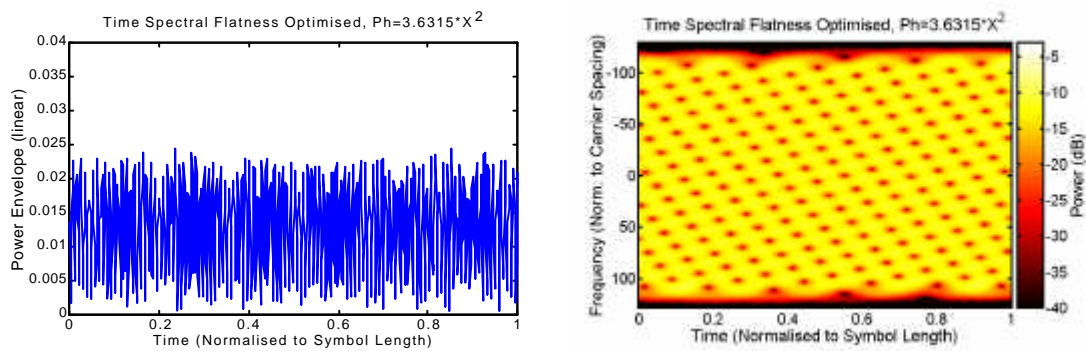


Figure 6-26, Time waveform and spectrogram of a 224 tone OFDM signal using the time spectral flatness optimised phasing scheme. (script s0055)

6.3.2 EXPERIMENTAL VERIFICATION

An experiment was performed to verify the effectiveness of the time spectral flatness optimised phasing scheme for use in null symbol time synchronisation. The performance was compared with a synchroniser using Narahashi low CF reference symbols (see section 6.2.3). The performance of this time synchronisation method is affected by multipath, as this filters the received signal, which can result in a non-uniform signal envelope. The amount of non-uniformity of the envelope will depend on the time spectral flatness of the symbols immediately before and after the null

synchronisation symbol.

Figure 6-27 shows the test set up. An OFDM generator was implemented on a SHARC DSP development board. The generated signal consisted of a 192 subcarrier OFDM signal using a bandwidth of 18 kHz, with a null symbol inserted every 30 symbols for time synchronisation. A real output signal was generated using a 512-point IFFT with a guard period of 64 samples.

The receiver's DSP performed time synchronisation on the signal. The receiver generated two output results, one being the null symbol time synchroniser and the other a straight though, showing the signal as seen by the receiver. The null symbol synchroniser consisted of taking the magnitude of the input signal and applying a moving average filter equal in length to the null symbol, corresponding to the IFFT size plus the guard period ($512+64 = 576$ samples). The resulting signal is high during the presence of the OFDM signal, changing to a 'V' shape during the null symbol. The minimum of this 'V' corresponds to the start of the OFDM frame. In order for a receiver to use this synchronisation signal, further processing would need to be applied to detect the minimum in the 'V'.

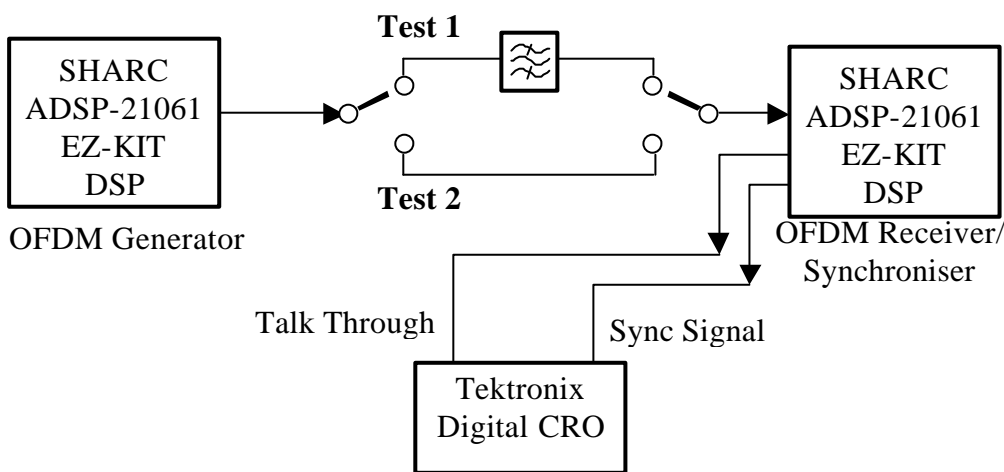


Figure 6-27, Experimental set up for investigating the performance of the time synchronisation method.

Test 2 is a straight through test. Test 1 shows the performance with simulated channel filtering.

Test 2 showed the performance of the synchroniser with no detrimental effects. Test 1 applied a low pass filter to the transmitted OFDM signal. The signal was filtered

with a 3rd order passive filter to simulate a distorted frequency response. This filter was a highly resonant low pass with a 6 dB peak just before the cut off frequency. The filter removed approximately 50% of the signal bandwidth. This filtering represents an extreme example of multipath frequency selective fading.

Figure 6-28 (a) – (c) show measured results for time synchronisation when using the S. Narahashi, T. Nojima phasing scheme. When no filtering was applied the performance is adequate, with the time synchroniser forming a reasonably sharp 'V'. The problem occurs when filtering is applied since this results in the signal envelope changing dramatically due to the frequency sweep nature of the signal. The envelope in fact tracks the frequency response of the filter. The resulting time synchronisation waveform is very poor, with no clear minimum occurring at the start of the frame. If this signal had a higher amount of noise the performance would be very poor.

Figure 6-28 (d)-(f) shows the same test using the phasing scheme developed. The 'V' formed by the synchroniser is very sharp with no filter, and remains sharp even when subjected to the low pass filtering. This verifies that the phasing scheme performs very well regardless of channel filtering.

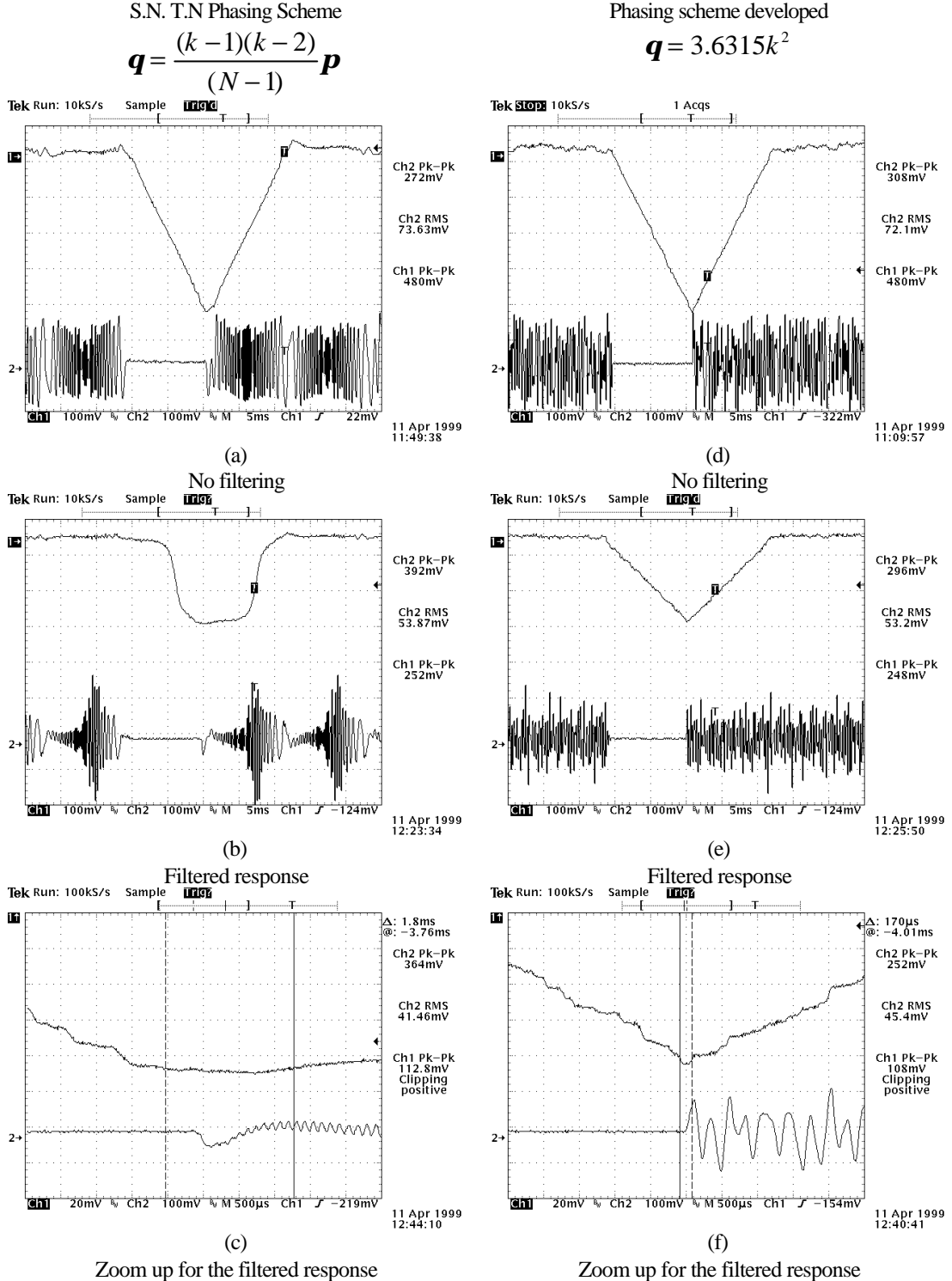


Figure 6-28, Measured time synchronisation accuracy for different reference symbols.

The bottom trace shows the OFDM signal, and the top signal is the frame detection signal. The actual time synchronisation is found by finding the minimum of this waveform. The filtered response was for a passive low pass filter removing 50% of the OFDM spectrum.

CHAPTER 7 CREST FACTOR MINIMISATION OF OFDM DATA SYMBOLS

A technique is described for a better than 5 dB reduction in the crest factor for data carrying OFDM signals. This improvement is achieved by inserting additional subcarriers into the signal referred to as peak reduction carriers (PRC). These PRC are set in phase and amplitude, using a codebook, to minimise the overall symbol CF. The codebook is obtained using a search of all possible signal combinations. This technique is optimised for signals using a low number of subcarriers, and low modulation schemes such as BPSK and QPSK, due to the brute force searching technique employed.

7.1 BACKGROUND

The CF of an OFDM signal can be reduced in several ways. Selective mapping [108], [109] involves generating a large set of data vectors all representing the same information. The data vector with the lowest resulting CF is selected. Information about which particular data vector was used is sent as additional subcarriers. However, there may be potential problems with decoding the signal in the presence of noise with selective mapping. Errors in the reverse mapping would result in whole symbols being lost.

Another technique similar to selective mapping is to use Golay sequences [113]. Information is transmitted by mapping each data word with a Golay sequence. Using Golay sequences result in a low CF, typically 3 - 6 dB, however the coding rate is poor, typically half, resulting in a large bandwidth increase. Cyclic coding [110]

involves adding extra subcarriers in which the phase of every fourth subcarrier is calculated based on an algorithm using the phase of the previous three information subcarriers. This method is similar to the presented technique except that it gives sub optimal results.

7.2 PEAK REDUCTION CARRIERS

This chapter presents a technique that combines selective mapping and cyclic coding. A reduction in the CF is achieved by adding extra subcarriers referred to as Peak Reduction Carriers (PRC). The phase and amplitude of the PRCs is varied to minimise the overall CF. The original information subcarriers are unaffected and can be decoded normally. The receiver can disregard the PRCs, or they can be used for error detection. The frequency of PRCs, or relative positioning of the PRCs can be varied with respect to the information subcarriers depending on the application. The results presented were found using a computationally intensive exhaustive search to find the optimal setting for the PRCs. However it is assumed that further work will allow a more efficient algorithm to be found.

An optimal setting for the PRCs corresponds to the combination of phase and amplitude that achieves the lowest CF of the overall OFDM symbol (information subcarriers and PRCs). In this paper the phase and amplitude of the PRCs was set in a coarse quantised manner to minimise the number of combinations needed to be searched. The phase of the PRCs was set to 0° or 180° and the subcarriers were turned on or off. There are therefore 3^M combinations for the PRCs for each information code word (where M is the number of PRCs). This level of quantisation was found to be appropriate for BPSK information subcarriers. Finer quantisation may produce improved results for higher modulation schemes.

An exhaustive search of all combinations of allowable phase and amplitude gives optimal PRCs, but is computationally intensive. This method can be used for small numbers of subcarriers where the optimal PRC coding can be stored in a look up table or code-book. This is impractical for more than 16 information subcarriers or for more than 10 PRCs as the number of combinations becomes too large to store and calculate. However for some multi-user OFDM applications 16 or less subcarriers

per user is sufficient.

The results shown were calculated based on all combinations of information code words, thus will give a good indication of the practical CF improvement.

For each experiment the inverse fast Fourier transform (IFFT) of the subcarrier configuration was used to give a complex base band signal.

For the simulations carried out, the base band subcarriers were centred on DC and the size of the IFFT was made at least 8 times greater than the number of subcarriers, oversampling the time domain signal. This ensures that peaks in the signal were accurately represented to get an accurate CF [111], [112].

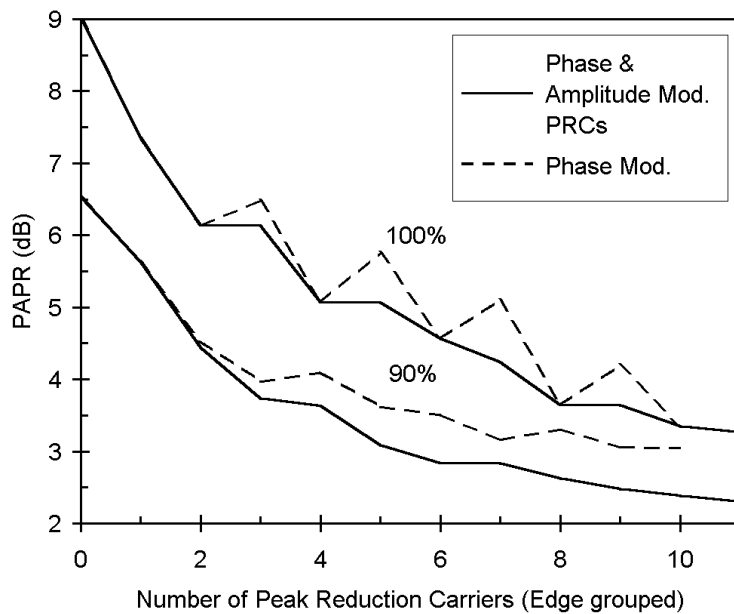


Figure 7-1, CF verses number of edge grouped PRCs (8 BPSK data subcarriers)

7.3 RESULTS

The simplest arrangement for the relative positioning of the data and PRCs is to have a block of data subcarriers immediately followed by a block of PRCs. This arrangement was used for the results shown in Figure 7-1 through to Figure 7-3.

Figure 7-1 shows the worst-case CF and the 90% point in the cumulative distribution of CF as the number of PRCs is increased. The maximum CF for the 8 information subcarriers is reduced by > 5.5 dB for the addition of 10 PRCs. Selecting the optimal amplitude and phase of the PRC improves the performance significantly as compared

with only setting the phase as used in cyclic coding [110]. For this reason phase and amplitude modulation of the PRCs was used in all later experiments due to the improved performance.

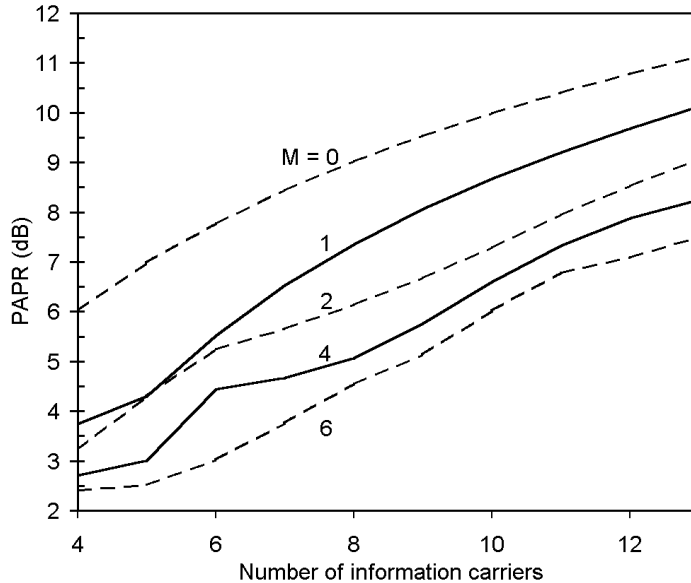


Figure 7-2, Maximum CF verses number of data subcarriers and edge grouped PRCs, where M is the number of PRCs.

Figure 7-2 shows the effect of adding PRCs to the CF as the number of information subcarriers is varied. The improvement in CF remains relatively constant as the number of information subcarriers is increased. This shows that this technique gives consistent performance gains as the number of information subcarriers is varied.

Adding PRCs reduces the CF at the expense of additional transmission power and bandwidth. Figure 7-3 shows the net improvement in CF due to the addition of PRCs. The CF reduction was calculated as the difference between the CF results for zero PRCs and the CF results with the addition of PRCs. The loss in signal power due to the PRCs was then subtracted from the CF reduction in order to give the net CF improvement. If the data signal power lost due to the transmission of the PRCs was more than the CF gain then there would be little point in adding the PRCs. It can be seen that for 10 BPSK subcarriers there is little improvement in adding more than 2 PRCs. In fact adding more than 5 PRCs results in a worsening of the average (50%) CF. This is due to the power cost of the PRCs.

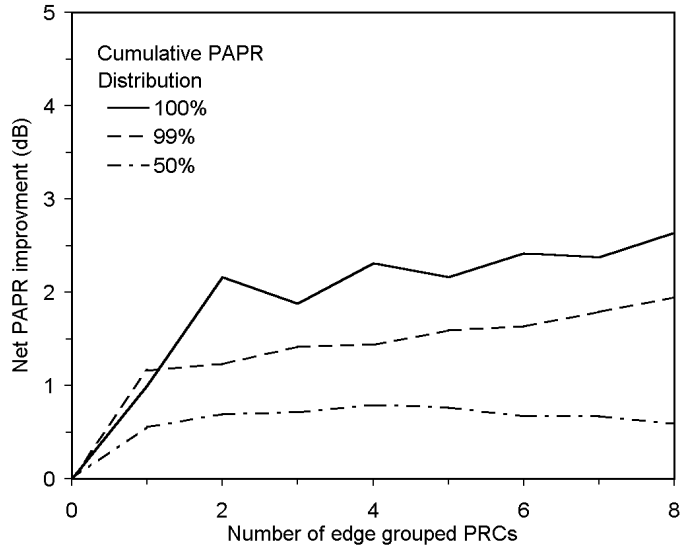


Figure 7-3, Net CF improvement verses number of edge grouped PRCs. (10 BPSK data subcarriers)

7.4 EFFECT OF PRC POSITION

Previous results are shown for grouped PRCs that were positioned immediately after the data subcarriers as shown in Figure 7-4 (a). Two different positioning tests were performed. One test kept the PRCs grouped together as in Figure 7-4 (a), however they were moved with respect to the data subcarriers as in Figure 7-4 (b). The second test positioned the PRCs in a spread out manner. The best spread pattern was established using a randomised search.

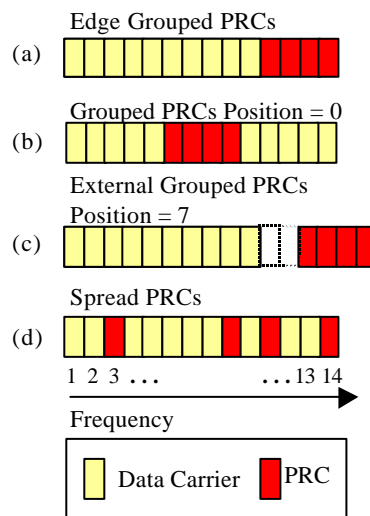


Figure 7-4, PRC position combinations

Adding PRCs use a significant amount of additional bandwidth. It is therefore important to minimise the number used, or to position the PRCs so that the bandwidth can be reused. For example, in a multi-user OFDM system where each user transmits a block of subcarriers, the PRCs can be overlapped, i.e. they are transmitted at the same frequency, effectively halving the bandwidth used by the PRCs.

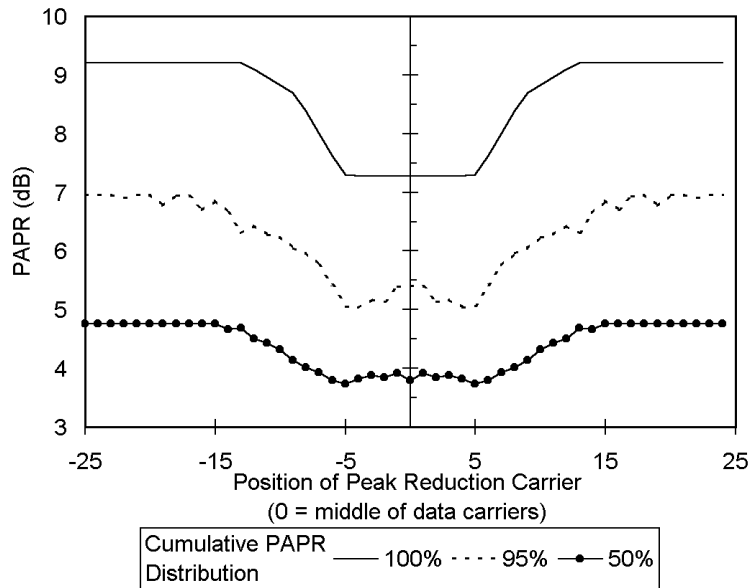


Figure 7-5, CF verses position of 2 grouped PRCs (10 BPSK data subcarriers)

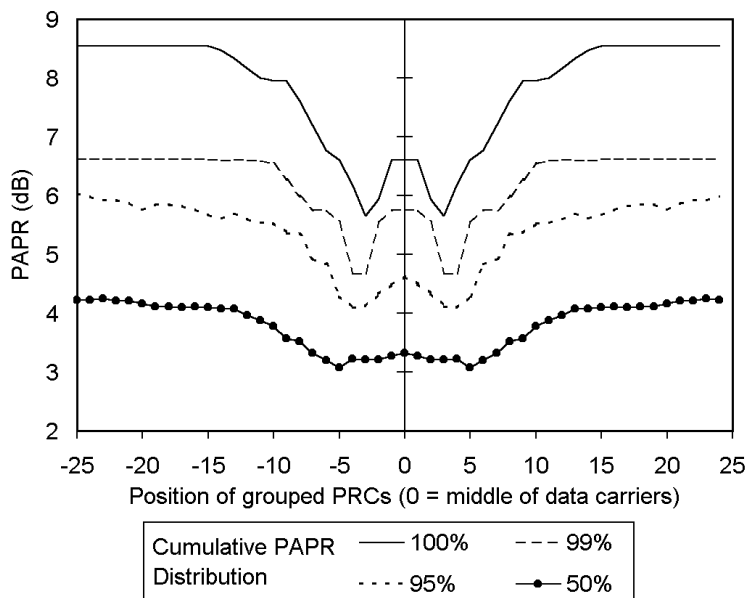


Figure 7-6, CF verses position of 4 grouped PRCs (10 BPSK data subcarriers)

7.5 GROUPED PRCs

In this scheme the PRCs were maintained as a group of subcarriers. They were repositioned by sliding them with respect to the data subcarriers. Figure 7-5 and Figure 7-6 show the effect of the position on effectiveness of the PRCs. Figure 7-5 shows that for a small number of PRCs the performance is not particularly dependent on the position of the PRCs within the data subcarriers. However with 4 or more PRCs the position has a significant effect on the performance of the PRCs. Placing the PRCs within the data subcarriers with an off centre of 3 subcarriers gives the best results. This gives a further reduction of 1 dB as compared with edge grouped PRCs. Not having edge grouped PRCs prevents the overlapping of the PRCs from different users in a multi-user OFDM system. As a consequence the bandwidth used by the PRCs will be effectively doubled.

7.6 SPREAD PRCs

The position of the 4 grouped PRCs had a significant effect on the PRC performance, thus it seemed likely that spreading the PRCs out might lead to further improvements. The exact relationship between the position of the PRCs and the CF distribution is currently unknown and so a random search was used for optimisation. The PRCs and data subcarriers were positioned randomly to form a block of subcarriers with no gaps as shown in Figure 7-4 (d). For each position combination the CF distribution was found and the combination that resulted in the lowest maximum CF was selected as the optimised PRCs position.

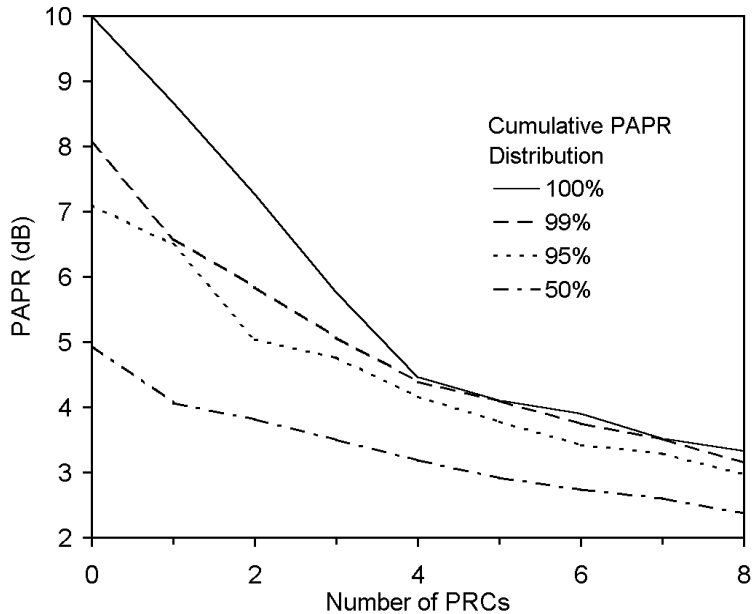


Figure 7-7, CF verses the number of spread PRCs (10 BPSK data subcarriers)

The CF distribution was found by testing all combinations of the data code words. For each data code word combination the optimum PRCs were found as described in section 3. The CF distribution verses the number of PRCs is shown in Figure 7-7. This result is for 10 data subcarriers and shows that spreading the PRCs can result in large reductions in the CF of the OFDM symbol. A reduction of greater than 6 dB is possible.

Figure 7-8 shows the overall net improvement in the CF using position optimised PRC. This can be directly compared to Figure 7-3 which shows the results for edge grouped PRCs. The maximum net gain for position optimised PRCs is approximately 2 dB better than that of the edge grouped PRCs. Figure 7-8 shows that the net CF gain increases rapidly up to 4 PRCs, after which the gain is minimal. Thus the optimal number of PRCs would be 4 for 10 data subcarriers. Other tests also show that the number of PRCs needs to be approximately 40% of the number of data subcarriers in order to get significant improvements in the CF.

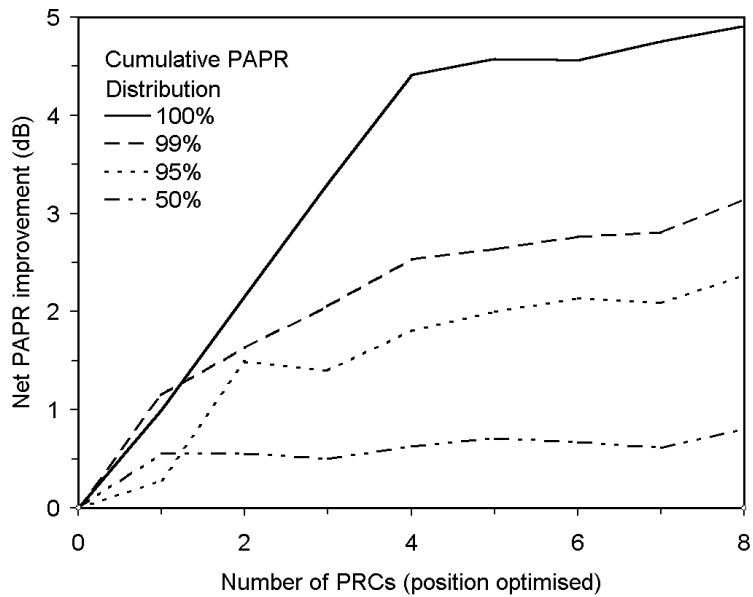


Figure 7-8, Net improvement in CF, position optimised PRCs (10 BPSK data subcarriers)

Overlapping of the spread PRCs in a multi-user OFDM system is more difficult as most of the PRCs will be bounded with data subcarriers. Thus simple overlapping may not be possible. This would be the case if the data and PRC are grouped. However if the subcarriers for each user are spread out, it might be possible to have spread out PRCs that overlap between the users, but still provide a large reduction in the CF.

The addition of 4 PRCs with 10 data subcarriers results in a large net gain of 4.5 dB, allowing more power to be transmitted. For a transmission with no PRCs at an error rate of 1×10^{-3} , adding the PRCs and maintaining the same peak power the error rate would be decreased to 1×10^{-7} .[117], [118] This is more efficient than adding simple error correcting bits at the same coding rate. For example Hamming coding at a rate of 4 parity bits for 11 data bits gives a gain of only 1.2 dB at a bit error rate of 1×10^{-4} which is significantly less than 4.5 dB.

Table 1 shows the number PRC positions tested, and the best combination found.

No. PRCs	Position tests simulated	Possible position combinations	Best Position Found, see fig. 4d for label method
1	11	11	1
2	66	66	2,3
3	286	286	3,4,6
4	262	1001	4,10,12,13
5	156	3003	1,3,7,10,15
6	68	8008	1,2,7,10,14,16
7	36	19448	1,2,7,9,11,14, 17
8	23	43758	1,2,3,4,11,12,16,18

Table 7-1, Optimised positions found for 10 BPSK data subcarriers

7.7 CONCLUSION

Adding peak reduction subcarriers can significantly improve the CF of an OFDM signal. The PRCs can result in a reduction of greater than 6 dB in the maximum CF and a net reduction of greater than 4.5 dB when the additional power for PRCs is taken into account. It was found that varying the amplitude as well as phase for the PRCs gave improved performance over just phase variation. It was also found that spreading the position of the PRCs resulted in a better performance than grouped PRCs. Adding more PRCs results in a lower CF, however the use of large numbers of PRCs is limited by the cost of additional transmission power, bandwidth and complexity limits.

CHAPTER 8 SUMMARY

8.1 FUTURE WORK

OFDM has a promising future for use in wireless LAN networks and for fixed and mobile communications. Its use is likely to be significantly increased over the next 10 years, due to its high spectral efficiency and flexibility in spectrum allocation and modulation. OFDM is mostly suited to low mobility high data rate networks, making it difficult to apply to mobile phone networks. At low user data rates, much of the adaptive techniques would not be suitable due to the high overhead of implementing such techniques. As a result, in multiuser applications at low data rates the overall efficiency of OFDM is much poorer with little advantage over CDMA techniques. Mobile networks of the future will shift away from low data rate voice applications to become primarily data terminals, striving for high data rates.

If OFDM is to be used in 4th generation mobile networks, a significant amount of research needs to be done in applying OFDM to cellular networks. Issues such as inter-cellular interference need to be studied, in the context of identifying the best frequency / time user allocation scheme. Ideally the networks should be self-organising in frequency reuse, and so an effective means of implementing this needs to be developed. Most current multiuser OFDM systems use TDMA as a method for providing multiple accesses. However the greatest performance gains can be made by jointly allocating users based on frequency and time. Due to the overlapping nature of subcarriers in OFDM signals, allocating users different subcarriers in the reverse link creates problems in maintaining subcarrier orthogonality. Each mobile user will have a different propagation delay and Doppler spread, making compensation for these factors in the reverse link a non-trivial problem. It is possible that the most robust schemes will use blocks of OFDM signals, which are band pass filtered to help separate signals from different users.

The effective use of adaptive modulation and adaptive user allocation will depend on the overhead required for implementation. Protocols need to be developed that will allow these techniques to be implemented efficiently. Research is needed to investigate the trade off between overhead and technique efficiency, so the optimal amount of overhead for each application can be established. Research is also needed for optimisation of the adaptive user allocation algorithm so as to satisfy the requirements of the different user in the system. This includes optimising so that the system throughput and quality of service is maximised. The optimisation will need to cope with variable and fixed data rate services. Additionally the effect of multi-cellular user allocation needs to be investigated.

Much of the development of effective allocation schemes will be dependent on improved modelling of wideband RF propagation. Much of the focus on propagation modelling has been on path loss modelling, statistical descriptions of fading, and discrete approximations of channel impulse using ray tracing. Ray tracing methods are improving rapidly, with much of the focus being on computation efficiency, and accurate prediction of path loss. Research needs to be done on wideband models that show the response of the radio channel with small changes in space, similar to the measurements presented in this thesis. These models need to be smooth in space to allow testing of multiuser user allocation schemes in terms of subcarrier SNR, the effects of Doppler spread, and propagation time. With accurate models it may be possible to develop a technique for predicting the channel response for a small time ahead, allowing adaptive techniques to cope with higher user mobility.

With the advent of OFDM, higher spectral efficiency modulation schemes (16-QAM, 64-QAM, etc) are now being used in terrestrial wireless networks. These modulation schemes are more susceptible to the effects of ISI caused by multipath propagation than previously used low spectral efficiency modulation schemes such as BPSK and QPSK. The use of OFDM helps to reduce the level of ISI by using a low symbol rate, and the use of a guard period. The guard period represents a significant time overhead and so should be minimised in length. The most suitable length depends on the multipath in the environment and the modulation scheme used. Traditionally the length of the required guard period has been estimated using the RMS delay spread of the propagation channel. This measurement is accurate for predicting the guard

period length required for BPSK and QPSK modulation schemes, but is inadequate for estimating the performance of high spectral efficiency modulation schemes. The estimated guard period length is too short for these modulation schemes, resulting in significant remaining ISI, resulting in degraded BER. The delay spread of indoor environments needs to be measured using a more appropriate multipath estimate than the RMS delay spread. Such a measurement might be, the delay spread over which a given percentage of the impulse energy arrives. For example if the length of the guard period matches the time over which 99.9% of the impulse energy arrives, then the ISI should only be 0.1%, resulting in an effective SNR of 30 dB, which is suitable for 64-QAM. A set of propagation experiments is needed using such a multipath measurement so the performance of OFDM systems using higher modulation schemes can more accurately be assessed.

This thesis presented the use of Access Point Repeaters as a method for low cost maximisation of signal strength in indoor environments. This technique could be extended to cellular networks as a method for controlling shape of cells, and for minimising shadowing within a cell. The effectiveness of using this technique in a cellular environment depends on the cost of installing extra base stations as compared with APRs, and with potential problems with combining APR with smart antenna technology. Research needs to be done to establish the amount of additional multipath created by using APRs, and the practical effectiveness of the technique.

Much work has been done on minimising the crest factor of data carrying OFDM signals. The high CF of OFDM signals requires a moderate power back off (6 - 9 dB) in the transmitting power amplifiers. However OFDM is very efficient in terms of the amount of power required for transmission, making this less significant. Most of the focus on minimisation techniques has been on minimising the worse case CF. However with sufficient data whitening the probability of very large CF symbols is so low that this is not a problem. Focus needs to be placed on CF minimisation techniques that will reduce the output power back off required. Currently published CF minimisation techniques only give minimal overall improvement, with most requiring large overheads in either complexity or throughput. The potential improvement for CF minimisation techniques is relatively small (2 – 4 dB) and so overhead in implementation must be small to justify its use.

8.2 CONCLUSION

This thesis has presented an investigation into the application of OFDM in multiuser systems, and has focused on techniques for improving the system spectral efficiency. Most current communication systems operate at a very low spectral efficiency, resulting in under utilisation of the radio spectrum. Future systems will have to improve the spectral efficiency to achieve the capacities required. This thesis has investigated techniques that exploit the flexibility of OFDM to maintain a maximum spectral efficiency, by matching the system parameters, such as subcarrier modulation and frequency, based on current conditions of the radio channel. The aim of this work is for the communication system to approach the maximum theoretical channel capacity given the constraints of the radio channel, transmitter power and quality of service. While many cellular systems are primarily limited by inter-cellular interference, this thesis has primarily focused on the performance of isolated communication networks. This work is thus appropriate for applications such as Wireless LAN systems, which tend to be partially shielded from interference by the outer walls of indoor environments.

With bi-directional communications, information from the receiver can be used to adaptively exploit the radio channel characteristics. The application of adaptive modulation was investigated and found to provide an effective means to mitigate the effects of fading. Adaptive modulation greatly decreases the BER, with it requiring 12 - 16 dB less SNR to achieve the same BER as compared with a fixed modulation system. In addition to this, it allows the data rate of the system to improve when the channel SNR is high. When using coherent QAM, every 3 dB improvement in SNR allows the spectral efficiency of the system to improve by 1 b/s/Hz. Implementation of adaptive modulation requires some information overhead as both the transmitter and receiver must know the modulation scheme currently being used on each subcarrier, and the subcarrier modulation must be updated to track the radio channel.

The required tracking rate for mobile systems employing adaptive modulation was found to be in the order of $0.05 - 0.1\lambda$, with the actual required rate depending on the required BER, the amount of link margin used in the modulation allocation, the delay in the allocation, and the subcarrier allocation scheme. This technique is suited to

pedestrian velocities as the overhead in modulation update becomes excessive at high velocities. In a mobile application at 5.2 GHz and at a velocity of 50 km/hr, a tracking rate of 2400 - 4800 Hz is required. This would result in an information overhead in the order of 5 - 10% for a system similar to HiperLAN2.

Adaptive User Allocation was presented as a method for optimising the subcarrier frequency allocation in multi-user applications. This technique exploits the variation in channel response between users, caused by frequency selective fading. This technique also reduces the effects of fading as users tend to be allocated strong subcarrier frequencies, with nulls in the frequency response of the channel being avoided. This technique can be used in conjunction with adaptive modulation, to provide an additional signal power gain of around 3 - 5 dB. This technique requires complete knowledge of the channel response to each user, and so implementation requires significant overheads, making this technique only suitable for relatively fixed wireless applications such as wireless LAN systems.

This thesis has also presented a method for maximising the signal strength within buildings, by using transmission repeaters. The implementation complexity and cost is low, as multiple repeaters are distributed from a single base station. This technique is similar to Single Frequency Networks used in DAB and DVB, except at a much smaller scale. This technique increases the multipath in most environments, but this is compensated for by the high multipath tolerance of OFDM. The performance of using Access Point Repeaters (APR) was measured by finding the reduction in path loss in a simulated WLAN system using a simple ray trace model. This was verified against direct measurement of the building that was simulated. It was found to decrease the path loss by 7 dB for a system with two APRs, and up to 20 dB for eight APRs.

In addition, two techniques were presented for reducing the Crest Factor (peak to average power ratio of the RF signal envelope) of OFDM signals.

The first technique is a phasing scheme for OFDM pilot symbols, which uses genetic algorithms to optimise the phase angle of each subcarrier to achieve very low CF waveforms. This technique achieves a lower CF than any previously published techniques, obtaining a CF as low as 0.65 dB, which is 2 dB lower than commonly

used techniques. These low CF symbols can be used for reference pilot symbols. The low CF of these symbols allows the average power to be boosted (up to 6 dB) while maintaining a peak power significantly lower than the data symbols. This boosted power reduces the noise in the channel equalisation, improving the system performance.

The second technique reduces the CF of data carrying symbols, by including additional subcarriers that are optimised in amplitude and phase to cancel out the peaks in the overall OFDM symbol. This was found to produce a net improvement of 4 dB to the worst-case symbol CF.

REFERENCES

UTMS AND THIRD GENERATION SYSTEMS

- [1] K. W. Richard, "UMTS overview", *IEE Electronics and Communication Engineering Journal*, Vol. 12, No. 3, June 2000, pp. 93 - 100
- [2] Ermanno Berruto, Giovanni Colombo, Pantelis Monogioudis, Antonella Napolitano, Kyriacos Sabatakakis, "Architectural Aspects for the Evolution of Mobile Communications Toward UMTS", *IEEE Journal on Selected Areas in Communications*, Vol. 15, No. 8, October 1997, pp. 1477 - 1487
- [3] Erik Dahlman, Björn Gudmundson, Mats Nilsson, Johan Sköld, "UMTS/IMT-2000 Based on Wideband CDMA", *IEEE Communications Magazine*, September 1998, pp. 70 - 80
- [4] Fumiyuki Adachi, Mamoru Sawahashi, Hirohito Suda, "Wideband DS-CDMA for Next-Generation Mobile Communications Systems", *IEEE Communications Magazine*, September 1998, pp. 56 - 69
- [5] Josef Huber, "3G Forum Leveraging Spectrum Capacity In Accordance with 3G Deployment", *3G Forum* 17th-18th April 2001, Washington D. C., Online: http://www.umts-forum.org/ipapers/Leveraging_Spectrum_Capacity.pdf
- [6] Douglas N. Knisely, Sarath Kumar, Subhasis Laha, Sanjiv Nanda, "Evolution of Wireless Data Services: IS-95 to cdma2000", *IEEE Communications Magazine*, October 1998, pp. 140 - 149
- [7] "Third Generation Mobile Phone Licensing in Europe", *TIA on line*, Online: <http://www.tiaonline.org/international/regional/nis/licensing.cfm>, October 2000.
- [8] "Auction of Third Generation Mobile Telecommunications Licences in the UK, Frequently Asked Questions", *Radiocommunications Agency of UK*, Online: <http://www.spectrumauctions.gov.uk/documents/faq2.htm>

-
- [9] “Spectrum Auctions”, Radiocommunications Agency of UK, Online: http://www.spectrumauctions.gov.uk/auction/auction_index.htm
 - [10] S. Dehghan, D. Lister, R. Owen, P. Jones, “W-CDMA capacity and planning issues”, *IEE Electronics and Communications Engineering Journal*, Vol. 12, No. 3, June 2000, pp. 101 - 118
 - [11] Sanjiv Nanda, Krishna Balachandran, and Sarath Kumar, “Adaptation Techniques in Wireless Packet Data Services”, *IEEE Communications Magazine*, January 2000, pp. 54 - 64

4TH GENERATION SYSTEMS

- [12] Terje Tjelta, Agne Nordbotten, Marco Annoni, Enrico Scarrone, Simone Bizzarri, Laurissa Tokarchuk, John Bigham, Chris Adams, Ken Craig, Manuel Dinis, “Future Broadband Radio Access Systems for Integrated Services with Flexible Resource Management”, *IEEE Communications Magazine*, August 2001, pp. 56 - 63
- [13] NTT DoCoMo Advertisement, “The Path to 4G Mobile”, *IEEE Communications Magazine*, March 2000, pp. 38 - 41

DIGITAL VIDEO BROADCASTING

- [14] “Digital Video Broadcasting”, ETSI, Online: <http://www.etsi.org/broadcast/dvb.htm>, October 2000
- [15] “A Guideline for the use of DVB specifications and standards”, DVB Blue Book A20, pp. 9, Online: www.dvb.org/news/pdf/dvb_cook.pdf
- [16] ETSI EN 300 421, “Framing Structure, channel coding and modulation for 11/12 GHz satellite services”, August 1997, pp. 6, Online: <http://www.etsi.org>
- [17] Ulrich Reimers, “Digital Video Broadcasting”, *IEEE Communications Magazine*, June 1998, pp. 104 - 110
- [18] ETSI ETS 300 744, “Framing Structure, Channel Coding and Modulation for Digital Terrestrial Television”, March 1997, Online: <http://www.etsi.org>

DIGITAL AUDIO BROADCASTING

- [19] Louis Thibault, Minh Thien Le, “Performance Evaluation of COFDM for Digital Audio Broadcasting Part I: Parametric Study”, *IEEE Transactions on Broadcasting*, Vol. 43, No.1, March 1997, pp. 64 – 75

- [20] “Digital Audio Broadcasting - Overview and Summary of the DAB System”, *World DAB Forum*,
Online: http://www.worlddab.org/public_documents/eureka_brochure.pdf
- [21] ETSI EN 300 401, “Radio Broadcasting Systems; Digital Audio Broadcasting (DAB) to mobile, portable and fixed receivers”, May 2001, Online: <http://www.etsi.org>

GSM NETWORKS

- [22] Michel Mouly, Marie-Bernadette Pautet, “The GSM System for Mobile Communications”, *M. Mouly et Marie-B. Pautet*, France, 1992, ISBN: 2-9507190-0-7
- [23] Siegmund Redl, Matthias Weber, Malcom Oliphant, “GSM and Personal Communications Handbook”, *Artech House Publishers*, Norwood, 1998, ISBN: 0 89006-957-3
- [24] Telstra, “Flexi-Plans”,
Online: <http://www.telstra.com.au/mobilenet/flexipln/dflex.cfm>, November 2001
- [25] Optus, “Rate Plans”, Online: <http://optusdirect.optus.com.au/shop/rateplans>, November 2001

CDMA OVERVIEW

- [26] William C. Y. Lee, “Overview of Cellular CDMA”, *IEEE Transactions on Vehicular Technology*, Vol. 40, No. 2, May 1991, pp. 291 - 302
- [27] Ryuji Kohno, Reuven Meidan and Laurence B. Milstein, “Spread Spectrum Access Methods for Wireless Communications”, *IEEE Communications Magazine*, January 1995, pp. 58 - 67

OFDM

- [28] Yiyan Wu, William Y. Zou, “Orthogonal Frequency Division Multiplexing: A Multi-Carrier Modulation Scheme”, *IEEE Transaction on Consumer Electronics*, Vol. 41, No. 3, August 1995, pp. 392 - 399
- [29] William Y. Zou, Yiyan Wu, “COFDM: An Overview”, *IEEE Transactions on Broadcasting*, Vol. 41, No. 1, March 1995, pp. 1 - 8
- [30] R. R. Mosier and R. G. Clabaugh, “Kineplex, a bandwidth-efficient binary transmission system”, *AIEE Transactions*, Vol. 76, January 1958, pp. 723 - 728

-
- [31] Robert Chang, “Synthesis of Band-Limited Orthogonal Signals for Multichannel Data Transmission”, *The Bell System Technical Journal*, December 1966, pp. 1775 - 1796
 - [32] Robert Chang, “Orthogonal frequency division multiplexing”, US. Patent 3,488,445, filed November 14, 1966, issued January 6, 1970
 - [33] S. B. Weinstein, Paul M. Ebert, “Data Transmission by Frequency-Division Multiplexing Using the Discrete Fourier Transform”, *IEEE Transactions on Communication Technology*, Vol. COM-19, No. 5, October 1971, pp. 628 - 634
 - [34] Carl Magnus Frodigh, Perols Leif Mikael Gudmundson, “Adaptive channel allocation in a frequency division multiplexed system”, US. Patent 5,726,978, Filed: June 22, 1995, Issued: March 10, 1998

SYNCHRONISATION FOR OFDM

- [35] J. Beek, M. Sandell, P. Borjesson, “ML Estimation of Time and Frequency Offset in OFDM Systems”, *IEEE Transactions on Signal Processing*, Vol. 45, No. 7, July 1997, pp. 1800 - 1805
- [36] P. Moose, “A Technique for Orthogonal Frequency Division Multiplexing Frequency Offset Correction”, *IEEE Transactions on Communications*, Vol. 42, No. 10, October 1994, pp. 2908 - 2914
- [37] L. Wei, C. Schlegel, “Synchronization Requirements for Multi-user OFDM on Satellite Mobile and Two-path Rayleigh Fading Channels”, *IEEE Transactions on Communications*, Vol. 43, No. 2/3/4, February/March/April 1995, pp. 887 - 895
- [38] Meng-Han Hsieh, Che-Ho Wei, “Channel Estimation for OFDM systems based on Comb-Type Pilot Arrangement in Frequency Selective Fading Channels”, *IEEE Transactions on Consumer Electronics*, Vol. 44, No. 1, February 1998, pp. 217 - 225
- [39] Ye Li, Nambirajan Seshadri, Sirikiat Ariyavitsakul, “Channel Estimation for OFDM Systems with Transmitter Diversity in Mobile Wireless Channels”, *IEEE Journal on Selected Area in Communications*, Vol. 17, No. 3, March 1999, pp. 461 - 471
- [40] Marco Luise, Ruggero Reggiannini, “Carrier Frequency Acquisition and Tracking of OFDM Systems”, *IEEE Transactions on Communications*, Vol. 44, No. 11, November 1996

-
- [41] Y. H. Ng, P. M. Grant, R. A. Stirling-Gallacher, "Carrier tracking techniques for OFDM signal transmissions", *Electronic Letters*, Vol. 32, No. 22, 24th October 1996, pp. 2047 - 2048
 - [42] T. M. Schmidl, D. C. Cox, "Blind synchronization for OFDM", *Electronic Letters*, Vol. 33, No. 2, 16th January 1997, pp. 113-114
 - [43] Uwe Lambrette, Michael Speth, Heinrich Meyr, "OFDM Burst Frequency Synchronisation by Single Carrier Training Data", *IEEE Communication Letters*, Vol. 1, No. 2, March 1997
 - [44] Jean Armstrong, "Analysis of New and Existing Methods of Reducing Intercarrier Interference Due to Carrier Frequency Offset in OFDM", *IEEE Transactions on Communications*, Vol. 47, No. 3, March 1999, pp. 365 - 369
 - [45] Hui Liu Ufuk Tureli, "A High-Efficiency Carrier Estimator for OFDM Communications", *IEEE Communications Letters*, Vol. 2, No. 4, pp. 104 - 106
 - [46] M. J. Fernández-Getino, S. Zazo, J. M. Páez-Borrallo, "Pilot patterns for channel estimation in OFDM", *Electronic Letters*, Vol. 36, No. 12, 8th June 2000, pp. 1049
 - [47] William Warner, Cyril Leung, "OFDM/FM Frame Synchronization for Mobile Radio Data Communication", *IEEE Transactions on Vehicular Technology*, Vol. 42, No. 3, August 1993, pp. 302 - 313
 - [48] J. Ahn, H. S. Lee, "Frequency Domain Equalisation of OFDM signals over Frequency Nonselective Rayleigh Fading Channel", *Electronics Letters*, Vol. 29, No. 16, 5th August 1993, pp. 1476 - 1477
 - [49] Marco Luise, Ruggero Reggiannini, Giorgio Vitetta, "Blind Equalization/Detection for OFDM Signals over Frequency-Selective Channels", *IEEE Journal on Selected Areas in Communications*, Vol. 16, No. 8, October 1998, pp. 1568 - 1577
 - [50] Donghoon Lee, Kyungwhoon Cheun, "A New Symbol Timing Recovery Algorithm for OFDM systems", *IEEE Transactions on Consumer Electronics*, Vol. 43, No. 3, pp. 767 - 775
 - [51] Ufuk Tureli, Didem Kivanc, Hui Liu, "Experimental and Analytical Studies on a High-Resolution OFDM Carrier Frequency Offset Estimator", *IEEE Transactions on Vehicular Technology*, Vol. 50, No. 2, March 2001, pp. 629 – 643

-
- [52] Yang-Seok Choi, Peter J. Voltz, Frank A. Cassara, “ML Esimation of Carrier Frequency Offset for Multicarrier Signals in Rayleigh Fading Channels”, *IEEE Transactions on Vehicular Technology*, Vol. 50, No. 2, March 2001, pp. 644-655

INFORMATION THEORY

- [53] C. E. Shannon, “A Mathematical Theory of Communication”, 1949, Online: <http://www.math.psu.edu/gunesch/Entropy/shannon.ps>

EFFECT OF DISTORTION ON OFDM

- [54] Minh T. Le, Louis Thibault, “Performance Evaluation of COFDM for Digital Audio Broadcasting Part II: Effects of HPA Nonlinearities”, *IEEE Transactions on Broadcasting*, Vol. 44, No. 2, June 1998, pp. 165 - 171
- [55] S. Merchán, A. García Armada, J. L. García, “OFDM Performance in Amplifier Nonlinearity”, *IEEE Transactions on Broadcasting*, Vol. 44, No. 1, March 1998, pp. 106 - 113
- [56] Qun Shi, “OFDM in Bandpass Nonlinearity”, *IEEE Transactions on Consumer Electronics*, Vol. 42, No. 3, August 1996, pp. 253 - 258
- [57] Maria-Gabriella Di Benedetto, Paolo Mandarini, “An Application of MMSE Predistortion to OFDM Systems”, *IEEE Transactions on Communications*, Vol. 44, No. 11, November 1996, pp. 1417 - 1420
- [58] Hyun Woo Kang, Yong Soo Cho, Dae Hee Youn, “On Compensating Nonlinear Distortions of an OFDM System Using an Efficient Adaptive Predistorter”, *IEEE Transactions on Communications*, Vol. 47, No. 4, April 1999, pp. 522 - 526
- [59] Won Gi Jeon, Kyung Hi Chang, Yong Soo Cho, “An Adaptive Data Predistorter for Compensation of Nonlinear Distortion in OFDM Systems”, *IEEE Transactions on Communications*, Vol. 45, No. 10, October 1997, pp. 1167 - 1171
- [60] James K. Cavers, “Amplifier Linearization Using a Digital Predistorter with Fast Adaption and Low Memory Requirements”, *IEEE Transactions on Vehicular Technology*, Vol. 39, No. 4, November 1990, pp. 374 - 382
- [61] Sante Andreoli, Howard G. McClure, Paolo Banelli, Saverio Cacopardi, “Digital Linearizer for RF Amplifiers”, *IEEE Transactions on Broadcasting*, Vol. 43, No. 1, March 1997, pp. 12 - 19

RADIO PROPAGATION

- [62] Fechtel, Stefan A., "A Novel Approach to Modelling and Efficient Simulation of Frequency-Selective Fading Radio Channels", *IEEE Journal on Selected in Communications*, Vol. 11, April 1993, pp. 422 - 431
- [63] Andersen Jørgen, Rappaport Theodore S., Yoshida Susumu, "Propagation Measurements and Models for Wireless Communications Channels", *IEEE Communications Magazine*, January 1995, pp. 42 - 49
- [64] Durgin Greg, Rappaport Theodore S., Xu Hao, "5.85 GHz Radio Path Loss and Penetration Loss Measurements In and Around Homes and Trees", *IEEE Communications Letters*, Vol. 2, No. 3, March 1998, pp. 70 - 72
- [65] Talbi L., "Effect of frequency carrier on indoor propagation channel", *Electronic Letters*, Vol. 36, No. 15, 20th July 2000, pp. 1309 - 1310
- [66] Takeshi Manabe, Yuko Miura, Toshio Ihara, "Effects of Antenna Directivity and Polarization on Indoor Multipath Propagation Characteristics at 60 GHz", *IEEE Journal on Selected Areas in Communications*, Vol. 14, No. 3, April 1996, pp. 441 - 447
- [67] Larbi Talbi, Gilles Y. Delisle, "Experimental Characterisation of EHF Multipath Indoor Radio Channels", *IEEE Journal on Selected Areas in Communications*, Vol. 14, No. 3, April 1996
- [68] McDonnel J.T.E, Spiller T.P., Wilkinson T.A., "RMS delay spread in indoor LOS environments at 5.2 GHz", *Electronic Letters*, Vol. 34, No. 11, 28th May 1998, pp. 1149 - 1150
- [69] Seong-Cheol Kim, Henry L. Bertoni, Miklos Stern, "Pulse Propagation Characteristics at 2.4 GHz Inside Buildings", *IEEE Transactions on Vehicular Technology*, Vol. 45, No. 3., August 1996, pp. 579 - 592
- [70] Donald C. Cox, Robert P. Leck, "Correlation Bandwidth and Delay Spread Multipath Propagation Statistics for 910 MHz Urban Mobile Radio Channels", *IEEE Transactions on Communications*, Vol. COM-23, No. 11, November 1975, pp. 1271 - 1280

-
- [71] Donald C. Cox, Robert P. Leck, "Distributions of Multipath Delay Spread and Average Excess Delay for 910-MHz Urban Mobile Radio Paths", *IEEE Transactions on Antennas and Propagations*, Vol. AP-23, No. 2, March 1975, pp. 206 - 213
- [72] Donald C. Cox, "Delay Doppler characteristics of multipath propagation at 910 MHz in a suburban mobile radio environment", *IEEE Transactions on Antennas and Propagation*, Vol. AP-20, September 1972
- [73] Homayoun Hashemi, David Tholl, "Statistical Modelling and Simulation of the RMS Delay Spread of Indoor Radio Propagation Channels", *IEEE Transactions of Vehicular Technology*, Vol. 43, No. 1 February, 1994, pp. 110 - 119
- [74] Robert J. C. Bultitude, Samy A. Mahmoud, William A. Sullivan, "A Comparison of Indoor Radio Propagation Characteristics at 910 MHz and 1.75 GHz", *IEEE Journal on Selected Areas in Communications*, Vol. 7, No. 1, January 1989, pp. 20 - 39
- [75] S. Y. Seidel and T. S. Rappaport, "914 MHz path loss prediction models for indoor communications in multifloored buildings", *IEEE Transactions on Antennas and Propagation*, Vol. 40, No. 2, February 1992, pp. 207 - 217
- [76] Laura Dossi, Guido Tartara, Fiorenzo Tallone, "Statistical Analysis of Measured Impulse Response Functions of 2.0 GHz Indoor Radio Channels", *IEEE Journal on Selected Areas in Communications*, Vol. 14, No. 3, April 1996, pp. 405 - 410
- [77] Theodore S. Rappaport, Scott Y. Seidel, Rajendra Singh, "900-MHz Multipath Propagation Measurements for U.S. Digital Cellular Radiotelephone", *IEEE Transactions on Vehicular Technology*, Vol. 39, No. 2, May 1990, pp. 132 - 139
- [78] Elvino S. Sousa, Vladan M. Jovanoviæ Christian Daigneault, "Delay Spread Measurements for the Digital Cellular Channel in Toronto", *IEEE Transactions on Vehicular Technology*, Vol. 43, No. 4, November 1994, pp. 837 - 847
- [79] Robert J. C. Bultitude, G. Keith Bedal, "Propagation Characteristics on Microcellular Urban mobile Radio Channels at 910 MHz", *IEEE Journal on Selected Areas in Communications*, Vol. 7, No. 1, January 1989, pp. 31 - 39

MULTIUSER OFDM

- [80] "Overcoming Multipath in Non-Line-of-Sight High-Speed Microwave Communications Links", Cisco Systems, Online:
http://www.cisco.com/warp/public/cc/pd/witc/wt2700/mulpt_wp.htm

-
- [81] M. Fattouche, "Method and Apparatus for Multiple Access between Transceivers in Wireless Communications using OFDM spread spectrum", U.S. Patent 5,282,222, Filed Mar. 31, 1992, Issued Jan. 25, 1994
- [82] T. Williams, R. Prodan, "Multiple User Access Method Using OFDM", U. S. Patent 5,815,488, Filed Sep. 28, 1995, Issued Sep. 29, 1998
- [83] L. Cimini, J. Chuang, N. Sollenberger, "Advanced Cellular Internet Service (ACIS)", *IEEE Communications Magazine*, Oct. 1998, pp. 150 - 159
- [84] M. Wahlqvist, C. Östberg, J. Beek, O. Edfors, P. Börjesson, "A Conceptual Study of OFDM-based Multiple Acess Schemes", Technical Report Tdoc 117/96, ETSI STC SMG2 meeting no 18, Helsinki, Finland, May 1996, Online: <http://www.sm.luth.se/csee/sp/publications>
- [85] L. Wei, C. Schlegel, " Synchronization Requirements for multi-user OFDM on Satellite Mobile and Two-path Rayleigh Fading Channels", *IEEE Transaction on Communications*, Vol. 43, No. 2/3/4, February/ March/ April 1995, pp. 887-895

ASDL TECHNOLOGY

- [86] Z. Papir, A. Simmonds, "Competing for Throughput in Local Loop", *IEEE Communications Magazine*, May 1999, pp. 61 - 66
- [87] M. Barton, L. Chang, T. R. Hsing, "Performance Study of High-Speed Asymmetric Digital Subscriber Lines Technology", *IEEE Transactions on Communications*, Vol. 44, No. 2, Feb 1996, pp. 156 - 157
- [88] J. Chow, J. C. Tu, J. M. Cioffi, "A Discrete Multitone Transceiver System for HDSL Applications", *IEEE Journal on Selected Areas in Communications*, Vol. 9, No. 6, Aug 1991

NETWORK DATA TRAFFIC

- [89] W. E. Leland, M. S. Taqqu, W. Willinger, and D. V. Wilson, "On the Self-Similar Nature of Ethernal Traffic", *IEEE Transactions on Networking*, Vol. 2, No. 1, February 1994, pp. 1 - 15

ADAPTIVE MODULATION

- [90] K. J. Hole, G. E. Øien, "Spectral Efficiency of Adaptive Coded Modulation in Urban Microcellular Networks", *IEEE Transactions on Vehicular Technology*, Vol. 50, No. 1, pp. 205 - 222.

- [91] M. C. Aguayo-Torres, J. T. Entrambasaguas, F. Ruiz, "Variable rate multitone system for multipath fading channels", *Electronic Letters*, 11th Jun 1998, Vol. 34, No. 12, pp. 1203 - 1204
- [92] Nilo C. Ericsson, Sorour Falahati, Anders Ahlén, and Arne Svensson, "Hybrid type-II ARQ/AMS supported by Channel Predictive Scheduling in a Multi-User Scenario", *IEEE Vehicular Technology Conference – VTC'00-Fall*, Boston, MA, USA, September 24-28, 2000, pp. 1804 - 1811
Online: <http://www.signal.uu.se/Publications/abstracts/c0015.html>
- [93] Mohamed-Slim Alouini, "Adaptive and Diversity Techniques for Wireless Digital Communications over Fading Channels", *Ph.D Thesis, Department of Electrical Engineering, California Institute of Technology*, Pasadena, California, June 1998.
Online: http://systems.stanford.edu/Publications/Alouini/alouini_phd.ps
- [94] Cheong Yui Wong, Roger S. Cheng, Khaled Ben Letaief, Ross D. Murch, "Multiuser OFDM with Adaptive Subcarrier, Bit, and Power Allocation", *IEEE Journal on Selected Areas in Communications*, Vol. 17, No. 10, October 1999, pp. 1747-1757
- [95] BeamReach Networks, "BeamReach's Adaptive MultiBeam OFDM Technology",
Online: http://www.beamreachnetworks.com/brn/technology/tech_descr.html

HIPERLAN2 AND WLAN SYSTEMS

- [96] B. Crow, I. Widjaja, J. G. Kim, P. Sakai, "IEEE 802.11 Wireless Local Area Networks", *IEEE Communications Magazine*, pp 116 - 126, September 1997
- [97] M. Johnsson, "HiperLAN/2 – The Broadband Radio Transmission Technology Operating in the 5 GHz Frequency Band",
Online: <http://www.hiperlan2.com/site/specific/specmain/specwh.htm>, 1999
- [98] ETSI, "Hiperlan/2-Technical Overview",
Online: <http://www.etsi.org/technicalactiv/Hiperlan/hiperlan2tech.htm>
- [99] ETSI TS 101 475 V1.1.1, "Broadband Radio Access Networks (BRAN); HIPERLAN Type 2; Physical (PHY) layer", April 2000, Online: <http://www.etsi.org>
- [100] "Part 11: Wireless LAN Medium Access Control (MAC) and Physical Layer (PHY) specifications: High-speed Physical Layer in the 5 GHZ Band", *IEEE Std 802.11a-1999*, September 1999

-
- [101] C. Lim, A. Nirmalathas, D. Novak, "Dynamic Range Of A Multi-Section Laser In A Millimetre-Wave Fibre-Wireless Uplink", *Proc. Asia Pacific Microwave Conference 2000*, Sydney, Australia, December 2000
- [102] U. Grob, A. L. Welti, E. Zollinger, R. Küng, H. Kaufmann, "Microcellular Direct-Sequence Spread-Spectrum Radio System Using NPath RAKE Receiver", *IEEE Journal on Selected Areas in Communications*, Vol. 8, No. 5, pp. 772 - 779, June 1990
- [103] Intersil, (May, 2000), Direct Sequence Spread Spectrum Baseband Processor with Rake receiver and Equalizer, HFA3863 Data sheet,
Online: <http://www.intersil.com/data/FN/FN4/FN4856/FN4856.pdf>

PHASING SCHEMES FOR LOW CREST FACTOR MULTITONE SIGNALS

- [104] S. Boyd, "Multitone signals with low crest factor", *IEEE Transactions on Circuits and Systems*, vol. CAS-33, pp. 1018 - 1022, Oct. 1986
- [105] D. J. Newmann, "An L1 extremal problem for polynomials," *Proc. Amer. Math. Soc.*, vol. 16, pp. 1287-1290, Dec. 1965
- [106] S. Narahashi, T. Nojima, "New phaseing scheme of N-multiple carriers for reducing peak-to-average power ratio", *Electronic Letters*, Vol. 30, No. 17, pp. 1382 - 1383, Aug. 1994
- [107] S. Narahashi, K. Kumagai and T. Nojima, "Minimising peak to average power ratio of multitone signals using steepest descent method", *Electronic Letters*, Vol. 31, No. 18, 31st August 1995, pp. 1552 - 1554

CREST FACTOR MINIMISATION OF OFDM DATA SYMBOLS

- [108] R.W. Bauml, R.F.H. Fischer, J.B. Huber, "Reducing the peak-to-average power ratio of multicarrier modulation by selected mapping", *Electronic Letters*, 1996, Vol. 32, pp. 2056 - 2057
- [109] Eetvelt J.Van, G. Wade, M. Tomlinson, "Peak to average power reduction for OFDM schemes by selective scrambling", *Electronic Letters*, 1996, Vol. 32, pp. 1963 - 1964
- [110] D. Wulich, 'Reduction of peak to mean ratio of multicarrier modulation using cyclic coding", *Electronic Letters*, 1996, Vol. 32, pp. 432 - 433
- [111] C. Tellambura, "Use of m-sequences for OFDM peak-to-average power ratio

reduction”, *Electronic Letters*, 1997, Vol. 33, pp. 1300 - 1301

[112] C. Tellambura, “Phase optimisation criterion for reducing peak-to-average power ratio in OFDM”, *Electronic Letters*, 1998, Vol. 34, pp. 169 - 170

[113] J.A. Davis, J. Jedwab, “Peak-to-mean power control and error correction for OFDM transmission using Golay sequences and Reed-Muller codes”, *Electronic Letters*, 1997, Vol. 33, pp. 267 - 268

APPLICATION OF GENETIC ALGORITHMS

[114] Moshe Sipper, Edmund M. A. Ronald, “A new species of hardware”, *IEEE Spectrum*, Vol. 37, No. 3, March 2000, pp. 59 - 64

[115] “The Genetic Algorithms Archive”, Navy Center for Applied Research in Artificial Intelligence, March 2001, Online: <http://www.aic.nrl.navy.mil/galist>

[116] “The Hitch-Hiker’s Guide to Evolutionary Computation”, Online:
<ftp://ftp.cerias.purdue.edu/pub/doc/EC/Welcome.html> or
<ftp://ftp.cs.wayne.edu/pub/EC/Welcome.html>

GENERAL COMMUNICATION TEXTBOOKS

[117] Gordon L. Stüber, “Principles of Mobile Communication”, Kluwer Academic Publishers, 1996, pp. 225 - 238

[118] B. Sklar, “Digital Communications Fundamentals and Applications”, *Prentice Hall*, 1988, pp. 300

[119] J. Gibson, “The Mobile Communications Handbook”, *CRC Press*, 1996, pp. 355 - 369

[120] Emmanuel C. Ifeachor, Barrie W. Jervis, “Digital Signal Processing, A Practical Approach”, Addison-Wesley, 1993, ISBN: 0-201-54413-X

[121] Martin S. Roden, “Analog and Digital Communication Systems”, *Prentice-Hall International, Inc*, 4th Edition, 1996, ISBN: 0-13-399965-3

[122] B. P. Lathi, “Modern Digital and Analog Communication Systems”, *CBS College Publishing*, 1983, ISBN: 0-03-058969-X

[123] Yoshihiko Akaiwa, “Introduction to Digital Mobile Communication”, *John Wiley & Sons, Inc*, 1997, ISBN: 0-471-17545-5

PUBLICATIONS RESULTING FROM THIS PHD

Eric Lawrey, Cornelis J. Kikkert, "Adaptive Frequency Hopping for Multiuser OFDM", *Second International Conference on Information, Communications and Signal Processing, ICICS'99*, Singapore, Dec 7-10, 1999, Proceedings: paper number 361, Publisher NTU, <http://www.ntu.edu.sg/eee/conferences/icics/icics.html>.

Eric Lawrey, Cornelis J. Kikkert, "Peak to average power ratio reduction of OFDM signals using peak reduction carriers", *Fifth International Symposium on Signal Processing and its Applications, ISSPA99*, Brisbane, Aug. 1999, pp. 737-740.

Eric Lawrey, "Multiuser OFDM", *Fifth International Symposium on Signal Processing and its Applications, ISSPA99*, Brisbane, Aug. 1999, pp. 761-764.

Eric Lawrey, Cornelis J. Kikkert, "Maximising Signal Strength inside Buildings for wireless LAN Systems using OFDM", *Asia Pacific Microwave Conference, APMC 2000*, Sydney, Dec 3-6, 2000, pp. 257-260

Eric Lawrey, Cornelis J. Kikkert, "Maximising Signal Strength for OFDM inside buildings", *IEEE Transactions on Microwave Theory and Techniques*, November 2001, Special Mini-issue from APMC 2000

A copy of these papers is attached to the end of this thesis.

APPENDIX A WINDOW FUNCTIONS

Window functions are used for frequency analysis and for designing FIR filters. For spectral analysis the time waveform is usually multiplied by a window function to reduce the effects of spectral spreading. Spectral analysis is normally performed using a Fast Fourier Transform (FFT). This calculates the frequency response of the cyclic extension of the time waveform. As a consequence if the time waveform is non-cyclic it results in a transient between the end of the time waveform and the start, resulting in spectral spreading. Applying a window function tapers the start and ends of waveform reducing these transients, and consequently spectral spreading.

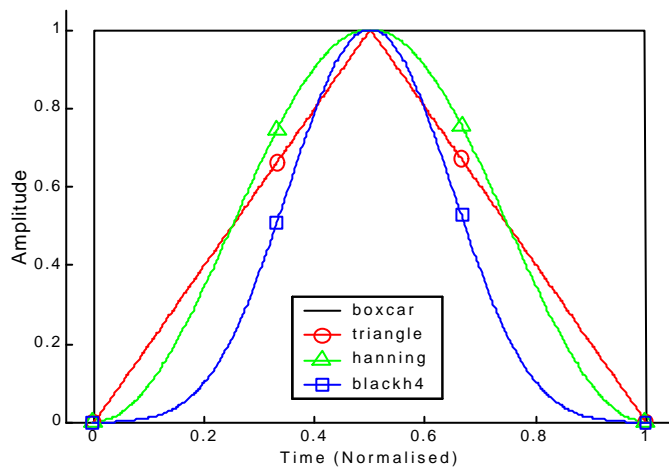


Figure A - 1, Time waveform for several common window functions.

(Blackh4 = 4 term Blackman Harris) (script s0072)

The power spectrum of a discrete time waveform $s(t)$, can be estimated using the following:

$$P(s) = 20\log_{10}(|\text{FFT}(s(t) \cdot w(t))|) - 20\log_{10}\left(\frac{N}{2}\right) + W_L$$

Where $w(t)$ is the window function being used, W_L is the window loss of the window function, N is the number of samples in $s(t)$, and $P(s)$ is the power spectrum in dB. N is also usually the length of the FFT. $|x|$ is the magnitude of the complex value x .

Figure A - 2 shows the application of window functions for spectral estimation. The spectrum shown is for a four-tone signal with a large variation in tone power. Figure A - 2 (a) shows the result for a boxcar window function. This is the same as having no window function at all. This spectral spreading in this result masks all but the strongest tone. Figure A - 2 (b) shows the result when using a Hanning window function. This allows for three of the tones to be seen clearly. The Blackman Harris window function allows the fourth tone to be just seen at a frequency of 0.25, however it is too close to the strong tone at a frequency of 0.2, to allow accurate estimation. Figure A - 2 (d) shows the estimation with the new presented Lawrey6 window function. Details of the implementation of this window function are shown in section A.4. The side-lobes of the window function are sufficiently low to allow all four tones to be easily distinguished. One other thing that can be seen is that the width of the main lobe of the tone becomes wider as the side-lobe power is reduced.

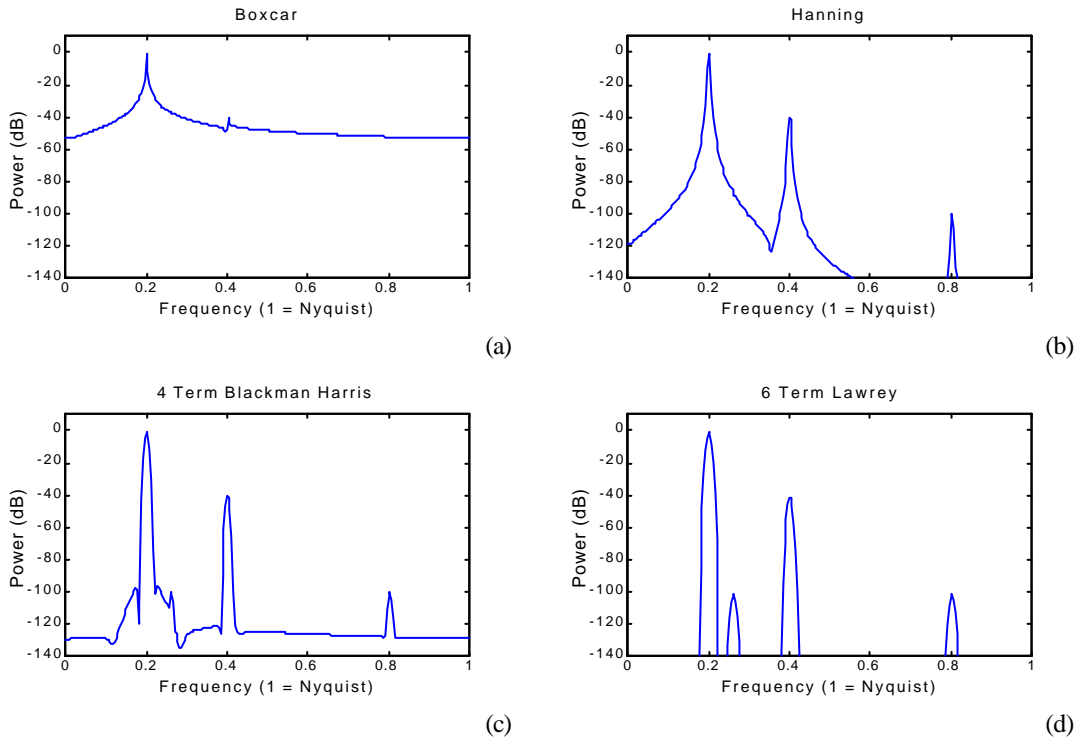


Figure A - 2, Power spectra of a 4 tone signal with power levels varying up to 100 dB. (script s0074)

A.1 WINDOW FUNCTION TRANSITION WIDTH AND SIDE-LOBE POWER

The performance of a window function is determined largely by two main parameters. These are the side-lobe power and the transition width of the window function. The transition width of a window function is measured by taking the magnitude of the Fourier transform of the time waveform of the window function. It is a measure of how fast the window function rolls off from DC to the first null. Figure A - 3 shows the spectrum of the Boxcar and Hanning window functions. The transition width for the Boxcar window function is 1.0 as the first null in the frequency response corresponds to a frequency that is the inverse of the symbol time. The Hanning window function has a transition width very close to 2.0.

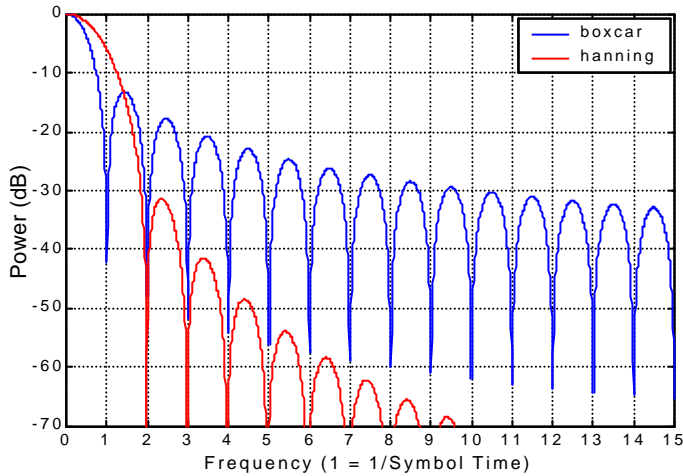


Figure A - 3, Spectrum of Boxcar and Hanning window functions. (script s0076)

There is a strict trade off between side-lobe power and the transition width of a window function. Decreasing the side-lobe power increases the transition width, thus using a window function with low side-lobe power for spectral analysis results in a lower frequency resolution. Figure A - 4 shows the side-lobe power for a number of window functions, as a function of the transition width. The Kaiser window function incorporates a side-lobe power control parameter, allowing a trade off between side-lobe power and transition width. See [120] for more details on the Kaiser window function.

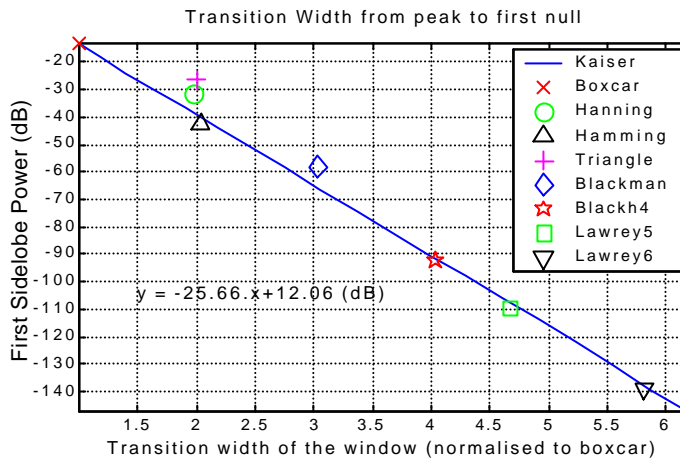


Figure A - 4, Transition width for a number of window functions, as a function of the side-lobe power. (script s0039)

Table A - 1 shows the transition width and side-lobe power for a variety of window functions. This is the performance that would be seen when using the window functions for spectral analysis.

Window Function	Transition width of window function DC to first Null (normalised to 1/symbol time) (W _T)	Maximum Side-Lobe Power for window function (dBc)
Boxcar	1.00	-13.3
Hanning	2.00	-31.5
Hamming	2.00	-42.6
Triangle	2.00	-26.5
Blackman	3.03	-58.1
4 term Blackman Harris	4.03	-92.0
5 term Lawrey	4.67	-109.9
6 term Lawrey	5.81	-139.1

Table A - 1, Transition width and side-lobe power of different window functions. (script s0039)

A.2 WINDOW FUNCTION PERFORMANCE WHEN USED FOR FIR FILTERS

Window functions can be used to design FIR filters. This is achieved by taking the inverse fourier transform of the required frequency response to find the time domain impulse response of the filter. This impulse response is the coefficients of the FIR design. If we take for example an ideal brick-wall low pass filter, the impulse

response corresponds to a *sinc* function. The *sinc* function is however infinite in length, and so truncation is required for implementation of the filter. However, this truncation results in spectral spreading. Windowing the truncated impulse response reduces the spectral spreading at the cost of broadening the transition width of the filter. For a more detail description of the window method for FIR filter design refer to [120].

Window Function	(b) Maximum Side-lobe Power, for FIR filter using window method (dBc)
Boxcar	-20.9
Hanning	-43.9
Hamming	-54.2
Triangle	-26.2
Blackman	-78.3
4 term Blackman Harris	-109.2
5 term Lawrey	-127.7
6 term Lawrey	-160.9

Table A - 2, Side-lobe power of different window functions when used with the window method of FIR filter design. (script s0071)

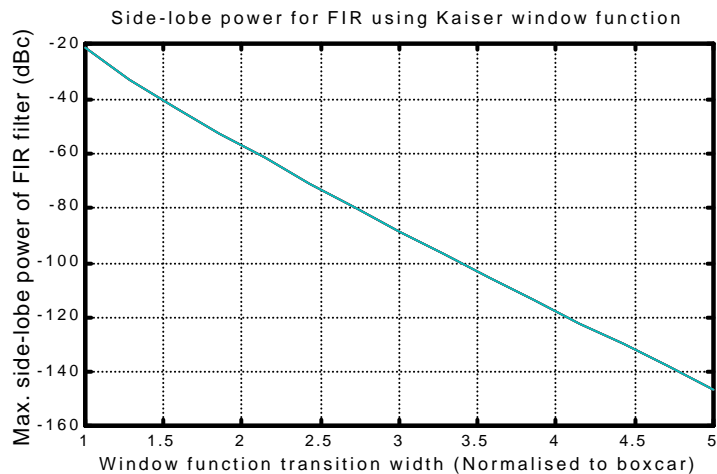


Figure A - 5, Side-lobe power for Kaiser window function when used with the window method of FIR filter design. (script s0071)

The x-axis is normalised to the transition width of the window function by itself, the same as used in Figure A - 4.

When a window function is used for FIR filter design the out of band attenuation is greater than the side-lobe power of just the window function itself. Table A - 2 shows the maximum side-lobe power for FIR filters designed using the window method for a range of window functions. Table A - 3 shows the transition width of

each of the window functions when used with the window method for FIR filter design. The transition width has been normalised to the number of taps in the filter. The transition width of an FIR filter will be approximately:

$$f_t = \frac{w_t}{N} f_s$$

Where f_t is the transition frequency width in Hz, w_t is the window function transition width as in Table A - 3, N is the number of taps in the filter, and f_s is the sample rate in Hz. For example if I used a 100 tap filter with a Hanning window function, a sample rate of 1 kHz, then the transition width from the pass band (6dB down) to the first null would be:

$$f_t = \frac{1.67}{100} 1000 = 16.7 \text{ Hz}$$

Also shown in Table A - 3 is the relative transition width from -6dBc to -20dBc for each of the window functions. This represents the ratio of the number of filter taps required to maintain the same rate of filter roll off and an example is shown in Figure A - 7.

Window Function	Transition Width of FIR filter (From X dB point to first null)			Transition Width for FIR filter from -6 dB to -20 dB, normalised to Boxcar
	1 dB	3 dB	6 dB	
Boxcar	1.05	0.83	0.62	1
Hanning	2.59	2.09	1.67	2.15
Hamming	2.65	2.17	1.76	2.04
Triangle	2.95	2.38	1.95	2.36
Blackman	4.18	3.54	3.03	2.67
4 term Blackman Harris	5.39	4.64	4.03	3.14
5 term Lawrey	6.00	5.19	4.53	3.41
6 term Lawrey	7.45	6.52	5.78	3.85

Table A - 3, Transition of FIR filters using different window functions. (script s0071)

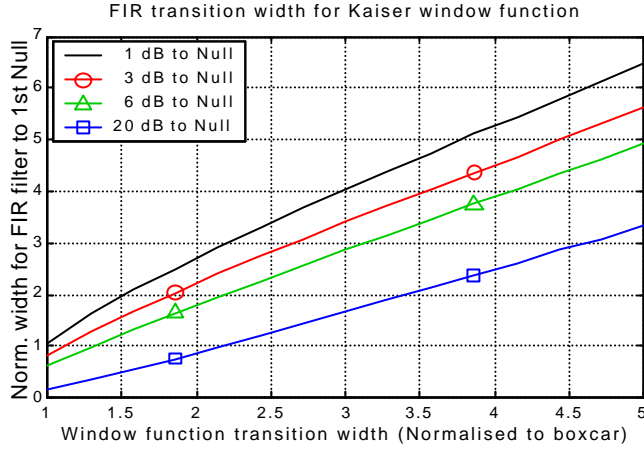


Figure A - 6, Transition of FIR filters using the Kaiser window function.

The x-axis is normalised to the transition width of the window function by itself, the same as used in Figure A - 4. The y-axis shows the transition width of FIR filter from X dB point to first null in the filter response.

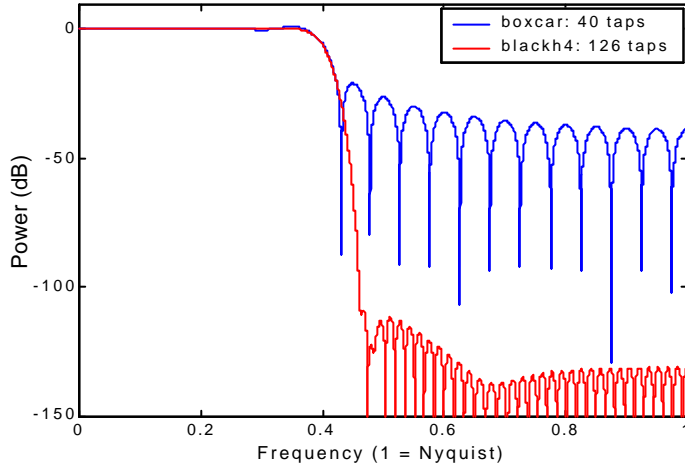


Figure A - 7, Frequency response of two FIR filters with the same rate of roll off. The FIR filter using the Blackman Harris window function requires 3.14 times more filter taps than the boxcar filter. (script s0073)

A.3 WINDOW LOSS

Applying a window function as part of spectral analysis tapers the start and end of the time waveform, resulting in a loss of power seen in the spectrum of the signal. This power loss is referred to as window loss. Table A - 4 shows the loss for each of the common window functions.

Window Function	Window Loss (dB)
Boxcar	0.000
Hanning	6.018
Hamming	5.354
Triangle	6.021
Blackman	7.537
4 term Blackman Harris	8.906
5 term Lawrey	9.583
6 term Lawrey	10.608

Table A - 4, Window loss for different window functions (script s0075)

A.4 LAWREY WINDOW FUNCTION

Window functions with low side-lobe power are especially important for spectral analysis and FIR filter design. The Kaiser window function is a flexible window function that can be used to generate side-lobes with arbitrary attenuation, however Bessel functions are required to calculate the window function. This makes it difficult to implement on a DSP.

Two window functions were developed to provide lower side-lobes than the 4-term Blackman Harris window function, and be simple to implement. Both window functions were calculated by approximating a Kaiser window function using a sum of sinusoids. The coefficients were optimised to maximise the side-lobe attenuation for the given number of coefficients.

$$\mathbf{q} = \frac{2\mathbf{p}}{(n-1) \cdot t} \quad t = 0, 1, \dots n-1$$

$$w(t) = c_1 + c_2 \cos(\mathbf{q}) + c_3 \cos(2\mathbf{q}) + \dots + c_m \cos((m-1)\mathbf{q})$$

where c is the coefficients of the window function, and m is the number of coefficients or terms.

Coefficient	Hanning	Hamming	Blackman	Blackh4	Lawrey5	Lawrey6
c ₁	0.5	0.54	0.42	0.35875	0.3318676	0.2949200
c ₂	-0.5	-0.46	-0.50	-0.48829	-0.4766027	-0.4531624
c ₃	—	—	0.08	0.14128	0.1675404	0.2004549
c ₄	—	—	—	-0.01168	-0.0234285	-0.0467364
c ₅	—	—	—	—	0.0006249	0.0046253
c ₆	—	—	—	—	—	-0.0001010

Table A - 5, Coefficients for Lawrey5 and Lawrey6 window functions, and other common window functions.

All digits are required to maintain window function performance. For Lawrey5 and Lawrey6 single precision representation of the coefficients is sufficient.

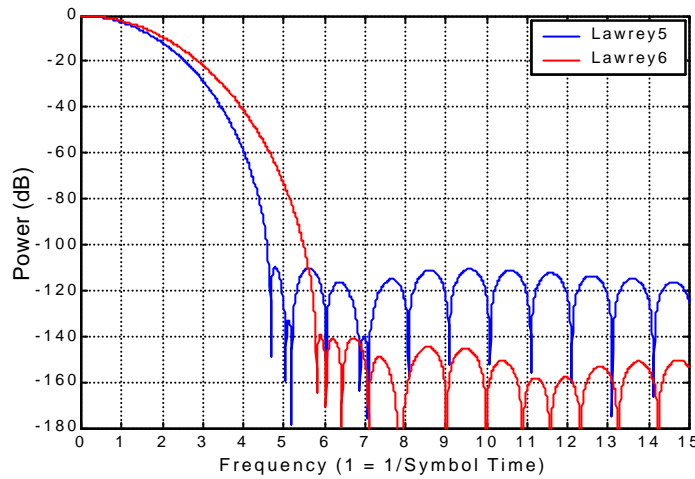


Figure A - 8, Spectrum of Lawrey5 and Lawrey6 window functions.

APPENDIX B BER VERSES SNR FOR OFDM IN AWGN

The performance of OFDM in the presence of AWGN was simulated. These tables show the same results as that shown in Section 2.6.9 but in tabular form.

B.1 COHERENT QUADRATURE AMPLITUDE MODULATION

EBNR (dB)	BPSK	QPSK	8QAM	16QAM	32QAM	64QAM
-6.0	2.393E-01	2.389E-01	2.944E-01	2.861E-01	3.801E-01	3.259E-01
-5.5	2.264E-01	2.268E-01	2.836E-01	2.749E-01	3.743E-01	3.165E-01
-5.0	2.137E-01	2.129E-01	2.714E-01	2.624E-01	3.685E-01	3.069E-01
-4.5	1.994E-01	1.993E-01	2.600E-01	2.495E-01	3.625E-01	2.974E-01
-4.0	1.868E-01	1.862E-01	2.475E-01	2.368E-01	3.555E-01	2.878E-01
-3.5	1.726E-01	1.720E-01	2.357E-01	2.245E-01	3.485E-01	2.781E-01
-3.0	1.584E-01	1.584E-01	2.225E-01	2.116E-01	3.404E-01	2.685E-01
-2.5	1.444E-01	1.443E-01	2.086E-01	1.992E-01	3.326E-01	2.588E-01
-2.0	1.310E-01	1.306E-01	1.968E-01	1.872E-01	3.236E-01	2.495E-01
-1.5	1.169E-01	1.171E-01	1.832E-01	1.750E-01	3.140E-01	2.403E-01
-1.0	1.039E-01	1.038E-01	1.694E-01	1.637E-01	3.045E-01	2.304E-01
-0.5	9.114E-02	9.114E-02	1.555E-01	1.523E-01	2.930E-01	2.208E-01
0.0	7.883E-02	7.847E-02	1.428E-01	1.414E-01	2.820E-01	2.113E-01
0.5	6.712E-02	6.700E-02	1.287E-01	1.299E-01	2.693E-01	2.017E-01
1.0	5.627E-02	5.627E-02	1.146E-01	1.188E-01	2.562E-01	1.919E-01
1.5	4.646E-02	4.639E-02	1.017E-01	1.084E-01	2.432E-01	1.824E-01
2.0	3.737E-02	3.756E-02	8.880E-02	9.792E-02	2.281E-01	1.723E-01
2.5	2.972E-02	2.960E-02	7.673E-02	8.739E-02	2.136E-01	1.626E-01
3.0	2.289E-02	2.291E-02	6.476E-02	7.741E-02	1.981E-01	1.534E-01
3.5	1.712E-02	1.724E-02	5.390E-02	6.802E-02	1.825E-01	1.436E-01
4.0	1.250E-02	1.254E-02	4.409E-02	5.847E-02	1.663E-01	1.334E-01
4.5	8.810E-03	8.803E-03	3.530E-02	5.000E-02	1.507E-01	1.243E-01
5.0	5.946E-03	5.968E-03	2.740E-02	4.182E-02	1.344E-01	1.144E-01
5.5	3.857E-03	3.865E-03	2.085E-02	3.440E-02	1.196E-01	1.050E-01
6.0	2.378E-03	2.382E-03	1.528E-02	2.786E-02	1.038E-01	9.582E-02
6.5	1.399E-03	1.412E-03	1.083E-02	2.197E-02	8.913E-02	8.637E-02
7.0	7.817E-04	7.699E-04	7.410E-03	1.708E-02	7.573E-02	7.720E-02
7.5	3.992E-04	3.941E-04	4.833E-03	1.272E-02	6.269E-02	6.836E-02
8.0	1.983E-04	1.872E-04	2.995E-03	9.253E-03	5.071E-02	5.979E-02

EBNR (dB)	BPSK	QPSK	8QAM	16QAM	32QAM	64QAM
8.5	8.630E-05	8.613E-05	1.773E-03	6.510E-03	4.034E-02	5.170E-02
9.0	3.448E-05	3.337E-05	9.704E-04	4.397E-03	3.152E-02	4.398E-02
9.5	1.270E-05	1.186E-05	5.051E-04	2.855E-03	2.357E-02	3.683E-02
10.0	4.163E-06	3.503E-06	2.423E-04	1.744E-03	1.741E-02	3.037E-02
10.5	7.740E-07	9.108E-07	1.057E-04	1.022E-03	1.214E-02	2.444E-02
11.0	2.111E-07	2.452E-07	4.179E-05	5.667E-04	8.342E-03	1.929E-02
11.5		3.528E-08	1.414E-05	2.904E-04	5.409E-03	1.486E-02
12.0			5.439E-06	1.365E-04	3.338E-03	1.109E-02
12.5			1.240E-06	6.156E-05	1.967E-03	8.065E-03
13.0			3.263E-07	2.361E-05	1.083E-03	5.643E-03
13.5			6.124E-08	8.827E-06	5.655E-04	3.803E-03
14.0				2.953E-06	2.736E-04	2.466E-03
14.5				7.995E-07	1.179E-04	1.512E-03
15.0				1.795E-07	4.740E-05	8.812E-04
15.5					1.626E-05	4.860E-04
16.0					6.175E-06	2.448E-04
16.5					1.347E-06	1.190E-04
17.0					2.681E-07	5.137E-05
17.5					8.838E-08	2.054E-05
18.0						6.733E-06
18.5						2.371E-06
19.0						4.025E-07
19.5						1.197E-07
20.0						2.359E-08
20.5						2.540E-08

EBNR (dB)	128QAM	256QAM	512QAM	1024QAM	2048QAM	4096QAM
-6.0	4.064E-01	3.529E-01	4.217E-01	3.719E-01	4.312E-01	3.858E-01
-5.5	4.030E-01	3.461E-01	4.188E-01	3.659E-01	4.289E-01	3.807E-01
-5.0	3.994E-01	3.388E-01	4.158E-01	3.604E-01	4.265E-01	3.762E-01
-4.5	3.962E-01	3.316E-01	4.127E-01	3.546E-01	4.235E-01	3.710E-01
-4.0	3.907E-01	3.241E-01	4.099E-01	3.485E-01	4.208E-01	3.661E-01
-3.5	3.870E-01	3.168E-01	4.062E-01	3.428E-01	4.181E-01	3.613E-01
-3.0	3.831E-01	3.095E-01	4.027E-01	3.371E-01	4.151E-01	3.561E-01
-2.5	3.774E-01	3.024E-01	3.987E-01	3.307E-01	4.119E-01	3.505E-01
-2.0	3.728E-01	2.946E-01	3.941E-01	3.250E-01	4.081E-01	3.457E-01
-1.5	3.664E-01	2.868E-01	3.906E-01	3.184E-01	4.048E-01	3.404E-01
-1.0	3.608E-01	2.791E-01	3.855E-01	3.118E-01	4.009E-01	3.352E-01
-0.5	3.529E-01	2.710E-01	3.807E-01	3.057E-01	3.970E-01	3.297E-01
0.0	3.461E-01	2.631E-01	3.764E-01	2.992E-01	3.928E-01	3.248E-01
0.5	3.393E-01	2.554E-01	3.710E-01	2.924E-01	3.882E-01	3.185E-01
1.0	3.311E-01	2.473E-01	3.656E-01	2.855E-01	3.838E-01	3.128E-01
1.5	3.227E-01	2.389E-01	3.601E-01	2.793E-01	3.792E-01	3.075E-01
2.0	3.132E-01	2.305E-01	3.529E-01	2.721E-01	3.741E-01	3.016E-01
2.5	3.039E-01	2.221E-01	3.470E-01	2.653E-01	3.694E-01	2.953E-01
3.0	2.941E-01	2.134E-01	3.406E-01	2.579E-01	3.643E-01	2.900E-01
3.5	2.835E-01	2.049E-01	3.337E-01	2.510E-01	3.590E-01	2.834E-01
4.0	2.717E-01	1.962E-01	3.254E-01	2.435E-01	3.537E-01	2.775E-01
4.5	2.599E-01	1.874E-01	3.187E-01	2.363E-01	3.480E-01	2.717E-01
5.0	2.472E-01	1.787E-01	3.100E-01	2.290E-01	3.426E-01	2.660E-01
5.5	2.345E-01	1.700E-01	3.020E-01	2.215E-01	3.363E-01	2.596E-01
6.0	2.205E-01	1.612E-01	2.931E-01	2.144E-01	3.300E-01	2.536E-01
6.5	2.062E-01	1.527E-01	2.846E-01	2.069E-01	3.238E-01	2.471E-01
7.0	1.924E-01	1.442E-01	2.754E-01	1.996E-01	3.170E-01	2.410E-01
7.5	1.784E-01	1.355E-01	2.663E-01	1.925E-01	3.109E-01	2.348E-01
8.0	1.636E-01	1.272E-01	2.563E-01	1.851E-01	3.043E-01	2.288E-01
8.5	1.493E-01	1.186E-01	2.459E-01	1.777E-01	2.973E-01	2.221E-01
9.0	1.343E-01	1.103E-01	2.355E-01	1.702E-01	2.897E-01	2.158E-01
9.5	1.198E-01	1.022E-01	2.244E-01	1.627E-01	2.822E-01	2.098E-01
10.0	1.057E-01	9.394E-02	2.130E-01	1.553E-01	2.752E-01	2.031E-01
10.5	9.207E-02	8.578E-02	2.007E-01	1.476E-01	2.673E-01	1.965E-01
11.0	7.991E-02	7.796E-02	1.890E-01	1.403E-01	2.595E-01	1.903E-01
11.5	6.718E-02	7.017E-02	1.770E-01	1.326E-01	2.511E-01	1.837E-01
12.0	5.573E-02	6.257E-02	1.639E-01	1.252E-01	2.428E-01	1.773E-01
12.5	4.551E-02	5.494E-02	1.517E-01	1.182E-01	2.347E-01	1.709E-01
13.0	3.650E-02	4.805E-02	1.391E-01	1.105E-01	2.258E-01	1.642E-01
13.5	2.841E-02	4.117E-02	1.256E-01	1.035E-01	2.165E-01	1.578E-01
14.0	2.160E-02	3.485E-02	1.131E-01	9.626E-02	2.074E-01	1.511E-01
14.5	1.594E-02	2.908E-02	1.008E-01	8.921E-02	1.975E-01	1.446E-01
15.0	1.137E-02	2.379E-02	8.868E-02	8.211E-02	1.876E-01	1.378E-01
15.5	7.780E-03	1.904E-02	7.743E-02	7.536E-02	1.775E-01	1.314E-01

EBNR (dB)	128QAM	256QAM	512QAM	1024QAM	2048QAM	4096QAM
16.0	5.153E-03	1.482E-02	6.613E-02	6.847E-02	1.672E-01	1.250E-01
16.5	3.254E-03	1.135E-02	5.610E-02	6.153E-02	1.561E-01	1.181E-01
17.0	1.925E-03	8.373E-03	4.612E-02	5.496E-02	1.453E-01	1.119E-01
17.5	1.081E-03	6.015E-03	3.791E-02	4.845E-02	1.342E-01	1.056E-01
18.0	5.841E-04	4.154E-03	3.008E-02	4.225E-02	1.230E-01	9.891E-02
18.5	2.964E-04	2.774E-03	2.327E-02	3.639E-02	1.119E-01	9.265E-02
19.0	1.299E-04	1.754E-03	1.767E-02	3.090E-02	1.010E-01	8.661E-02
19.5	5.496E-05	1.061E-03	1.303E-02	2.580E-02	8.987E-02	7.995E-02
20.0	2.129E-05	6.079E-04	9.309E-03	2.113E-02	7.968E-02	7.424E-02
20.5	6.151E-06	3.288E-04	6.342E-03	1.700E-02	6.929E-02	6.786E-02
21.0	2.154E-06	1.631E-04	4.148E-03	1.331E-02	5.999E-02	6.199E-02
21.5	7.778E-07	7.463E-05	2.628E-03	1.024E-02	5.042E-02	5.584E-02
22.0	2.881E-08	3.149E-05	1.539E-03	7.615E-03	4.229E-02	5.033E-02
22.5		1.136E-05	8.855E-04	5.448E-03	3.448E-02	4.484E-02
23.0		4.251E-06	4.542E-04	3.803E-03	2.778E-02	3.901E-02
23.5		1.363E-06	2.210E-04	2.538E-03	2.161E-02	3.368E-02
24.0		2.121E-07	9.954E-05	1.627E-03	1.661E-02	2.896E-02
24.5		4.079E-08	4.203E-05	9.820E-04	1.226E-02	2.432E-02
25.0			1.554E-05	5.705E-04	8.855E-03	2.005E-02
25.5			5.512E-06	3.051E-04	6.091E-03	1.629E-02
26.0			1.121E-06	1.541E-04	4.100E-03	1.301E-02
26.5			6.662E-07	7.323E-05	2.588E-03	1.002E-02
27.0			2.273E-07	2.959E-05	1.551E-03	7.533E-03
27.5				1.173E-05	8.843E-04	5.548E-03
28.0				4.118E-06	4.735E-04	3.894E-03
28.5				1.299E-06	2.387E-04	2.656E-03
29.0				2.937E-07	1.148E-04	1.739E-03
29.5				1.115E-07	4.632E-05	1.083E-03
30.0					1.838E-05	6.360E-04
30.5					5.618E-06	3.580E-04
31.0					2.522E-06	1.847E-04
31.5					6.329E-07	9.174E-05
32.0					1.686E-07	4.014E-05
32.5						1.662E-05
33.0						6.369E-06
33.5						1.851E-06
34.0						5.385E-07
34.5						8.733E-08
35.0						3.538E-08

B.2 COHERENT PHASE SHIFT KEYING

EBNR (dB)	8PSK	16PSK	32PSK	64PSK	128PSK	256PSK
-6.0	2.712E-01	3.058E-01	3.320E-01	3.479E-01	3.612E-01	3.734E-01
-5.5	2.596E-01	2.964E-01	3.229E-01	3.412E-01	3.552E-01	3.670E-01
-5.0	2.473E-01	2.862E-01	3.142E-01	3.342E-01	3.495E-01	3.620E-01
-4.5	2.330E-01	2.744E-01	3.051E-01	3.272E-01	3.431E-01	3.565E-01
-4.0	2.214E-01	2.634E-01	2.962E-01	3.190E-01	3.366E-01	3.511E-01
-3.5	2.093E-01	2.529E-01	2.866E-01	3.119E-01	3.302E-01	3.451E-01
-3.0	1.960E-01	2.416E-01	2.788E-01	3.050E-01	3.243E-01	3.403E-01
-2.5	1.830E-01	2.296E-01	2.692E-01	2.975E-01	3.180E-01	3.340E-01
-2.0	1.715E-01	2.188E-01	2.604E-01	2.895E-01	3.115E-01	3.289E-01
-1.5	1.582E-01	2.074E-01	2.518E-01	2.823E-01	3.058E-01	3.235E-01
-1.0	1.467E-01	1.963E-01	2.429E-01	2.750E-01	2.993E-01	3.181E-01
-0.5	1.339E-01	1.855E-01	2.338E-01	2.682E-01	2.935E-01	3.129E-01
0.0	1.226E-01	1.742E-01	2.251E-01	2.603E-01	2.873E-01	3.076E-01
0.5	1.116E-01	1.636E-01	2.159E-01	2.534E-01	2.808E-01	3.021E-01
1.0	1.007E-01	1.535E-01	2.066E-01	2.463E-01	2.750E-01	2.967E-01
1.5	9.031E-02	1.435E-01	1.979E-01	2.394E-01	2.687E-01	2.916E-01
2.0	8.062E-02	1.336E-01	1.890E-01	2.312E-01	2.625E-01	2.864E-01
2.5	7.141E-02	1.249E-01	1.797E-01	2.250E-01	2.567E-01	2.808E-01
3.0	6.221E-02	1.156E-01	1.706E-01	2.175E-01	2.504E-01	2.758E-01
3.5	5.423E-02	1.069E-01	1.628E-01	2.103E-01	2.444E-01	2.706E-01
4.0	4.587E-02	9.898E-02	1.535E-01	2.031E-01	2.384E-01	2.652E-01
4.5	3.839E-02	9.070E-02	1.453E-01	1.961E-01	2.325E-01	2.603E-01
5.0	3.219E-02	8.290E-02	1.372E-01	1.891E-01	2.265E-01	2.552E-01
5.5	2.590E-02	7.549E-02	1.286E-01	1.818E-01	2.200E-01	2.497E-01
6.0	2.040E-02	6.808E-02	1.207E-01	1.743E-01	2.145E-01	2.445E-01
6.5	1.585E-02	6.110E-02	1.131E-01	1.673E-01	2.086E-01	2.393E-01
7.0	1.197E-02	5.421E-02	1.055E-01	1.599E-01	2.022E-01	2.338E-01
7.5	8.597E-03	4.790E-02	9.864E-02	1.523E-01	1.960E-01	2.283E-01
8.0	6.231E-03	4.135E-02	9.141E-02	1.449E-01	1.902E-01	2.232E-01
8.5	4.164E-03	3.542E-02	8.476E-02	1.379E-01	1.841E-01	2.181E-01
9.0	2.755E-03	3.007E-02	7.862E-02	1.303E-01	1.782E-01	2.131E-01
9.5	1.696E-03	2.495E-02	7.194E-02	1.234E-01	1.719E-01	2.080E-01
10.0	1.001E-03	2.022E-02	6.611E-02	1.163E-01	1.657E-01	2.027E-01
10.5	5.531E-04	1.608E-02	6.008E-02	1.098E-01	1.598E-01	1.972E-01
11.0	2.925E-04	1.264E-02	5.436E-02	1.031E-01	1.533E-01	1.919E-01
11.5	1.430E-04	9.483E-03	4.884E-02	9.638E-02	1.475E-01	1.866E-01
12.0	6.302E-05	7.074E-03	4.356E-02	9.034E-02	1.414E-01	1.817E-01
12.5	2.686E-05	4.908E-03	3.836E-02	8.426E-02	1.348E-01	1.765E-01
13.0	8.881E-06	3.388E-03	3.319E-02	7.825E-02	1.286E-01	1.710E-01
13.5	3.354E-06	2.296E-03	2.859E-02	7.256E-02	1.225E-01	1.656E-01
14.0	8.503E-07	1.434E-03	2.406E-02	6.769E-02	1.160E-01	1.605E-01
14.5	3.779E-07	8.333E-04	2.009E-02	6.229E-02	1.097E-01	1.552E-01
15.0		4.840E-04	1.621E-02	5.714E-02	1.039E-01	1.499E-01
15.5		2.506E-04	1.297E-02	5.204E-02	9.782E-02	1.443E-01
16.0		1.252E-04	1.021E-02	4.746E-02	9.213E-02	1.389E-01
16.5		5.547E-05	7.691E-03	4.282E-02	8.647E-02	1.340E-01

EBNR (dB)	8PSK	16PSK	32PSK	64PSK	128PSK	256PSK
17.0		2.300E-05	5.634E-03	3.846E-02	8.074E-02	1.280E-01
17.5		9.212E-06	4.022E-03	3.381E-02	7.588E-02	1.228E-01
18.0		3.224E-06	2.754E-03	2.958E-02	7.072E-02	1.174E-01
18.5		8.858E-07	1.832E-03	2.549E-02	6.591E-02	1.117E-01
19.0		2.126E-07	1.158E-03	2.170E-02	6.082E-02	1.065E-01
19.5		3.543E-08	6.865E-04	1.825E-02	5.664E-02	1.011E-01
20.0			3.884E-04	1.483E-02	5.208E-02	9.547E-02
20.5			2.029E-04	1.205E-02	4.784E-02	9.013E-02
21.0			1.024E-04	9.369E-03	4.377E-02	8.515E-02
21.5			4.569E-05	7.275E-03	3.950E-02	7.994E-02
22.0			1.919E-05	5.406E-03	3.539E-02	7.505E-02
22.5			7.228E-06	3.929E-03	3.151E-02	7.030E-02
23.0			2.494E-06	2.703E-03	2.777E-02	6.584E-02
23.5			8.362E-07	1.842E-03	2.425E-02	6.108E-02
24.0			1.984E-07	1.189E-03	2.087E-02	5.724E-02
24.5			7.086E-08	7.163E-04	1.760E-02	5.279E-02
25.0				4.189E-04	1.459E-02	4.885E-02
25.5				2.253E-04	1.205E-02	4.526E-02
26.0				1.169E-04	9.515E-03	4.139E-02
26.5				5.604E-05	7.431E-03	3.784E-02
27.0				2.361E-05	5.598E-03	3.404E-02
27.5				8.846E-06	4.180E-03	3.058E-02
28.0				3.319E-06	2.998E-03	2.733E-02
28.5				9.803E-07	2.061E-03	2.395E-02
29.0				3.897E-07	1.366E-03	2.093E-02
29.5				8.267E-08	8.787E-04	1.788E-02
30.0				2.062E-08	5.236E-04	1.516E-02
30.5					2.961E-04	1.249E-02
31.0					1.595E-04	1.028E-02
31.5					8.013E-05	8.145E-03
32.0					3.717E-05	6.336E-03
32.5					1.597E-05	4.816E-03
33.0					6.195E-06	3.538E-03
33.5					1.832E-06	2.537E-03
34.0					5.467E-07	1.758E-03
34.5					7.086E-08	1.141E-03
35.0					4.049E-08	7.230E-04
35.5						4.301E-04
36.0						2.424E-04
36.5						1.297E-04
37.0						6.474E-05
37.5						2.847E-05
38.0						1.262E-05
38.5						4.765E-06
39.0						1.444E-06
39.5						4.606E-07
40.0						1.143E-07
40.5						3.376E-08

B.3 DIFFERENTIAL QAM

EBNR (dB)	DBPSK	DQPSK	D16QAM	D64QAM	D256QAM	D1024QAM	D4096QAM
-6.0	3.885E-01	4.150E-01	4.890E-01	4.835E-01	4.799E-01	4.773E-01	4.765E-01
-5.5	3.775E-01	4.051E-01	4.856E-01	4.800E-01	4.758E-01	4.739E-01	4.730E-01
-5.0	3.651E-01	3.949E-01	4.804E-01	4.748E-01	4.718E-01	4.700E-01	4.694E-01
-4.5	3.510E-01	3.837E-01	4.741E-01	4.696E-01	4.667E-01	4.660E-01	4.657E-01
-4.0	3.357E-01	3.702E-01	4.674E-01	4.636E-01	4.616E-01	4.612E-01	4.616E-01
-3.5	3.208E-01	3.554E-01	4.596E-01	4.578E-01	4.565E-01	4.565E-01	4.574E-01
-3.0	3.021E-01	3.418E-01	4.510E-01	4.508E-01	4.510E-01	4.519E-01	4.535E-01
-2.5	2.850E-01	3.253E-01	4.414E-01	4.438E-01	4.450E-01	4.468E-01	4.485E-01
-2.0	2.664E-01	3.079E-01	4.312E-01	4.364E-01	4.386E-01	4.413E-01	4.438E-01
-1.5	2.455E-01	2.896E-01	4.200E-01	4.288E-01	4.323E-01	4.361E-01	4.396E-01
-1.0	2.260E-01	2.699E-01	4.082E-01	4.199E-01	4.257E-01	4.302E-01	4.344E-01
-0.5	2.045E-01	2.502E-01	3.951E-01	4.111E-01	4.187E-01	4.247E-01	4.296E-01
0.0	1.846E-01	2.293E-01	3.815E-01	4.014E-01	4.117E-01	4.187E-01	4.249E-01
0.5	1.630E-01	2.080E-01	3.659E-01	3.914E-01	4.046E-01	4.126E-01	4.193E-01
1.0	1.415E-01	1.874E-01	3.508E-01	3.820E-01	3.967E-01	4.068E-01	4.140E-01
1.5	1.215E-01	1.666E-01	3.334E-01	3.715E-01	3.893E-01	4.003E-01	4.086E-01
2.0	1.036E-01	1.457E-01	3.152E-01	3.611E-01	3.810E-01	3.934E-01	4.035E-01
2.5	8.454E-02	1.264E-01	2.966E-01	3.504E-01	3.733E-01	3.873E-01	3.979E-01
3.0	6.804E-02	1.068E-01	2.770E-01	3.389E-01	3.654E-01	3.809E-01	3.923E-01
3.5	5.326E-02	8.935E-02	2.568E-01	3.273E-01	3.569E-01	3.738E-01	3.863E-01
4.0	4.047E-02	7.264E-02	2.365E-01	3.154E-01	3.479E-01	3.671E-01	3.806E-01
4.5	2.966E-02	5.857E-02	2.162E-01	3.020E-01	3.393E-01	3.601E-01	3.745E-01
5.0	2.105E-02	4.578E-02	1.951E-01	2.892E-01	3.299E-01	3.531E-01	3.690E-01
5.5	1.434E-02	3.497E-02	1.745E-01	2.754E-01	3.214E-01	3.461E-01	3.627E-01
6.0	9.401E-03	2.598E-02	1.551E-01	2.609E-01	3.118E-01	3.385E-01	3.569E-01
6.5	5.793E-03	1.853E-02	1.359E-01	2.463E-01	3.017E-01	3.313E-01	3.506E-01
7.0	3.349E-03	1.289E-02	1.174E-01	2.307E-01	2.924E-01	3.236E-01	3.446E-01
7.5	1.789E-03	8.499E-03	9.992E-02	2.153E-01	2.827E-01	3.165E-01	3.384E-01
8.0	9.148E-04	5.500E-03	8.415E-02	1.994E-01	2.730E-01	3.092E-01	3.322E-01
8.5	4.147E-04	3.258E-03	6.927E-02	1.832E-01	2.625E-01	3.016E-01	3.263E-01
9.0	1.800E-04	1.898E-03	5.609E-02	1.674E-01	2.519E-01	2.939E-01	3.199E-01
9.5	6.823E-05	1.026E-03	4.415E-02	1.512E-01	2.408E-01	2.859E-01	3.132E-01
10.0	2.277E-05	5.138E-04	3.414E-02	1.353E-01	2.297E-01	2.780E-01	3.069E-01
10.5	6.388E-06	2.456E-04	2.563E-02	1.197E-01	2.185E-01	2.695E-01	3.001E-01
11.0	1.699E-06	1.021E-04	1.863E-02	1.047E-01	2.062E-01	2.617E-01	2.937E-01
11.5	3.664E-07	3.802E-05	1.309E-02	9.063E-02	1.939E-01	2.536E-01	2.871E-01
12.0		1.360E-05	8.761E-03	7.729E-02	1.815E-01	2.450E-01	2.806E-01
12.5		4.424E-06	5.688E-03	6.456E-02	1.687E-01	2.367E-01	2.740E-01
13.0		1.019E-06	3.537E-03	5.355E-02	1.558E-01	2.279E-01	2.675E-01
13.5		2.446E-07	2.097E-03	4.308E-02	1.429E-01	2.194E-01	2.609E-01
14.0			1.142E-03	3.374E-02	1.298E-01	2.101E-01	2.536E-01
14.5				5.867E-04	2.627E-02	1.169E-01	2.010E-01
15.0				2.804E-04	1.965E-02	1.043E-01	1.916E-01

EBNR (dB)	DBPSK	DQPSK	D16QAM	D64QAM	D256QAM	D1024QAM	D4096QAM
15.5			1.209E-04	1.426E-02	9.213E-02	1.818E-01	2.330E-01
16.0			4.838E-05	9.889E-03	8.025E-02	1.722E-01	2.261E-01
16.5			1.787E-05	6.775E-03	6.891E-02	1.618E-01	2.190E-01
17.0			5.227E-06	4.335E-03	5.826E-02	1.513E-01	2.118E-01
17.5			1.687E-06	2.686E-03	4.840E-02	1.406E-01	2.046E-01
18.0			2.852E-07	1.560E-03	3.967E-02	1.303E-01	1.970E-01
18.5			2.480E-08	8.550E-04	3.178E-02	1.196E-01	1.899E-01
19.0				4.353E-04	2.482E-02	1.087E-01	1.821E-01
19.5				2.106E-04	1.916E-02	9.772E-02	1.743E-01
20.0				9.327E-05	1.415E-02	8.759E-02	1.664E-01
20.5				3.600E-05	1.010E-02	7.714E-02	1.582E-01
21.0				1.240E-05	6.994E-03	6.782E-02	1.498E-01
21.5				4.295E-06	4.635E-03	5.813E-02	1.410E-01
22.0				1.133E-06	2.959E-03	4.928E-02	1.324E-01
22.5				2.852E-07	1.794E-03	4.135E-02	1.234E-01
23.0				7.949E-08	1.021E-03	3.384E-02	1.144E-01
23.5				8.585E-09	5.423E-04	2.714E-02	1.055E-01
24.0					2.714E-04	2.108E-02	9.607E-02
24.5					1.279E-04	1.625E-02	8.699E-02
25.0					5.255E-05	1.226E-02	7.844E-02
25.5					2.075E-05	8.682E-03	6.928E-02
26.0					6.969E-06	6.092E-03	6.095E-02
26.5					2.052E-06	4.029E-03	5.278E-02
27.0					5.022E-07	2.627E-03	4.523E-02
27.5					9.074E-08	1.582E-03	3.809E-02
28.0						9.098E-04	3.134E-02
28.5						4.976E-04	2.541E-02
29.0						2.545E-04	2.018E-02
29.5						1.149E-04	1.579E-02
30.0						4.812E-05	1.188E-02
30.5						1.983E-05	8.584E-03
31.0						6.665E-06	6.072E-03
31.5						2.054E-06	4.198E-03
32.0						4.859E-07	2.731E-03
32.5						1.196E-07	1.692E-03
33.0							1.014E-03
33.5							5.607E-04
34.0							2.929E-04
34.5							1.416E-04
35.0							6.349E-05
35.5							2.548E-05
36.0							9.663E-06
36.5							3.142E-06
37.0							1.026E-06
37.5							2.501E-07

B.4 DIFFERENTIAL PHASE SHIFT KEYING

EBNR (dB)	D8PSK	D16PSK	D32PSK	D64PSK	D128PSK	D256PSK
-6.0	4.285E-01	4.341E-01	4.372E-01	4.402E-01	4.427E-01	4.451E-01
-5.5	4.204E-01	4.271E-01	4.313E-01	4.353E-01	4.384E-01	4.414E-01
-5.0	4.127E-01	4.203E-01	4.257E-01	4.299E-01	4.334E-01	4.373E-01
-4.5	4.050E-01	4.134E-01	4.198E-01	4.242E-01	4.289E-01	4.327E-01
-4.0	3.946E-01	4.060E-01	4.131E-01	4.183E-01	4.239E-01	4.279E-01
-3.5	3.840E-01	3.977E-01	4.062E-01	4.127E-01	4.185E-01	4.232E-01
-3.0	3.736E-01	3.892E-01	3.997E-01	4.069E-01	4.132E-01	4.195E-01
-2.5	3.625E-01	3.809E-01	3.919E-01	4.009E-01	4.080E-01	4.141E-01
-2.0	3.514E-01	3.718E-01	3.851E-01	3.951E-01	4.029E-01	4.100E-01
-1.5	3.387E-01	3.629E-01	3.778E-01	3.886E-01	3.969E-01	4.053E-01
-1.0	3.255E-01	3.535E-01	3.703E-01	3.827E-01	3.921E-01	4.004E-01
-0.5	3.128E-01	3.436E-01	3.628E-01	3.762E-01	3.868E-01	3.955E-01
0.0	2.981E-01	3.351E-01	3.550E-01	3.697E-01	3.811E-01	3.908E-01
0.5	2.834E-01	3.244E-01	3.476E-01	3.636E-01	3.759E-01	3.858E-01
1.0	2.681E-01	3.143E-01	3.400E-01	3.575E-01	3.710E-01	3.816E-01
1.5	2.524E-01	3.042E-01	3.320E-01	3.506E-01	3.652E-01	3.769E-01
2.0	2.370E-01	2.938E-01	3.241E-01	3.443E-01	3.598E-01	3.720E-01
2.5	2.209E-01	2.837E-01	3.164E-01	3.384E-01	3.545E-01	3.668E-01
3.0	2.045E-01	2.729E-01	3.085E-01	3.316E-01	3.484E-01	3.617E-01
3.5	1.876E-01	2.625E-01	3.013E-01	3.252E-01	3.431E-01	3.570E-01
4.0	1.701E-01	2.513E-01	2.931E-01	3.185E-01	3.375E-01	3.526E-01
4.5	1.545E-01	2.401E-01	2.850E-01	3.120E-01	3.320E-01	3.473E-01
5.0	1.377E-01	2.290E-01	2.767E-01	3.055E-01	3.267E-01	3.425E-01
5.5	1.216E-01	2.168E-01	2.684E-01	2.986E-01	3.208E-01	3.378E-01
6.0	1.063E-01	2.050E-01	2.603E-01	2.925E-01	3.148E-01	3.328E-01
6.5	9.163E-02	1.927E-01	2.516E-01	2.860E-01	3.097E-01	3.279E-01
7.0	7.798E-02	1.795E-01	2.428E-01	2.788E-01	3.038E-01	3.230E-01
7.5	6.511E-02	1.663E-01	2.344E-01	2.725E-01	2.982E-01	3.179E-01
8.0	5.365E-02	1.535E-01	2.260E-01	2.656E-01	2.925E-01	3.133E-01
8.5	4.324E-02	1.400E-01	2.169E-01	2.590E-01	2.866E-01	3.077E-01
9.0	3.368E-02	1.269E-01	2.078E-01	2.517E-01	2.813E-01	3.032E-01
9.5	2.594E-02	1.138E-01	1.984E-01	2.451E-01	2.749E-01	2.978E-01
10.0	1.950E-02	1.011E-01	1.894E-01	2.380E-01	2.690E-01	2.929E-01
10.5	1.416E-02	8.868E-02	1.792E-01	2.311E-01	2.638E-01	2.882E-01
11.0	9.755E-03	7.768E-02	1.689E-01	2.235E-01	2.574E-01	2.828E-01
11.5	6.644E-03	6.663E-02	1.585E-01	2.167E-01	2.520E-01	2.782E-01
12.0	4.256E-03	5.575E-02	1.480E-01	2.099E-01	2.462E-01	2.727E-01
12.5	2.599E-03	4.632E-02	1.380E-01	2.019E-01	2.403E-01	2.678E-01
13.0	1.524E-03	3.752E-02	1.274E-01	1.949E-01	2.344E-01	2.624E-01
13.5	8.250E-04	3.002E-02	1.157E-01	1.869E-01	2.284E-01	2.577E-01
14.0	4.195E-04	2.321E-02	1.053E-01	1.797E-01	2.224E-01	2.522E-01
14.5	1.977E-04	1.764E-02	9.424E-02	1.715E-01	2.165E-01	2.470E-01
15.0	8.560E-05	1.295E-02	8.412E-02	1.635E-01	2.105E-01	2.424E-01

EBNR (dB)	D8PSK	D16PSK	D32PSK	D64PSK	D128PSK	D256PSK
15.5	3.468E-05	9.227E-03	7.447E-02	1.554E-01	2.045E-01	2.372E-01
16.0	1.207E-05	6.288E-03	6.441E-02	1.466E-01	1.976E-01	2.316E-01
16.5	3.695E-06	4.154E-03	5.550E-02	1.385E-01	1.918E-01	2.265E-01
17.0	8.434E-07	2.597E-03	4.707E-02	1.295E-01	1.857E-01	2.215E-01
17.5	4.712E-07	1.545E-03	3.874E-02	1.199E-01	1.793E-01	2.163E-01
18.0		8.655E-04	3.183E-02	1.117E-01	1.730E-01	2.109E-01
18.5		4.559E-04	2.523E-02	1.023E-01	1.664E-01	2.057E-01
19.0		2.224E-04	1.958E-02	9.335E-02	1.599E-01	2.004E-01
19.5		1.022E-04	1.483E-02	8.417E-02	1.535E-01	1.951E-01
20.0		4.181E-05	1.086E-02	7.507E-02	1.465E-01	1.899E-01
20.5		1.507E-05	7.756E-03	6.665E-02	1.397E-01	1.841E-01
21.0		4.881E-06	5.328E-03	5.806E-02	1.324E-01	1.789E-01
21.5		1.596E-06	3.544E-03	5.047E-02	1.246E-01	1.732E-01
22.0		4.313E-07	2.226E-03	4.241E-02	1.171E-01	1.678E-01
22.5		4.372E-08	1.355E-03	3.591E-02	1.091E-01	1.626E-01
23.0			7.485E-04	2.931E-02	1.018E-01	1.569E-01
23.5			4.003E-04	2.363E-02	9.400E-02	1.514E-01
24.0			1.939E-04	1.867E-02	8.575E-02	1.451E-01
24.5			8.853E-05	1.435E-02	7.795E-02	1.397E-01
25.0			3.670E-05	1.072E-02	7.050E-02	1.341E-01
25.5			1.346E-05	7.758E-03	6.267E-02	1.284E-01
26.0			4.681E-06	5.449E-03	5.519E-02	1.215E-01
26.5			1.166E-06	3.633E-03	4.822E-02	1.154E-01
27.0			4.211E-07	2.326E-03	4.153E-02	1.090E-01
27.5			9.718E-08	1.412E-03	3.505E-02	1.022E-01
28.0				8.387E-04	2.897E-02	9.537E-02
28.5				4.499E-04	2.392E-02	8.847E-02
29.0				2.309E-04	1.920E-02	8.185E-02
29.5				1.092E-04	1.491E-02	7.498E-02
30.0				4.736E-05	1.128E-02	6.802E-02
30.5				1.779E-05	8.368E-03	6.079E-02
31.0				5.840E-06	6.014E-03	5.439E-02
31.5				2.055E-06	4.169E-03	4.791E-02
32.0				6.684E-07	2.760E-03	4.160E-02
32.5				2.814E-08	1.750E-03	3.563E-02
33.0				1.437E-08	1.052E-03	3.020E-02
33.5					5.993E-04	2.497E-02
34.0					3.186E-04	2.035E-02
34.5					1.581E-04	1.620E-02
35.0					7.317E-05	1.278E-02
35.5					3.121E-05	9.642E-03
36.0					1.143E-05	7.112E-03

EBNR (dB)	D8PSK	D16PSK	D32PSK	D64PSK	D128PSK	D256PSK
36.5					4.004E-06	5.069E-03
37.0					1.335E-06	3.518E-03
37.5					3.720E-07	2.292E-03
38.0					4.310E-08	1.452E-03
38.5						8.686E-04
39.0						4.952E-04
39.5						2.643E-04
40.0						1.283E-04
40.5						5.971E-05
41.0						2.333E-05
41.5						9.001E-06
42.0						3.023E-06
42.5						7.854E-07
43.0						2.377E-07
43.5						3.100E-08

APPENDIX C RF MEASUREMENTS

These results are from the measurements presented in section 3.8 starting page 104. The location of each of the measurements is shown in Figure 3-9.

The frequency response of the channel measurement set up is shown in Figure A - 9. The combined frequency response of the two antennas and the preamplifier was difficult to measure due to the effects of multipath, causing frequency selective fading. To overcome this, the frequency response was estimated by averaging the radio channel response from all the measurement sets taken. This frequency response was used to calibrate the measurements taken. The error in calibration is about ± 1 dB.

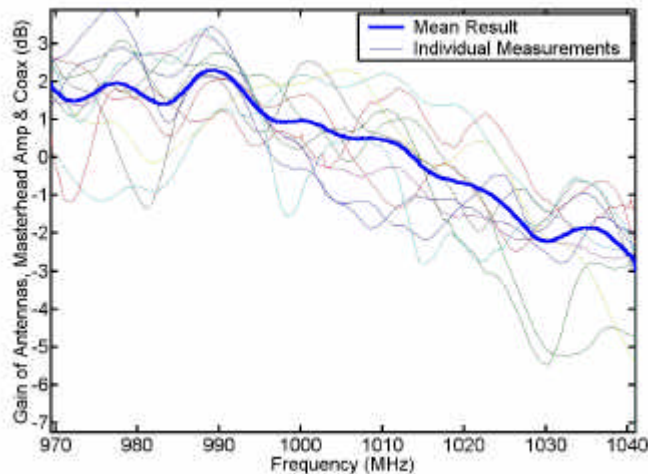


Figure A - 9, Frequency response of the radio channel measurement set up, including antennas, and pre-amplifier.

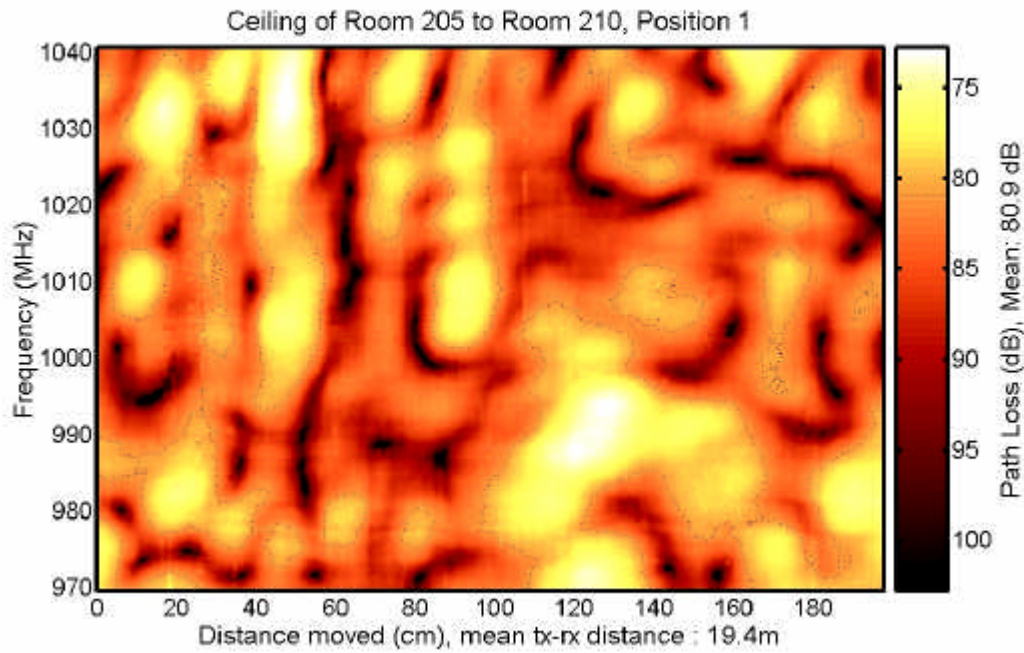


Figure A - 10, Wide bandwidth frequency fading over distance for room 205 to 210.

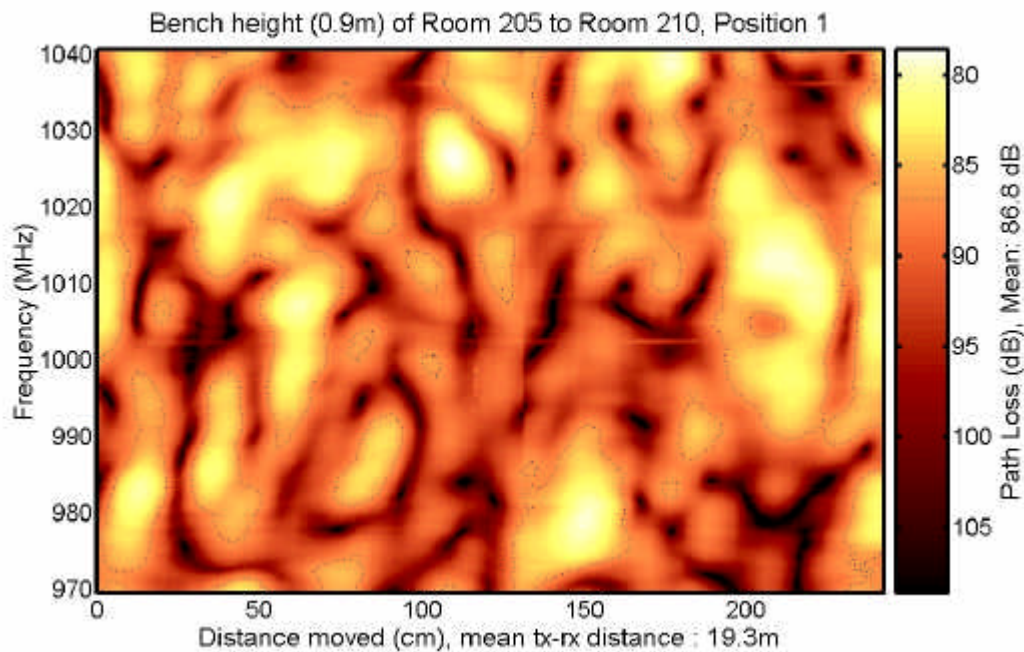


Figure A - 11, Wide bandwidth frequency fading over distance for room 205 to 210.

Streaks in the response are due to narrow band interfering transmissions.

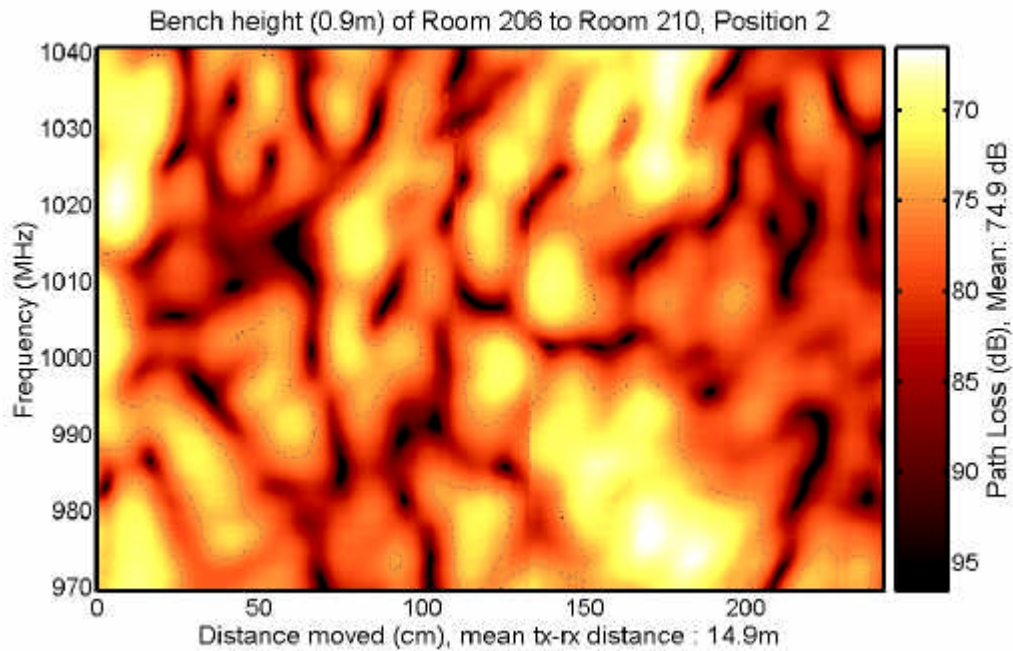


Figure A - 12, Wide bandwidth frequency fading over distance for room 206 to 210.

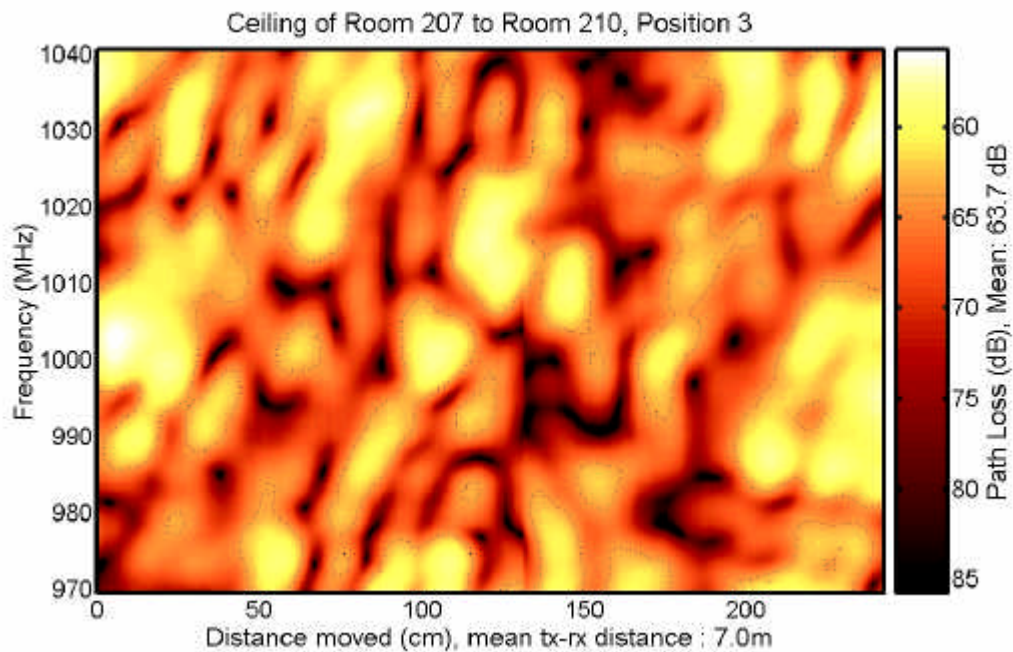


Figure A - 13, Wide bandwidth frequency fading over distance for room 207 to 210.

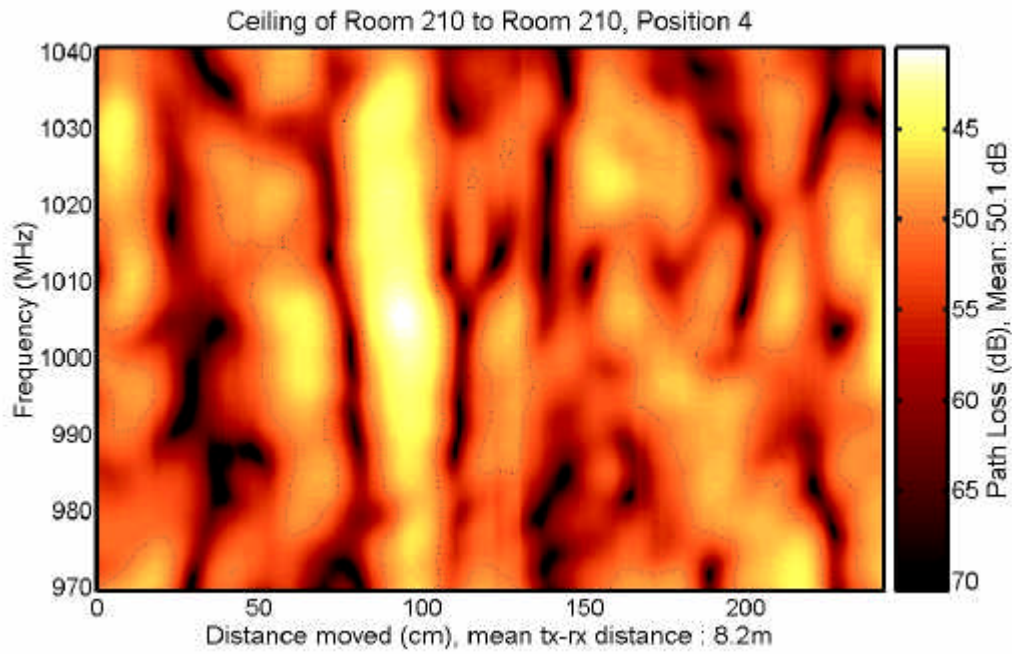


Figure A - 14, Wide bandwidth frequency fading over distance for room 210 to 210. This is a LOS link, as a result the correlation bandwidth is wider.

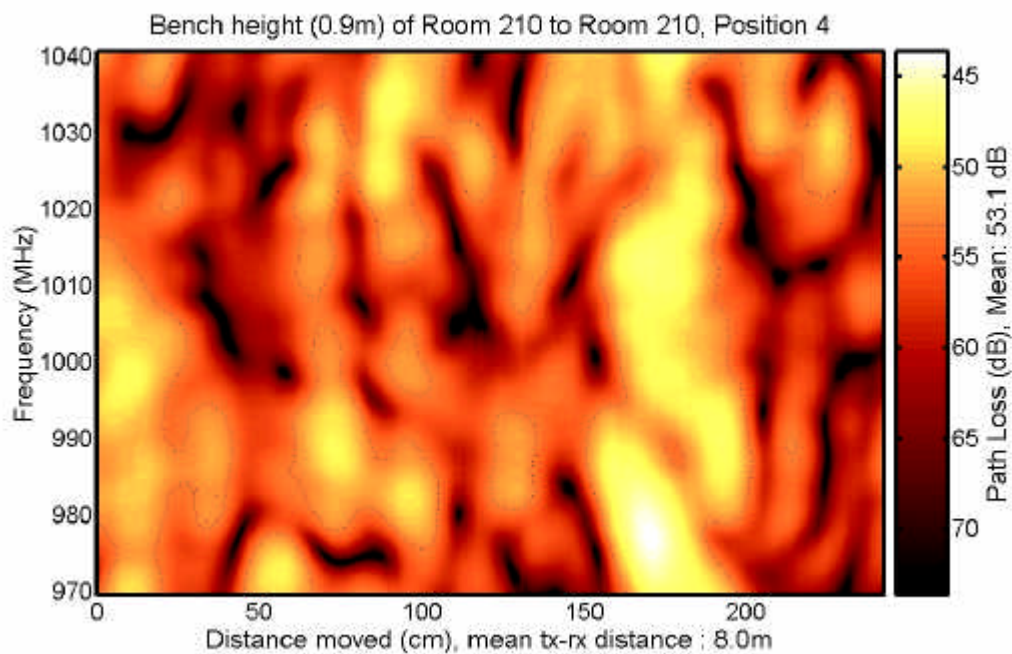


Figure A - 15, Wide bandwidth frequency fading over distance for room 205 to 210. This is a LOS link.

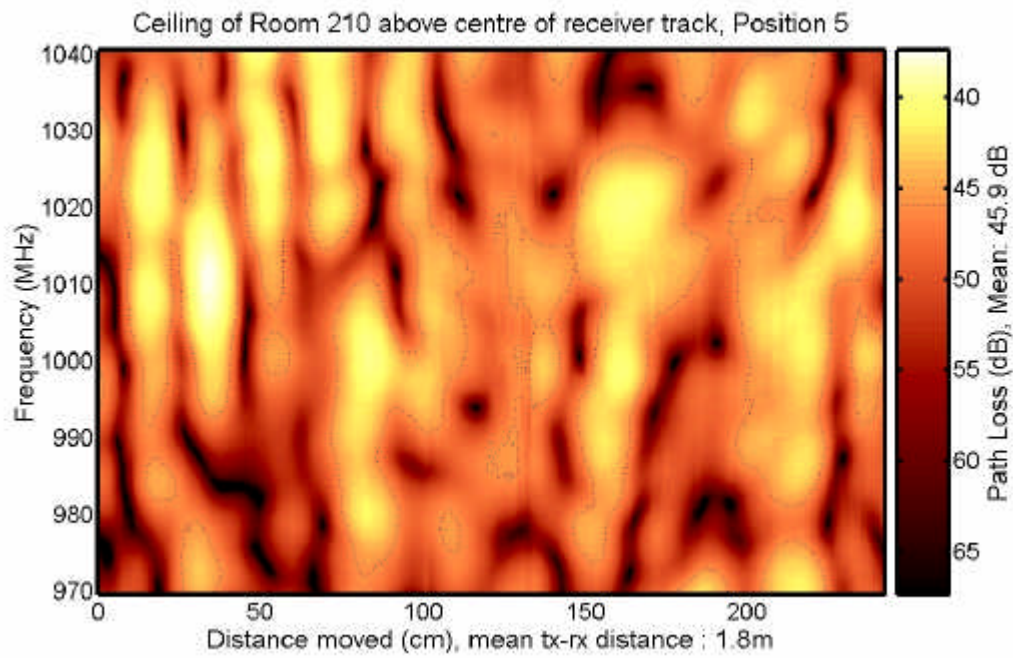


Figure A - 16, Wide bandwidth frequency fading over distance for room 210 above the centre of the receiver track to the guide track also in room 210.

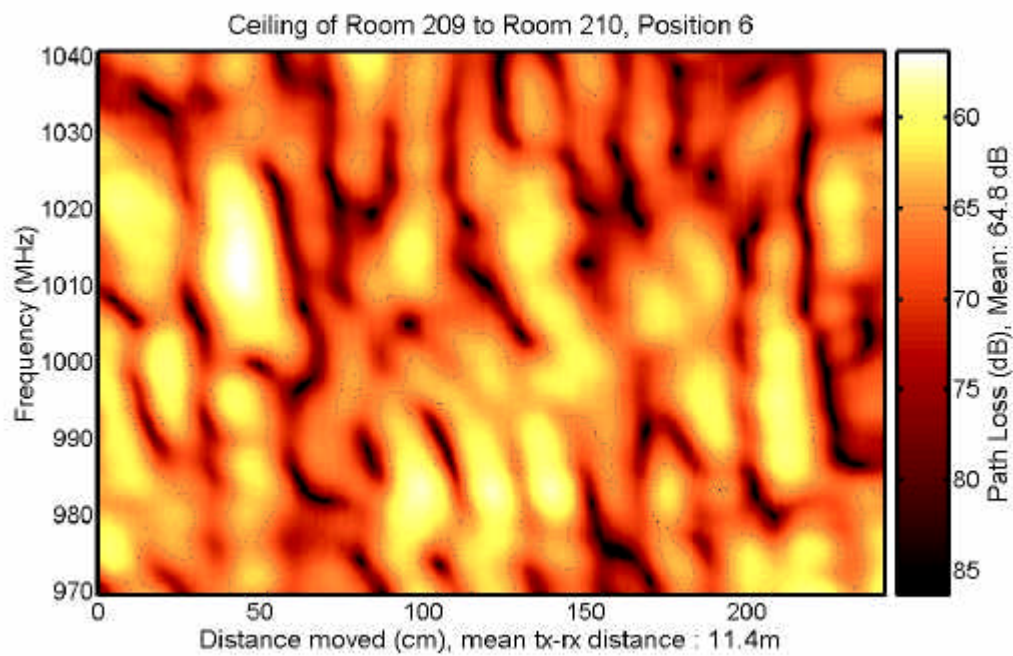


Figure A - 17, Wide bandwidth frequency fading over distance for room 209 to 210.

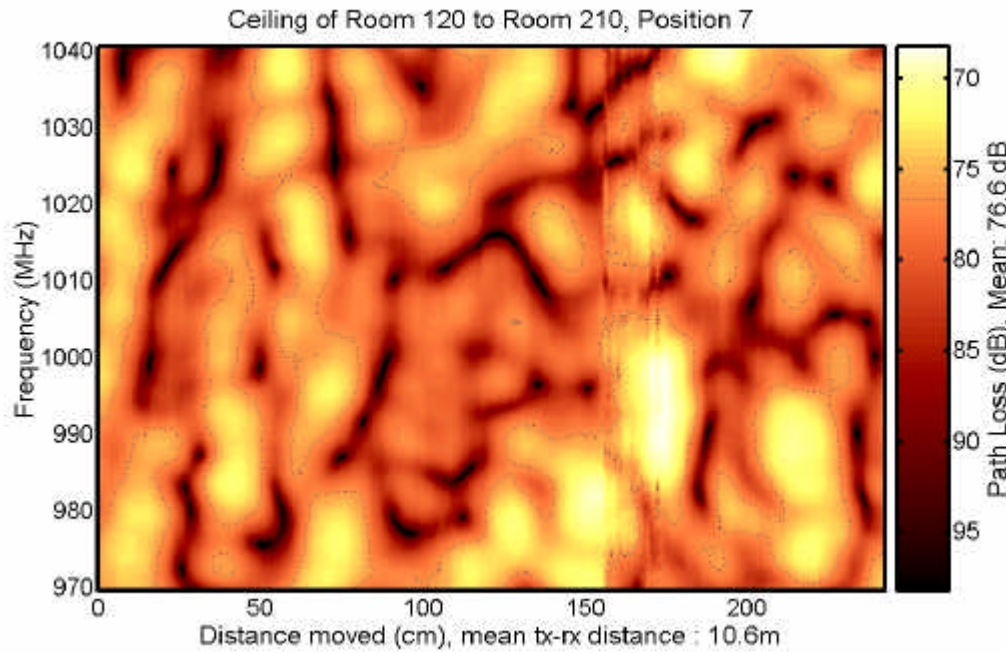


Figure A - 18, Wide bandwidth frequency fading over distance for room 120 to 210.

Rm120 is on the next floor down. From 155 –170 cm the data is blurred due to movement within the building during the measurement.

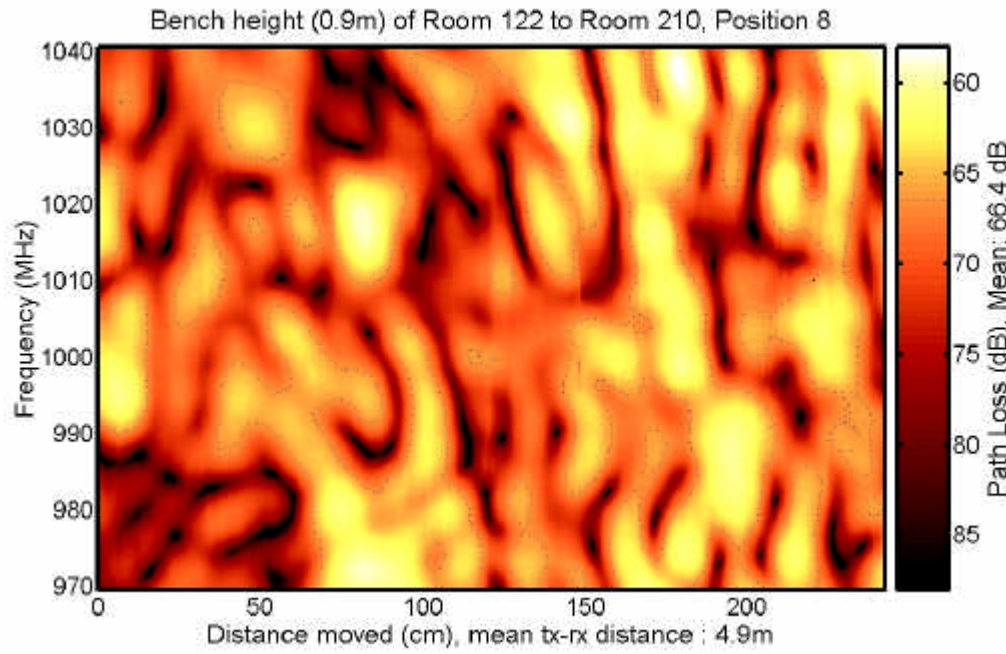


Figure A - 19, Wide bandwidth frequency fading over distance for room 122 to 210.

Rm122 is on the next floor down, resulting in additional path loss and a lower correlation bandwidth for the short transmission distance.

C.1 DIVERSITY

The performance of an optimal power combining diversity receiver was simulated for the channel response measurements taken in Appendix C. The performance of the diversity receiver was estimated for different antenna spacings. The measurements shown in Appendix C were taken along a linear track 2.4 m in length. As part of the simulation virtual antennas were placed along this measurement track, and the power from these antennas were combined to obtain the estimated performance of a diversity receiver. These virtual antennas were slid along the measurement track in order to obtain the fading nature of the simulated diversity receiver.

The probability distribution of the fading depth was found by taking the statistics across each of the frequency bins and each of the different measurement locations. The results from all 10 measurement-sets in Appendix C were used to estimate the performance.

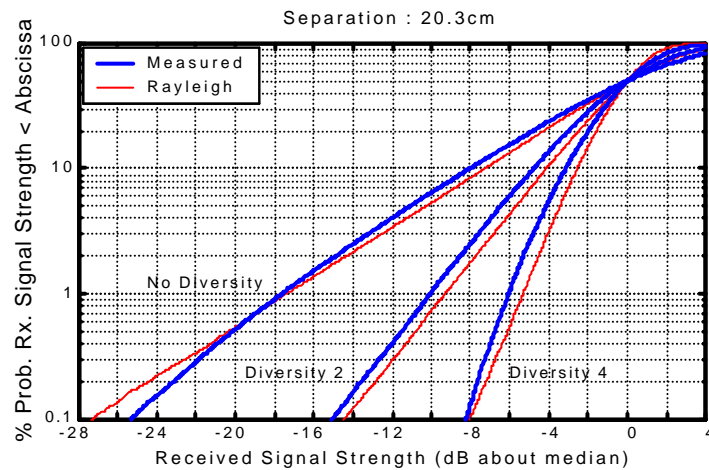


Figure A - 20, Simulated fading distribution for optimal power combining diversity reception.

Note: The data has been normalised about the median. The average power for an antenna diversity of 2 was 3.0 dB higher, and for an antenna diversity of 4 it was 6.0 dB higher. (script s0030)

Figure A - 20 shows the fading probability distribution as the amount of diversity is increased. The “No diversity” measurement shows the fading probability for a single antenna. The “Diversity 2” results show the performance of a simulated diversity

receiver using the measurement sets taken. The distance between the two antennas in this result were 20.3 cm. The “Diversity 4” result shows the result for the fading depth when the power is combined from 4 virtual antennas spaced 20.3 cm apart. Also shown on the plot is the fading depth that would be expected in a Rayleigh fading channel with zero correlation between the diversity antennas. The simulated diversity performance based on the measured channel fading show a greater fading depth than Rayleigh fading. This is likely to be partly due to correlation between the antennas spaced at 20.3 cm apart. This simulation was repeated for an antenna separation of 40 cm with similar results. The increased fading in the measured results compared with Rayleigh fading may also be due to small amounts of shadowing along the path of the measurement.

Figure A - 21 shows the fading depth as a function of the antenna separation for a receiver using an antenna diversity of 4. This shows that for antenna separations must be greater than approximately 10 cm (1/3 wavelength) in order to achieve the best performance from the diversity receiver.

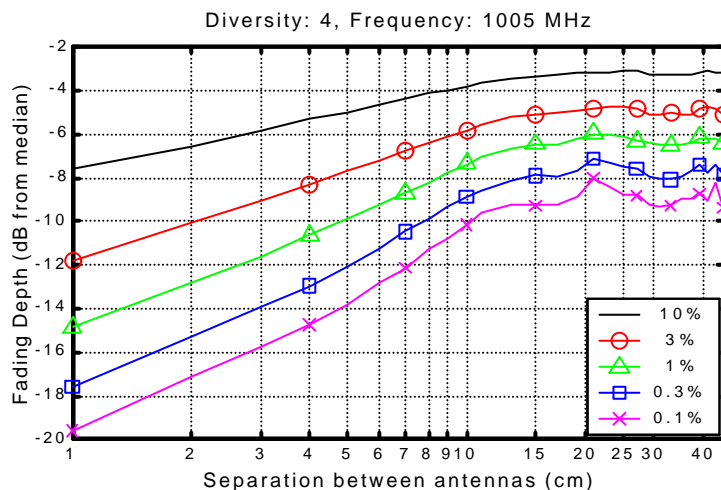


Figure A - 21, Effect of antenna separation on the fading depth for diversity reception. (script s0030)

The five results show the probability of the fading exceeding the value shown. For example, for a separation of 10 cm there is a 0.1% chance of the fading exceeding 10.1 dB. The non-smooth characteristics of the 0.1% and 0.3% probability curves are due to measurement variation.

APPENDIX D PHASE TABLES FOR EVOLVED LOW CREST FACTOR DISCRETE MULTI-TONE SIGNALS

The following tables show the phase angles of each subcarrier in radians for the phase sequence found to have the lowest crest factor. These phase sequences were developed using the genetic algorithm optimisation algorithm outlined in section 6.2.

Each column in the table represents the phase sequence for a given number of tones in the signal. Each row specifies the phase angle for each of the tones (c1, c2, etc) in the signal. For example: for a DMT signal with 9 tones the best phase sequences is:

{-0.1506, 0.8477, 1.1603, 2.7360, -0.3339, 2.0445, -0.2213, -1.2250, -2.9157}

where the lowest frequency tone (**c1**) is set to a phase of -0.1506 radians, the next tone (**c2**) is set to 0.8477 radians, through to the highest frequency tone set to a phase of -2.9157 radians (**c9**). All the tones must have the same amplitude.

N	2	3	4	5	6	7	8	9	10	11	12	13
CF (dB)	3.0096	2.2180	1.8401	1.7562	1.9353	1.9959	1.1357	0.9195	1.3760	2.0681	1.6585	1.2855
c1	0.3227	0.1739	0.0698	-0.0337	-0.2617	0.3423	0.1494	-0.1506	-0.4931	-0.0515	-0.2348	-0.1128
c2	1.4762	0.7015	0.6043	0.3935	-0.1001	0.6874	1.3464	0.8477	0.5232	0.2956	-0.2604	0.9819
c3		-1.9125	2.9478	3.0420	2.9791	1.5422	1.1741	1.1603	1.2104	1.1168	1.0707	1.5980
c4			0.8174	-0.8563	-0.6664	-2.4205	3.0161	2.7360	2.6591	2.6873	-2.9699	2.2874
c5				-2.5333	1.5292	0.6219	-0.5100	-0.3339	-0.7343	-1.9001	-1.4402	-2.4297
c6					0.3593	-1.1533	-3.1208	2.0445	2.0989	1.0755	-0.3012	0.6287
c7						-2.4180	2.5664	-0.2213	-1.4154	-2.4557	-2.1887	1.9462
c8							0.6028	-1.2250	2.7908	1.5700	0.2226	-1.2270
c9								-2.9157	1.4838	-0.5681	-1.8615	1.8849
c10									-0.1529	-1.9320	1.7537	0.2902
c11										-2.8432	1.0931	-1.1668
c12										0.0312	-1.2351	
c13											-2.7297	

N	14	15	16	17	18	19	20	21	22	23	24	25
CF (dB)	1.5296	1.4061	1.0676	1.3035	1.1744	1.2271	1.3548	1.3244	1.0552	1.2040	1.1719	0.9441
c1	-0.3143	-0.1263	-0.5219	-0.4220	-0.3229	-0.5961	-0.4055	-0.0107	-0.4534	0.2200	-0.1952	-0.2114
c2	0.2432	0.4711	0.2380	0.3865	0.2420	0.2429	0.2536	1.1275	0.6360	0.8695	0.2656	0.8631
c3	0.5139	1.2162	1.2461	0.8953	0.0416	0.4724	0.2400	0.8363	0.4350	0.9187	1.0006	0.5844
c4	1.7704	1.5999	1.2962	1.6693	1.3563	0.8890	1.0576	1.4033	1.0431	1.4434	1.0848	1.2006
c5	-2.3605	2.9087	2.6942	2.4072	-2.8477	3.0993	2.7334	2.1464	2.0145	1.7812	1.7638	1.7043
c6	-0.6212	-0.2779	-0.4868	-1.6116	-1.8718	-2.2509	-2.3239	-3.1319	-2.9506	2.7395	2.9505	-3.0657
c7	1.9108	1.5417	1.0382	1.1731	0.1778	-0.5172	-0.8969	-0.7769	-0.9944	-1.6769	-1.4679	-1.6283
c8	-1.4077	-2.7183	-2.9410	2.6807	2.3801	2.6164	1.5054	0.8011	0.9142	0.1213	0.1237	-0.5484
c9	1.8683	1.1185	0.0036	-0.8592	-1.3292	-1.8447	-1.6609	2.8528	2.3265	1.9701	2.4190	2.0344
c10	-0.3490	-1.1290	-2.6962	2.3154	1.6415	1.1984	-0.2321	-0.5192	-0.8118	-1.9034	-2.1511	-2.6010
c11	-2.9433	1.6382	1.6725	0.4448	-1.2756	-2.1785	-2.3851	2.8782	2.3203	1.8072	0.4510	-0.8429
c12	1.7131	-0.0948	-1.8216	-2.7057	2.4617	1.9484	0.0099	-1.0587	-0.9372	-1.2398	-2.1815	2.6975
c13	0.9508	-0.8998	2.6614	0.9486	0.0636	-1.5241	-2.0682	2.3418	1.9614	0.7807	0.8952	-0.7629
c14	-0.0831	-2.0682	2.2164	-0.1557	-1.2543	2.6941	1.6879	0.3070	-1.5622	-2.4343	-3.0688	2.1955
c15		-3.0921	0.8151	-1.2969	2.6074	1.4298	-0.0698	-1.8807	2.9414	1.8431	0.3025	-1.0723
c16			-0.3348	-2.1686	0.9460	-1.1177	-2.1905	2.0249	0.9088	-0.3910	-1.7525	-2.7590
c17				2.9411	0.7987	-1.8713	1.8195	0.3572	-1.3860	-2.5124	2.0835	0.8732
c18					-0.1094	-2.4346	1.3435	-0.4166	-2.9621	1.4247	0.1917	-1.5739
c19						2.6738	0.4657	-1.7183	2.0559	0.3541	-1.9411	-2.8132
c20							-0.4869	-1.8388	1.2277	-1.1698	2.8961	1.5308
c21								-3.0810	1.1041	-0.8913	1.9613	-0.1880
c22									-0.1812	-2.3530	1.6802	-0.8995
c23										-3.1265	0.7232	-2.1706
c24											-0.0529	-1.9480
c25												2.8559

Appendix D

Phase tables for evolved low Crest Factor Discrete Multi-Tone signals

N	26	27	28	29	30	31	32	34	36	38	40	42
CF (dB)	0.8956	1.0133	1.1251	1.1699	1.2577	1.0325	1.1387	0.9430	0.9542	1.1888	1.1130	0.9188
c1	-0.5829	-0.9571	-0.7045	-0.4533	-0.3604	-0.5336	-0.4014	-0.3149	-0.8210	-0.5677	-0.4621	-0.6650
c2	0.3906	-0.0206	0.6325	0.6797	0.4653	0.3320	0.3673	0.4108	0.0075	0.3619	0.3729	0.2501
c3	0.3867	0.1552	0.3764	0.4762	0.1261	0.6501	0.7934	0.5717	0.2890	0.3591	0.6553	0.4720
c4	1.1177	0.8282	1.3278	1.5319	0.7180	0.5086	1.0739	1.1594	0.8382	0.7963	0.4722	0.7403
c5	1.4465	1.3389	1.8584	1.4224	1.2045	1.3927	1.2120	1.2048	1.2137	1.2182	1.4019	0.8690
c6	2.9086	2.8253	-2.9376	2.7094	2.5228	2.2783	2.4187	2.0015	1.5555	1.8393	1.4324	1.5233
c7	-1.7391	-2.1450	-2.2856	-2.9256	-2.3025	-2.2570	-2.6220	-3.1093	2.7923	2.8033	2.8631	2.8752
c8	-0.2711	-0.3521	-0.4919	-1.3678	-1.3458	-1.4864	-0.7328	-1.7771	-2.1231	-2.5376	-2.5514	-2.2075
c9	1.6222	1.4643	2.1462	1.1630	0.4167	-0.1381	-0.0796	-0.0199	-0.7593	-1.1638	-1.1878	-1.0911
c10	-2.3949	-2.7933	2.8563	2.2907	2.2077	1.8730	1.7388	1.2619	1.1484	0.2462	0.0834	-0.6207
c11	-0.7489	-0.5723	-1.5618	-2.1579	-2.0624	-2.5096	3.1500	2.8907	2.7525	2.0819	1.9094	1.1940
c12	2.1981	1.4586	1.3100	0.8547	0.3606	-0.4489	-0.7996	-1.5420	-2.2753	-2.5713	-3.1608	3.1359
c13	-0.8726	-0.9790	-3.1740	2.3575	2.7569	2.3360	1.3554	0.6230	-0.3638	-1.2097	-1.3888	-1.8455
c14	2.1356	1.5357	-0.0985	-0.3045	-0.6869	-0.6500	-2.3914	-3.0363	2.1613	1.3177	1.0749	-0.1139
c15	-1.3128	-1.2534	2.5837	2.0418	1.7489	1.4047	0.9445	-0.4022	-1.1893	-2.8029	2.8850	2.1152
c16	1.7840	0.9763	-0.5141	-0.4666	-1.5344	-2.3154	2.9156	2.3104	1.3805	-0.0982	-0.8644	-1.8366
c17	-0.0779	-1.3895	2.4841	1.8283	2.0342	1.2316	-0.5656	-1.7308	-2.0996	2.5932	1.7838	0.7421
c18	-2.5874	2.5171	0.8816	-0.2637	-0.9305	-1.0011	-3.1489	1.3148	-0.3464	-0.8781	-2.5896	2.8478
c19	1.5684	0.1765	-1.3547	-2.2402	2.7093	1.7453	1.3227	-1.1314	2.8437	1.7511	0.1747	-1.0847
c20	-0.1587	-1.9856	2.3095	1.3832	0.2070	-1.2617	-1.9902	2.2394	0.5848	-1.6820	-3.0595	1.8793
c21	-2.0296	2.5702	1.0751	-0.4963	-2.0972	2.8037	1.6270	-0.5740	-2.2136	1.7913	0.1660	-0.9072
c22	2.5737	0.9878	-0.3762	-2.2303	2.1859	0.6821	-1.0669	2.8915	1.2249	-1.1803	3.0464	2.2257
c23	2.0077	-0.7581	-1.8973	2.4868	0.2709	-1.4959	-2.8259	0.5376	-1.4301	2.5155	0.4225	-1.4130
c24	1.0272	-1.4714	2.7017	0.6037	-0.8273	-3.0624	1.6379	-1.5150	1.8821	0.5050	-2.3310	1.6738
c25	0.7693	-2.4172	1.6071	-0.5767	-2.5348	2.2266	-0.3347	2.9585	-0.0296	-2.7667	1.3548	-0.8591
c26	-0.4273	-2.6937	1.4484	-1.0221	2.2722	0.2583	-1.6185	1.4737	-1.9153	1.4545	-1.5782	-3.0616
c27		2.4435	0.8836	-2.0902	1.4935	-0.7889	-2.8143	-0.4702	2.5881	-0.7649	2.1346	0.5837
c28			-0.0145	-2.2062	0.6615	-1.9006	2.2819	-1.9919	1.2642	-2.6260	0.7646	-2.0106
c29				2.7755	0.7787	-1.8910	1.6006	2.9169	-0.2843	2.2196	-1.3526	1.8169
c30					-0.1720	-2.4314	1.3488	1.9349	-2.5088	1.0373	-3.0078	0.0015
c31						2.7566	0.9095	1.6870	2.3292	-1.3894	1.6859	-1.4456
c32							-0.0790	0.9137	1.9995	-2.6045	0.1360	2.7574
c33								0.5499	1.2610	2.6657	-1.0742	0.7891
c34								-0.3637	0.8912	2.0626	-2.4307	0.0535
c35									0.3888	1.7345	2.4731	-1.1556
c36									-0.5790	1.0586	1.8962	-2.4971
c37										0.5361	1.2238	2.3982
c38										-0.7169	0.8796	1.5205
c39											0.5340	1.2946
c40											-0.3249	0.9101
c41												0.5586
c42												-0.5792

Appendix D

Phase tables for evolved low Crest Factor Discrete Multi-Tone signals

N	44	46	48	50	52	54	56	58	60	62	64	68
CF (dB)	1.0488	0.8532	1.0083	0.6722	1.0039	1.0210	1.0769	0.8749	0.9523	0.8729	0.6497	0.9294
c1	-0.3672	-0.7000	-0.4721	-0.7352	-0.6789	-0.7884	-0.4569	-0.6801	-0.7019	-0.6667	-0.7835	-0.5704
c2	0.3432	0.3875	0.1339	0.3779	0.1906	-0.0295	0.3630	0.0328	0.1436	0.2478	0.1563	0.1868
c3	0.5836	0.2467	0.4575	0.3017	0.4815	0.1621	0.5291	0.1928	0.4523	0.2959	0.5840	0.3545
c4	0.7219	0.7115	0.7983	0.9442	0.6655	0.5736	0.4339	0.7313	0.4302	0.7634	0.6903	0.7806
c5	1.2275	0.9359	0.9406	1.0287	0.8392	0.7504	0.8594	0.5182	0.9408	0.7533	1.1734	0.8108
c6	1.3225	1.4730	1.3388	1.4566	1.4530	1.1877	1.1233	1.1379	0.9331	1.1853	1.1812	1.1655
c7	2.5813	2.0500	1.9793	1.9028	1.9162	1.4858	1.5157	1.2884	1.5048	1.4275	1.6980	1.5260
c8	-2.9130	3.0362	2.8013	2.7648	-3.0122	2.8974	2.6563	2.4689	2.2287	2.1635	1.9463	1.9038
c9	-1.6215	-1.9820	-2.1956	-2.3763	-2.3523	-2.3066	-2.5743	-2.9679	3.1185	-2.9599	2.6055	2.8857
c10	-0.1148	-0.6402	-0.6336	-0.8215	-1.1346	-1.5871	-1.5045	-1.9419	-2.1950	-2.2701	-2.7304	-2.6889
c11	0.9026	0.7848	0.2664	0.3426	-0.0766	-0.2847	-0.5095	-0.6344	-1.1982	-0.9832	-1.4055	-1.7162
c12	2.2961	1.9352	1.5782	1.4733	1.4008	0.8171	0.4431	0.1380	0.1677	-0.1305	0.1101	-0.1916
c13	-2.4891	-2.9942	2.9442	2.9686	2.7835	2.3480	1.5955	1.6668	1.2287	1.0528	0.8676	0.5077
c14	-0.6867	-1.0353	-1.8006	-1.8313	-2.2711	-2.6512	-3.0269	2.8013	2.6587	2.4118	2.0974	1.6667
c15	1.3393	0.9616	-0.1107	-0.6294	-0.5667	-1.2032	-1.4292	-2.0510	-2.4811	-2.6299	2.9992	2.8141
c16	-2.5187	2.8628	2.2626	1.5694	0.9741	0.6087	-0.3139	-0.3167	-0.9637	-1.3186	-1.9585	-2.3353
c17	-0.6639	-0.5815	-1.8677	-2.2438	2.7530	2.3404	1.8224	1.4508	0.9293	0.0809	-0.4962	-0.7795
c18	1.8657	1.1936	0.5809	-0.3744	-0.8721	-1.8494	-1.9364	-2.8582	2.8924	2.1213	1.3926	0.7742
c19	-2.3839	3.0835	2.5210	2.1426	1.0696	0.4444	-0.6170	-0.5493	-1.1724	-1.9283	-2.9933	2.4492
c20	0.0889	-0.5971	-1.7114	-2.0635	-3.0606	2.6097	1.7261	1.3563	0.3667	-0.2694	-0.6423	-1.7441
c21	-2.8912	2.0551	0.6757	-0.4308	-0.9262	-1.7029	-2.5369	2.9154	2.3373	1.8720	1.2220	-0.0628
c22	0.3033	-0.9431	-2.6329	2.1787	1.0332	0.3565	-0.7227	-1.1108	-2.1961	-2.5529	2.8977	2.1223
c23	-2.9116	1.8758	0.3225	-1.0803	-2.3703	3.0093	2.1748	0.9232	-0.0318	-0.8347	-1.4798	-2.6220
c24	0.0258	-1.3403	-2.8739	2.2229	0.5155	-0.7822	-0.9733	-2.7273	2.4565	1.3890	0.2800	-0.6854
c25	2.8702	1.9808	-0.0042	-1.2851	-2.9012	2.3798	1.3279	0.3433	-1.0163	-2.0489	2.5534	1.3666
c26	0.2683	-1.4494	-2.8411	1.7615	-0.4085	-1.2429	-2.6372	2.9597	1.6513	0.6896	-0.5654	-2.4149
c27	-1.9066	2.0542	0.1173	-1.2243	2.7218	1.7050	0.4609	-1.1158	-2.0357	2.9681	2.3140	-0.1885
c28	1.7153	-0.7006	-2.9921	1.6631	-0.0010	-1.3516	-3.0237	1.6976	0.6948	-0.6911	-1.5420	2.4267
c29	-0.2730	-2.7771	1.0007	-1.4652	-3.0028	1.8828	-0.1642	-1.6372	-2.9798	2.0081	1.3881	-1.3311
c30	-2.8585	1.6437	-1.0190	2.0946	0.2127	-1.0003	-3.0967	1.3636	0.2506	-1.4256	-2.3820	1.1651
c31	1.2455	-1.3606	2.7344	0.2802	-2.6815	2.3665	0.5005	-1.6701	-3.0891	1.4110	0.1274	-2.3946
c32	-0.7053	2.8467	0.5492	-1.8986	1.4559	-0.3768	-2.6081	1.6232	-0.0492	-1.7298	2.8932	0.3747
c33	-2.3283	0.7961	-1.8102	1.7008	-0.8815	2.9570	1.1446	-0.9255	-2.8405	1.5877	-0.3090	-0.0881
c34	2.4368	-1.3169	2.0218	-0.2990	3.1091	0.6540	-1.8752	2.7487	1.1903	-1.4759	-3.1493	-0.6730
c35	1.2489	-2.8254	0.0873	-2.8069	1.1070	-1.4388	1.8172	-0.1022	-1.5990	1.9953	0.5707	2.5292
c36	-0.3926	2.2126	-1.6138	1.0969	-1.5870	2.4983	-0.0499	-3.0374	1.6111	-0.7370	-2.1429	-0.0798
c37	-1.8174	0.6240	-3.0148	-0.1580	2.6815	0.3348	-2.2540	1.1117	-1.2978	3.0216	1.1638	-2.9887
c38	-2.7548	-0.8536	1.8347	-1.6587	1.1917	-2.1628	1.5175	-1.2671	2.3931	0.2769	-1.3367	0.3024
c39	2.1135	-2.2546	0.6339	2.9571	-0.4992	2.1011	-0.4935	-3.0846	-0.0142	-2.5463	1.9122	-2.3995
c40	1.9022	2.9083	-1.1641	1.6481	-2.1881	0.3947	-2.0663	1.4485	-1.8393	1.3008	-1.2923	1.3895
c41	1.2528	2.2125	-2.3612	0.2191	2.5539	-1.1368	1.7524	-1.0391	2.3669	-0.6000	2.6550	-1.3474
c42	0.9751	1.4862	2.8254	-1.3656	1.0655	-2.7156	0.1328	3.1166	0.3053	-2.3550	0.8180	2.2887
c43	0.5931	1.1656	2.0170	-2.5138	0.1223	1.7299	-1.4355	1.2083	-1.7704	1.5442	-1.2039	-0.0083
c44	-0.2685	0.5731	1.4102	2.7592	-1.1403	0.6352	-2.6827	-0.5498	2.4762	-0.3322	-2.9384	-2.6748
c45	0.5402	0.9778	2.1742	-2.1715	-0.6424	2.3331	-2.1088	0.6573	-2.3587	1.2920	1.5029	
c46	-0.6584	0.6993	1.5828	2.6519	-1.5142	0.5475	2.8748	-0.9696	1.6590	-1.1409	-0.4603	
c47		0.0871	1.3137	2.0792	-2.6212	-0.5064	1.3968	-2.3428	0.1694	-3.1044	-2.3329	
c48		-0.5210	0.5684	1.3803	2.2131	-1.7908	0.3041	2.3522	-1.1659	1.2369	1.7310	
c49			0.5436	1.0299	1.7482	-2.5594	-0.9327	1.1951	-2.6036	-0.3547	0.2683	
c50				-0.6785	0.7499	1.0925	2.4951	-2.1376	0.2201	2.2904	-1.7418	-1.9861
c51					0.3466	0.9813	1.7183	-3.0444	-1.1460	0.9572	-2.7516	2.3589
c52					-0.5345	0.4964	1.1610	1.9861	-2.3085	0.0232	2.1755	0.8216
c53						0.3370	0.4787	1.7187	2.9152	-1.3000	1.3396	-0.8130
c54						-0.6012	0.5756	1.0270	2.1406	-2.2198	-0.3440	-2.1344
c55							0.1020	1.0400	1.4442	2.9698	-1.7062	2.9409
c56							-0.7951	0.4752	1.4224	2.0668	-2.7104	1.5242

Appendix D

Phase tables for evolved low Crest Factor Discrete Multi-Tone signals

N	44	46	48	50	52	54	56	58	60	62	64	68
c57							0.2111	0.8376	1.7619	2.7551	0.8373	
c58							-0.6500	0.5449	1.1821	2.4264	-0.8283	
c59							0.2177	1.0896	1.7888	-1.7630		
c60							-0.6123	0.5940	1.6728	-2.6455		
c61							0.4198	0.4198	1.0345	2.5010		
c62							-0.5951	0.7952	2.1024			
c63							0.3031	0.3031	1.5230			
c64							-0.6640	1.1232	1.0375			
c65									0.5432			
c66									0.1909			
c67									-0.6021			
c68												

N	72	76	80	84	88	92	96	100	104	108	112	116
CF (dB)	0.9224	0.9004	0.8051	0.8633	0.9003	0.8837	0.8998	0.6708	0.8852	0.8263	0.8374	0.8069
c1	-0.6861	-0.6972	-0.7469	-0.7355	-0.8858	-0.6389	-0.7659	-1.0036	-0.7377	-0.7658	-0.7753	-0.9469
c2	0.0671	-0.0120	-0.0116	-0.1188	-0.0457	0.0231	0.0154	-0.0002	-0.0764	0.0072	-0.3397	-0.2138
c3	0.4416	0.3344	0.2892	0.5384	0.4424	0.4863	0.2398	0.2398	0.4068	0.4141	0.2850	0.1987
c4	0.6019	0.3765	0.3344	0.4895	0.4715	0.3326	0.4169	0.4514	0.4454	0.5016	0.3990	0.4265
c5	0.6375	0.8151	0.9408	0.7691	0.5208	0.7694	0.6500	0.6684	0.6839	0.7828	0.5517	0.4817
c6	0.9717	0.8289	1.0345	0.8654	0.7716	0.7614	0.9996	0.6667	0.8385	0.7309	0.6932	0.4959
c7	1.3853	1.3681	1.3855	1.2637	0.9632	1.2176	1.0433	1.1146	1.1183	1.0695	1.0401	1.0356
c8	1.6246	1.6048	1.5176	1.5870	1.4363	1.2933	1.3393	1.1450	1.3025	1.2948	0.9633	1.0141
c9	2.7834	2.6674	2.2400	2.0021	1.8708	1.7746	1.6643	1.6031	1.6671	1.6310	1.4882	1.5177
c10	-2.8044	-2.8573	2.9111	2.9602	2.9601	2.4941	2.3653	2.1290	2.0159	1.7216	1.6235	1.5938
c11	-1.8176	-2.0895	-2.5009	-2.8036	-2.6516	-2.8566	3.0443	-3.1611	3.0787	2.8995	2.6346	2.6478
c12	-0.8856	-1.1437	-1.7297	-1.6187	-1.8695	-1.9055	-2.3639	-2.5192	-2.6973	-2.9583	-3.0622	-2.8323
c13	-0.1275	-0.0518	-0.2932	-0.6464	-1.3170	-1.3676	-1.5927	-1.6074	-1.8753	-2.1581	-2.4541	-2.4789
c14	1.2794	0.9746	0.5979	0.2201	-0.3309	-0.2810	-0.3647	-0.7230	-1.0212	-1.3435	-1.5075	-1.6779
c15	2.4086	2.2262	1.5301	1.0814	0.6919	0.2593	0.2070	-0.1738	-0.1728	-0.4016	-0.7752	-0.9228
c16	-2.7184	-3.0929	2.7031	2.2221	2.1507	1.4053	1.0833	0.9185	0.5795	0.3389	0.0317	-0.2864
c17	-1.6562	-1.9219	-2.4549	-3.0267	3.0035	2.4688	2.1560	1.7356	1.5719	1.4006	0.7645	0.7529
c18	-0.2459	-0.6345	-1.4926	-1.8980	-2.4203	-2.4918	-2.9158	2.9797	2.6868	2.0650	1.7852	1.8157
c19	1.6097	0.9672	0.0237	-0.5255	-1.1236	-1.4686	-2.0656	-2.3355	-2.4615	3.0692	2.8636	2.7581
c20	3.1309	2.7993	1.3832	0.5278	0.1325	-0.3694	-0.8161	-1.4017	-1.7914	-2.3070	-2.5992	-2.6080
c21	-1.0041	-1.7787	3.0201	2.4505	1.8730	1.1968	0.3760	-0.2339	-0.5234	-1.1926	-1.6144	-1.8518
c22	0.9375	-0.1004	-1.1431	-2.0812	3.0417	2.6468	1.8348	1.1226	0.4545	0.1007	-0.4089	-0.8077
c23	2.5232	1.9582	0.4427	-0.4302	-1.2424	-2.0269	-2.7773	2.7050	2.0629	1.3485	0.8068	0.4794
c24	-1.9461	-3.0654	2.3819	1.3692	0.2823	-0.2191	-1.0387	-1.8679	-2.7561	2.5806	2.2174	1.7830
c25	-0.1862	-1.2147	-2.4055	2.9360	2.0503	1.0815	0.2426	-0.4825	-1.0706	-1.9250	-2.5544	2.9035
c26	2.0442	0.5070	-0.7708	-1.6896	-2.8649	2.6278	2.1404	1.3058	0.2855	-0.2796	-0.8179	-1.6241
c27	-1.7175	2.6819	1.1059	-0.0968	-0.9999	-2.0802	-2.8470	2.8351	1.9844	1.2717	0.4857	-0.3113
c28	0.8779	-1.1901	3.0395	2.0294	0.3687	-0.4539	-1.4186	-2.1100	-2.8905	2.6578	2.0677	1.3172
c29	-3.1097	1.2490	-0.7513	-1.9350	2.4674	1.4949	0.2562	-0.7079	-1.3576	-2.3257	3.0588	2.7049
c30	-1.1233	-2.8021	1.8023	0.3951	-1.4218	-2.6548	2.2465	0.9628	0.0417	-0.9015	-1.6343	-2.3766
c31	1.5811	-0.4043	-2.1077	2.5590	0.7627	-0.4297	-2.1279	2.8420	1.7231	0.7235	-0.0612	-0.9348
c32	-1.7815	1.9089	0.0959	-1.6143	2.8720	1.7372	-0.0009	-1.0626	-2.6406	2.6697	1.5301	0.5498
c33	0.6051	-1.8087	2.5106	0.5654	-1.1565	-2.4155	2.3330	1.1234	-0.6329	-1.3239	-2.8177	2.3433
c34	-2.9583	0.8689	-1.0872	3.1468	0.7188	-0.5696	-1.9034	3.1033	1.7888	0.4549	-0.4780	-2.0182
c35	0.0248	-2.4081	1.3842	-0.6702	-3.0616	1.8001	0.2340	-1.2758	-2.5175	2.4601	1.4845	-0.0251
c36	2.8981	0.2654	-2.3920	1.9211	-0.3502	-2.3031	2.3810	0.7853	-0.7884	-1.9776	3.0729	2.1948
c37	-0.3168	-3.0333	0.5058	-1.9033	2.1946	-0.0612	-1.6561	2.7275	1.4331	0.0351	-1.1308	-2.2287
c38	3.0766	0.2555	-2.8174	0.3182	-1.4208	2.6383	0.7548	-0.9836	-2.7191	2.1437	0.8961	-0.7003
c39	0.0601	-2.5411	0.0383	-3.1111	1.0603	-1.0572	-3.1186	1.3982	-0.3860	-1.8098	2.6770	1.4583
c40	-2.6936	0.0030	-2.9493	0.2392	-2.6014	1.4675	-0.8389	-2.5771	1.9429	0.2397	-1.1609	-2.8583
c41	0.8634	-3.0807	0.4816	-2.8592	0.4419	-2.0855	2.0238	-0.1267	-2.0419	2.4140	0.8404	-0.7853

N	72	76	80	84	88	92	96	100	104	108	112	116
c42	-2.0177	0.3177	-2.4826	-0.1961	-2.8667	1.1797	-1.3930	2.2203	0.4488	-1.5700	-3.1907	1.5227
c43	1.4951	-2.5935	0.4849	2.8889	0.1705	-2.5735	1.4013	-1.3171	2.9062	0.6431	-0.7292	-2.3322
c44	-0.5638	0.8095	-2.9585	0.3204	-2.9636	-0.2011	-2.0799	1.7967	-0.7242	-3.0534	1.5113	-0.3342
c45	-2.7434	-1.6741	0.2981	-2.8779	0.2069	2.9329	0.6749	-1.6232	2.0079	-0.2172	-2.4031	2.0317
c46	0.6716	2.1891	-2.1759	-0.0675	2.8942	0.1070	-2.6298	0.9656	-1.5583	2.4954	0.4096	-1.7712
c47	-1.8162	-0.5177	1.5117	-2.8619	-0.1515	-3.0283	0.1355	-2.4869	1.2521	-1.2666	3.0225	0.7812
c48	2.1157	-2.7164	-1.2387	0.9096	-2.9905	-0.0428	2.9670	0.5701	-2.1251	1.1752	-0.8643	-2.9156
c49	0.1736	1.3620	2.6642	-1.7735	0.7792	-3.1128	-0.2146	-2.8821	0.8185	-2.1634	1.8476	-0.3969
c50	-1.6722	-1.3635	0.5259	1.7702	-2.0721	0.8315	3.0280	-0.4373	-2.6679	0.8705	-1.5430	2.2173
c51	2.8352	2.4864	-2.0268	-0.7533	1.3306	-2.2092	0.1068	2.6013	0.1766	-2.6780	1.1712	-1.2458
c52	0.9984	0.5620	1.6712	3.0899	-1.3773	0.8415	-2.7691	0.0887	-2.9540	-0.0642	-2.3982	1.5444
c53	-1.3271	-1.2187	-0.7918	0.7079	2.3569	-2.0355	0.7887	-2.6666	0.0248	2.9313	0.4401	-2.1686
c54	-3.0749	-2.8662	-2.9573	-1.5378	-0.1726	1.5102	-2.0651	0.5131	3.1644	0.0787	-2.8679	0.2299
c55	1.3259	1.6179	1.2412	2.6066	-2.7266	-1.0009	1.4074	-2.3760	0.3385	-2.8547	0.2759	-3.0749
c56	-0.0329	-0.0716	-0.5799	0.1037	1.3551	2.5854	-1.5262	1.1753	-2.4858	-0.1880	-2.7742	0.3728
c57	-1.3320	-2.0636	-2.2175	-2.3412	-0.8539	0.3665	1.8211	-1.7545	0.6473	2.9078	0.3229	-2.7035
c58	-2.6034	2.2896	2.1795	1.8205	-2.8624	-2.0818	-0.5466	1.4018	-2.2158	0.2763	-2.7532	0.2076
c59	2.4443	0.7491	0.6701	0.0622	1.0095	1.7978	-3.0620	-1.5150	1.2184	-2.5950	0.1274	-3.0063
c60	1.0160	-0.6902	-1.3607	-1.5604	-1.5219	-0.2034	0.8035	2.3252	-1.5287	0.4950	-3.0808	0.2353
c61	0.1063	-2.0320	-3.0140	-3.0502	2.6636	-2.2782	-1.6594	-0.0421	1.9524	-2.2933	0.5267	-2.8597
c62	-0.9924	2.9758	1.4980	1.1936	0.9563	1.4910	2.3577	-2.4315	-0.9064	1.4329	-2.3453	0.0314
c63	-1.9425	1.7720	0.0260	-0.3707	-0.8957	-0.8523	0.3532	1.4451	2.8212	-1.1005	1.0182	-3.1401
c64	-2.8248	0.7931	-1.4147	-2.2732	-2.4266	-2.9009	-1.9252	-1.2333	0.5110	2.4801	-1.8734	0.5307
c65	2.2536	-0.2054	-2.4270	2.0397	2.0508	1.4884	2.0050	2.9692	-2.0299	-0.4942	1.7033	-1.9827
c66	1.8256	-1.2716	2.3824	0.7175	0.4364	0.0002	-0.1110	0.8825	1.7890	-3.0720	-0.8239	1.4337
c67	1.3196	-2.3383	1.7019	-0.5662	-1.7780	-1.8250	-2.1724	-1.2021	-0.4167	0.8239	2.7558	-1.3706
c68	0.9003	3.1519	0.4377	-1.7440	2.9128	3.0465	2.0333	3.0915	-2.7478	-1.4074	0.0251	2.0911
c69	0.7405	2.1388	-0.5969	-2.9219	1.6010	1.3961	0.4020	0.8461	1.3127	2.6906	-2.5482	-0.5203
c70	0.4973	1.7964	-1.8181	2.1911	0.4633	-0.4259	-1.2518	-1.5093	-0.4498	0.0665	1.5492	-2.9986
c71	-0.0178	1.1865	-2.6996	1.1423	-0.9774	-2.1782	-2.5410	2.8179	-2.7783	-1.9632	-1.0056	0.6881
c72	-0.8284	1.2249	2.6187	0.3590	-2.1490	2.5983	1.7239	1.1136	1.2356	2.0999	-3.1290	-1.7378
c73		0.8148	2.2143	-0.7781	2.8014	0.9609	0.4867	-0.3724	-0.7943	0.0586	0.8471	1.9667
c74		0.6875	1.9329	-2.0153	1.7344	-0.2504	-1.3121	-1.7864	-2.8426	-1.8047	-1.5785	-0.2102
c75		0.2836	1.4958	-2.4958	1.0341	-1.3296	-3.0224	2.8255	1.5869	2.4570	2.8117	-2.4847
c76		-0.6144	1.4039	2.6945	0.0060	-2.4597	1.6995	1.1563	0.2840	0.1865	0.9469	1.3983
c77			0.8729	2.3011	-0.7725	2.7181	0.3158	-0.3789	-1.3542	-1.7887	-1.2090	-0.7006
c78			0.7725	1.7931	-1.7108	1.3831	-0.9101	-2.1069	-2.8506	2.6368	-3.0035	-2.8922
c79			0.3563	1.5292	-2.5232	0.5130	-1.9390	2.4379	1.6728	0.9221	1.3405	1.3369
c80			-0.5579	1.0539	2.5431	-0.5725	-3.0024	1.0925	0.5126	-0.6257	-1.0974	-0.3373
c81				1.1664	2.0256	-1.2022	2.0205	-0.1696	-1.5072	-2.0306	-2.9022	-2.2106
c82				0.6653	1.6257	-2.2044	1.1068	-1.1539	-2.8432	2.7829	1.5777	1.8132
c83				0.3064	1.1989	-3.0229	0.2823	-2.1756	1.6894	1.1543	0.1836	-0.0160
c84				-0.6421	1.2513	2.3089	-0.8583	2.8138	0.5859	-0.5095	-1.5793	-2.1995
c85					0.5739	1.8568	-1.7861	1.9468	-0.6071	-2.2028	-2.7414	2.1630
c86					0.6339	1.4073	-2.5308	0.7093	-1.4727	2.7692	2.0058	0.7235
c87					0.1103	1.2557	2.8707	0.0074	-2.7245	1.4961	0.6612	-0.8172
c88					-0.6099	0.8507	2.2122	-0.8430	2.5004	0.1810	-1.2049	-2.2212
c89						0.6870	1.7197	-1.8312	1.4523	-1.0191	-2.5939	2.7018
c90						0.4272	1.4970	-2.4640	0.8080	-2.2010	2.0889	1.0312
c91						0.1431	1.2120	2.7894	-0.3709	-3.0702	0.8514	-0.3606
c92						-0.8474	0.9322	2.1596	-1.0840	2.4456	-0.3341	-2.1550
c93							0.5962	1.6452	-2.0584	1.2618	-1.3403	2.8524
c94							0.4992	1.5605	-2.6752	0.4539	-2.4015	1.4829
c95							0.0482	1.0452	2.5349	-0.4378	2.9214	0.4138
c96							-0.7330	0.9521	2.1728	-1.3209	1.7945	-0.6603
c97								0.7100	1.7766	-2.3394	0.9670	-1.8051
c98								0.4766	1.5803	-2.7186	0.1169	-2.6548

N	72	76	80	84	88	92	96	100	104	108	112	116
c99							0.1485	1.1497	2.4057	-0.6887	2.3440	
c100							-0.9304	0.9462	2.1433	-1.5434	1.2983	
c101							0.6292	1.7351	-2.4048	1.0119		
c102							0.5707	1.5692	-2.9808	-0.1187		
c103							0.0477	0.9804	2.2931	-0.6227		
c104							-0.7345	0.8391	2.0836	-1.4272		
c105							0.6945	1.5164	-2.4593			
c106							0.5567	1.4124	-3.1239			
c107							-0.0242	1.1343	2.2061			
c108							-0.7372	0.8605	1.9351			
c109							0.8073	1.5512				
c110							0.4219	1.5053				
c111							0.0069	1.1244				
c112							-0.6813	0.9867				
c113								0.6648				
c114								0.6057				
c115								0.1390				
c116								-0.6981				

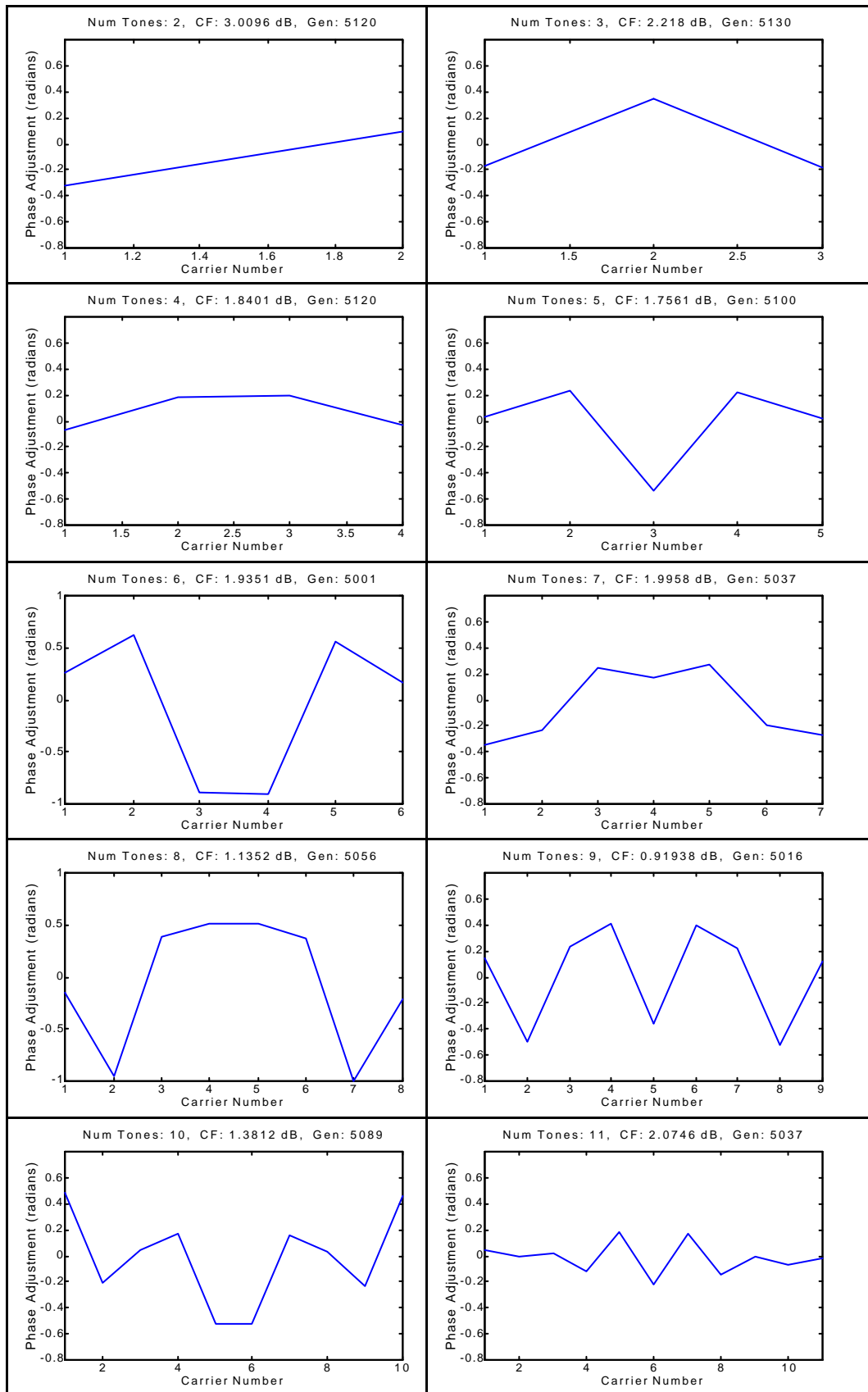
D.1 PHASE DIFFERENCE BETWEEN EVOLVED LOW CF DMT SYMBOLS AND NEWMANN'S PHASING SCHEME

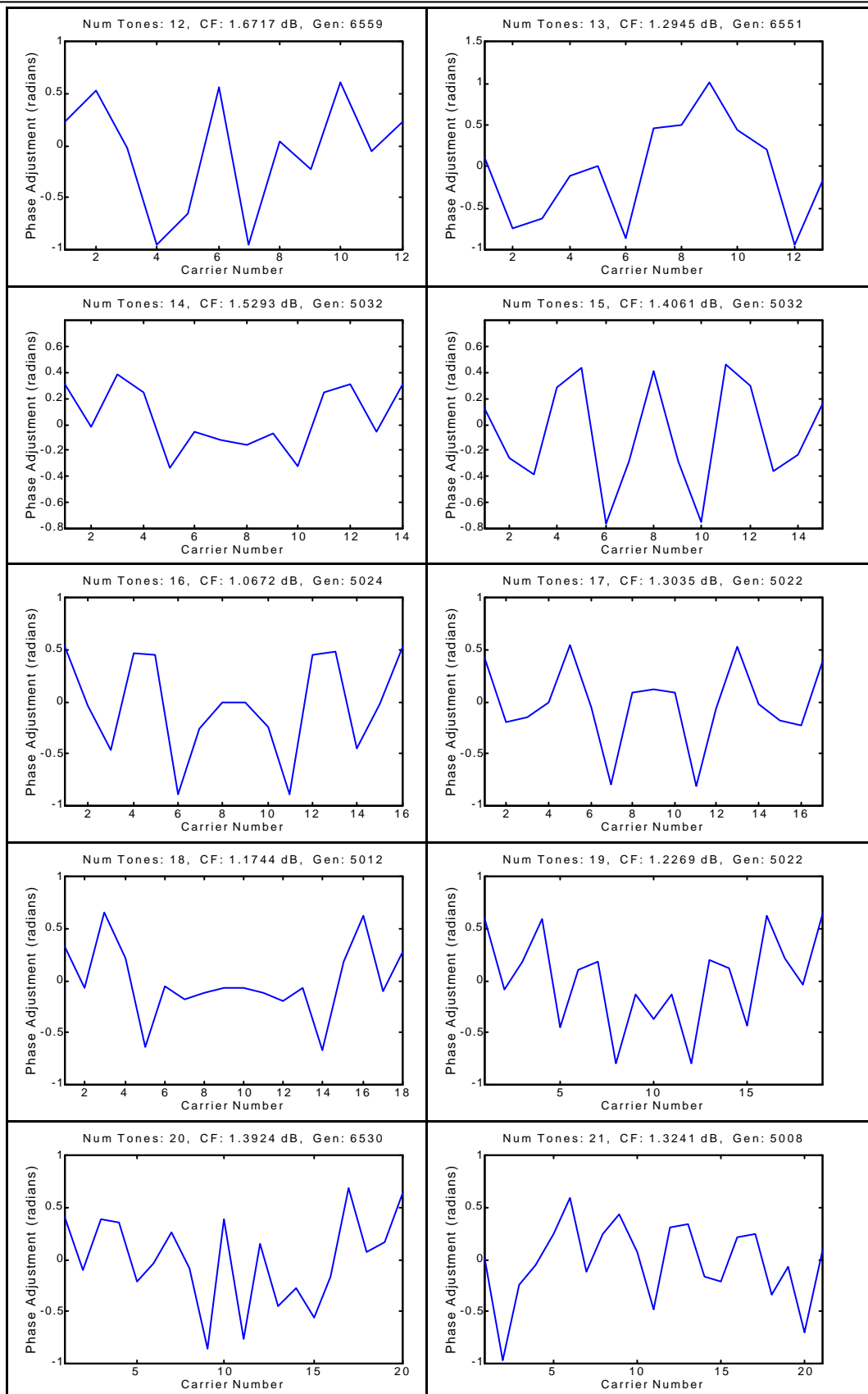
These plots show the difference between the evolved phase sequences outlined in Appendix D and the original starting point using Newmann's phasing scheme as shown in equation A3-1

$$\mathbf{q} = \frac{\mathbf{p}(k-1)^2}{N} \quad \text{A3-1}$$

The evolved phase sequences correspond to the phase shown in A3-1 plus the phase difference shown here in D.1. The results show that the difference is a complex sequence, which is almost fractal in nature. It is important to remember that due to the process of evolution the results shown may not be the global minima but local minima. In addition, if the evolution was run again the results might vary slightly. The main variations appear to be mirroring in the X or Y axis, or resulting in a completely different sequence. Sequences for tones from 2 – 30 have been simulated twice. The only major variations between the different evolution runs was for 12 tones the sequence was mirrored in the X axis and for 13 tones the sequence was quite different.

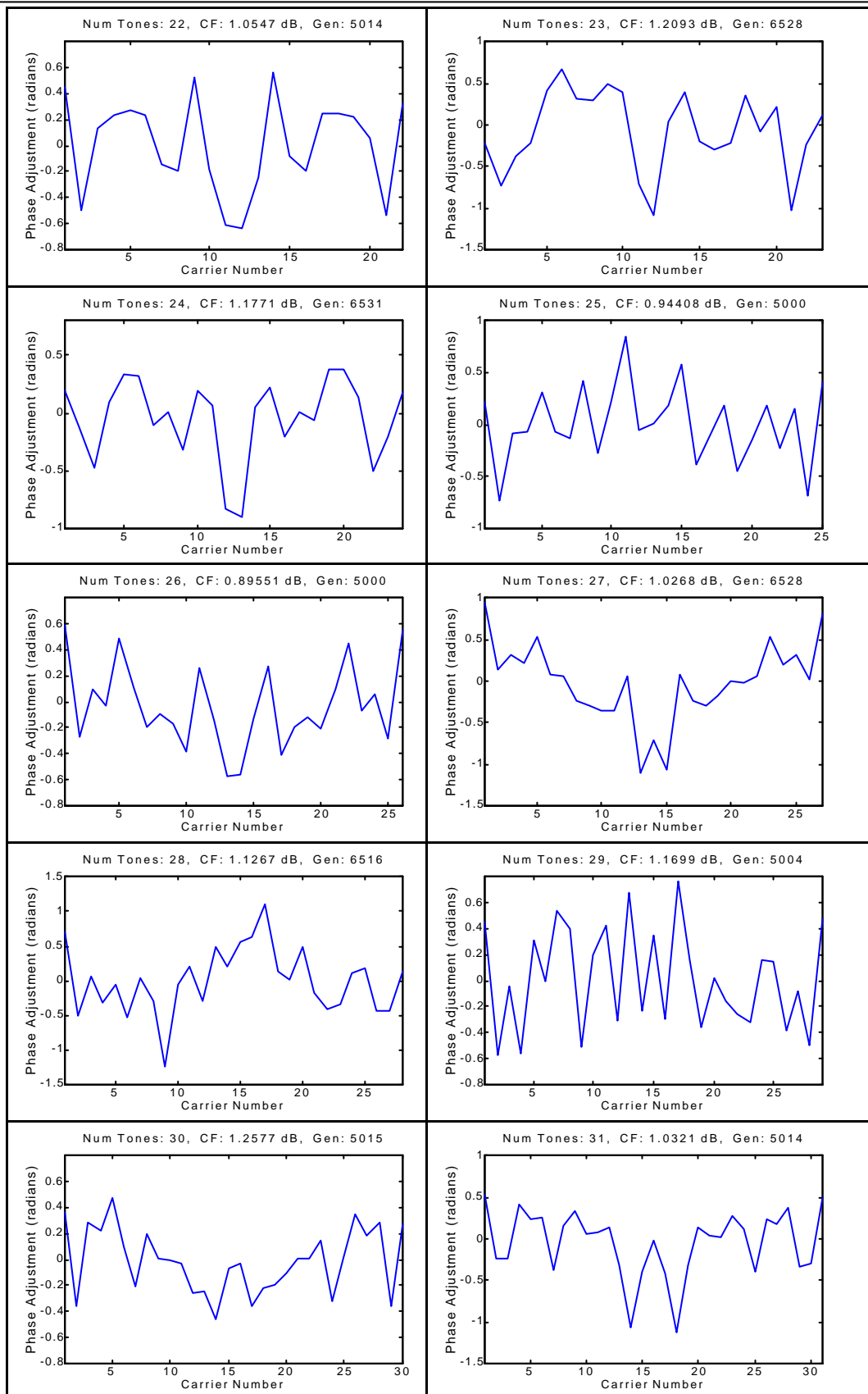
The evolved results give a clue as to the optimal phasing scheme to achieve the minimum CF for a DMT signal. There may exist a direct mathematical method for deriving this phasing scheme, which is left for future research.





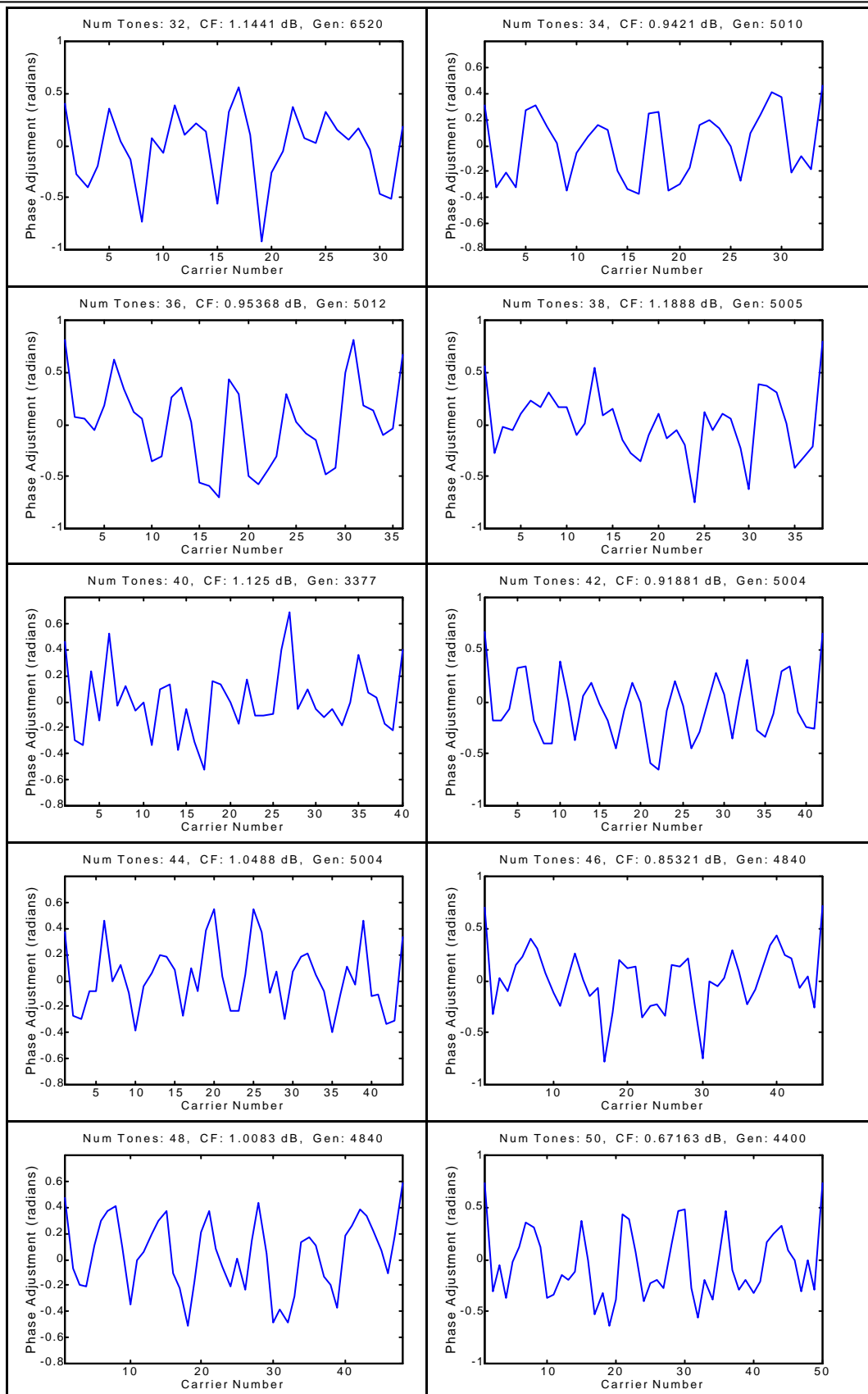
Appendix D

Phase tables for evolved low Crest Factor Discrete Multi-Tone signals



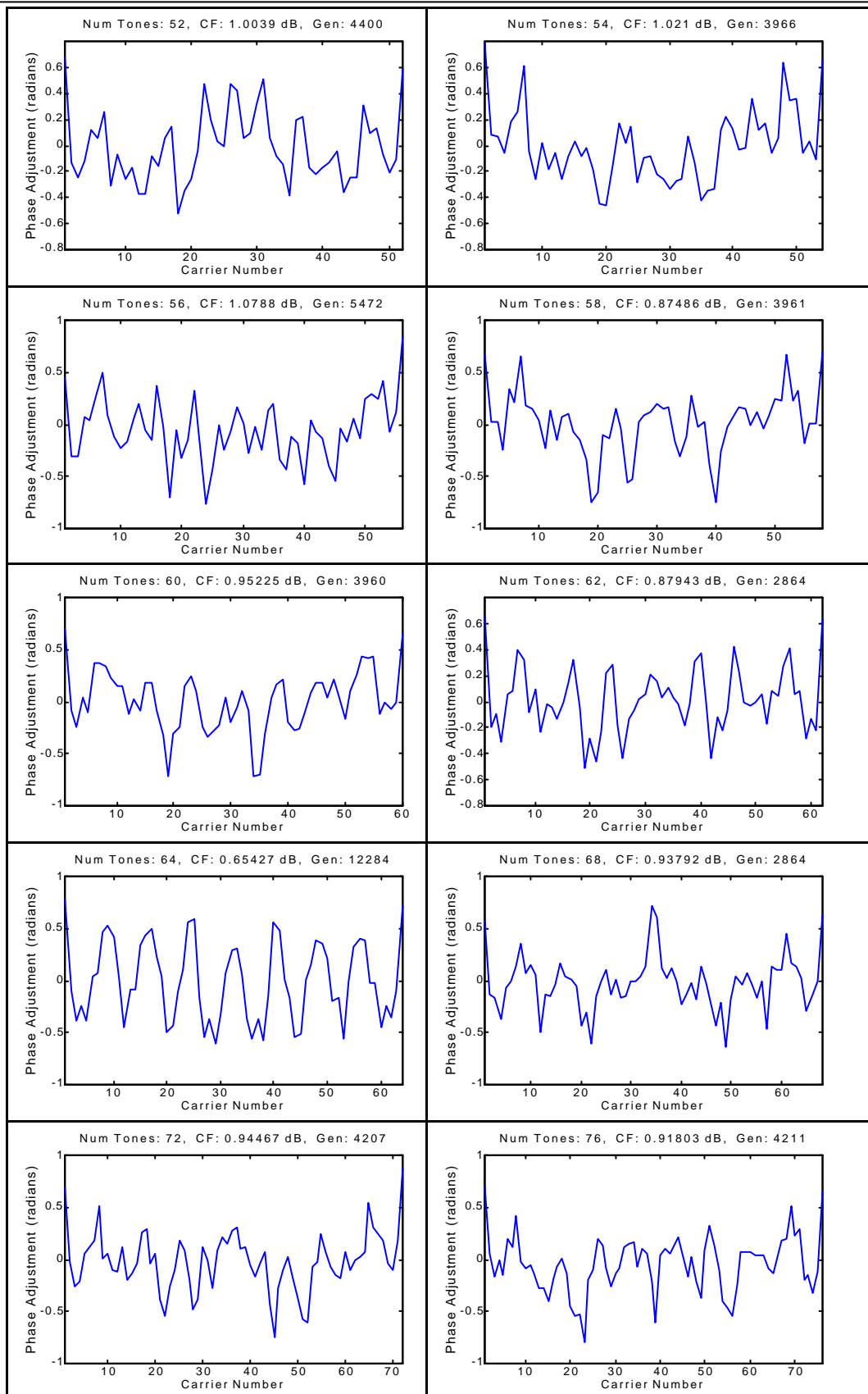
Appendix D

Phase tables for evolved low Crest Factor Discrete Multi-Tone signals



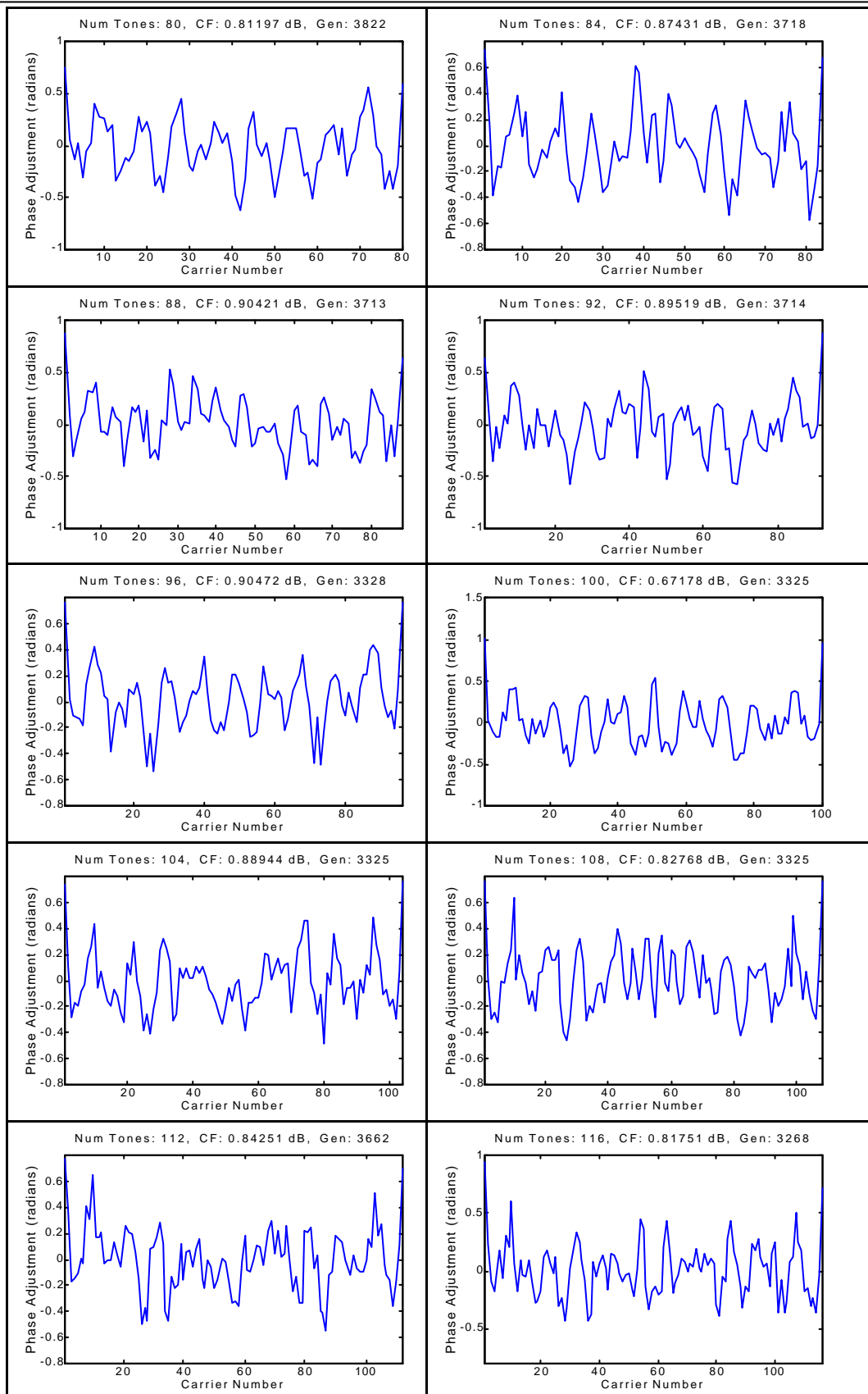
Appendix D

Phase tables for evolved low Crest Factor Discrete Multi-Tone signals



Appendix D

Phase tables for evolved low Crest Factor Discrete Multi-Tone signals



Appendix D

Phase tables for evolved low Crest Factor Discrete Multi-Tone signals

